

**Proteomic analysis of disease associated changes in animal models of
dilated cardiomyopathy**

Inaugural dissertation

Zur

Erlangung des akademischen Grades
Doktor rerum naturalium (Dr. rer. nat.) an der Mathematisch-
Naturwissenschaftliche Fakultät
der
Ernst-Moritz-Arndt-Universität Greifswald

Vorgelegt von
Krishnatej Nishtala
geboren am 16.08.1981
in Kakinada – India

Greifswald, April 2012

Dekan: Prof. Dr. rer. nat. Klaus Fesser

1. Gutachter : Prof. Dr. rer. nat. Uwe Völker

2. Gutachter: Dr. Thomas Bock

Tag der Promotion: 15.06.2012

Table of contents

Summary	I
1. Introduction	1
2. Materials & Methods.....	21
2.1 Materials	21
2.1.1. Chemicals.....	21
2.1.2. Instruments.....	23
2.1.3. Softwares.....	23
2.2. Methods	24
2.2.1. Biological samples	24
2.2.2. Histology.....	25
2.2.4. Protein Quantitation by Bradford assay	25
2.2.5. CyDye labeling and Differential In-gel Electrophoresis (DIGE)	26
2.2.6. Two dimensional gel electrophoresis.....	27
2.2.7. Spot detection, quantification and protein identification	31
2.2.8. Gel-Free liquid chromatography- mass spectrometric analysis	33
2.3. Phosphoprotein analysis	36
2.3.1. Visualizing of phosphorylated proteins using ProQ staining.....	36
2.3.2. Identification of phosphorylated proteins	37
2.4. Western blot analysis.....	39
2.5. Validation of proteins by immunohistological staining.....	41
2.6. Detection of protein oxidation using Oxyblot technique.....	42
3. Results	43
3.1. Comparison of protein quantitation methods for data recorded by gel-free LC-MS/MS using HL-1 cells	43
3.2. Analysis of the CVB3 induced DCM animal model	47
3.2.1. Pathological changes in mouse hearts due to CVB3 induced dilated cardiomyopathy.....	47
3.2.2. Characterisation of changes in the proteome of hearts infected with CVB3 in A.BY/SnJ mice.....	48
3.2.3. Decreased activities of mitochondrial respiratory chain complexes in A.BY/SnJ mice hearts infected with dilated cardiomyopathy	68
3.2.4. Phosphorylation of proteins associated to dilated hearts of CVB3 infected A.BY/SnJ mice.....	69
3.3. Age related changes in the protein profile of non-infected A.BY/SnJ mice hearts.....	72
3.3.1. 2D-DIGE analysis of age dependent changes in the proteome profile of mouse hearts	72
3.3.2. Gel free LC-MS/MS analysis of age dependent changes in the proteome profile of mice heart.....	77
3.3.3. Comprehensive analysis of the data of the 2D-DIGE and gel free LC-MS/MS analysis.....	81
3.3.4. Validation of proteins displaying age dependent changes in A.BY/SnJ mice hearts by immunohistochemistry	85
3.4. Analyses of heart tissues of rats overexpressing ANT-1 in comparison to wild type animals.....	87
3.4.1. Changes in the total proteome of adenine nucleotide translocase 1/ANT1 over expressing (ANT-OE) rat hearts in comparison to wild type hearts.....	87

3.4.2. Influence of ANT1 over expression on the mitochondrial proteome of rats infected with CVB3	92
3.5. Proteomic analysis of dilated cardiomyopathy in rats immunized with peptides of Fcγ receptor	98
4. Discussion	104
4.1. Dilated cardiomyopathy associated changes in A.BY/SnJ mice hearts at 84 days post CVB3 infection	105
4.1.1. Dilated cardiomyopathy is associated with an increase in fibrosis as a consequence of cardiac remodeling	106
4.1.2. Compromised myocardial contractility as a result of virus induced dilated cardiomyopathy.....	108
4.1.3. Dilated cardiomyopathy is associated with decreased levels of proteins involved in energy metabolism	111
4.1.4. Changes in the phosphorylation of proteins associated with virus induced dilated cardiomyopathy in mice hearts 84 d p.i.	112
4.2. Age dependent changes in the proteome profile of A.BY/SnJ mouse hearts	114
4.2.1. Altered mitochondrial function in 4 months old A.BY/SnJ mice hearts	115
4.2.2. Increased intracellular protein transport in 4 months old A.BY/SnJ mice hearts compared to young 1 month old hearts	118
4.3. Alterations in the whole heart proteome of rats due to over expression of Adenine nucleotide translocase 1	120
4.3.1. Comparative proteomic analysis of mitochondrial fractions of rat hearts over expressing adenine nucleotide translocase 1 and wild type hearts upon infection with Coxsackievirus B3	122
4.4. Proteomic analysis of experimental rat model developing dilated cardiomyopathy and severe heart failure after immunization with peptides of Fc receptor gamma IIa(CD32).....	125
5. References	130

Summary

Dilated Cardiomyopathy is a chronic myocardial disease characterized by progressive depression of contractile function and ventricular dilatation. It is the leading cause of heart failure and the most common reason for heart transplantation. Besides genetic causes, viral infection and autoimmune response are considered to play a major role in the etiology of the disease. Among different viruses that cause the disease, Coxsackievirus B3 (CVB3) is predominantly associated with the development and progression of the disease. Moreover, Coxsackievirus induced myocarditis in the mouse mimics human myocarditis and dilated cardiomyopathy. In the murine model, the disease progresses over a period of 90 days from acute myocarditis to chronic myocarditis and further develops into dilated cardiomyopathy and congestive heart failure. Though much is known about the progression of the disease, the molecular events occurring after infection with CVB3 are not completely understood.

In the current study, comparative proteomic analysis of A.BY/SnJ mouse hearts 84 days post infection (84 d p.i.) with CVB3 and age-matched non-infected mouse hearts was performed. 2D-DIGE and gel-free LC-MS/MS were used to characterize the changes occurring at the molecular level and Western Blot analysis as well as immunohistochemical staining was carried out for validation of results.

A total of 101 distinct proteins were identified as displaying dilated cardiomyopathy-associated changes in A.BY/SnJ mouse hearts 84 d p.i. compared to age matched controls. Comprehensive analysis by both DIGE and gel-free proteomics revealed proteins related to lipid metabolism (18%), carbohydrate metabolism (14%), cell morphogenesis (14%) and respiratory electron transport chain (9%) to display significantly altered levels in diseased mouse hearts. The significant increase in extracellular matrix proteins observed in mouse hearts 84 d p.i. indicated extensive fibrosis. On the other hand, proteins related to energy metabolism were identified at lower levels in infected mouse hearts than in controls. These proteomics data and the decrease in activities measured for complexes I-IV of the respiratory electron transport chain in A.BY/SnJ mouse hearts 84 d p.i compared to age matched controls, indicate a diminished energy supply in the dilated hearts of CVB3 infected mice. Furthermore, proteins associated with muscle contraction were identified at lower levels in mouse hearts 84 d p.i. compared to age matched controls indicating compromised myocardial contractility due to virus induced dilated cardiomyopathy.

While extracellular matrix proteins and contractile proteins were identified in the DIGE analysis, proteins of lipid metabolism which are mostly mitochondrial in origin and have a $pI > 7$ were identified by gel-free proteomics indicating the advantages of both methods. Gel based analysis also aided in the identification of protein isoforms/ species which allows conclusions on post translational modifications and protein processing. Thus, the current study also identified infection related changes in the phosphorylation of selected proteins. Phosphospecific staining of the gels demonstrated increased phosphorylation of myosin regulatory light chain - ventricular isoform, actin - aortic smooth muscle isoform, heat shock protein 90B, and heat shock protein beta-1 in infected mouse hearts. Extensive degradation of proteins was not observed in the dilated heart.

As described earlier, virus induced dilated cardiomyopathy develops over a period of 90 days in the murine model during which the mice also grow and undergo aging. Since aging is one of the factors influencing the susceptibility of animals to disease, age dependent changes in the proteome of mouse hearts were also studied by comparing 4 months old (84d) A.BY/SnJ mice with 1 month old mice as controls. Complementary analyses by 2D-DIGE and gel-free LC-MS/MS analysis revealed 96 distinct proteins displaying age associated differences in intensity. These proteins are related to lipid metabolism (19%), protein transport (17%) and electron transport chain (12%). Mitochondrial proteins such as carnitine-o-palmitoyltransferase 1, carnitine-o-palmitoyltransferase 2, and carnitine-O-acetyltransferase involved in lipid metabolism and transport were identified at significantly higher levels indicating higher energy demand in 4 months old mice compared to controls. This conclusion is complemented by observation of decreases in the levels of respiratory electron transport chain proteins especially of subunits of ATP synthase as a member of complex V.

Furthermore, an increase in intracellular transport proteins was also observed in 4 months old mouse hearts compared to one month old controls. An increase in the level of vesicular transport proteins likely constitutes a secondary effect leading to endoplasmic reticulum associated protein degradation.

In the two studies described above, altered mitochondrial functioning and thereby decreased energy/ATP production was very prominent indicating the role of mitochondria in health and disease. The exchange of ADP/ATP across the mitochondrial membrane is carried out by the carrier protein adenine nucleotide translocase1 (ANT1). To improve

understanding of the influence of ANT1 in the heart, comparative proteomic analysis using gel-free LC-MS/MS was performed with hearts of 3 months old rats over-expressing ANT1 using hearts from age-matched wild type animals as controls. A total of four hundred and thirty three proteins were identified with at least two peptides, of which eighty seven proteins displayed small but significant ($p < 0.05$) changes in intensity. Proteins related to integrin linked kinase signalling and myocardial contraction displayed increased levels whereas proteins of the mitochondrial respiratory electron transport chain displayed decreased levels in ANT1 overexpressing hearts compared to wild type animals. Oxyblot analysis performed to study changes in the protein oxidation did not reveal any significant difference in the oxidative state of the proteins between the wild type and transgenic animals.

To understand the influence of ANT1 overexpression in virus induced dilated cardiomyopathy, comparative proteomic analyses was performed for the mitochondrial fractions from the hearts of 8 months old rats of the wild type and ANT1 transgenic animals infected with CVB3. Of a total of 370 identified proteins, 83 proteins displayed altered levels in ANT1 overexpressing animals compared to controls. Proteins related to mitochondrial electron transport chain, fatty acid metabolism, contractility and cell structure displayed decreased levels in the infected transgenic animals compared to controls indicating decreased energy metabolism and myocardial contractility besides compromised cell structure.

Besides viral causes of dilated cardiomyopathy, autoimmunity also plays a major role in the development of myocarditis and dilated cardiomyopathy. Therefore proteomic analyses of experimental models of autoimmune myocarditis generated by active immunization of rats with peptides of Fc γ IIa receptor -CEPPWIQVLKEDTVTL (peptide 1) designated as FcR animals and CRCRMEETGISEPI (peptide 2) designated as FcR2 animals- was performed. Of the 303 proteins identified with at least two peptides by gel-free LC-MS/MS analysis. 43 proteins displayed intensities greater than 1.2 fold in FcR rat hearts and 49 proteins displayed intensities greater than 1.2 fold in FcR2 rat hearts compared to animals injected with KLH adjuvant treated as controls. The majority of the alterations (>70%) were observed in both autoimmune models. Thus, immunization leading to an induction of the acute phase response signalling was observed in both experimental setups. Furthermore, the increased amount of proteins such as lumican or procollagen alpha 1,

type 1 indicated the presence of fibrosis after immunization independent of the peptide used.

In summary, using proteomics the current thesis addresses the changes in protein profiles of two models of dilated cardiomyopathy, namely, virus induced dilated cardiomyopathy and autoimmunity induced dilated cardiomyopathy in mouse and rat models of disease. 2D-DIGE and gel-free LC-MS/MS analysis are complementary techniques which provided a comprehensive view of the changes in the protein profile of hearts of the different animal models.

Altered mitochondrial function resulting in decreased energy metabolism and compromised myocardial contractility were prominent in viral models of cardiomyopathy whereas intense acute phase response signalling was observed as a characteristic feature of autoimmune dilated cardiomyopathy. Altered mitochondrial function was also prominent in age associated changes in the heart of A.BY/SnJ mice indicating the role and influence of mitochondria in health and in disease.

1. Introduction

Cardiomyopathies, as defined by American Heart Association (AHA) are a heterogeneous group of diseases of the myocardium associated with mechanical and/or electrical dysfunction that usually (but not invariably) exhibit inappropriate ventricular hypertrophy or dilatation and are caused by a variety of factors that are genetic, non-genetic or acquired (Maron et al., 2006). Based on the factors that cause disease, cardiomyopathies are classified into:

- a. Primary Cardiomyopathy:** Primarily confined to heart muscle and due to either genetic, acquired, or mixed (genetic/non-genetic) reasons (Maron et al., 2006).

Examples: Hypertrophic cardiomyopathy (HCM), and dilated cardiomyopathy (DCM) are two prominent types of primary cardiomyopathy

- b. Secondary Cardiomyopathy:** Shows myocardial involvement and is caused by extrinsic factors like infection, hypertension and generalized systemic disorders (Maron et al., 2006, Towbin & Bowles, 2002).

Example: Amyloidosis, toxicity due to drugs, heavy metals, hyper- and hypothyroidism, neuromuscular disorders such as ataxia, neurofibromatosis etc.

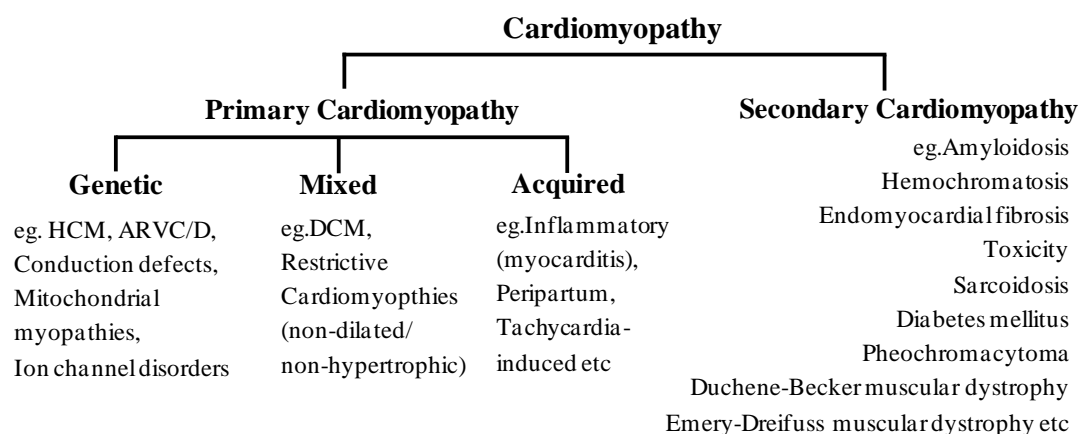


Fig. 1. Classification of Cardiomyopathies by American Heart Association (AHA). Classification of cardiomyopathies into primary and secondary cardiomyopathies based on the factors that cause the disease. The most prominent of these cardiomyopathies are hypertrophic cardiomyopathy (HCM) and dilated cardiomyopathy (DCM). Modified from Maron et al., 2006

Dilated cardiomyopathy (DCM) is characterized by an increase in the ventricular chamber with normal or reduced wall thickness and systolic dysfunction associated with decreased myocardial contractility which progresses into congestive heart failure and/or sudden death (Fig.2). It mostly presents between 18 and 50 years of age, though children and elderly can also be affected. Men are more frequently affected by DCM than women (2.5:1). It is the third most common form of heart muscle disease with an estimated prevalence of 1:2500 and the most common cause of heart transplantation with approximately 50% of the individuals with severe forms (LVEF < 30 %) reported to die within 5 years of diagnosis if they do not receive heart transplantation (Towbin & Bowles, 2002, Maron et al., 2006, Mohan et al., 2002).

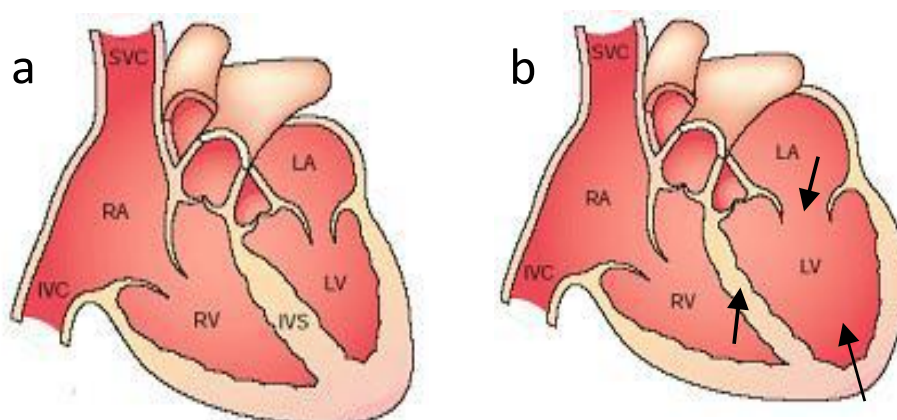


Fig. 2. Diagrammatic representation of a heart affected with dilated cardiomyopathy. Illustration of a dilated heart. a-represents a healthy heart with no infection. LV-left ventricle, LA-left atrium, RV-right ventricle, RA-right atrium, IVS-intraventricular septum, IVC-inferior vena cava, SVC-supra ventricular septum. b- represents heart infected by dilated cardiomyopathy showing dilated left atrium and left ventricle with bulging intraventricular septum (Towbin and Bowles, 2002).

Three major factors contribute to DCM: genetic factors, auto-immune components and enteroviral infection. Besides these, toxins, chemotherapeutic agents like anthracycline, doxorubicin, daunorubicin, chronic alcohol consumption, neuromuscular disorders, mitochondrial, endocrine, metabolic disorders and infectious agents like bacteria, fungi, parasites (chagas disease-*T.cruzi*) etc. have also been implicated as causes for the disease.

Genetic predisposition is considered to be the major cause of dilated cardiomyopathy. Around 30% of the cases reported have genetic reasons. Familial DCM is diagnosed at an earlier age than in individuals with non-familial DCM. More than 20% of the patients affected by DCM were also reported to have an affected first degree relative. Population

studies on DCM patients have shown that the disease can be transmitted as autosomal dominant or recessive, X-linked or mitochondrial traits (Table.1). Although genetically heterogeneous, the most common mode of inheritance is autosomal dominant. X-linked and autosomal recessive mutations are less frequent and autosomal recessive inheritance is associated with infantile forms of DCM (Schönberger & Seidman, 2001, Fatkin & Graham, 2002). More than twenty gene mutations such as those in genes encoding for muscle LIM protein, desmin, δ -sarcoglycan, actin, lamin A/C have been associated with DCM (Arber et al., 1997, Milner et al., 1996, Nigro et al., 1997, Olson et al., 1998, Sullivan et al., 1999). Availability of polymorphic genomic markers and successful strategies for selecting candidate genes dramatically increased the number of identified human DCM gene mutations. Decoding the genetic causes of DCM aided in the development of two models- the final common pathway model which states DCM to be a non-specific degenerative state and an alternative model which states that several independent pathways play a role in remodeling of heart leading to DCM (Ahmad et al., 2005).

Table 1. Genetic causes of DCM. Mutations in genes encoding proteins belonging to sarcomere, structural proteins and others have been identified to cause DCM. Most of the genes involved are transmitted by autosomal dominant inheritance. (Data adopted and modified from Schönberger & Seidman, 2001 and Carolyn & Seidman, 2003).

Gene Class	Gene	Inheritance
Proteins in sarcomere	β -myosin heavy chain	autosomal dominant
	cardiac troponin T	autosomal dominant
	α -tropomyosin	autosomal dominant
	actin	autosomal dominant
Structural proteins	δ -sarcoglycan	autosomal dominant
	desmin	autosomal dominant
	desmoplakin	autosomal recessive
	plakoglobin	autosomal recessive
Others	lamin A/C	autosomal dominant
	dystrophin	X-linked

Viral infection has been documented as another major causative agent of dilated cardiomyopathy besides genetic reasons, contributing to almost equal percentage (20-25%) of the cases (Bowles et al., 1989, Bendig et al., 2003, Klingel et al., 2004, Kuhl et al., 2005b). For more than 50 years, viral myocarditis has been implicated as leading to congestive heart failure (CHF). Myocarditis is defined as an inflammatory disease of the

cardiac muscle caused by myocardial infiltration of immunocompetent cells following any kind of cardiac injury (Kühl & Schultheiss, 2009). According to the definition and classification of the World Health Organization/International Society and Federation of Cardiology (WHO/ISFC), myocarditis is a heterogeneous final common pathway for myocardial inflammation and necrosis and/or degeneration of adjacent myocytes resulting from a variety of diverse etiologies such as infection, immunity and toxic insults. Viral genomes have been detected in endomyocardial biopsies of patients with acute heart failure and might be the initiator of myocarditis. A broad spectrum of viruses is known to cause myocarditis leading to DCM (Table 2) (Kearney et al., 2001, Pauschinger, 2004).

Table 2. Viral causes of myocarditis. Viruses of different taxonomy are known to cause myocarditis. (Data obtained from Kearney et al., 2001 & Mathias Pauschinger, 2004)

Viruses causing myocarditis	
Coxsackievirus B1-B5	Epstein-Barr virus
Serotypes of Coxsackievirus A	Polio virus
Adenovirus type2 and type 5	Mumps virus
Parvovirus B19	Hep B virus
Influenza virus A and B	Rabies virus
Cytomegalovirus	Varicella zoster virus
Toga Viruses	Vaccinia & Variola virus

The most common viruses associated with DCM are adenoviruses and enteroviruses. Among the enteroviruses, coxsackieviruses, in particular B3 (CVB3) and B5- belonging to the family *Picornaviridae*- were commonly found in DCM patients (Orthopolous et al., 2004). CVB3 is the predominant cause of myocarditis and is implicated in 20-40% of the cases of dilated cardiomyopathy (DCM) (Esfanderei & McManus, 2008). Beside the viral genotype as a critical factor which determines the disease expression in the heart, a set of factors such as sex, age, presence of virus specific receptors, nutritional status, pregnancy, exercise, immunological response and genetic predisposition to viral myocarditis influences the susceptibility of the host to the disease. The impact of these factors has been extensively studied in murine models, but most of them have also been found important in humans (Martino, 1994, Yajima, 2009).

Of all the viruses, the **mechanisms associated with coxsackieviral infection** have been most widely studied in mice since mice models of CVB infection mimic human chronic myocarditis with progression to DCM (Klingel et al., 1992, Rutschow et al., 2010). Coxsackievirus causes cell destruction either by direct cytolytic infection of the heart or by contributing to autoimmune reactions in an indirect manner (Pallansch, 1997, Lane et al., 1993). Interaction between the virus and the cell receptor plays a critical role in the infection cycle. Viral entry and subsequent replication require receptors and additional co-factors.

Myocarditis in mice is best studied by intraperitoneal administration of CVB3 to susceptible mice resulting in heart disease which is then strikingly similar to human myocarditis. The disease progresses over a period of 90 days (Fig.3) from acute myocarditis to chronic myocarditis, subsequently leading to dilated cardiomyopathy and congestive heart failure (Klingel et al., 1992, Esfanderei & McManus, 2008, Yajima, 2009).

Acute phase of myocarditis comprises the initial 4-7 days of infection-viral entry into the host cardiomyocyte, viral replication and spreading of the virus, virus mediated cardiac injury and host immune response.

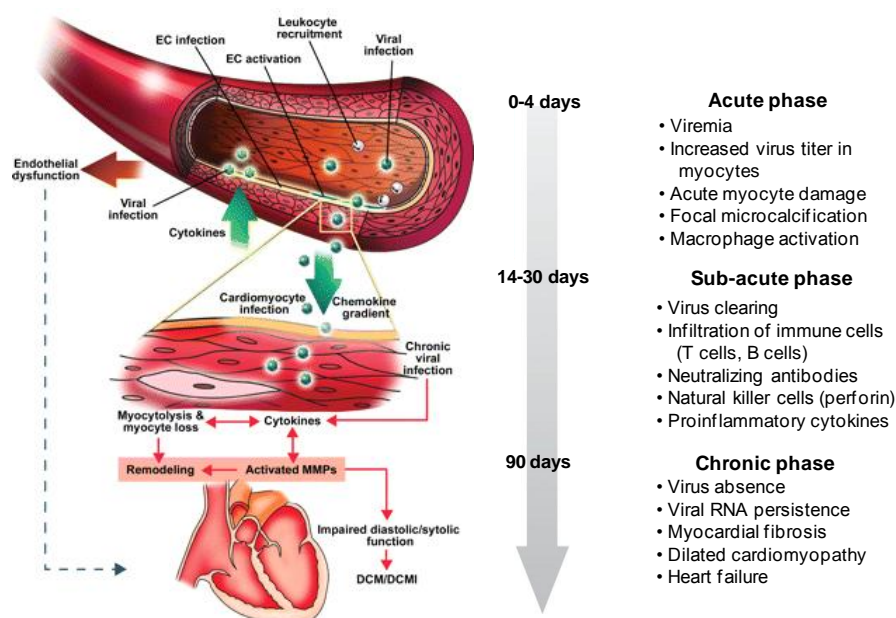


Fig. 3. Stages of viral myocarditis leading to dilated cardiomyopathy. High viral titer and acute myocardial damage with activation of innate immune response is observed in the initial 4days of infection. Activation of adaptive immune response in 7-14days of infection removes virus, pro-inflammatory cytokines are secreted and infiltration of natural killer cells (NK) is observed. However viral RNA still persists. Chronic phase of the disease is associated with severe myocardial fibrosis leading to dilated cardiomyopathy and heart failure (Adopted and modified from Esfanderei & McManus, 2008, Schultheiss et al., 2011).

The infectious cycle is initiated by binding of the virus to decay accelerating factor (DAF) which acts as a primary attachment protein/co-receptor. DAF is a membrane glycosyl-phosphatidyl-inositol (GPI) anchored protein and associates with the Src family of protein tyrosine kinases (Bergelson et al., 1997, Nicholson-Weller et al., 1994). Besides DAF, another receptor which is critical for the virus to infect the cell is coxsackievirus and adenovirus receptor (CAR), which helps in the internalization of the virus at the tight junctions of the epithelial cells. The virus hijacks GPI anchored DAF mediated Src-family tyrosine signaling pushing the virus-DAF complex towards tight junction via actin cytoskeleton remodeling which is not usually accessible to the virus, (Shinoy-Scaria et al., 1992, Liu et al., 2000, Coyne & Bergelson, 2006). Expression of CAR as a viral receptor in the cardiomyocyte influences the susceptibility of the host to infection. Its expression is highest in the early post natal period and decreases with age which to a certain extent may explain the susceptibility of myocarditis in children (Kashimura et al., 2004, Noutsias et al., 2001). Significant decrease in CAR expression in mouse heart with increasing age indicates age-related pattern of host susceptibility and tissue tropism to CVB3 (Honda et al., 2000). No myocardial inflammation or cardiomyopathy developed in the absence of CAR in cardiomyocytes (Shi et al., 2009).

CVB3 contains a 74kb single strand positive-sense RNA as its genetic material. The 5' end has a virus encoded protein, VPg (3B) instead of the usual eukaryotic 7-methyl guanosine cap. Following entry of the virus into the cardiomyocyte, the VPg (3B) protein is essential for viral RNA and protein synthesis (Flanagan et al., 1977). Viral replication in the myocytes results in high titers of infectious progeny in blood, spleen, pancreas and the myocardium during acute viremic stage. 3 days post infection (p.i.), myocytes with CVB3 RNA are distributed randomly through the myocardium. By this time the majority of the myocytes lose their contractile ability (Yoneda et al., 1979). High viral replication within 3-4 days p.i. results in virus-mediated cardiomyocyte injury, necrotic and apoptotic myofibres, and formation of vesicles and vacuoles in the cytoplasm (McManus et al., 1993).

In response to the virus, cells intrinsic to the myocardium such as endothelial cells, cardiomyocytes, fibroblasts, and dendritic cells release cytokines triggering the host innate immune response. Besides cytokines, levels of interleukins IL-1 α , IL-1 β , IL-6, IL-18, TNF- α , TNF- β and interferon γ are elevated prior to infiltration by immune cells leading to an inflammatory reaction. Around day 4 p.i., neutralizing antibodies also play an

important role in limiting the viral replication (Seko et al., 1997, Fuse et al., 2005, Cho et al., 1982).

Viruses which successfully avoid elimination by the innate immune system replicate and cause myocardial injury by producing viral proteins. Viral protein, protease 2A is known to cleave eukaryotic initiation factor-4 γ resulting in inhibition of the host cell mRNA translation and protein synthesis (Lamphear et al., 1993, Ehrenfeld, 1982, Ventoso et al., 1998). Viral protease 2A also induces apoptosis by activating extrinsic and intrinsic apoptotic pathways. Protease 2A was shown to contribute to myocardial injury by cleavage and disruption of cytoskeletal proteins dystrophin and associated glycoproteins α -sarcoglycan and β -dystroglycan both *in vitro* and in *in vivo* models. Another viral protease, protease 3C cleaves and inactivates several transcription factors resulting in shut down of the host transcriptional and translational machinery. It also induces apoptosis through the intrinsic apoptotic pathway (Chau et al., 2007, Badorff et al., 1999, Clark et al., 1993). Viral 3D^{Pro}, a RNA dependent RNA polymerase uses viral positive sense RNA as a template to generate negative-sense RNA which in turn can produce several positive strands. These positive strands, which are packed into the progeny virus, are eventually released to initiate new cycles of infection (Van Dyke & Flanagan, 1980). The release of progeny virus though not clearly understood, is thought to be facilitated by viral protein 2B by increasing the permeability of the plasma membrane (Doedens & Kirkegaard, 1993, van Kuppeveld et al., 1997).

The release of progeny virus into the interstitium stimulates migration of NK cells activated by IL-2 and macrophages to the site of injury and an increase in inflammatory cytokines. NK cells following activation by IL-2 kill the virus infected cardiomyocyte to curb the spread of virus. In murine models of myocarditis, mice deficient in NK cells showed severe myocarditis emphasizing the cardioprotective role of NK cells (Lodge et al., 1987). However, extended presence of NK cells aggravates myocardial damage due to the release of cytotoxic molecules within the myocardium such as perforin. The cytotoxic molecules form multifocal inflammatory lesions on the membrane surface of cardiomyocytes and contribute to disruption of the cytoskeleton (Young et al., 1990, Godney et al., 1986, Koike et al., 2001). The expression of proinflammatory cytokines is associated with a second wave of infiltrating immune cells especially antigen specific T-lymphocytes. T-cytotoxic (T_C) and T-helper (T_H) cells infiltrate the myocardium initiating the adaptive immune response. T_C cells target the viral antigens associated with MHC-I

presented on the cell surface of infected cardiomyocytes (Fuse et al., 2005, Kishimoto et al., 1985, Seko et al., 1980). This infiltration of the heart by T-cells peaks 7-14days p.i. and is considered to be the most severe phase of myocardial damage since T-cells play an important role in both viral clearance from the infected myocytes and immune mediated myocardial injury or necrosis. At this stage, cell mediated immune response rather than viral mechanisms are responsible for the ongoing destruction of the cardiac tissue and its progression into chronic heart disease (Kishimoto et al., 1985, Martino et al., 1994). The T-cell response to the virus differs based on the susceptibility of the host to infection. The strain of the mice as a genetic determinant plays a critical role in the intensity of the T-cell response through which either the virus is completely eliminated or the disease progresses further into a chronic phase. C57BL/6 and DBA/1J strains of mice are resistant and successfully eliminate the virus after acute infection whereas A.BY/SnJ and SWR/J mice are susceptible strains which likely develop ongoing myocarditis after acute infection (Klingel et al., 1992).

The **chronic phase of myocarditis** is observed in immune competent hosts with a complete removal of virus from the blood and peripheral tissues and lasts from 15-90 days p.i.. The inflammation resolves with the clearance of the virus, however, the viral RNA still persists along with viral capsid protein VP1 in heart and in reservoir organs such as spleen and lymphnodes (Kyu et al., 1992, Li et al, 2000). The viral RNA is capable of replication, albeit in a restricted manner, and might contribute to continuous triggering of the immune response. Subsequently, interstitial fibrosis, myocardial necrosis and ventricular dilation develop as a result of ongoing myocardial damage. The continuous viral replication and immune cell infiltration may be responsible for the progression of viral myocarditis to dilated cardiomyopathy (Chow et al., 1991, Klingel et al., 1992). Also, myocardial antigens that bear similarity to viral proteins cause T-cells aimed at the virus to cross react with host antigens in a phenomenon of “molecular mimicry” resulting in autoimmune myocarditis (Woodruff & Woodruff, 1974). Coxsackievirus shares epitopes with proteins in the cell or plasma membrane and stimulates autoimmune responses. Coxsackievirus B3 in particular, shares epitopes with human and mouse cardiac myosins (Gaunt et al., 1995). Myosin heavy chain, an autoantigen is mostly associated with chronic viral myocarditis (Neu et al., 1987). Cardiac myosin released during the inflammatory process is taken up either by dendritic cells present in the heart or by macrophages whereupon the myosin is fragmented and presented with class-II major histocompatibility

complex (MHC) on the surface of an antigen-presenting cell (APC). The myosin-MHC-II-APC complex is recognized by CD4⁺ T_H cells triggering an autoimmune response (Rose & Susan, 1996). During chronic myocarditis, CD4⁺ T-cells predominantly infiltrate the myocardium. Activated CD4⁺ T-cells might participate in the immunity by regulating the production of autoantibodies by B cells or infiltrating into the myocardium leading to myocyte damage through production of cytokines or cytolytic molecules, such as perforin (Eriksson *et al.*, 2003). These effects are assumed to cause contractile dysfunction leading to long-term remodeling and dilated cardiomyopathy.

As discussed above, viral myocarditis, over a span of 90 days progresses into dilated cardiomyopathy leading to sudden death. During this period, the mice also grow older and considering the fact that age is one of the factors influencing the susceptibility of the mice to the virus and the disease, the changes occurring due to **aging** should also be taken into consideration. Especially in case of diseases which progress over a period of time, studying the age related changes emphasizes the importance of considering age matched controls. Cardiovascular diseases such as hypertension, myocardial infarction, coronary heart disease, arteriosclerosis have been shown to have significant age and sex dependency (Diedrich *et al.*, 2007). Structural and functional changes occur in the heart as a result of aging. Left ventricular thickening and decrease in left ventricular cavity size, decrease in the number of myocytes and decreased diastolic function are the most significant changes of cardiac aging (Lakatta *et al.*, 2000, Dai *et al.*, 2009).

Echocardiographic studies showed significant age-dependent trends in the structural changes of the heart in mice. The left ventricle continuously goes through series of structural and functional changes with age (Lakatta & Levy, 2003). Murine hearts were characterized with increased left ventricular mass index (LVMI) and myocardial performance index (MPI) indicating LV systolic and diastolic dysfunction (Dai *et al.*, 2009). Histopathology of the aged mice hearts showed subendocardial and interstitial fibrosis, vacuolization of the cytoplasm, collapse of sarcomeres, mineralization and arteriosclerosis. Most of these changes are also observed in case of cardiomyopathy and hence can be designated as age-associated cardiomyopathy (Treuting *et al.*, 2008). Boyle *et al.* recently reported that 18 months old C57/Bl6 mice developed contractile dysfunction associated increased fibrosis and hypertrophy compared to young mice (Boyle *et al.*, 2011). Fibrosis is more frequently observed in the ventricular subendocardium of old mice hearts. Matrix metalloproteinases (MMPs) and tissue inhibitors of matrix

metalloproteinases (TIMPs), indicators of fibrosis, showed differential expression with age. These findings in conjunction with an age related decrease in cardiac fibroblast proliferation indicates impaired left ventricular repair capacity in aged hearts (Lindsey et al., 2005, Dai et al., 2007). Besides structural changes, molecular changes such as enhanced production of stress-related substances, increased expression of angiotensin-II receptors, enhanced apoptosis and desensitization of β -adrenergic receptors have been observed as a result of aging (Simkhovich et al., 2003).

Aged hosts have higher incidence, severity and mortality from infections than an adult heart. Higher susceptibility to infections such as viral myocarditis has been associated to dysregulation of the immune system leading to inability of the host to ward off the infection through an effective immune response (Gay et al., 2006). A significant decline in the adaptive immunity and activation of innate immunity has been associated with aging. Transcriptional analysis done in 18 months old C57Bl/6 mice showed increased expression of genes related to the immune system with an increase in immune related mechanisms. These genes are thought to play a key role in innate immunity which is thought to respond to pathogens in a generic manner though it does not provide long-lasting protective immunity to the host as in the case of adaptive immunity (Brink et al., 2009, Boyle et al., 2011).

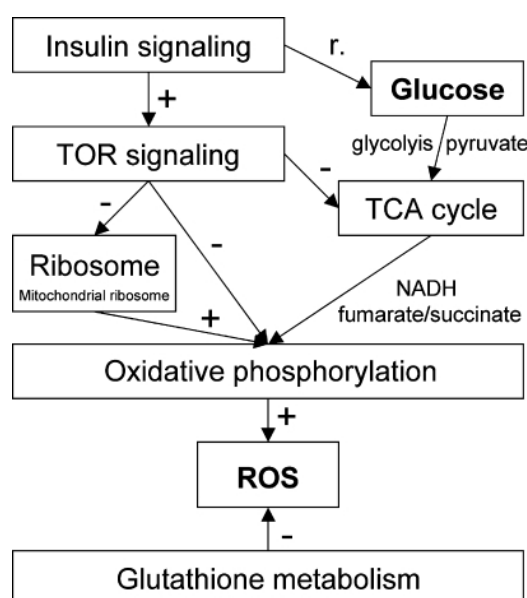


Fig. 4. Interconnected network of pathways regulated due to aging in mice heart. Increased insulin signaling induces increased TOR signalling which affects mitochondrial ribosome genes, genes related to oxidative phosphorylation (OxPhos) and TCA cycle. Besides, Insulin signalling also regulates glucose levels linked to TCA cycle which is further related to OxPhos by Complex I of the electron transport chain. Decreased OxPhos produces reactive oxygen species (ROS) which is deleterious to the cell (Brink et al., 2009).

Cardiac myocytes house numerous mitochondria which ensure the high energy supply necessary for efficient contractility of the cells. Mitochondrial dysfunction in aging heart might affect the cellular energy production and metabolism. Alteration in the mitochondrial function leads to increased oxidative stress and causes oxidative damage to proteins associated with aging and various cardiac pathologies (Fig.4). Mitochondria play an important role in cellular loss as observed in cardiomyopathy, ischemia, myocardial infarction and congestive heart failure (Lenaz et al., 2002, Gustaffson & Gottlieb., 2008, Shih et al., 2010). This indicates the overlapping role of mitochondria in aging and in disease. Hence, it is imperative to use age matched controls for the study of diseases where age has significant influence in the susceptibility and progression of the disease as mentioned above.

The structural and molecular changes occurring in the heart have a major implication on the age related decrease in cardiac performance and in tolerance to disease related injury. Cardiac aging is an irreversible process and is associated with instability and damage rendering the heart susceptible to disease. In this process mitochondria play a major role.

Electrons generated from various pathways such as β -oxidation of fatty acids, glycolysis and TCA cycle feed the respiratory electron transport chain where ATP is generated within the mitochondria. For the transport of ATP across the mitochondrial membrane, cells need carrier molecules. One such carrier molecule located in inner membrane of the mitochondria is adenine nucleotide translocase (ANT). ANT is a dimeric protein complex encoded by three nuclear genes ANT 1-3 expressed in a tissue specific pattern. ANT1 is specific to tissues like heart, skeletal muscle and brain rich in mitochondria while ANT2 was found in kidney, liver and spleen (Dörner et al., 2006). ANT homodimers form selective channels that facilitate the efflux of nascent ATP out to the cytoplasm accompanied by influx of ADP to the mitochondrial matrix (Levy et al., 2000, Stepien et al., 1992).

Deficit of ANT has been shown to influence the pathogenesis of myocardial remodeling and cardiac insufficiency (Portman, 2002). Moreover excessive proliferation of mitochondria in skeletal and heart muscle, exercise intolerance and defective mitochondrial oxidative phosphorylation were reported in ANT1 knock-out mice. The mitochondrial energy insufficiency raised by defective OxPhos in ANT knock-out mice was reported to cause severe cardiac hypertrophy leading to loss in contractile function

and abnormal Ca^{+2} transport in the sarcolemma and sarcoplasmic reticulum. Furthermore, defective OXPHOS translates to increased production of reactive oxygen species which damage the mitochondrial DNA and cause cellular dysfunction (Graham et al., 1997, McMullen & Jennings, 2007). Besides mitochondrial energy production and cytosolic energy consumption, ANT plays a significant role in apoptosis by binding to pro-apoptotic and anti-apoptotic proteins, transcription factors, cell signaling proteins and viral proteins (Belzacq et al., 2003, Bottero et al., 2001, Goldmacher et al., 1999, Jacotot et al., 2001). ANT-specific antibodies were observed in patients with DCM indicating their involvement in the pathophysiology of DCM triggering an autoimmune response. This supposedly might be due to molecular mimicry between homologous amino acid sequences of ANT and CVB3. These antibodies are organ- and conformation specific and inhibit the nucleotide exchange by blocking the substrate binding site of the protein. This might cause imbalance of energy supply and demand by disturbance of cellular function which is a crucial factor in myocarditis and dilated cardiomyopathy (Schultheiss et al., 1985, Schwimmbeck et al., 1993, Schultheiss et al., 1984, Schulze et al., 1989).

Mitochondrial oxidative damage influences the activity of ANT in dilated cardiomyopathy. A significant decline in the ANT transport activity was reported in explanted heart tissues of patients with DCM accompanied by elevation of total ANT protein. This might be compensation to the decrease in the activity of ANT (Bäumer et al., 2000, Schultheiss et al., 1992, Sylven et al., 1993). Furthermore, a shift in the isoform expression of ANT with elevated ANT1 was also observed in inflammatory heart disease associated with enterovirus infection indicating DCM specific mechanism associated with altered ANT function and expression (Dörner et al., 2006).

Transgenic over-expression of ANT1 seems to revert the effects caused by ANT dysfunction. It induces an intracellular cardioprotective program that influences various cellular processes. ANT1 over expression increased the efficiency of mitochondrial ADP/ATP flux and energetic coupling of oxidative phosphorylation. Tissue destruction and cardiac dysfunction in hypertrophic and diabetic cardiomyopathy was prevented in ANT1 over expressing animals (McLeod et al., 2004, Walther et al., 2007, Wang et al., 2009). In rat hearts, transgenic over expression of ANT1 resulted in improved contractility and in abundance of myofibrillar proteins. The improved contractility might be due to increased expression of SERCA 2a, a reticular Ca^{2+} ATPase which facilitates enhanced sarcoplasmic reticulum Ca^{2+} uptake (Vogelpohl et al., 2011). These observations illustrate

the importance and protective role of ANT and in particular ANT1 protein in improving cardiac performance and mitochondrial oxidative phosphorylation in heart failure.

While mitochondrial dysfunction may lead to deleterious effects to the myocardium in dilated cardiomyopathy, the immune response and in particular humoral immunity also plays a significant role in the pathogenesis of DCM. Antibodies against various cardiac proteins such as mitochondrial proteins (e.g. ANT), contractile proteins, e.g. myosin heavy chain and β -1 receptors and others were identified in DCM (Schulze et al., 1990, Caforio et al., 1992, Limas et al., 1989). The IgG autoantibodies on one hand bind to the antigens with their Fab fragments and on the other hand with their Fc fragments, they bind to the Fc_γ -receptor (Fc_γR) expressed on cardiomyocytes. By simultaneously binding to the antigen and Fc_γ -receptor, the autoantibodies can affect the cells by inducing signals either through Fab fragment or through Fc_γ -receptor. The Fc_γR mediated mechanism is thought to be responsible for the negative inotropic effects induced by IgG autoantibodies in cardiomyocytes (Koolwijk et al., 1989, Kurlander et al., 1983, Staudt et al., 2007).

Cell membrane receptors specific for the Fc portion of IgG were shown to play an important role in the immunity and resistance towards infection. While FcRs have been described for all classes of immunoglobulins, Fc_γ receptors are specific to IgG. These receptors are involved in diverse biological responses such as endocytosis, phagocytosis, antibody-mediated cell toxicity, regulation of B-cell function and release of inflammatory mediators based on their binding to IgG-antibody complexes. The Fc part of the antibody is responsible for the diverse biological effects since it interacts with Fc_γ receptors expressed on many cells as leukocytes, platelets and others (Hulett & Hogarth, 1994, Staudt et al., 2007). The IgG receptor family comprises of numerous activating receptors and a single inhibiting receptor, $\text{Fc}_\gamma\text{RIIIb}$. Only two of the several activating receptors, $\text{Fc}_\gamma\text{RI}$ and $\text{Fc}_\gamma\text{RIIIa}$ are common to humans and mice. Both these receptors signal via $\text{FcR } \gamma$ -chain which contains specialized motifs such as immunoreceptor tyrosine based activation motif (ITAM). These motifs signal cell activating pathways via *src* and *syk* tyrosin kinases. Humans and rats express an additional activating receptor $\text{Fc}_\gamma\text{RIIa}$. It is of particular importance since other Fc receptors require $\text{Fc}_\gamma\text{RIIa}$ to initiate cell activation. The inhibitory receptor, $\text{Fc}_\gamma\text{RIIIb}$ mediates its effect via immunoreceptor tyrosine based inhibiting motif (ITIM) located in its cytoplasmic tail (Ravetch & Bolland, 2001, Daeron, 1997, Staudt et al., 2007, Tamir et al., 2000). FcRs are involved in different steps of the immune process such as maintenance of B-cell tolerance, formation of autoantigen-

antibody immune complexes and subsequent maturation of dendritic cells to antigen presenting cells. During the 50s' and 60s', antibody induced destruction of Type III hypersensitivity was thought to be majorly dependant on complement system. However, a strong inflammatory response was visible even after experimental depletion of the complement system. FcRs were not known during that period and it was only in the 80s' that FcRs were considered major effectors of antibody-based inflammation. This was demonstrated using soluble recombinant forms of the ectodomains of human FcRIIa in rats as a competitive inhibitor of Fc receptor function. Inhibited Type III hypersensitivity indicates FcRs may be responsible for antibody-based inflammation (Ierino et al., 1993). Together with complement system, FcR, through these processes described above probably elicit an autoimmune response (Schmidt & Gessner, 2005, Hogarth, 2002).

Genetic studies and disease models have identified FcRs as risk factors of autoimmune disease. The presence of anti- Fc γ antibodies were demonstrated in strains of autoimmune mice using truncated recombinant Fc γ RII (Hogarth, 2002, Boros et al., 1990). Fc γ RIIa was detected on the sarcolemmal membrane of rat ventricular cardiomyocytes and was shown to have potential functional role in DCM. The Fc γ receptors IIa are thought to induce an activating signal in cardiomyocytes through its cytoplasmic domains thereby triggering a negative inotropic effect (Staudt et al., 2007). However, the role of Fc γ receptors IIa in autoimmunity and DCM is still not clear and further studies need to be done to understand its mechanism.

Though much is known about the cause of heart disease, the pathogenic mechanisms underlying the disease are not yet clearly understood. Though gene expression studies have made considerable contributions to the understanding the molecular changes, one gene does not encode for one protein and protein expression and post-translational modifications (PTM) determine cardiac function.

The term proteomics describes a suite of technologies that offer the option to identify the changes occurring in the proteome and to understand what such changes translate into. However, *proteome* is a complex term. So far, 5079 human cardiac proteins have been annotated and 4906 proteins have been characterized in the mouse heart (Prasad et al., 2009, Bousette et al., 2009). The factor of complexity has to be overcome in order gain access to individual proteins and hence, separation of the proteins is essential which marks the foundation of the proteomics workflow. Two dimensional gel electrophoresis (2-DE)

has been widely used for the separation of complex protein mixtures obtained from whole cells, tissues and organisms. Developed in 1975, this method uses a combination of isoelectric point (pI) based first dimension separation under denaturing conditions called isoelectric focusing (IEF) combined with second-dimension separation based on molecular mass (M_r) using sodium dodecyl sulphate polyacrylamide gel electrophoresis (SDS-PAGE) (O'Farrell, 1975, Klose, 1975). This orthogonal separation using combination of charge with mass results in proteins distributed across the gel as distinct intact spots.

Sample preparation involving solubilization, denaturation and reduction of the samples with a reducing agent, is an important step for proteomic studies. Usually the sample proteins are solubilized in sample lysis buffer containing 7-9 M urea, non-ionic or zwitterionic detergent such as CHAPS and a reducing agent as dithiothreitol. Certain protein samples require additional solubilizing agents such as thiourea for enhanced solubility due to the presence of membrane or membrane associated proteins. Approximately 2000 protein species/spots from cell and tissue extracts can be separated on 18cm immobilized pH gradient strip (IPG) combined with 24cm long SDS-PAGE gels (Dunn, 1987, Herbert, 1999, Klose & Kobalz, 1995). The separated proteins are visualized employing a highly sensitive detection method and which should also be compatible to mass spectrometry such as silver staining, coomassie brilliant blue etc. However, these methods differ in sensitivity, specificity and MS compatibility and hence should be selected upon individual merits (Lauber et al., 2001, Miller et al., 2006). A pre-electrophoretic fluorescent staining method called differential in-gel electrophoresis (DIGE) based on the labelling of proteins with the CyDyes is currently considered the gold standard for gel-based proteomics analysis (Lilley and Friedman, 2004). Each protein sample can be labeled separately with Cy3 or Cy5 dye and then separated together on a single 2-D gel. Images of protein pattern are acquired by scanning at different wavelengths. To reduce technical variations, a pooled internal standard labeled with another dye (Cy2) is included in the sample mixture (Alban et al., 2003). Peptide mass fingerprinting (PMF) has been the primary way of identification of proteins. A set of peptide masses obtained from MS after proteolytic digestion of the protein are compared to theoretical peptide masses obtained from *in silico* digestion of the protein or predicted from nucleotide sequence databases.

2DE has been extensively used for the detection and identification of cardiac proteins and for studying disease related changes in the protein profile in human and in animal models.

As many as 100 proteins have been identified to show DCM related changes in explanted hearts and biopsies. These have been classified into cytoskeletal and myofibrillar proteins, mitochondrial proteins and stress related proteins (McGregor & Dunn, 2006). The changes in protein profile of mice heart due to acute and chronic viral myocarditis were characterized in A.BY/SnJ mice using 2D-DIGE. A total of 136 distinct proteins were identified to show disease related changes in their intensity (Hammer et al., 2010). Using 2-DE cardiac antigens that react with autoantibodies in dilated cardiomyopathy and myocarditis have been identified in human as well as animal models. Cardiac autoantigens myosin light chain 1, myosin heavy chain muscle α isoform, tropomyosin, α -cardiac actin, heat shock protein 60, mitochondrial aconitate hydratase, glyceraldehyde 3-phosphate dehydrogenase and brain glycogen phosphorylase were identified by 2-DE (Latif et al., 1993, Buse et al., 2008). 2-DE was also used to characterize changes in heart failure due to arrhythmogenic right ventricular cardiomyopathy (ARVC). Comparison of hearts from patients suffering from ARVC (n=8) with non-failing hearts by 2-DE allowed identification of proteins like heat shock protein 70 (Hsp70), desmin and α -actin, which showed disease specific changes with significant elevation in Hsp70 (Wei et al., 2009).

Besides disease related changes in the expression of the proteins, 2-DE is also used to identify post-translational modifications (PTM) of the proteins and in particular, phosphorylation. Phosphorylation of proteins on both 1D and 2D gels can be detected by phosphor-specific ProQ staining which can be identified further by mass spectrometry. PTMs influence the activity and functionality of the proteins in eukaryotes and play an important role in maintaining the physiology of the cells in health and in disease. Proteins like myosin regulatory light chain, ventricular isoform and myosin binding protein C3 were identified as phosphorylated in A.BY/SnJ mice in acute and chronic myocarditis induced by Coxsackievirus B3 infection (Hammer et al., 2010). Phosphorylation of myosin binding protein C is essential for regular cardiac function and novel phosphorylation sites on myosin binding protein have been detected by 2-DE in canine and in rat hearts (Yuan et al., 2006).

Though two dimensional electrophoresis has several advantages like reproducibility, detection of isoforms, identification of post-translational modifications and easy quantitation, it also has certain limitations. Proteins with high hydrophobicity, extremely high or low molecular weight, or having strong basic or acidic pH cannot be displayed by

2-D gels. These limitations can be overcome by alternate techniques called gel-free or LC-MS/MS approaches.

LC-MS/MS analysis can be performed in two ways- one in which the proteins are enzymatically digested with proteases into peptides, separated on a reverse-phase liquid chromatography column (RPLC) and identified by mass spectrometry called the bottom-up approach or by analysis of intact protein, especially for smaller molecules by measuring the mass of the molecule first and then its fragments -the top down approach (McDonald & Yates, 2003, Breuker et al., 2008). The bottom –up approach is most popular and is similar to shotgun genome sequencing. Hence it is also termed as shotgun proteomics (Opiteck & Jorgenson, 1997, Walters et al., 2001, Yates, 2004). The limitation in 2-DE to separate proteins with high hydrophobicity is resolved by reverse phase liquid chromatography (RPLC) where proteolytic peptides of the proteins are separated based on their hydrophobicity. RPLC has the advantages of high resolution, reproducibility, efficiency and mobile phase compatibility with electrospray ionization (ESI) (Shen & Smith, 2002).

Quantitation of data is necessary to learn about the changes in the protein concentrations and to understand the influence of such changes at the molecular level when comparing two different physiological conditions or samples. Data generated from shotgun proteomics experiments can be quantified by *stable-isotope labeling* such as stable isotope labels with amino acids in cell culture (SILAC) (Mann, 2006), isotope coded affinity tags (ICAT) (Ross et al., 2004, Gygi et al., 1999), spiking synthetic peptides or artificial proteins derived from detected peptides e.g. QconCAT (Gerber et al., 2003, Beynon et al., 2005). Though labeling strategies provide option for relative or absolute quantitation of the proteins, they are limited in certain aspects such as expensive isotope labels, need of specific software and -much more important- they cannot be applied to all types of samples (Karlie et al., 2010). Thus, samples of humans cannot be subjected to metabolic labeling or SILAC like cell cultures. Alternatively, proteins can also be quantified using *label-free* methods.

Label free methods can be broadly classified into two distinct groups- intensity based measurement and spectral counting (Fig.5). Intensity based quantitation is done by MS signal intensity measurement based on the precursor ion. It uses integrated measurement of any given peptide in LC-MS runs and helps in protein quantitation. In contrast spectral

counting is based on the number of spectra matched to all peptides of a single protein and therefore related to the number of MS/MS events assigned to a protein. Since more abundant peptides are selected for fragmentation, the protein amount in a data dependent mode will therefore be proportional to the number of MS/MS spectra (Liu et al., 2004). Since its inception, spectral counting has undergone several changes to overcome its shortcomings such as variability and bias towards peptides with different physicochemical properties, considering the protein length since longer proteins generate more peptides and has also been used with other quantitation techniques as selected reaction monitoring (SRM) and LCMS^E method (Lu et al., 2007, Pavelka et al., 2008, Mailstrom et al., 2009).

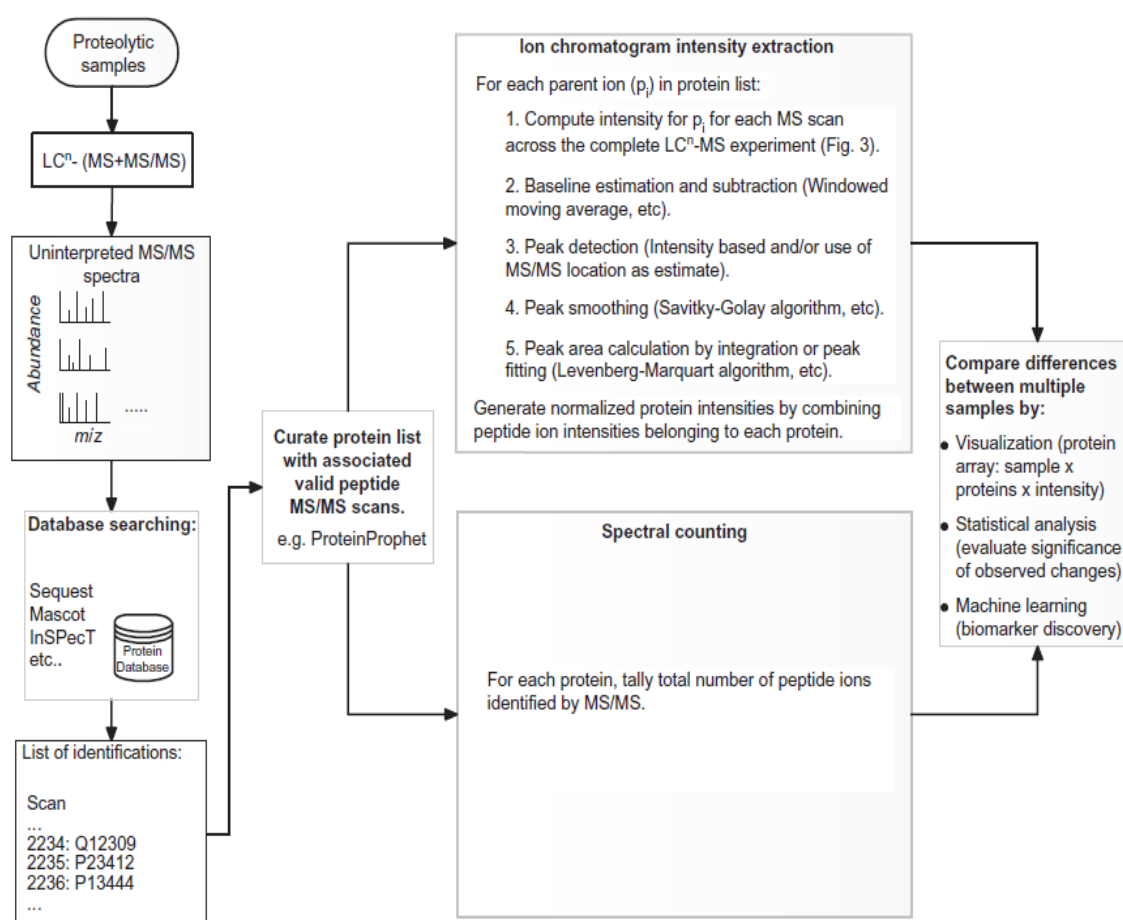


Fig. 5. Schematic representation of label-free quantitative proteomics by LC-MS/MS method. (Wong et al., 2007)

Shotgun proteomics has been successfully applied to identify and characterize DCM related changes in mice models and in human biopsies. 6190 proteins were identified of which 593 showed DCM specific changes in a phospholamban mutant mouse model (Gramolini et al., 2007). Recently, comparison of endomyocardial biopsies of 10 patients

with idiopathic dilated cardiomyopathy (iDCM) with 7 controls with normal left ventricular function by label-free approach resulted in 485 proteins identified among which 174 proteins belonging to cytoskeleton, mitochondrion and metabolic pathways showed iDCM specific changes (Hammer et al., 2011). Also PTMs in cardiac myosin binding protein C have been deciphered using top-down approach (Ge et al., 2008).

Proteomics has evolved significantly in the past decade. The advent of new methods and technologies has helped in reducing the complexity of the proteome and provided better coverage which ultimately leads to a better understanding of the molecular events inside the cell. Using complementary methods of gel-based and gel-free/LC-MS/MS, a comprehensive picture of the proteomic profile of cells, a tissue or organ can be obtained.

Aim of the study

Viral myocarditis and dilated cardiomyopathy were best studied in mice since murine models of myocarditis mimic human myocarditis. The susceptibility of mice to the disease varies as certain strains of mice are resistant while others are susceptible to disease due to the genetic variability among the strains. A.BY strain mice are one such breed which is susceptible to viral myocarditis by Coxsackievirus infection and further develops dilated cardiomyopathy leading to heart failure. The aim of the current study was to identify and characterize the changes in the proteome pattern of dilated A.BY/SnJ mice hearts infected with coxsackievirus B3 at 84 days p.i. by comparing with age-matched non-infected hearts using complementary techniques of 2D-DIGE and LC-MS/MS analysis. Since mice also age during the period of development of the disease, age dependent changes in the total proteome of 4 month A.BY/ SnJ mice hearts were also characterized in comparison to young 1 month hearts.

On the other hand, DCM is also associated with mitochondrial dysfunction. Overexpression of ADP/ATP translocase 1 (ANT1) in transgenic rats is reported to have a protective effect against heart failure. Therefore, in this study, the question was addressed if ANT1 overexpression (ANT-OE) triggers alterations in the protein profile of the heart and if so, what are the pathways that are affected. Furthermore, the impact of ANT1 overexpression on the protein profile in rat hearts infected with CVB3 was investigated using gel free LC-MS/MS

Another aspect of DCM is autoimmunity. Active immunization of rat hearts with peptides against Fc gamma receptor (Fc γ) has been reported to elucidate a response similar to autoimmune dilated cardiomyopathy. Hence using proteomics, the changes in the proteome of rat hearts due to active immunization with certain peptides against Fc γ IIa receptor were characterized.

2. Materials & Methods

2.1 Materials

2.1.1. Chemicals

Name	Source
Acetic acid	Roth
Acetonitrile	J.T Baker
Acrylamide 40%, (37.5:1)	AppliChem
Agarose 0.5%	Invitrogen
Ammonium Bicarbonate	Sigma
Ammonium sulfate	Sigma
Ammoniumpersulfate (APS) 10%	PlusOne
Bradford reagent	BioRad
Bromophenol Blue	Sigma
CHAPS	AppliChem
Collagen a 1Type VI: rabbit polyclonal antibody (H-200)	Santa Cruz Biotechnology
Coomassie brilliant blue G-250	Merck
Cy2, Cy3,Cy5 dyes for DIGE	GE Healthcare
Dithiothreitol (DTT)	PlusOne
Ethanol	Roth
Formaldehyde	Roth
Formic acid	Merck
Glyceraldehyde-3-phosphatedehydrogenase, rabbit monoclonal antibody (14C10)	Cell Signalling
Glycerol 87%	PlusOne
Glycin	Roth
Goat Anti Rabbit IgG (H+L) Peroxidase conjug.	Jackson Immunoresearch
Heat Shock Protein 70	Cell Signalling
Heterogeneous ribonucleoprotein K	Bethyl Laboratories
Hydrochloric acid	Roth
Iodoacetamide	Sigma

Name	Source
Isopropanol	Merck
Immobiline dry strip cover fluid	PlusOne
Lumican polyclonal AB Mouse- Anti Human	Abcam
Lysozyme C	Sigma
Methanol	Roth
Milk powder	Roth
Phosphoric acid 85%	Roth
Pelican Ink 4001	Pelikan
Pharmalyte 3-10	Amersham
Potassium ferrocyanide	Sigma
ProQ Diamond Phosphoprotein gel kit	Invitrogen
PVDF membrane	Millipore
Rho GDP dissociation inhibitor 2	Novus Biologicals
Silver nitrate	AppliChem
Sodium carbonate	Merck
Sodium chloride	Roth
Sodium dodecyl Sulfate(SDS) 20%	Roth
Sodium thiosulfate penta hydrate	Merck
β-Mercaptoethanol	Sigma
Super- Signal West Femto Maximum Sensitivity Substrate	Thermoscientific
Sypro Ruby	BioRad
TEMED	PlusOne
Thiourea	Sigma
Tris	Sigma
Trypsin	Sigma
Tween-20	Sigma
Urea	Merck

2.1.2. Instruments

Name	Source
BioRad-protein plus Dodeca Cell	BioRad
Epson Expression 1680 pro scanner	Epson
Heareus Fresco17 Centrifuge	Thermo Scientific
LTQ-Orbitrap Velos	Thermo Electron
LTQ-Orbitrap XL	Thermo Electron
Lumi Imager	Roche
Mikro dismembrator	Braun
Milli Blot™ Graphite Electroblotter II	Millipore
Multiphor II	GE Healthcare
Sonicator	Bandelin Sonoplus
Typhoon 9400 Scanner	GE Healthcare
Ultrasonification bath	Bandelin Sonorex
Ultrospec 2100 pro Spectrophotometer	Amersham Biosciences

2.1.3. Softwares

Name	Source
Bioworks 3.2	Thermo Scientific
Delta 2D	Decodon
Elucidator	Rosetta
Image Quant 5.2	Molecular Dynamics
Scaffold 2.6	Proteome Software

2.2. Methods

2.2.1. Biological samples

2.2.1.1. Cultivation of HL-1 cells

As cell culture model for testing of proteomic quantitation methods the permanent murine heart cell line HL-1 was used. Cells were cultivated in the presence of norepinephrine, growth factors and a specific foetal bovine serum (F2442, Sigma, Taufkirchen, Germany) on gelatin-fibronectin coated plates (Claycomb et al., 1998).

2.2.1.2. Animal models of CVB3 induced dilated cardiomyopathy

For all mice experiments A.BY/SnJ mice (H-2^b) were used. Animals were hosted, infected and sacrificed at Department of Molecular Pathology, University Hospital Tübingen, Germany.

Four to five week old mice (n=4) were infected intraperitoneally with 5×10^4 plaque-forming units (PFU) of purified CVB3 derived from the infectious cDNA copy of the cardiotropic Nancy strain as previously described (Klingel et al., 1992). A.BY/SnJ mice (H-2^b) susceptible for ongoing myocarditis following CVB3 infection were kept under specific pathogen-free conditions at the animal facilities of the Department of Molecular Pathology, University Hospital Tübingen and experiments were conducted according to the German animal protection law. Two males and two females were considered for each of the conditions. At 84 days p.i., mice were sacrificed and hearts were collected for analysis. Non-infected age matched mice were considered as controls. For proteomic analysis, parts of the hearts were snap frozen in liquid nitrogen. For histology, part of the hearts were fixed in 4% phosphate-buffered paraformaldehyde (pH 7.2) and embedded in paraffin.

2.2.1.3. ANT 1 overexpression in rats

The animal model with cardiac overexpression of ANT1 (TGRMHCrANT1 [ANT]) in rats was generated in the group of A. Dörner at Charité, Berlin using the rat α -myosin heavy chain promoter as first described in Walther et al. (2007). Hearts of male WT and ANT1-TG rats were quickly excised and immersed in an ice-cold solution containing 130 mmol/L NaCl, and 30 mmol/L KCl. Left ventricular (LV) tissue samples were shock-frozen in liquid nitrogen and stored at -80 °C until analysis (Vogelpohl et al., 2011).

2.2.1.4. Immunization of rats with Fc gamma (Fc γ) receptors peptides

Rat models of autoimmune cardiomyopathy were generated in the lab of Dr. Lars Herda at the Department of Cardiology, University medicine Greifswald. Four to six week old male lewis rats (n=4), were injected with 1 mg of CD-32 peptide emulsion containing peptides CEPPWIQVLKEDTVTL (peptide 1) and CRCRMEETGISEPI (peptide 2) bound to glutathione-S-transferase (GST) every 4 weeks over a period of 5 months. Animals injected with adjuvants (KLH) bound to GST were considered as controls.

2.2.2. Histology

Paraffin-embedded hearts were cut into 5-mm-thick tissue sections and stained with hematoxylin/eosin (H&E) and picosirius red to evaluate the extent of myocardial injury at 84 days p.i. in comparison to non-infected animals. For the detection of CVB3 positive-strand genomic RNA in hearts we performed in situ hybridization experiments using single-stranded ³⁵S-labeled RNA probes, which were synthesized from the dual-promoter plasmid pCVB3-R1 as previously described. Slide preparations were subjected to autoradiography, exposed for 3 weeks at 41°C, and counterstained with H&E (Klingel et al., 1992).

2.2.3. Preparation of whole heart protein extracts

Heart tissues snap frozen in liquid nitrogen were powdered in a Mikro dismembrator at 2600 rpm for 2 min in 150 μ l of rehydration buffer containing urea 8M, thiourea 2M, and CHAPS 2%. The powdered tissue was reconstituted in about 1.5-2.0 ml of rehydration buffer and was sonicated on ice three times each for 5 sec with nine cycles at 80% energy. The extract was then centrifuged at 14000 rpm for 1h at 4°C to separate the cell debris. The supernatant was collected in separate vials and the protein concentration was estimated using Bradford assay kit (BioRad). The protein samples after estimation were stored at -80°C.

2.2.4. Protein Quantitation by Bradford assay

For Bradford assay, a series of known concentrations of bovine serum albumin (BSA)-standard solution were made for preparation of a standard curve as described in the following table (Table 3).

Table 3. BSA concentrations used for standard curve

Amount (μg)	0	1	2	4	6	8	10	12
0.1 μg/μl BSA (μl)	0	10	20	40	60	80	100	120
Water (μl)	800	790	780	760	740	720	700	680

To each of the above solutions 200 μl of Bradford reagent was added and the mixture was incubated at room temperature for 5 min. The BSA standard curve was prepared by measuring the absorbance at 595 nm in a UV spectrophotometer. The protein samples were diluted 10 fold with rehydration buffer and 10 μl of the diluted sample was used for estimation of the concentration. Three replicates of each sample were analyzed and the mean absorbance value was used for calculating the concentration of the sample by plotting on the standard curve.

2.2.5. CyDye labeling and Differential In-gel Electrophoresis (DIGE)

Prior to DIGE samples were labeled with fluorescent dyes. The CyDye solutions were prepared by reconstitution of the powder in high quality dimethylformamide (DMF). The CyDye powder stored at -20°C was allowed to thaw at room temperature for 5 min before a specified volume of DMF was added to give a stock solution of 1 mM. The mixture was vortexed vigorously for 30 sec and then centrifuged for 30 sec at 13000 rpm. Afterwards, the CyDye stock solution could be used or stored in the dark at -20°C. It has to be noted that the DMF must be anhydrous and fresh (3 months shelf life once opened) since degradation products of DMF such as amines compete with the proteins for dye during labeling and might cause degradation of the dye. Since CyDyes Cy2, Cy3 and Cy5 are fluorescent dyes, all following reactions were performed in the dark. The CyDye working solution was prepared by adding one volume of CyDye stock solution to 1.5 volumes of DMF to make 400 pmol CyDye solution which could then be used for labeling.

100 μg of each protein sample was adjusted to a pH of 8.5 with 50 mM NaOH using pH indicator strips and the protein concentrations were recalculated. 50 μg of the protein sample from individual mice were minimally labeled with 400 pmol of either Cy3 or Cy5 dye. 50 μg of protein from all animals was pooled and labeled with 400 pmol of Cy2 to be used as an internal standard. The reaction was carried out on ice for 30 min and the labeling was stopped by adding 10 mM lysine equal to the volume of dye used. The

reaction mixture was kept on ice in the dark for 15 min. At this stage the samples were considered ready for separation by 2-DE. The samples could also be stored at -80°C for a period of three months in dark.

Due to fluorescent nature of the CyDyes, care was taken to reduce the exposure of gels to light during separation.

2.2.6. Two dimensional gel electrophoresis

2.2.6.1. Rehydration of IPG Strips

For separation of the proteins in the first dimension, the IPG strips were rehydrated to their original thickness of 0.5 mm by incubating them in a mixture of the sample solution with the rehydration buffer (Table 4) prepared at 20°C in a thermomixer for 30 min. The reswelling trays were properly cleaned and levelled before loading the samples on the IPG strips. The appropriate volume of the sample with rehydration buffer was carefully spread to avoid air bubbles along the wall of the slot to an approximate length of the IPG strip. The dry strip cover was removed using forceps and the strip was laid carefully with the gel side of the strip facing the sample mixture. The ends of the strip were slightly lifted and lowered to remove any air bubbles. The sample evaporation and crystallization of urea were prevented by adding a layer of Immobiline dry strip cover fluid. Rehydration was performed at 20°C for 24 h. High or low temperature (> 37°C or < 10°C) should be avoided to minimize the carbamidomethylation of proteins or crystallization of urea.

Table 4. Rehydration of Immobiline dry strips pH 4-7

Components	Final Concentration
Urea	8 M
Thiourea	2 M
CHAPS	2%
Pharmalyte 3-10	2%
DTT	0.03M
Bromophenol Blue	Trace amount

2.2.6.2. Iso-Electric Focusing (IEF)/First dimensional separation of proteins

After rehydration, the gel strips after rehydration were dried off the cover strip fluid by blotting the strips carefully on moderately moist Whatman paper since excess water might cause streaking during first dimension. Prior to IEF, the focusing trays were cleaned with ethanol and blot dried. Whatman paper strips moistened with water were placed transversely at either end of the strips for better conductance. Additionally, a strip moistened with 15 mM DTT was placed at the cathode end. The IEF was carried out in GE Multiphor IEF apparatus at 20°C under the conditions specified in Table 5.

Table 5. Voltage-time gradient for separation of proteins on 24cm IPG strip pH4-7

	Voltage (V, mA, Watts)			Volt-hours (Vh)	Time (in hrs)
Step 1	500V	2mA	5W	1	0:01
Step 2	3500V	2mA	5W	3000	1:30
Step 3	3500V	2mA	5W	57000	16:20
Total				60000	17:50

2.2.6.3. Equilibration of IPG strips

Prior to second dimension separation of the proteins by SDS-PAGE, the IPG strips were equilibrated in the equilibration buffer (Table 6) for reduction and alkylation of the proteins.

Table 6. Composition of equilibration buffer

Components	Final concentration
Urea	6 M
1.5 M Tris-HCl pH 8.8	0.375 M
Glycerol 87%	20%
SDS 20%	4%

The proteins separated by IEF were reduced and alkylated before second dimension. For this purpose equilibration solutions were prepared by adding fresh solutions of 1% DTT and 2.5% IAA to equilibration buffer (Table 6), respectively. The strips were first incubated in reduction solution containing DTT for 15 min with gentle agitation, followed by a second incubation in alkylating solution with IAA for another 15 min.

2.2.6.4. Second dimension separation of proteins

After equilibration the IPG strips were carefully placed on SDS-polyacrylamide gels casted between low fluorescent glass plates. The strips were placed with the acidic end to the left side of the gel. 0.5% agarose prepared in running buffer (Table 8) was melted and laid on top of the IPG strip as a sealant.

Second dimension separation was carried out on 12.5% SDS-polyacrylamide gels (SDS-PAGE) according to Laemmli (Laemmli, 1970). Polyacrylamide gels were prepared with or without 5% stacking gel layer. The composition of gels and running buffers is given in tables below (Table 7 & Table 8).

Table 7. Composition of 12.5% SDS-polyacrylamide gel

Components	Resolving gel	Stacking gel
Acrylamide/Bis acrylamide	12.50%	5%
Tris-HCl pH 8.8	0.375 M	-
Tris-HCl pH 6.8	-	0.125 M
SDS	0.10%	0.10%
APS	0.05%	0.05%
TEMED	0.03%	0.07%

Table 8. Composition of SDS electrophoresis gel-running buffer

Components	Final concentration
Glycin	0.30%
Tris	1.44%
SDS	0.10%

2.2.6.5. Visualization of proteins on DIGE gels

In order to prevent drying and shrinkage of gels, the DIGE gels were scanned without removing from the glass plates using Typhoon 9400 scanner. The appropriate voltage of photomultiplier tubes was set for the three channels (Cy2, Cy3 and Cy5) by initially scanning the gels under low resolution 1000µm pixel size to ensure the spot intensity is not

above 100,000. The gels were scanned at high resolution of 100 μm pixel size with three different excitation wavelengths as described below (Table 9).

Table 9. Different excitation wavelengths for Cy2, Cy3 and Cy5 channels in DIGE Scans

Channel	Filter	Laser	Sensitivity	PMT
Cy2	520BP40	Blue (488 nm)	Normal	535
Cy3	580BP30	Green (532 nm)	Normal	520
Cy5	670BP30	Red (633 nm)	Normal	495

After scanning, the gels were stained with Coomassie brilliant blue for visualizing the spots.

2.2.6.6. Different methods of protein staining

2.2.6.6.1. Colloidal Coomassie staining

The procedure for colloidal coomassie staining was as follows:

1. The gels were initially placed for 1-2 h in a fixative containing 40% ethanol and 10% acetic acid with gentle shaking. This removed the SDS and fixed the proteins in the gel.
2. The gels were then washed twice for 10 min each with distilled water.
3. After washing, the gels were placed in the staining solution (Table 10) and left over night at room temperature with gentle shaking.
4. The gels were destained twice with 20% methanol for 15min each until the gel was transparent and devoid of any background.

Table 10. Composition of Colloidal Coomassie staining solution

Components	Final concentration
Coomassie brilliant blue G-250	0.08%
Ammonium sulfate	8%
Ortho-phosphoric acid	1.60%
Methanol (to be freshly added)	20%

2.2.6.6.2. Staining of the gels with silver nitrate

The following solutions were used for visualizing the proteins by staining with silver nitrate:

- Fixing solution: 50% ethanol, 12% acetic acid and 0.05% formaldehyde
- Washing solution: 50% ethanol
- Sensitizing solution: 0.02% $\text{Na}_2\text{S}_2\text{O}_3$, 5 x H_2O
- Silver staining solution: 0.2% AgNO_3 and 0.075% formaldehyde
- Developing solution: 6% Na_2CO_3 , 0.0004% $\text{Na}_2\text{S}_2\text{O}_3$ 5 x H_2O and 0.05% formaldehyde
- Stopping solution: 1% glycine

After second dimension the gels were placed in fixing solution with gentle agitation for 30 min. The gels were then washed with 50% ethanol twice, each for 20 min. Prior to staining, the gels were sensitized with 0.02% sodium thiosulfate for 1min and were washed thrice with distilled water for 20 sec each. The gels were then incubated in silver staining solution in the dark with gentle shaking. After 30 min, the staining solution was removed and the gels were washed twice for 20 min with distilled water to remove any remaining stain. In order to visualize the protein spots, the gels were developed in the developing solution for a period of 1-3 min. After achieving optimal intensity of protein signals on the gel, the process was quickly stopped by adding 1% glycine as stopping solution and incubating for 10-30 min. The gels were then washed with distilled water for 30 min with gentle shaking. At the end, the gels were scanned using an Epson Expression 1680 Pro Scanner at 254 dpi resolution in positive mode, 48 bit colour scale.

2.2.7. Spot detection, quantification and protein identification

2.2.7.1. Statistical analysis of 2-DE data

After scanning the gels by Typhoon scanner, the images were analyzed with Delta-2D software version 3.4 (Decodon, Greifswald, Germany). The protein spots showing disease related and age related changes were identified by initially matching all internal standard (Cy2) images applying the exact warp mode. This was followed by merging all the gel

images in the project to generate a fusion image using Union fusion function of the software. Spots on the fusion image were automatically detected and were manually validated by comparison of the fused image with the original image. The spot map (spot boundaries of detected spots) created by the software were transferred to all gel images to ensure uniform analysis. Spot volumes were calculated based on the area and pixel intensities of spots. The relative spot intensities of the individual animals at different time points were analyzed by Genespring software package (version 7.3.1, Agilent Technologies, Waldbronn, Germany) to identify infection dependent and age-dependent changes. Firstly, interchannel and intergel differences (Cy3, Cy5 and Cy2) in the intensities were corrected by dividing the background corrected values of the spot volumes by the median of all spots of the channel (Cy2, Cy3 or Cy5). The fluorescence intensities of each spot were then calibrated with the internal standard (Cy2) by dividing the median normalized spot volumes of the Cy3- and Cy5-channels by their corresponding spot value of the Cy2 channel. Later the spot intensities for each comparison (infected vs. non-infected and aging time points) were normalized with their respective control time points. Statistically significant differences among the comparisons were derived by applying stringent filters of as follows: (i) the change in the intensity ratio between the particular time point and non-infected control group had to exceed a factor of 1.5; (ii) the p-value of the corresponding Welch t-test had to be lower than 0.05. The spots showing significant changes were picked up for identification by mass spectrometry.

2.2.7.2. In-gel digestion and analysis by liquid chromatography – electrospray tandem mass spectrometry

For identification of the spots displaying significant changes, three preparative gels were run each with 300 µg of the pooled samples and the protein spots were visualized by staining with silver nitrate as described earlier (section 2.2.6.2). The spots were manually excised from the preparative gels and collected in individual tubes. The spots were then destained with 30 mM potassium hexacyanoferrate and 100 mM sodium thiosulfate thrice, each for 10 min until colourless. After destaining, the spots were washed in 200 mM ammonium bicarbonate in 50% acetonitrile for 15 min. The gel pieces were then dehydrated in 100% acetonitrile for 15 min, which removes the water from the gel and renders the gel spot dry to absorb trypsin. The gel spots were then soaked with trypsin (Promega, Madison, WI, USA) and subjected to proteolysis overnight (16 h) at 37°C. The peptides were extracted from the gel piece by ultrasonication first in 0.1% acetic acid and

afterwards in 0.05% acetic acid in 50% acetonitrile, each for 30 min at 30°C. The peptide aliquots were concentrated to a volume of 2 µl and mixed with 7 µl of 0.1% acetic acid and 2% acetonitrile for MS analysis.

The tryptic peptides were separated on an Acclaim PepMap 100 reverse phase column (3 µm, 75 µm i.d. x 150mm, LC Packings, Dionex, Idstein, Germany) with a nano-HPLC (EASY-nLC, Proxeon Biosystems A/S, Odense, Denmark) coupled with a LTQ-Orbitrap-XL mass spectrometer (Thermo Electron, Bremen, Germany) using a 35 min linear gradient ranging from 5-60% ACN in 0.1% acetic acid (0 min -5%B -3 min-5% -23 min-35% -28 min-60% -30 min-100% -32 min-100% -35 min-0%) at a constant flow rate of 0.3 µL/min.

2.2.7.3. Protein identification

A SEQUEST (Bioworks 3.2 / SEQUEST 2.7, Thermo Electron) search was done for the resultant MS/MS spectra against Swissprot mouse database release 57.1 with a mass tolerance of 10ppm and fragment ion tolerance of 0.8Da for the peptide identifications. The search was performed considering oxidation of methionine and carbamidomethylation of cysteine as variable and static aminoacid modifications.

Proteins were identified by at least two peptides passing the following filter criteria: charge dependent Xcorrelation score for two-fold charged peptides >2.2; three and four-fold charged peptides >3.70, RSp value =4; ion percent >60%.

2.2.8. Gel-Free liquid chromatography- mass spectrometric analysis

2.2.8.1. In-solution digestion of proteins

2 µg of protein of each of the samples were initially reduced to break the disulfide bonds. 25 mM DTT prepared in 20 mM ammonium bicarbonate was added to the samples (final concentration 2.5 mM) and the mixtures were incubated at 60°C for 1h. Following reduction, the protein samples were carbamidomethylated with 100 mM iodoacetamide in 20 mM ammonium bicarbonate (final concentration 10 mM) and incubated at 37°C in the dark. After 30min, the protein samples were subjected to proteolysis using a combination of LysC and trypsin to ensure efficient digestion and elimination of missed cleavages. Initially LysC (Sigma-Aldrich Chemie GmbH, Munich, Germany) was added to the samples in the ratio of 1:100 (enzyme:protein) and were incubated for 3 h followed by

overnight (16 h) proteolysis with trypsin in a ratio of 1:10. 1% acetic acid was added to stop digestion of the samples. The samples were then purified to remove the impurities that might interfere with MS analysis.

2.2.8.2. Purification of the peptide extracts prior to mass spectrometry

The samples were purified using C-18 resin tips with binding capacity of 2 µg (OMIX, Varian, Pittcon, U.S.A.). Purification of the samples involved the following steps:

1. The C18 tips were initially equilibrated by aspirating three times 10 µl of 100% acetonitrile followed by aspiration 10 µl of 80%, 50% and 30% acetonitrile in 1% acetic acid, 5times each.
2. This was followed by slowly aspirating the tip three times with 10 µl of 1% acetic acid.
3. The peptides were bound to the matrix by aspirating the sample slowly ten times. Care was taken to avoid the formation of air bubbles while aspiration as it might interfere with the binding of peptides to the resin.
4. After binding the peptides to C-18 resin the tip was washed 5 times with 10 µl of 1% acetic acid.
5. The bound peptides were eluted with 50% and 80% acetonitrile, 5 µl each.

The samples were then concentrated to a volume of 2 µl and mixed with 2% acetonitrile in 0.1% acetic acid before MS analysis.

2.2.8.3. Mass spectrometric analysis

The purified peptides were separated on an Acclaim PepMap 100 reverse phase column with an EASY-nLC (Proxeon Biosystems) using a 300 min non-linear gradient ranging from 0-100% ACN in 0.1% acetic acid (0 min-0%B -15 min-0% -27 min 5-30% -290 min -60%-291min-100% -295 min-100% -300 min-0%) at a constant flow rate of 0.3 µL/min.

The separated peptides were monitored with a LTQ-Orbitrap-XL mass spectrometer (Thermo Electron, Bremen, Germany). The MS was operated in data dependent mode to automatically switch between Orbitrap-MS and LTQ MS/MS acquisition. Survey full scan MS (from m/z 300 to 2000) were acquired in the Orbitrap with resolution R=60,000 at m/z 400 at a target value of 1,000,000 ions. For MS/MS sequential isolation and fragmentation of the five most intense ions, in the linear ion trap, collision induced dissociation at a

target value of 10,000 ions was performed. Target ions already selected for MS/MS were dynamically excluded for 30sec. Following parameters were used: electrospray voltage, 2 kV; no sheath and auxiliary gas flow; MS/MS parameters: ion selection threshold: 1000 counts, activation Q-value: 0.25, activation time: 30 ms.

2.2.8.4. Protein identification and quantitation by spectral counting

Proteins were identified via automated SORCERER/SEQUEST search (Sorcerer built 4.04, Sage-N Research Inc., Milpitas, CA, U.S.A.) against a Swissprot mouse database release 57.1 as described above (2.2.7.3). SORCERER/SEQUEST generated output files were loaded into SCAFFOLD software version 2.6 (Proteome Software, Portland, USA) for analysis by spectral counting. Proteins identified with at least two peptides throughout the whole dataset at a probability of 90 % were included in quantitation by spectral counting method (Old et al., 2005). Before considering the data for spectral counting, the homologous peptides shared among various proteins were omitted from the data to narrow down the quantitation to proteins on basis of unique peptides only. The data from the assigned spectra were normalized across all bioreplicates and categories using a normalization factor. The normalization factor was calculated by the following method:

1. The total number of spectra per each animal was calculated by summing up the spectra of all proteins identified.
2. The average of the summed spectra of all individual animals was calculated.
3. The normalization factor for each biosample was calculated by dividing individual summed spectra by the average value across all biosamples (point 2).

$$\text{Normalization factor} = \frac{\text{Sum of spectra for each bioreplicate}}{\text{Average of total spectra across all bioreplicates}}$$

4. Normalization was carried out by dividing individual protein values by the normalization factor calculated for the respective biosample.

After normalization, proteins with \geq six assigned spectra per condition were considered for analysis and Students t-test was applied for statistical evaluation. The proteins were then filtered for p -value ≤ 0.1 and a ratio fold change of > 1.2 since proteins with more than 30 spectra reportedly not display linear increase in the spectral counts with increasing amounts (Old et al., 2005, Cima et al., 2011).

2.2.8.5 Protein quantitation by Rosetta Elucidator

The obtained Raw data were analyzed with the Rosetta Elucidator software version 3.3 (Rosetta Inpharmatics LLC, Seattle, WA) employing the following workflow: (i) feature detection, (ii) feature alignment across all MS runs (adjusting for mean retention times shifts of 0.025 up to 1.2 min), (iii) filtering for features $p < 0.05$, (iv) feature annotation, (v) median normalization by a feature set containing search results and therefore discriminating features arising from single-charged contaminants, (vi) combination of signal intensities of technical replicates, (vii) filtering for unique peptides, (viii) statistical analyses by a two sided, two-sample t test ($p < 0.05$), and (ix) application of a fold change of 1.2. Steps (iii) to (viii) were carried out with an inhouse- created visual script (Hammer et al., 2011).

2.3. Phosphoprotein analysis

2.3.1. Visualizing of phosphorylated proteins using ProQ staining

Phosphoproteins were detected by staining the gels using a ProQ Diamond phosphoprotein gel stain kit. ProQ Diamond dye is a fluorescent phosphosensor that binds directly to the phosphate moiety of phosphoproteins with high sensitivity.

1. After the second dimension separation of proteins, the gels were fixed with a solution of 50% ethanol and 12% acetic acid with gentle shaking.
2. The gels were then either washed four times with distilled water for 15 min each or left in distilled water over night with gentle shaking
3. The staining was performed with ProQ Diamond phosphoprotein gel stain kit for 2 h in the dark.
4. The gels were then destained for 2 h with a solution of 20% propylene glycol and 50 mM sodium acetate, pH 4.0, by changing the solution every 30 min.
5. After destaining, the gels were washed with distilled water twice, each for 10 min and the images were scanned using Typhoon 9400 scanner with laser excitation source at 532 nm using a PMT voltage of 630V.
6. The gels were later stained with SYPRO Ruby dye overnight with gentle agitation to visualize the total protein pattern on the gel.

7. Destaining of the gels was done by rinsing the gels in 10% ethanol and 7% acetic acid twice for a total of 1 h.
8. After destaining, the gels were washed with distilled water twice for 10 min each and were later scanned using Typhoon 9400 scanner.
9. For cutting of spots prior to protein identification by mass spectrometry, the gels were stained with Coomassie brilliant blue (see 2.2.6.1.).

2.3.2. Identification of phosphorylated proteins

To identify the phosphorylated proteins, preparative gels were made from the pooled samples of 84d infected and 84d non-infected mice hearts and the spots were visualised by Coomassie staining. The spots phosphorylated according to ProQ stain were cut from the Coomassie stained gels. The spots were analyzed by mass spectrometry using LTQ Orbitrap Velos with a run time of 35 min using data dependent neutral loss method. The neutral loss masses were defined as 32.66, 49.00, 65.33, 98.00 and 147.00 m/z representing the loss of single or multiple PO_4 groups from the precursor ion at different charge states. The MS parameters were as follows: survey scan: 300-1700m/z. The most intense ion from the survey scan was considered for MS/MS as follows: activation type: CID, isolation width: 2.0, activation Q: 0.25, activation time: 20ms. For MS3, most intense neutral loss from MS/MS was considered. MS3 was performed with multistage activation. A Sequest search for serine, threonine and tyrosine phosphorylation was performed on the raw files against Swissprot mouse forward reverse database rel 57.1 using Thermo Proteome Discoverer 1.3. The peptides for the identified spots were screened by “phosphoRS” of Proteome discoverer 1.3., which calculates the probability of the putative phosphorylation sites in the peptide sequence and gives a confidence value as pRS score (Fig.6).

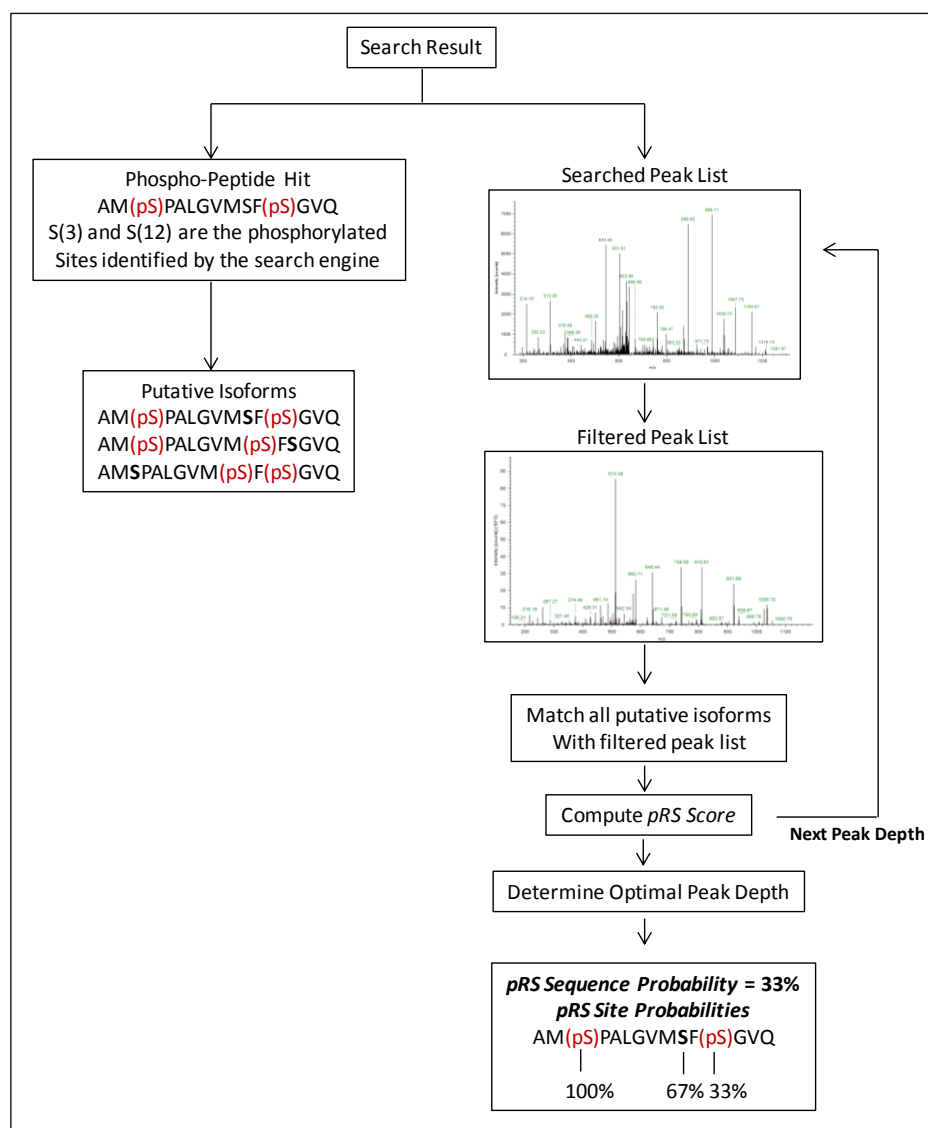


Fig.6 Phosphoprotein identification by Proteome Discoverer. A-represents the workflow for protein identification and phosphor prediction. B- represents the algorithm applied by the software for predicting the phosphosite frequency and probability which determines the phosphopeptide confidence score (pRS).

2.4. Western blot analysis

The proteins were initially separated using 1D SDS-PAGE. 20µg of protein from each of the samples was loaded onto the gel and separated on 12.5% SDS-polyacrylamide gels of 1mm thickness. After 1D gel electrophoresis the proteins were transferred onto PVDF membrane using a semidry transfer apparatus.

Prior to transfer of proteins, the gels were equilibrated in transfer buffer for 5 min. Six sheets of Whatman paper cut to the size equal to that of the gel were soaked with transfer buffer for 5 min. Immobilon-P PVDF membrane also cut to the size of the gel was initially activated in 100% methanol for a few seconds and then placed in transfer buffer for 5 min before use (Table.11).

Table 11. Components of transfer buffer, pH 8.5

Components	Final concentration
Tris	0.02 M
Glycine	0.15 M
Methanol (freshly added before use)	20%

For the transfer of proteins from the gel onto the PVDF membrane, the gel was placed towards the cathode on top of the PVDF membrane. This assembly was sandwiched between three layers of wet Whatman paper on either side in the following manner (Fig.7):

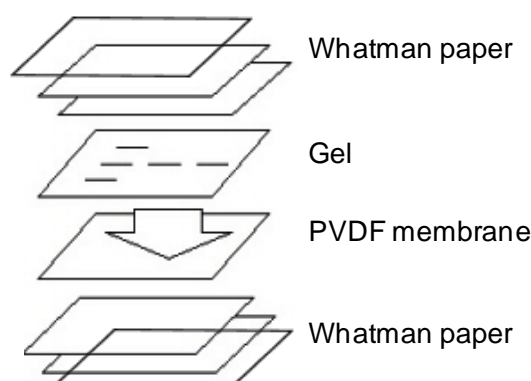


Fig.7 Procedure for Western Blotting. Western blot assembly for transfer of proteins onto the membrane using semidry transfer apparatus (Adopted from Institute for Physiology, EMAU, Greifswald)

Air bubbles formed between the layers during the assembly were carefully removed by using a roller since air bubbles may interfere with the transfer process. For transfer of proteins onto the membrane, 80 mA current was applied for 8cm x 7cm membrane for a period of 2 h. The gel was removed after transfer and stained with colloidal coomassie for evaluation of the efficiency of the transfer. The membrane was also tested for efficient transfer by staining with 0.1% pelican ink in a solution of PBS-T containing 1% acetic acid for 20 min (Table 12). The membrane was destained with PBS-T twice for 10min each and was scanned with Epson Expression 1680 Pro Scanner at 254 dpi resolution in positive mode, 16bit grey scale.

Table 12. Components of PBS-T buffer

Components	Final Concentration
NaCl	138 mM
KCl	2 mM
Na ₂ HPO ₄	10 mM
KH ₂ PO ₄	1.8 mM
pH 7.4 adjusted with HCl	
Tween-20	0.10%

The blot was first washed in TBS-T buffer (Table 13) for at least 5 min. To eliminate non-specific binding of the antibodies which might cause high background, the membrane was initially blocked with 5% non-fat dry milk prepared in TBS-T for 1.5 h at room temperature. The blot was briefly washed with TBS-T and incubated overnight with the primary antibody with 5% milk in TBS-T. The following primary antibodies were used: Collagen alpha 1 type VI: rabbit polyclonal antibody (H-200) directed against the epitope corresponding to 51–250 amino acids near N-terminus (Santa Cruz Biotechnology, Santa Cruz, CA,USA); dilution of 1:500; Lumican: mouse polyclonal antibody directed against full-length human protein (Abcam, Cambridge, UK), dilution of 1:500; Glyceraldehyde-3-phosphatedehydrogenase: rabbit monoclonal antibody (14C10) raised against a synthetic peptide near the carboxy terminus of human cross reacting to mouse epitope (Cell signalling, Boston, MA, USA) was used at a dilution of 1:50000. Following primary antibody incubation, the blot was washed with TBS-T buffer six times, each for 5 min, at room temperature to remove primary antibodies not bound to the protein targets. The

immunoreactive bands were visualized using a secondary antibody conjugated with HRP enzyme (Jackson ImmunoResearch, Suffolk, UK) for 1 h at room temperature with gentle agitation.

Table 13. Components of TBS-T buffer

Components	Final Concentration
Tris	20 mM
NaCl	137 mM
pH 7.6 adjusted with HCl	
Tween-20	0.10%

After six washes with TBS-T buffer, the immunoreactive bands on the membrane were detected by enhanced chemiluminescence using Super- Signal West Femto Maximum Sensitivity Substrate (Thermo Scientific, Rockford, IL, USA), followed by scanning with a Lumi-Imager for an appropriate exposure time.

2.5. Validation of proteins by immunohistological staining

Paraffin tissue sections of 5µm size from mouse hearts were incubated with primary antibodies rabbit polyclonal anti-collagen type VI, rabbit polyclonal anti-collagen type I (Abcam, Cambridge, UK), goat polyclonal anti-lumican (R&D Minneapolis, USA), heterogeneous nuclear ribonucleoprotein K (Bethyl Laboratories, Texas, USA), heat shock protein 70 (Cell Signalling, Germany), Rho GDP dissociation inhibitor 2 (Novus Biologicals, Cambridge, UK) for 1 h at room temperature. The sections were then heated with 10 mM citrate buffer (pH 6.0) for 4 min at 120°C for antigen retrieval. The sections were incubated with biotinylated secondary antibodies (Vector Laboratories, Inc., Burlingame, CA) for 30min at room temperature, and a streptavidin-biotin-immunoperoxidase system (Vectastain Elite StreptABC, Vector Laboratories) followed by 3,3 diaminobenzidine (Dako, Glostrup, Denmark) or HistoGreen (Linaris, Wertheim, Germany) as substrate and were counterstained with hematoxylin. Species-matched IgG was used as negative control and the slides were viewed under Zeiss Axioskop 40 microscope.

2.6. Detection of protein oxidation using Oxyblot technique

Oxyblot analysis was performed using Millipore Oxyblot detection kit (Millipore, MA, USA).

1. The concentration of the protein samples was initially adjusted to a uniform value of 4 $\mu\text{g}/\mu\text{l}$ with 50 mM Tris-HCl, pH 7.5, in order to facilitate considering equal volumes as well as concentration of the samples.
2. 5 μl of each sample corresponding to 20 μg was taken to which 5 μl of 12% SDS was added to make final concentration of 6% SDS.
3. 10 μl of dinitrophenylhydrazine (DNPH) from the kit was added to the above sample solution (1:1) and was incubated for 15 min (not more than 30min) at room temperature.
4. 7.5 μl neutralizing solution from the kit was added to the sample solution (1:0.375). The samples were then separated by 1D SDS-PAGE and western blotting was performed as described above (2.3.)
5. For detection of the oxidized proteins, the immunoblots were incubated for 1 h with rabbit-anti-DNPH primary antibody at a 1:150 dilution in 5% non-fat milk solution. The blot was then washed six times each for 5 min with TBS-T and was afterwards incubated for 1h with goat anti-rabbit HRP secondary antibody at 1:300 dilution with gentle agitation.
6. The immunoreactive bands on the membrane were detected by enhanced chemiluminescence using Super- Signal West Femto Maximum Sensitivity Substrate, followed by scanning with a Lumi-Imager for an appropriate exposure time.

3. Results

3.1. Comparison of protein quantitation methods for data recorded by gel-free LC-MS/MS using HL-1 cells

Accurate quantitation of protein levels is important for the analyses of proteomics data, hence the method most suitable producing the most accurate quantitation has to be chosen. This is no problem for gel-based analysis since DIGE experiments employ by default an internal standard and thus allow very reliable quantitation. However as described earlier, a wide variety of methods for quantitation of the proteins based on gel free LC-MS/MS exist. Among these, quantitation of proteins based on the intensity of the identified peptides is considered one of the reliable methods besides labelling methods. Hence before proceeding with the analyses of the mouse heart samples for CVB3 infection related changes, preliminary experiments for comparative quantitation of proteins based on their intensities and spectral counts were performed using protein extracts from a mouse HL-1 cardiac cell line (Claycomb et al., 1998).

2 µg of protein extract from HL-1 cells was subjected to overnight (16 h) digestion with trypsin in an enzyme to protein ratio of 1:50. After purification using C-18 resin containing tips the resultant peptides were spiked with 50, 100 and 200 femtomol of yeast alcohol dehydrogenase (ADH). This protein can serve as an internal standard for the absolute quantitation of proteins but was used within this experiment for the determination of technical variance of mass spectrometric measurements as well as comparison of quantitation methods. The peptides were monitored with an LTQ-Orbitrap-Velos mass spectrometer and identification was accomplished by searching against Swissprot mouse forward reverse database rel.57.1 extended by the forward reverse sequence of ADH. Raw data were analysed on one hand for peptide intensities using Rosetta Elucidator software. The sum of the intensities of the unique peptides per protein gives protein intensity. On the other hand the data from HL-1 cells were quantified based on their spectral counts obtained from the Sequest search output files by analysing the files in the Scaffold software. Data in Table 14 show that both methods give more reliable data with increasing protein amount in the sample which can be concluded from the decrease in coefficient of variation (CV) calculated from 3 technical replicates. Protein intensity based quantitation seemed to be a bit more robust with lower CV value at 100 fmol spike in than the spectral count method.

Table 14. Comparison of intensity and spectral count based quantitation of HL1 protein extract

Quantitation method	Amount of Yeast Alcohol dehydrogenase					
	50fmol	CV [†]	100fmol	CV	200fmol	CV
Protein intensity [#]	1.51E+07	31.5%	3.95E+07	0.5%	7.86E+07	8.1%
Spectral counts [#]	4	35.3%	5	28.3%	10	14.1%

CV- Coefficient of Variation; # average of values from 3 technical replicates

Absolute quantitation of proteins in a sample can be carried out by the top three method (Silva et al., 2006). Here, an universal signal response factor (USR) is calculated based on the average intensity of the 3 most intense peptides of ADH per 1 femtomol of the standard peptide mixture (Table 15). The USR value is applied to the average intensity of the top 3 intense peptides for the identified proteins which gives the femtomoles of each protein identified in the sample of interest.

Table 15. Quantitation of proteins spiked with ADH standard using the top 3 intense peptide method

Amount of ADH spiked	Amount on column	Top 3 peptides of ADH (50, 100 and 200fmol)	Avg.Intensity	USR (intensity/fmol)
50 fmol	8.82 fmol	SISIVGSYVGNR	3.32E+06	3.77E+05
100 fmol	18.82 fmol	VVGLSTLPEIYEK	6.10E+06	3.36E+05
200 fmol	31.25 fmol	GVIFYESHGK	1.33E+07	4.25E+05

Since the amount of HL-1 protein considered for the analysis was the same (2 µg), the femto moles of each protein calculated based on the USR from 50 fmol, 100 fmol and 200 fmol should be approximately the same and the variation observed provides further information of the technical variance of the measurements. Below are few examples of proteins quantified using the top 3 intense peptide method using the USR value for 50, and 100 fmol as mentioned above (Table 16) that show that technical variance is really low.

Table 16. Examples of proteins identified in similar amounts in the samples spiked with 50 and 100fmol of ADH.

Swissprot Entry name	Protein Annotation	Top 3 intense peptides	Avg. Intensity (50fmol)	CV [†]	Amount (fmol)	Spectral Count (50fmol)	CV ^{††}	Avg. Intensity (100fmol)	Amount (fmol)	Spectral Count (100fmol)	CV [†]	CV ^{††}
1433B	14-3-3 protein beta/alpha	AVTEQGHLSNEER YLILNATQAESK TAFDEAIAELDTLNEESYK	2.36E+06	0.02	6.3	8.0	0.00	2.66E+06	5.0	8.3	0.08	0.07
ADHX	Alcohol dehydrogenase class-3	AAVAWEAGKPLSIEEIEVAPPK VDEFVTGNLSFDQINQAFDLMHSGDSIR VEPGSTCAVFGGLGGVGLAVIMGCK	9.28E+05	0.02	1.8	2.0	0.00	6.07E+05	1.4	7.3	0.09	0.25
1433E	14-3-3 protein epsilon	EAAENSLVAYK AAFDDAIAELDTLSEESYK LICCDILDVLDK	3.49E+06	0.02	9.3	12.0	0.00	3.34E+06	8.0	11.7	0.10	0.00
ALDH2	Aldehyde dehydrogenase	VAEQTPLTALYVANLIK LGPALATGNVVVMK YGLAAAVFTK	2.42E+06	0.02	4.0	7.7	0.08	1.72E+06	3.7	7.7	0.03	0.20
AL1B1	Aldehyde dehydrogenase X	VAEQTPLSALYLASLIK LFINNEWHDAVSK LAPALATGNTTVVMK	1.32E+06	0.04	3.5	5.6	0.10	1.07E+06	3.2	4.6	0.05	0.25

CV[†]-Coefficient of variation from intensities, CV^{††}- Coefficient of variation from spectral counts

With prior information available from the HL-1 cell analysis, it was decided to adopt intensity based quantitation method also for observing the changes in A.BY/SnJ mice hearts dilated due to infection with CVB3 compared to age matched controls. Protein (2 μ g) from mice infected for 84d and non-infected mice hearts was digested using Lys C and trypsin for 16 h and the resulting peptides were measured on an LTQ-Orbitrap XL using a 300min gradient. The .raw files were loaded into Rosetta Elucidator version 3.3 (Rosetta Biosoftware) for intensity based label free quantitation of the proteins. However, a look at the chromatograms revealed that the presence of CHAPS in the extraction buffer resulted in a predominant CHAPS peak in the chromatogram which led to inconsistent retention time shifts making intensity based quantitation of proteins impossible (Fig.8). Therefore, the analysis had to be performed by a method independent of chromatographic alignment i.e. spectral counting. Hence, a SORCERER/Sequest search was performed against Swissprot mouse forward database reverse rel 57.1 and the output files generated were then loaded into SCAFFOLD software version 2.6 (Proteome software, USA) for quantitation of the proteins by spectral counting.

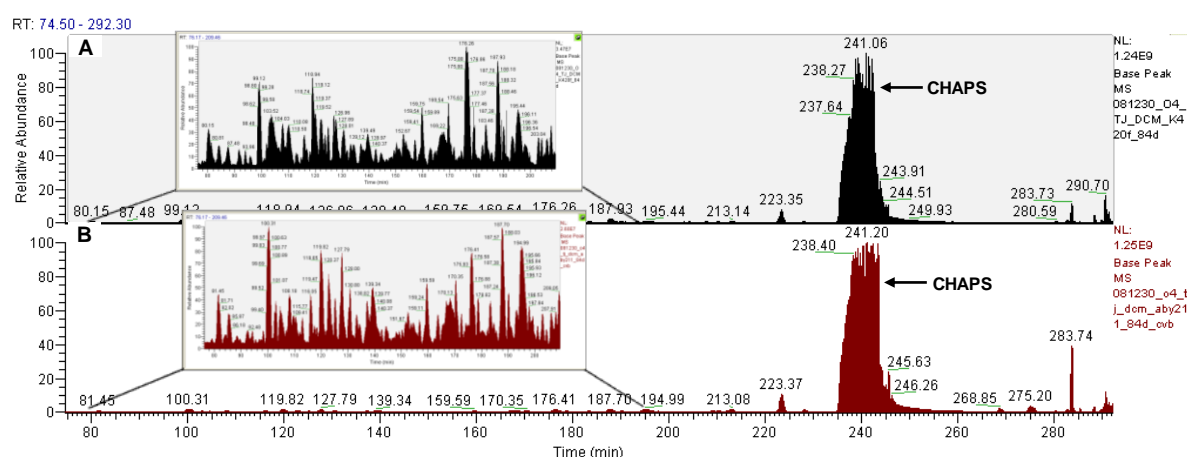


Fig. 8. Presence of CHAPS interferes with intensity based quantitation of proteins. CHAPS present in the extraction buffer resulted in the generation of a predominant CHAPS peak in the chromatogram and hampered quantitation of the proteins based on their intensities. A-The top row shows CHAPS in 84 d non-infected hearts around 240 min in a 300min gradient, B- the bottom row of the figure displays the same in 84 d infected hearts. The inner sections display the magnified sections of the chromatograms between 80 min and 200 min displaying abundance of peptides in the samples.

Since CHAPS showed a strong interference in quantitation of the samples, it was eliminated from further extraction of the protein from samples for animals models of DCM such as adenine nucleotide transporter – over expressing (ANT-OE) rats and for rats immunized against peptides of Fc γ receptor (FcR) which enabled intensity based quantitation of the proteins in these additional projects. The results for the above analyses are described in later sections.

3.2. Analysis of the CVB3 induced DCM animal model

3.2.1. Pathological changes in mouse hearts due to CVB3 induced dilated cardiomyopathy

Coxsackievirus B3 induced dilated cardiomyopathy develops over a period of 90 days in A.BY/SnJ mice. To study the chronic stages of the disease, mouse hearts at 84 d p.i. were compared to age matched non-infected hearts as controls. The pathological changes in the heart over the time course of infection were characterized by immunohistochemical analysis. Thin sections of the tissue (5µm) cut from the mice hearts stained with hematoxylin/eosin (H&E) showed necrosis of the myocytes at 8 d p.i. with numerous inflammatory cells at 28 d p.i. (Hammer et al., 2010). However, at 84 d p.i., the inflammation was replaced by severe fibrosis with dilation of the left ventricle visualised with H&E. The presence of virus during the course of infection monitored by radioactive in situ hybridization with ³⁵S-labeled CVB3-specific probes showed strong viral replication at 8 d p.i.. Though the viral titre decreased during acute and chronic phases of the infection, the virus was not completely eliminated and trace amounts of viral plus-strand RNA were detected in single myocytes at 28 d p.i. (Hammer et al., 2010) and 84 d p.i. consistent with the previous observations of CVB3 persistence in A.BY/SnJ mice (Fig.9).

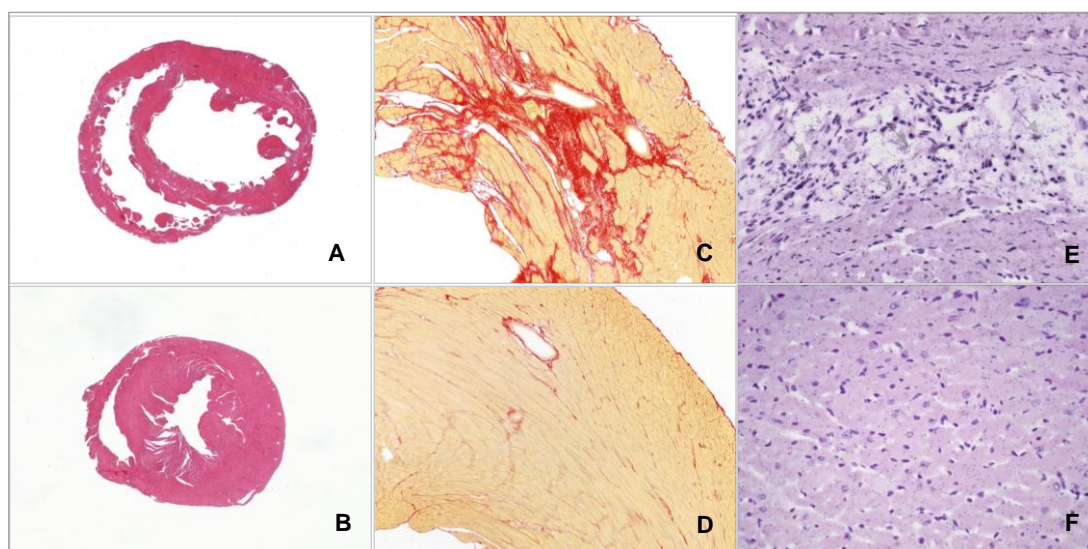


Fig. 9. Pathological changes in A.BY/SnJ mice 84 day p.i. with CVB3. Tissue sections from hearts of CVB3 infected mice obtained at day 84 d p.i. (A, C,) showing dilation (A, hematoxylin/eosin stainings, x12.5) and severe fibrosis (C, picosirius red stainings, x100); hearts of non-infected mice (B, D) are shown for comparison; E-F-Images of radioactive in situ hybridization (x100) illustrate very low levels of persistent virus infection in single myocytes 84 d p.i. (E) compared to control heart (F).

3.2.2. Characterisation of changes in the proteome of hearts infected with CVB3 in A.BY/SnJ mice

3.2.2.1. Quantitation of the infection related changes by DIGE analysis

To study the changes in the proteome profile of mice infected with CVB3, the hearts from mice at 84 d p.i. and age matched non-infected controls (n=4) were labelled with 400 pmol of Cy2, Cy3 and Cy5 dyes for analysis by differential in gel electrophoresis (DIGE) according to manufactures' suggestion (GE Healthcare, Germany). The labelling strategy incorporated a dye swap method wherein each sample from each condition is labelled with Cy3 and Cy5. A pooled internal standard with aliquots of all the samples in the experiment was labelled with Cy2 dye (Fig 10).

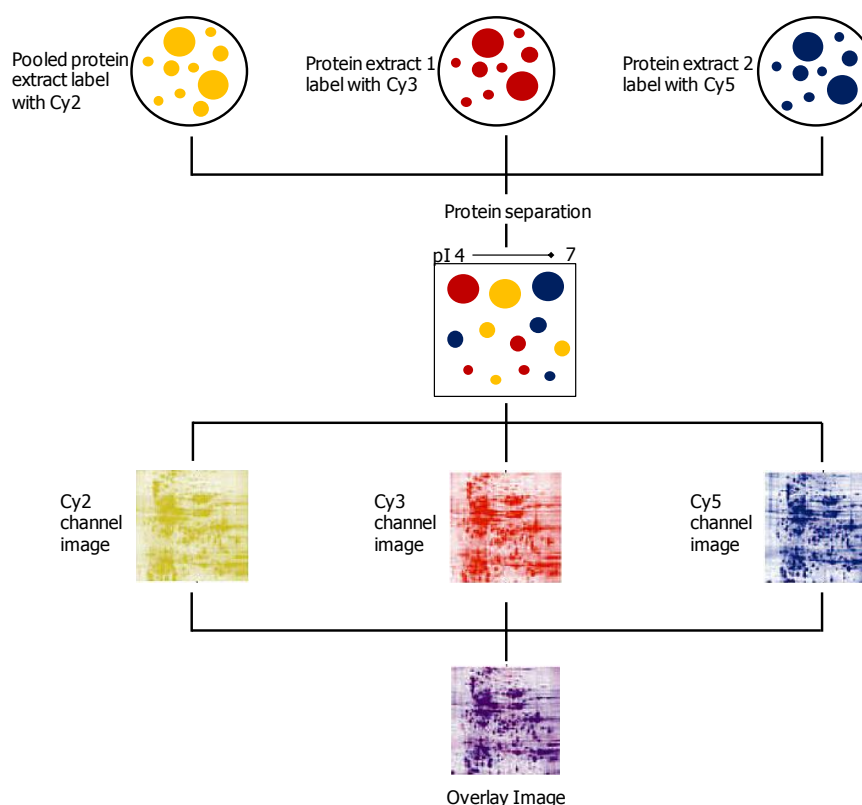


Fig. 10. Schematic representation of DIGE experiment. The samples were labelled using dye swap strategy where each animal in the control group and the group infected for 84 d has been labelled both with Cy3 and Cy5 for comparison. A pooled mixture of protein extracts from all the samples was labelled with Cy2 dye as an internal standard. After 2DE separation the images were scanned with a Typhoon scanner (GE Healthcare) for each channel. Each fluorescent image was loaded in Delta-2D software for quantitative analysis of the differences due to CVB3 infection.

The fluorescent images obtained by scanning the DIGE gels were then loaded into the Delta 2D software (Decodon, Germany) for image analysis. The gel images were segregated into infected and non-infected groups for spot matching. The Cy2 images from each comparison were grouped into a standard group. The image with the best separation among the Cy2 images was defined as a master and the remaining images were warped to the master by applying the “exact” warp mode. Since Cy2 images are a pool of all the samples, matching the images in exact warp mode ensures that the spots on all the gels are correctly matched. The Cy3 and Cy5 images from the same gel were set to “identical” warp mode and the images from different gels were set to “implicit” warp mode for comparison between the infected and non-infected groups. An in silico fusion image which is representative of all the images was created by fusing the images in the project. The fusion image was used for detection of the spots by the software which was later manually validated. A total of 1683 spots were detected on the fusion image and were transferred onto all the gels to have equal number of spots on the gel images.

For quantitative analysis, the spot volumes from the gels along with the spot labels were loaded into Genespring GX 7.3.1 software (Agilent Technologies). PCA analysis showed significant differences between samples from non-infected hearts and hearts infected for 84 d (all 4 months old mice). Hearts of non-infected mice (1 month old, day 0) were also included in the set for comparison (Fig.11). Statistically significant differences among the spots between infected and non-infected mice were calculated by applying one-way ANOVA and Welch t-test with a cut off value of $p < 0.05$ and fold difference > 1.5 in the spot intensity after normalising the samples as described in 2.2.7.1. One gel had to be eliminated from the analysis because of improper separation at the basic end as it might interfere with the intensity normalisations. This analysis resulted in 158 spots showing disease related changes in their intensities. 71 spots were observed with higher intensities in mice hearts 84 d p.i. whereas intensities of 87 spots were observed to be lower in infected hearts compared to healthy controls.

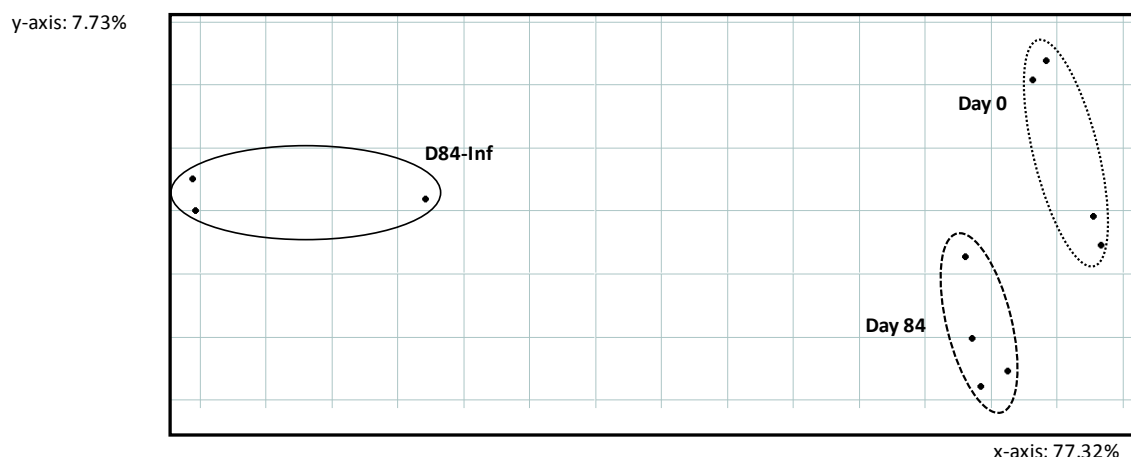


Fig.11. Principal Component Analysis of spots displaying age and infection dependent changes. Principal Component Analysis (PCA) based on spots displaying age dependent and infection dependent changes in intensity shows largest differences between d84 p.i. (continuous line) compared to d84 control mice (dashed line). Non-infected mice at day 0 (1 month) mice (dotted line) and d84 (4 month) show less differences in comparison to infected ones.

3.2.2.2. Identification of spots displaying disease associated changes after CVB3 infection using mass spectrometry

Quantitative analysis of the spots by Delta 2D and Genespring software revealed significant changes in the proteome of 84d infected mice hearts compared to healthy controls. To understand which proteins show infection related changes, 300µg of protein extract pooled from all the samples was separated by 2DE on three preparative gels as described in 2.2.6. 50µg of the pooled sample labelled with Cy2 dye was mixed with the 300µg pooled protein extract prior to separation to facilitate matching with the analytical gels. The gels were subsequently stained with silver nitrate for visualising the spots as described in 2.2.6.6.2.

After scanning, the gel images were loaded into the Delta 2D software for spot matching with fusion gel which will ensure picking up the spots of interest from the quantitative DIGE experiment from the preparative gels. The 158 spots were cut and 92 out of them could be identified by MS analysis. 48 spots were identified out of 71 spots displaying higher intensities in mice hearts 84d p.i. and 44 spots were identified out of 87 spots displaying lower intensities in infected hearts compared to controls (Fig.12). A representative gel image displaying the location of the identified spots with altered intensities is shown below (Fig.13).

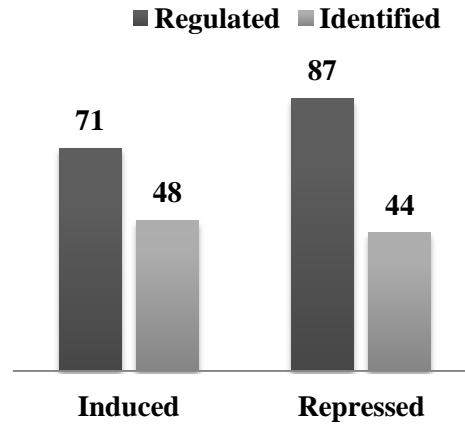


Fig. 12. Number of spots with altered intensity identified by 2D-DIGE analysis. 92 spots out of 158 quantified were identified by mass spectrometric analysis. 48 (71) spots displaying higher intensities and 44 (87) spots displaying lower intensities were identified in infected mice hearts compared to healthy controls.

pI 4.0

pI 7.0

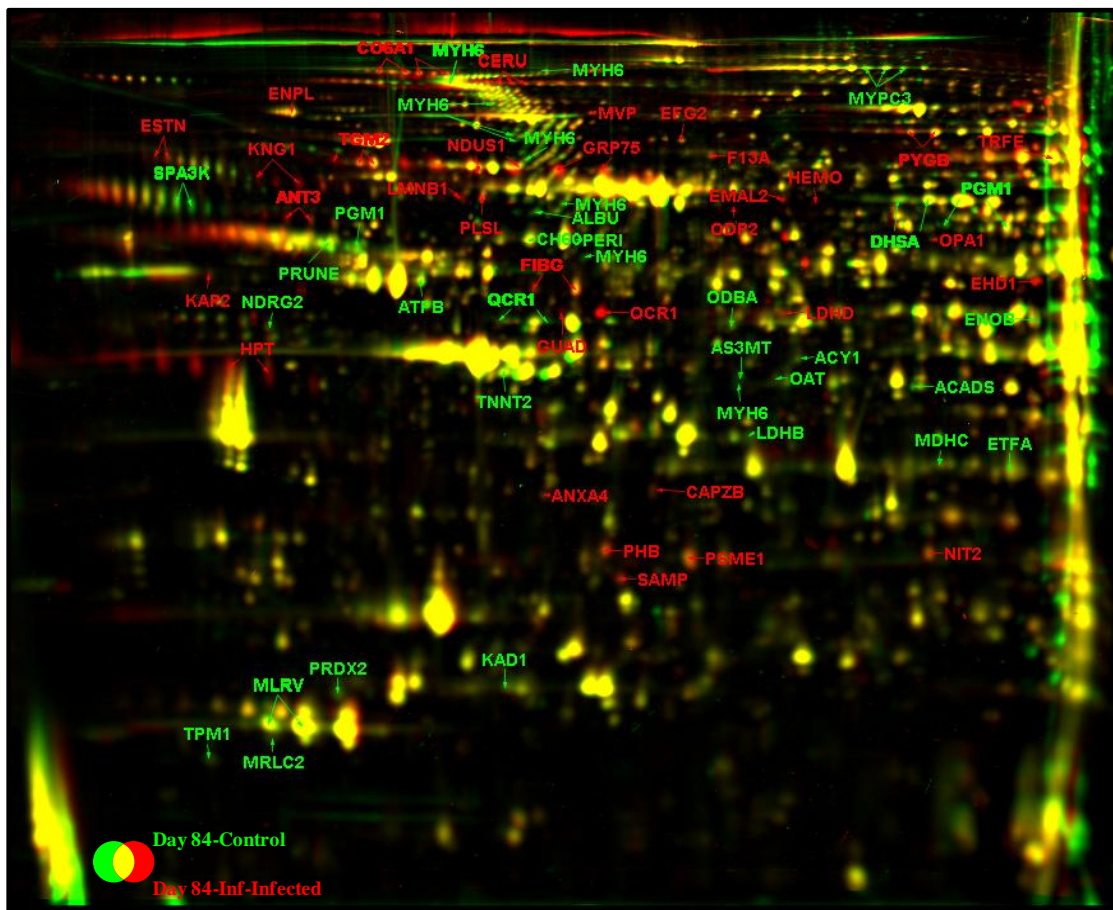


Fig. 13. Dual channel overlay displaying a comparison of protein patterns of dilated hearts at 84 days post infection with CVB3 and age-matched non-infected control mice. Protein spots in red and green colour indicate induction and repression during infection and the spots in yellow indicate proteins that do not show significant changes due to infection. Labels in red indicate the identified proteins for the induced spots and labels in green indicate protein identifications for the repressed spots.

The 92 spots identified comprised 74 distinct proteins. Eighteen proteins have been identified in more than one spot on the gel (Table 17). The presence of proteins in multiple spots suggests possible post-translational modifications, protein degradation products or protein species. Proteins collagen 6 alpha 1 (CO6A1), myosin binding protein C3 (MYPC3), myosin light chain ventricular isoform (MLRv), haptoglobin (HPT), serine protease inhibitor A3K (SPA3K) and antithrombin 3 (ANT3) are a few examples of proteins identified as a trace/chains of spots indicating their existence in multiple species on the gel (Fig.14).

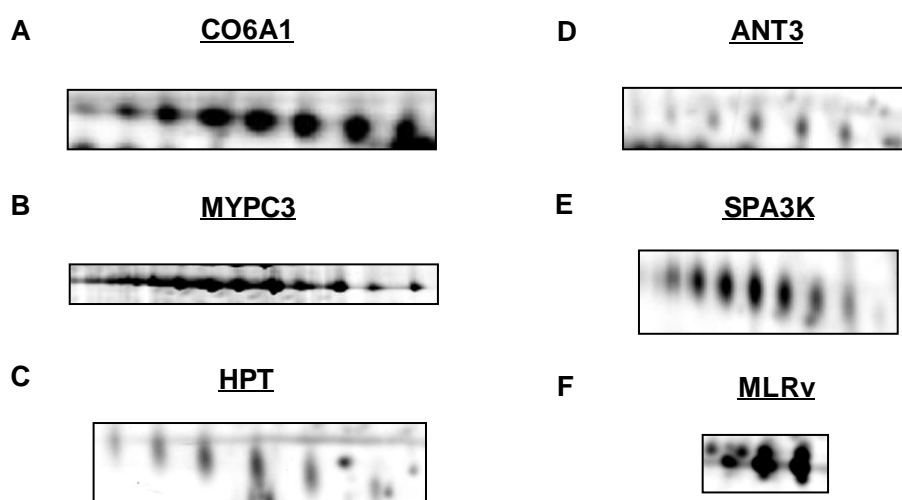


Fig. 14. Identification of protein species in 2D-DIGE analysis. Of the 92 spots identified on the gel in DIGE analysis, 18 proteins have been identified in multiple spots. Here are a few examples of proteins identified as a chain of spots representing different protein species. A- Collagen 6 alpha 1 (CO6A1), B- Myosin binding protein C3 (MYPC3), C- Haptoglobin (HPT), D- Antithrombin 3 (ANT3), E- Serine protease inhibitor A3K (SPA3K) and F- Myosin light chain ventricular isoform (MLRv).

Apart from those mentioned above, proteins belonging to the respiratory electron transport chain such as mitochondrial NADH-ubiquinone oxidoreductase 75 kDa subunit (NDUS1), succinate dehydrogenase (ubiquinone) flavoprotein subunit (DHSA), and cytochrome b-c1 subunit (QCR1) were also identified in multiple spots. Since all these proteins were identified in the same molecular weight range, they are more likely to be post-translationally modified rather than truncated products. The identification of QCR1 in three spots confirms such an assumption. Two out of three spots were identified at lower amounts (0.48 and 0.63 fold) while the third spot was identified at remarkably higher amounts (~43fold) and shifted towards the basic end of the gel in infected mice. However one particular protein, myosin heavy chain 6 (MYH6) was identified in 10 spots out of 92 spots showing infection related changes. The 10 spots were distributed over the entire gel at different ranges of molecular weight and pI suggesting degradation. Similar results for MYH6 were also observed during

early stages of acute and chronic myocarditis after CVB3 infection (Hammer et al., 2010). Besides MYH6, tropomyosin alpha 1 chain (TPM1) was also assumed to be processed by degradation since it was identified at a much lower molecular weight region (21kDa) than expected (32kDa).

The proteins identified by DIGE analysis were searched for their subcellular location in Uniprot (www.uniprot.org) (Fig.15). Mitochondrial proteins formed the major class of proteins followed by cytoplasmic proteins, secretory proteins and proteins related to cytoskeleton. Very few of the identified proteins belong to endoplasmic reticulum, nucleus, extracellular space and cell membrane. The large proportion of mitochondrial proteins indicates strong alterations in the mitochondrial function during manifestation of DCM subsequent to CVB3 infection.

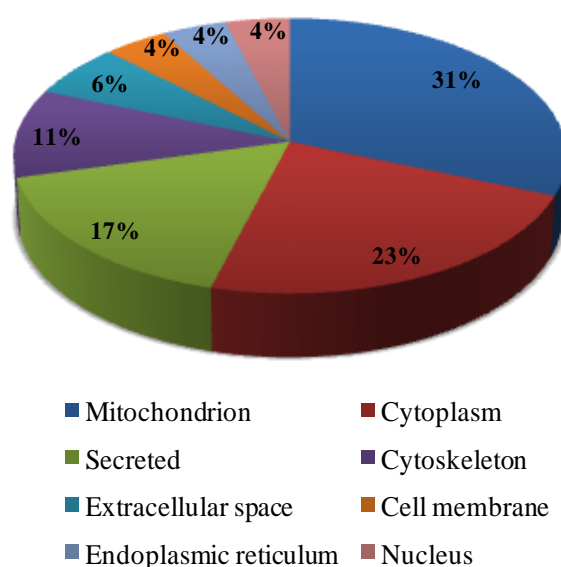


Fig. 15. Subcellular location of proteins altered in mouse hearts 84 d p.i. in comparison to controls identified by DIGE analysis. The proteins identified were searched for the subcellular location using Uniprot. The majority of the proteins belong to mitochondria and cytoplasm.

Though 2D-DIGE helped in the identification of protein species, PTMs and degradation products, the restricted pI range of 4-7 limited our analysis. The identification of only few membrane proteins also sheds light on the disadvantages of 2DE. Hence, in order to get a more comprehensive view of the molecular changes occurring in the dilated hearts, gel-free LC-MS/MS analysis was performed.

Table 17. Proteins identified from 2D -DIGE displaying altered intensity in mouse hearts with DCM 84 d p.i compared to age-matched 84d control hearts

Swissprot Entry	Acc no.	Protein Annotation	Spot-ID	Peptide Count	Seq. Coverage (%)	Fold Change	Direction	p-Value	Protein Score	CV D84	CV D84 Inf	CV*
Cytoplasm												
PLSL	Q61233	Plastin-2	ID106495	5	10.4	4.6	↑	2.08E-03	50.19	23.16	57.01	96.21
EMAL2	Q7TNG5	Echinoderm microtubule-associated protein-like 2	ID106485	5	8.3	4.3	↑	2.27E-02	50.19	36.17	25.89	79.61
CAPZB	P47757	F-actin-capping protein subunit beta	ID106859	9	28.5	2.2	↑	4.87E-03	90.19	20.37	33.18	49.70
MVP	Q9EQK5	Major vault protein	ID643481	8	8.2	1.9	↑	7.03E-04	80.21	15.22	22.18	41.92
KAP2	P12367	cAMP-dependent protein kinase typeII-alpha regulatory subunit	ID106618	6	14.7	1.8	↑	3.25E-02	60.23	11.98	28.80	44.67
F13A	Q8BH61	Coagulation factor XIIIa chain	ID106372	4	5.5	1.6	↑	1.66E-02	40.25	11.69	17.23	35.90
NIT2	Q9JHW2	Nitrilase homolog 2	ID106905	3	15.2	1.5	↑	8.76E-03	30.19	9.37	12.62	30.33
NDRG2	Q9QYG0	Protein NDRG2	ID106690	2	7.5	0.7	↓	1.11E-02	20.23	9.15	14.55	20.19
ENOB	P21550	Beta-enolase	ID167188	3	7.8	0.7	↓	6.55E-03	30.19	3.05	6.36	16.84
MDHC	P14152	Malate dehydrogenase, cytoplasmic	ID106828	4	14.4	0.6	↓	3.73E-02	40.19	25.03	37.68	29.83
ACY1	Q99JW2	Aminoacylase-1	ID106719	3	7.6	0.6	↓	3.83E-03	30.20	18.79	10.82	28.48
LDHB	P16125	L-lactate dehydrogenase B chain	ID106808	8	22.5	0.6	↓	1.93E-03	80.18	12.18	8.00	24.22
KAD1	Q9R0Y5	Adenylate kinase isoenzyme 1	ID107917	4	18.6	0.6	↓	4.56E-02	40.19	18.30	18.11	29.28
PRDX2	Q61171	Peroxiredoxin-2	ID107008	2	9.6	0.6	↓	2.34E-02	20.14	10.75	15.27	27.83
TPM1	P58771	Tropomyosin alpha-1 chain	ID107038	6	15.5	0.5	↓	2.24E-02	56.15	18.15	21.04	35.74
PRUNE	Q8BIW1	Protein prune homolog	ID106554	2	4.8	0.4	↓	2.50E-02	20.13	21.40	26.73	42.23
AS3MT	Q91WU5	Arsenite methyl transferase	ID106743	7	20.5	0.3	↓	5.40E-03	70.18	37.57	24.34	69.69
MYH6	Q02566	Myosin-6	10 spots	23	11.9	0.3-0.5	↓	1.11E-02	230.31	17.68	53.17	58.12
PGM1	Q9D0F9	Phosphoglucomutase-1	3 spots	11	21.4	0.3-0.4	↓	3.11E-03	110.26	4.95	113.04	44.67

Swissprot Entry	Acc no.	Protein Annotation	Spot-ID	Peptide Count	Seq. Coverage (%)	Fold Change	Direction	p-Value	Protein Score	CV D84	CV D84 Inf	CV*
Mitochondria												
ODP2	Q8BMF4	Dihydrolipoyllysine-residue acetyl transferase component of pyruvate dehydrogenase complex	ID121643	3	5.9	5.6	↑	3.81E-02	30.18	75.62	81.41	117.76
GRP75	P38647	Stress-70protein	2 spots	5	9.7	3.1	↑	2.02E-02	50.21	9.40	49.31	71.10
PHB	P67778	Prohibitin	ID106903	8	30.9	2.8	↑	1.37E-05	80.18	7.12	25.62	60.10
NDUS1	Q91VD9	NADH-ubiquinone oxidoreductase 75kDa subunit	2 spots	18	22.6	1.8	↑	2.94E-02	180.28	15.08	17.79	39.49
OPA1	P58281	Dynamin-like 120kDa protein	ID120537	9	10.7	1.7	↑	8.03E-03	90.19	13.41	21.63	37.53
RRF2M	Q8R2Q4	Elongation factor G2	ID106341	5	7.6	1.6	↑	7.97E-03	50.29	18.16	31.12	38.44
LDHD	Q7TNG8	Probable D-lactate dehydrogenase	ID135646	5	15.5	1.5	↑	1.26E-02	50.20	13.47	19.20	33.65
CH60	P63038	60 kDa heat shock protein	ID106533	19	35.4	0.7	↓	7.77E-03	190.30	4.16	10.85	16.82
OAT	P29758	Ornithine aminotransferase	ID106747	2	4.8	0.7	↓	1.32E-02	20.16	10.75	43.81	21.31
ETFA	Q99LC5	Electron transfer flavoprotein subunit alpha	ID106837	10	34.5	0.7	↓	9.50E-04	100.24	3.59	7.82	16.24
DHSA	Q8K2B3	Succinate dehydrogenase [ubiquinone] flavoprotein subunit,	ID106447	7	9.3	0.6	↓	2.50E-02	70.21	18.48	11.69	23.32
ODBA	P50136	2-oxoisovalerate dehydrogenase subunit alpha, mitochondrial	ID624970	11	20.4	0.6	↓	2.07E-02	110.28	7.10	18.52	22.68
ACADS	Q07417	Short-chain specific acyl-CoA dehydrogenase, mitochondrial	ID106748	3	1.8	0.6	↓	8.97E-04	30.19	10.69	20.53	22.75
ATPB	P56480	ATP synthase subunit beta, mitochondrial	ID106621	13	22.5	0.6	↓	2.23E-02	130.29	23.72	4.20	32.86
QCR1	Q9CZ13	Cytochrome b-c1 complex subunit 1, mitochondrial	3 spots	6	11.3	0.5-0.6, 42	↑	8.03E-04	60.19	5.76	9.46	31.28
Secretory/ Extracellular Matrix												
HPT	Q61646	Haptoglobin	2 spots	4	10.7	6.3-11.0	↑	1.77E-02	40.14	50.50	81.02	119.52
KNG1	O08677	Kininogen-1	2 spots	3	5.9	5.0-7.0	↑	1.61E-02	30.14	34.41	68.38	103.25
HEMO	Q91X72	Hemopexin	ID106481	4	10.0	6.3	↑	4.05E-03	40.19	38.94	53.44	101.12
CO6A1	Q04857	Collagen alpha-1(VI) chain	4 spots	5	6.4	1.5-3.5	↑	2.95E-02	50.22	7.67	24.34	34.37
ANT3	P32261	Antithrombin-III	2 spots	5	14.0	3.2	↑	1.98E-02	50.19	42.40	51.60	79.10
SAMP	P12246	Serum amyloid P-component	ID106926	3	17.9	2.9	↑	5.99E-03	30.35	15.93	39.78	63.59
FIBG	Q8VCM7	Fibrinogen gamma chain	2 spots	9	17.9	1.5-2.3	↑	3.30E-02	90.24	13.46	38.83	33.39
TRFE	Q921I1	Serotransferrin	ID106311	14	21.7	2.2	↑	6.23E-03	138.28	18.95	27.53	48.58

Swissprot Entry	Acc no.	Protein Annotation	Spot-ID	Peptide Count	Seq. Coverage (%)	Fold Change	Direction	p-Value	Protein Score	CV D84	CV D84 Inf	CV*
Secretory/ Extracellular Matrix (Continued)												
CERU	Q61147	Ceruloplasmin	3 spots	4	4.7	2.1	↑	1.93E-02	40.14	34.93	39.90	50.47
ALBU	P07724	Serum albumin	ID106506	3	5.8	0.3	↓	2.31E-02	30.20	16.85	58.09	50.07
SPA3K	P07759	Serine protease inhibitor A3K	2 spots	8	16.0	0.2	↓	1.48E-02	80.29	26.40	74.99	74.47
Cell Membrane												
EHD1	Q9WVK4	EH domain-containing protein 1	ID126263	6	10.9	2.7	↑	6.38E-03	60.20	8.19	26.94	61.68
Endoplasmic reticulum												
EST1C	P23953	Liver carboxylesterase N	2 spots	7	11.0	1.9	↑	6.21E-03	70.19	17.40	25.29	47.74
ENPL	P08113	Endoplasmin	ID106245	13	17.7	1.7	↑	8.67E-03	130.26	5.17	31.14	36.70
Nucleus												
LMNB1	P14733	Lamin-B1	ID140918	13	20.4	5.8	↑	1.56E-02	130.27	21.15	51.72	99.74
Unclassified												
GUAD	Q9R111	Guanine deaminase	ID137349	10	20.5	14.1	↑	2.49E-03	100.21	65.98	35.79	113.59
TGM2	P21981	Protein-glutamine gamma-glutamyl transferase2	3 spots	6	11.7	2.0-14.0	↑	4.56E-02	60.22	11.95	44.42	59.37
PSME1	P97371	Proteasome activator complex subunit 1	ID591049	12	40.2	2.2	↑	8.49E-05	120.26	8.44	21.54	48.85
ANXA4	P97429	AnnexinA4	ID106871	10	37.0	2.0	↑	1.96E-02	100.23	24.13	33.89	48.32
PYGB	Q8CI94	Glycogen phosphorylase,brain form	2 spots	13	14.2	1.8	↑	2.80E-03	128.22	2.32	17.88	39.71
MRLC2	Q3THE2	Myosin regulatory light chain MRLC2	ID111420	5	24.4	0.6	↓	1.88E-02	50.19	6.54	11.46	18.05
TNNT2	P50752	Troponin T, cardiac muscle	ID234383	5	13.6	0.6	↓	2.90E-02	50.19	6.85	13.47	19.59
MLRV	P51667	Myosin regulatory light chain 2, ventricular/cardiac muscle	2 spots	9	42.2	0.6	↓	1.04E-03	90.26	5.41	15.35	20.92
PERI	P15331	Peripherin	ID128355	8	16.4	0.5	↓	3.18E-02	80.18	26.32	27.93	44.12
MYPC3	O70468	Myosin-binding protein C, cardiac-type (3 spots)	3 spots	23	12.1	0.5	↓	3.28E-02	160.25	24.41	25.69	42.41

Fold change- protein intensity ratio of mouse hearts 84 d p.i. to 84 d control hearts, Direction-infection associated increase (↑) or decrease (↓) in protein levels indicated by arrows

3.2.2.3. Identification of proteins displaying dilated cardiomyopathy associated changes by gel-free LC-MS/MS analysis

Since the samples couldn't be quantified based on their peptide intensities, the .dta and .out files derived from a SORCERER/SEQUEST search against Swissprot mouse forward reverse database rel 57.1 were loaded into SCAFFOLD software version 2.6 (Proteome software, USA) for quantitation of the proteins by spectral counting. The proteins were identified with at least two peptides passing the filters as described in 2.2.8.4. The assigned spectra values given by the SCAFFOLD software were considered for quantitation. To restrict quantitation to distinct protein-specific peptides, the homologous peptides shared among the identified proteins were removed and the proteins with a sum of six spectra in at least one of the two conditions were considered for spectral counting.

A total of 391 proteins with at least two unique peptides per protein were identified using gel-free LC-MS/MS approach. The total number of proteins identified is listed in the appendix (A3.2.2.3). One third of the proteins (101) identified were membrane proteins belonging to ER-, mitochondrial-, nuclear- or cytoplasmic membrane (Fig.16A). Besides, 152 proteins had a pI >7 which falls beyond the identification range of the DIGE analysis. 322 proteins with ≥ 6 spectra in at least one of the two conditions were considered for quantitation by spectral counting (Old et al., 2005). Hence proteins satisfying the filters of a ratio fold change of > 1.2 and a two tailed student's *t*-test with $p \leq 0.1$ were considered as displaying statistically significant infection related changes (Cima et al., 2011).

Applying the above mentioned statistical cuts, 46 proteins were identified to show disease dependent changes in mice hearts 84 d p.i. compared to age- matched non-infected controls (Table 18). The proteins could be primarily assigned to three biological classes: lipid metabolism, respiratory electron transport chain, and extracellular matrix. Proteins long-chain specific acyl-CoA dehydrogenase, mitochondrial (ACADL), very long-chain specific acyl-CoA dehydrogenase, mitochondrial (ACADV), 3-hydroxy acyl-CoA dehydrogenase type-2 (HCD2), hydroxyacyl-CoA dehydrogenase, mitochondrial (HCDH) involved in lipid metabolism were identified in lower amounts in infected hearts. A similar pattern was observed for proteins of the respiratory electron transport chain cytochrome c oxidase 6C (COX6C), NADH dehydrogenase [ubiquinone] 1 beta subcomplex subunit 3. Proteins related to extracellular matrix such as collagen 6 alpha 1 (CO6A1), collagen 6 alpha 2 (CO6A2),

collagen 1 alpha 1(CO1A1), lumican (LUM) and decorin (PGS2) were identified in higher amounts in infected mice.

Among the regulated proteins, the majority were mitochondrial proteins. Also a significant percentage of the regulated proteins comprised membrane proteins belonging to either, inner/outer mitochondrial membrane, ER and cytoplasmic membrane. Though extracellular proteins accounted for only a small portion of the identified proteins, they showed significant changes in CVB3 infection and were identified as strongly regulated (Fig.16B).

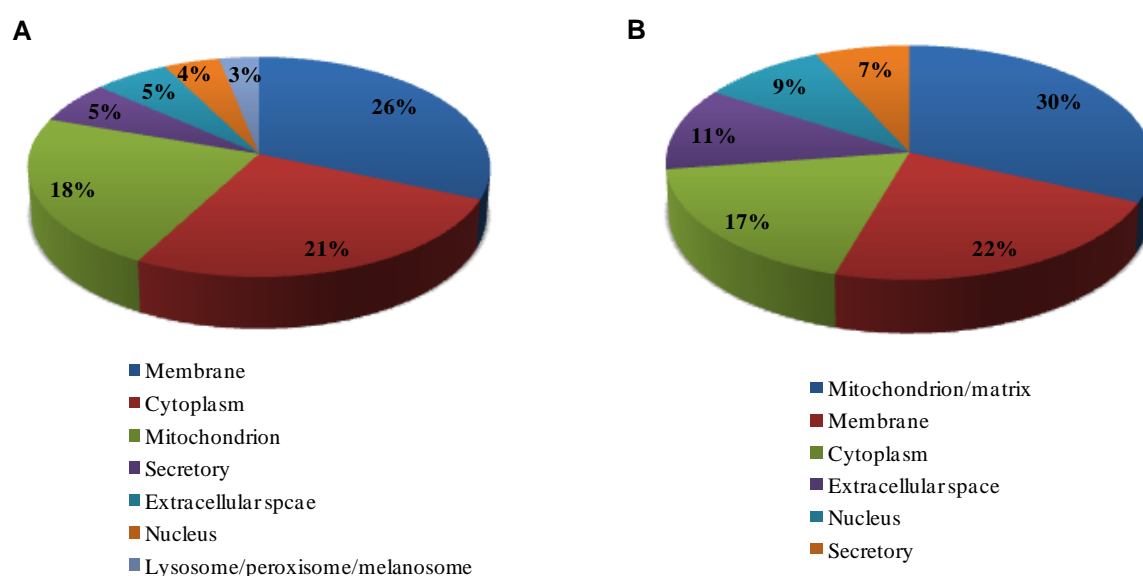


Fig. 16. Subcellular location of proteins covered by gel free LC-MS/MS analysis. The majority of the proteins identified by gel free analysis were membrane proteins which includes outer- and inner mitochondrial membrane, cytoplasmic- and ER membrane. Most of these proteins could not be covered by DIGE analysis. A- subcellular location of total proteins quantified (322). B- subcellular location of proteins identified as regulated (46).

Table 18. Proteins identified from gel-free LC-MS/MS analysis displaying altered levels in mouse hearts with DCM 84d p.i compared to age-matched 84d control hearts

Swissprot Entry	Protein Annotation	Acc. No	Mol.Wt	pI	No. of peptides	Sum of Norm. Spectra		Seq. Coverage (%)	Fold Change	Direction	p-value	Coeff. Of Var (CV)	
						84d-Inf	84d					84d-Inf	84d
Mitochondria													
ATP5L	ATP synthase subunit g	Q9CPQ8	11 kDa	9.74	2	13.8	1.5	33.0%	6.9	↑	8.3E-02	66.86	0.00
ACADL	Long-chain specific acyl-CoA dehydrogenase	P51174	48 kDa	6.50	10	103.4	97.5	21.0%	0.8	↓	1.4E-02	9.90	6.58
ODO2	Dihydrolipoyllysine-residue succinyltransferase component of 2-oxoglutarate dehydrogenase complex	Q9D2G2	49 kDa	5.98	4	37.8	36.2	12.0%	0.8	↓	4.8E-02	17.55	7.82
THIM	3-ketoacyl-CoA thiolase	Q8BWT1	42 kDa	8.33	13	155.5	155.5	48.0%	0.7	↓	2.1E-02	16.61	4.98
ACADV	Very long-chain specific acyl-CoA dehydrogenase	P50544	71 kDa	7.72	10	75.2	76.3	22.0%	0.7	↓	6.5E-02	3.54	12.54
ACS2L	Acetyl-coenzyme A synthetase 2-like	Q99NB1	75 kDa	5.98	7	21.4	21.9	16.0%	0.7	↓	6.8E-02	26.28	0.60
MMSA	Methylmalonate-semialdehyde dehydrogenase	Q9EQ20	58 kDa	7.02	6	30.0	32.1	13.0%	0.7	↓	5.2E-02	5.01	13.17
HCDH	Hydroxyacyl-coenzyme A dehydrogenase	Q61425	34 kDa	8.26	7	47.0	51.1	36.0%	0.7	↓	6.9E-02	28.96	15.55
EFTU	Elongation factor Tu	Q8BFR5	50 kDa	6.20	5	34.9	38.1	17.0%	0.7	↓	4.0E-02	27.81	9.48
ACSL1	Long-chain-fatty-acid--CoA ligase 1	P41216	78 kDa	6.81	11	34.6	42.2	13.0%	0.6	↓	4.5E-02	29.96	18.20
COX6C	Cytochrome c oxidase subunit 6C	Q9CPQ1	8 kDa	10.13	2	12.3	15.9	25.0%	0.6	↓	2.9E-02	17.59	16.73
HCD2	3-hydroxyacyl-CoA dehydrogenase type-2	O08756	27 kDa	8.56	3	12.8	17.9	22.0%	0.5	↓	7.4E-02	65.53	8.22
PCCB	Propionyl-CoA carboxylase beta chain	Q99MN9	58 kDa	6.38	2	9.9	14.8	5.5%	0.5	↓	8.1E-02	55.19	29.27
NDUB3	NADH dehydrogenase [ubiquinone] 1 beta subcomplex subunit 3	Q9CQZ6	12 kDa	9.01	2	4.1	7.7	17.0%	0.4	↓	6.3E-02	103.38	7.02
ADCK3	Chaperone activity of bc1 complex-like	Q60936	72 kDa		2	5.3	9.8	3.1%	0.4	↓	3.9E-02	83.41	22.79
MCCA	Methylcrotonoyl-CoA carboxylase subunit alpha	Q99MR8	79 kDa	6.68	2	4.0	7.7	4.2%	0.4	↓	4.8E-02	99.50	7.02
DECR	2,4-dienoyl-CoA reductase	Q9CQ62	36 kDa	8.78	2	4.0	8.6	8.4%	0.3	↓	2.5E-02	99.50	17.73
ODBA	2-oxoisovalerate dehydrogenase subunit alpha	P50136	50 kDa	6.05	3	3.0	7.5	10.0%	0.3	↓	5.9E-02	66.22	36.22
ACOT2	Acyl-coenzyme A thioesterase 2	Q9QYR9	50 kDa	6.14	2	5.0	12.7	6.4%	0.3	↓	2.5E-02	119.52	6.98

Swissprot Entry	Protein Annotation	Acc. No	Mol.Wt	pI	No. of peptides	Sum of Norm. Spectra		Seq. Coverage (%)	Fold Change	Direction	p-value	Coeff. Of Var (CV)	
						84d-Inf	84d					84d-Inf	84d
Extracellular Matrix/ Basement membrane													
LUM	Lumican	P51885	38 kDa	6.01	3	31.5	1.5	17.0%	15.8	↑	6.7E-03	27.89	0.00
PGS2	Decorin	P28654	40 kDa	8.98	3	13.4	1.5	7.1%	6.7	↑	8.3E-03	27.25	0.00
CO6A2	Collagen alpha-2(VI) chain	Q02788	110 kDa	5.92	4	17.8	2.6	3.9%	5.1	↑	5.2E-02	53.21	74.42
KN1G	Kininogen-1	O08677	73 kDa	6.02	2	14.6	2.5	3.6%	4.4	↑	7.3E-03	29.15	68.44
CO6A1	Collagen alpha-1(VI) chain	Q04857	108 kDa	5.15	8	50.2	13.8	10.0%	2.7	↑	1.8E-02	28.98	22.18
CO1A1	Collagen alpha-1(I) chain	P11087	138 kDa	9.28	5	44.1	12.8	5.1%	2.6	↑	3.2E-02	34.95	36.99
LAMC1	Laminin subunit gamma-1	P02468	177 kDa	5.03	11	46.2	22.9	9.1%	1.5	↑	4.5E-02	20.71	19.09
NID1	Nidogen-1	P10493	137 kDa	5.27	6	24.6	13.7	4.7%	1.4	↑	5.9E-02	16.18	16.23
Cytoplasm/ Cytoskeleton													
HS90A	Heat shock protein HSP 90-alpha	P07901	85 kDa	4.93	2	7.4	1.5	3.7%	3.7	↑	8.1E-02	56.39	0.00
ACTG	Actin, cytoplasmic 2	P63260	42 kDa	5.31	7	88.1	33.0	29.0%	2.0	↑	3.6E-04	9.25	12.46
TGM2	Protein-glutamine gamma-glutamyltransferase 2	P21981	77 kDa	4.98	8	41.4	16.6	11.0%	1.9	↑	3.7E-02	26.87	30.82
1433Z	14-3-3 protein zeta/delta	P63101	28 kDa	4.73	4	24.9	12.7	22.0%	1.5	↑	8.7E-02	22.96	24.53
DESM	Desmin	P31001	53 kDa	5.21	23	247.5	153.0	51.0%	1.2	↑	7.2E-02	12.89	8.53
SODC	Superoxide dismutase [Cu-Zn]	P08228	16 kDa	6.03	4	30.8	35.2	25.0%	0.7	↓	1.9E-02	24.51	4.66
FHL2	Four and a half LIM domains protein 2	O70433	32 kDa	7.31	4	25.8	35.2	22.0%	0.6	↓	3.2E-04	14.89	4.66
Peripheral membrane													
FLNC	Filamin-C	Q8VHX6	291 kDa	5.63	12	34.6	10.6	5.1%	2.4	↑	4.4E-02	37.19	45.98
GDIB	Rab GDP dissociation inhibitor beta	Q61598	51 kDa	5.93	2	6.2	9.8	7.0%	0.5	↓	7.2E-02	79.08	22.37
SDPR	Serum deprivation-response protein	Q63918	47 kDa	5.15	2	4.9	8.6	7.4%	0.4	↓	2.9E-02	74.31	16.88

Swissprot Entry	Protein Annotation	Acc. No	Mol.Wt	pI	No. of peptides	Sum of Norm. Spectra		Seq. Coverage (%)	Fold Change	Direction	p-value	Coeff. Of Var (CV)	
						84d-Inf	84d					84d-Inf	84d
Nucleus													
LMNA	Lamin-A/C	P48678	74 kDa	6.54	14	54.6	10.3	22.0%	4.0	↑	3.35E-02	43.40	75.45
ROA2	Heterogeneous nuclear ribonucleoproteins A2/B1	O88569	37 kDa	8.97	2	7.32	1.5	7.1%	3.7	↑	2.77E-02	36.18	0.00
HNRPK	Heterogeneous nuclear ribonucleoprotein K	P61979	51 kDa	5.39	4	12.38	5.56	10.0%	1.7	↑	3.66E-02	19.62	28.68
Secreted													
FETUA	Alpha-2-HS-glycoprotein	P29699	37 kDa	5.94	3	37.2	18.7	20.0%	1.5	↑	2.17E-02	13.55	18.34
ALBU	Serum albumin	P07724	69 kDa	5.53	32	884.3	515.1	63.0%	1.3	↑	5.81E-02	6.24	14.77
Miscellaneous													
APOA4	Apolipoprotein A-IV	P06728	45 kDa	5.27	3	13.4	2.5	9.4%	4.0	↑	6.7E-03	27.25	68.44
CATD	Cathepsin D	P18242	45 kDa	5.63	3	17.4	4.4	15.0%	3.0	↑	8.5E-02	15.06	114.29
HYES	Epoxide hydrolase 2	P34914	63 kDa	5.85	4	14.1	19.8	14.0%	0.5	↓	7.7E-02	62.53	22.46
Unclassified													
ANXA5	Annexin A5	P48036	36 kDa	4.83	7	35.6	12.7	26.0%	2.1	↑	4.04E-02	30.57	6.98

*Norm. spectra-Normalized spectra, Fold change- mean spectral count ratio of mouse heart proteins 84 d p.i. to 84 d control hearts , Direction-infection associated increase (↑) or decrease (↓) in protein levels

3.2.2.4. Comprehensive analysis of DIGE and gel free LC-MS/MS experiments

Each of the methods employed i.e. DIGE and gel free LC-MS/MS analysis, due to their advantages resulted in identification of different sets of proteins. This approach allowed for better protein coverage and a better understanding of the changes occurring at the molecular level in dilated cardiomyopathy. In order to derive a meaningful conclusion from the analyses, the proteins identified by both approaches were loaded together into the PANTHER software suite for their functional prediction. The protein classes' lipid metabolism (19), carbohydrate metabolism (15), respiratory electron transport chain (10) and cell morphogenesis (15) were among the most significantly affected in the dilated hearts of CVB3 infected mice 84 d p.i. (Fig.17).

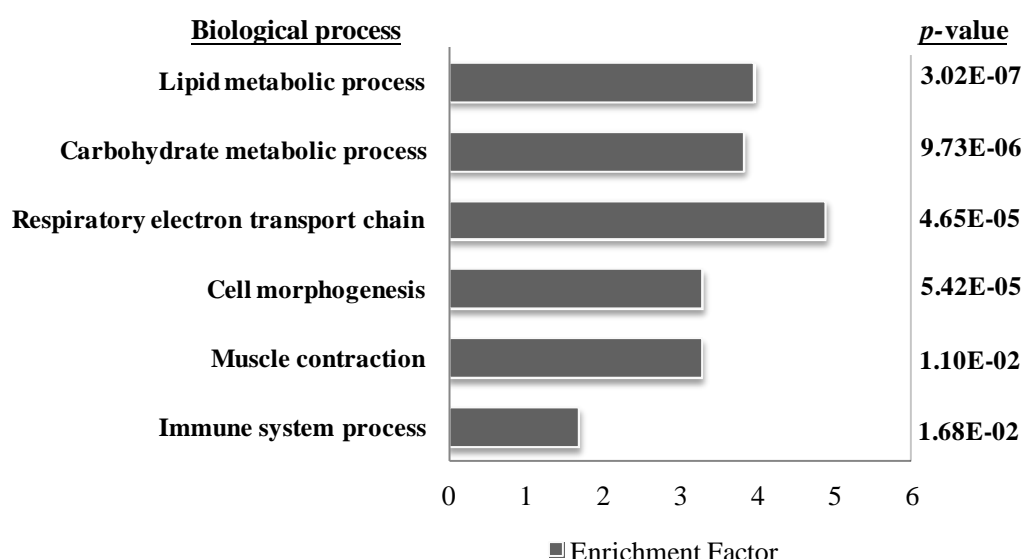


Fig. 17. Significantly affected protein classes in mice hearts 84 d p.i. Functional classification of the identified proteins was done using the PANTHER software suite. The enrichment factor for the protein class is calculated by taking the ratio of the number of expected proteins (PANTHER) to the number of identified proteins per class of protein. p-value as given by PANTHER (www.pantherdb.org).

Proteins of lipid metabolism were predominantly identified by gel free LC-MS/MS analysis and were observed in lower amounts in hearts 84 d p.i.. Also proteins involved in carbohydrate metabolism were observed in decreased amounts in infected mice. On the other hand, proteins of cell morphogenesis and immune system showed increased levels in disease condition. Proteins related to muscle contraction myosin regulatory light chain, ventricular isoform (MLRv), myosin regulatory light chain, smooth muscle isoform (MLRC2), myosin 6 (MYH6), tropomyosin 1, alpha (TPM1), troponin T2 were observed to have decreased in

amounts in 2D-DIGE indicating impaired muscle contraction in dilated cardiomyopathy (Fig.18).

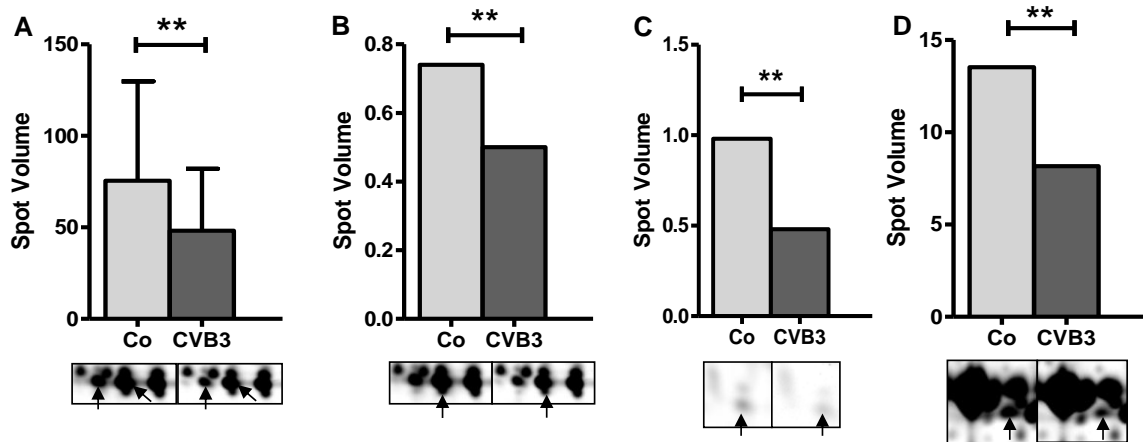


Fig. 18. Decrease in contractile proteins identified by DIGE analysis. Proteins (A) myosin regulatory light chain, ventricular isoform (MLRv), (B) myosin regulatory light chain (MLRC2), (C) tropomyosin alpha 1 (TPM1), (D) troponin T2 (TNNT2) were identified to have decreased in CVB3 mice compared to controls. ** - $p < 0.05$, arrows indicate spots quantified. Co-represents control D84 mouse hearts, CVB3-represent D84 infected mouse hearts, arrow heads point towards the identified spots.

Combination of 2D-DIGE and gel free LC-MS/MS analyses helped in improving coverage of proteins especially of the respiratory electron transport chain. Though total protein content of the respiratory electron transport chain did not alter, few subunits of complexes I, II, III and V were identified by both analyses as displaying infection-related changes in intensity. NADH-ubiquinone oxidoreductase 75kDa subunit, mitochondrial (NDUS1) of complex I was identified as two spots by 2D-DIGE and showed increase in amount at 84 d p.i. (Fig.19A). On the contrary, succinate dehydrogenase [ubiquinone] flavoprotein subunit, mitochondrial (DHSA) of complex II, also identified as two spots in 2D-DIGE, was observed at lower levels in 84 d p.i. compared to healthy controls (Fig.19B). Interestingly, cytochrome b-c1 complex subunit1, mitochondrial (QCR1), was identified in three spots on the gel. One of the spots showed a remarkable increase of 43 fold in its levels and showed a shift in pI towards basic range while the remaining two spots were identified at lower amounts in CVB3 mice. Since all three spots were identified in the same molecular weight range, these were considered as post-translationally modified as de/acetylated or de/phosphorylated (Kim et al., 2006). However this assumption couldn't be supported so far by our MS data (Fig.19 C-D). Besides, ATP synthase subunit beta, mitochondrial (ATPB) of complex V was observed to have decreased in levels at 84 d p.i. (Fig. 19E).

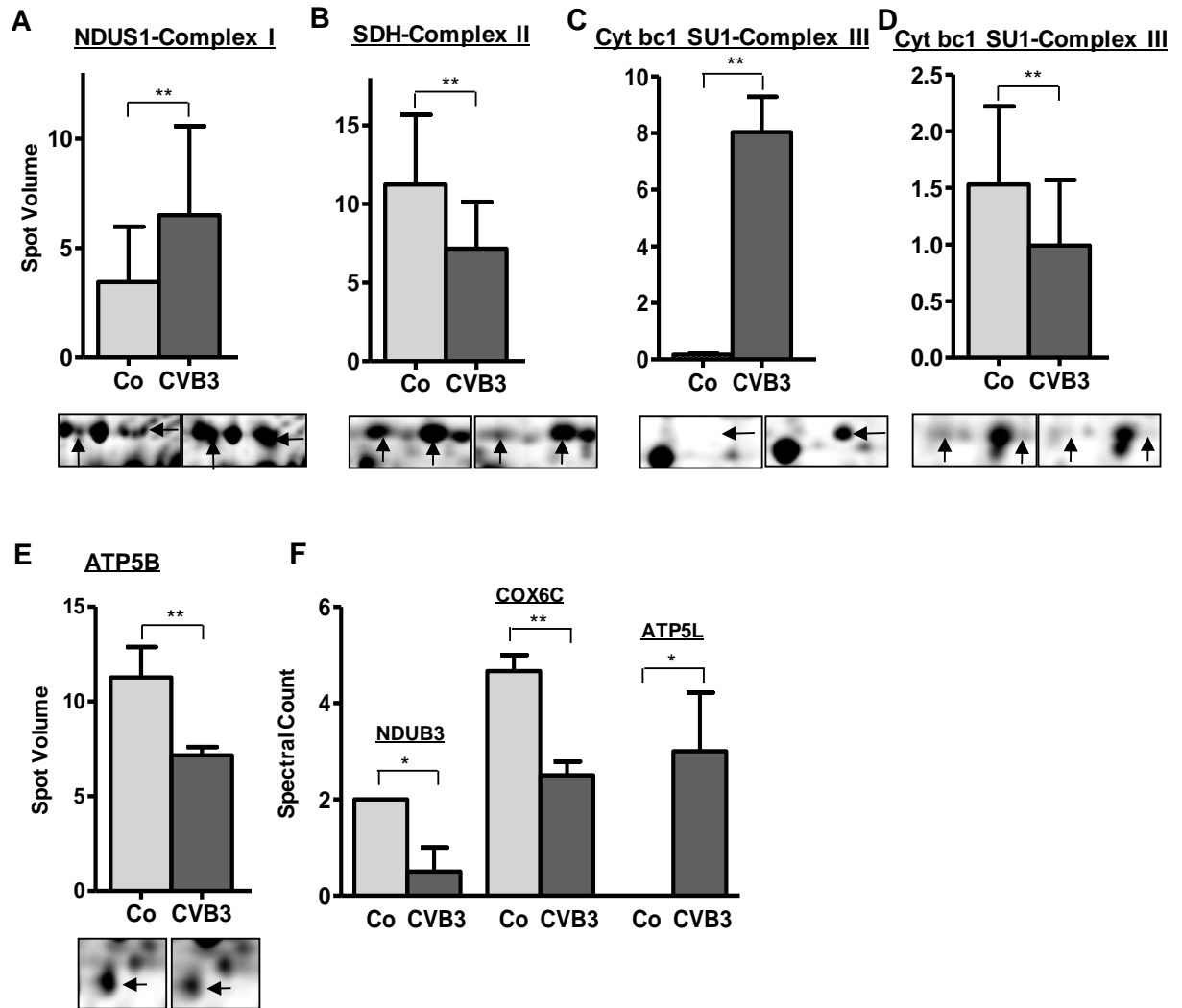


Fig. 19. Changes in levels of proteins of the respiratory electron transport chain in 84d mice infected with CVB3. A-E represent changes in levels of complex I, II, III and V of electron transport chain determined by 2D DIGE analysis (Bars). Gel segments show the spot intensities. Cyt bc1 subunit 1 (complex III) was observed in three different spots on gels. One spot was observed only in CVB3 infected mice (C) indicating an altered posttranslational modification in the dilated heart while two spots showed decreased levels during dilatation (D). Bars in A, B and D represent the sum of the intensities of the two spots identified as the same protein. F-Changes in levels of ETC proteins as identified by gel free LC-MS/MS analysis. Grey bars: control; dark bars: CVB3 infected mice. NDUS1: NADH ubiquinone oxidoreductase, 75kDa subunit, DHSA: Succinate dehydrogenase, QRC1: Cytochrome b-c1 complex, ATP5B: ATP synthase beta subunit, NDUB3: NADH dehydrogenase (ubiquinone) 1 beta subcomplex, COX6C: Cytochrome c Oxidase subunit 6C, ATP5L- ATP synthase subunit g. **p-value < 0.05, *p-value < 0.1.

In the gel free LC-MS/MS analysis, NADH dehydrogenase [ubiquinone] 1 beta subcomplex subunit 3 (NDUB3) of complex I and cytochrome c oxidase subunit 6C (COX6C) were identified at lower levels in CVB3 mice whereas ATP synthase subunit g, mitochondrial (ATP5L) of complex V was identified in higher amounts compared to non-infected mice hearts (Fig. 19F).

Another class of proteins identified at altered levels in both 2D-DIGE and gel free LC-MS/MS analysis were proteins belonging to extracellular matrix. CO6A1, CO6A2, CO1A1, LUM and PGS2 were identified at higher levels in hearts 84 d p.i. compared to organs of non-infected mice at day 84 and are known to play a significant role in fibrosis which is prominently observed in mice infected with CVB3. While CO6A1 was identified in DIGE as well as gel free LC-MS/MS analysis, the other proteins were identified in the gel free LC-MS/MS analysis only (Fig.20).

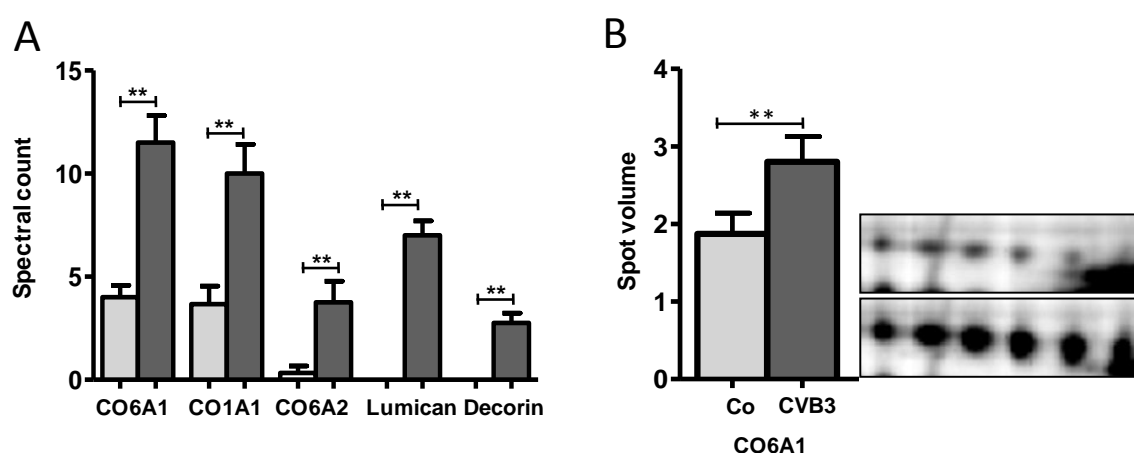


Fig. 20. Increase in levels of extracellular matrix proteins in mice infected with CVB3 for 84 d indicates extensive fibrosis as a result of DCM. A-shows increased extracellular matrix proteins in DCM mice identified by gel-free LC-MS/MS analysis. B-Collagen 6 alpha 1 was identified as a train of spots in DIGE analysis which showed increase in intensity in 84d infected mice compared to controls. The columns display summarized spot volumes of all 5 spots of CO6A1. Grey bars: control; dark bars: CVB3 infected mice. CO6A1 and 2: Collagen 6 alpha subunits 1 and 2; CO1A1: Collagen 1 alpha subunit 1. Grey bars: control; dark bars: CVB3 infected. **-p<0.05.

Proteins of respiratory chain and fibrosis could be identified in both the 2D-DIGE analysis and the gel free LC-MS/MS analysis. The advantage of gel free approach over 2DE was very prominent particularly in identifying proteins involved in lipid metabolism. Since the majority of the identified proteins of lipid metabolism have a pI above 7 and are mostly located in either the inner or outer mitochondrial membrane, they couldn't be identified by DIGE analysis performed only in pI range 4-7. Proteins of lipid metabolism were identified in lower levels in mice infected for 84 d pointing towards a reduced energy production in DCM (Fig.21).

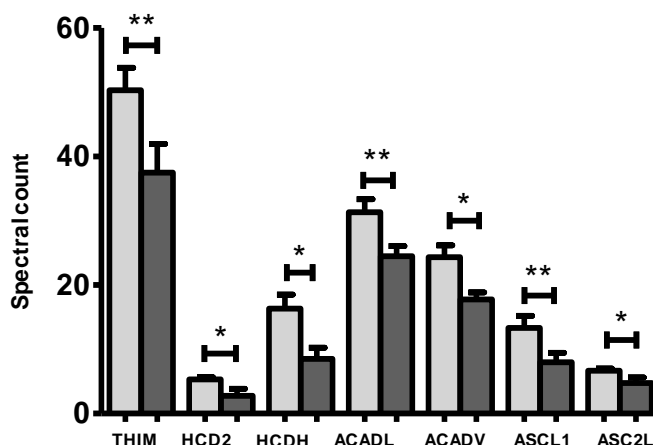


Fig. 21. Proteins with a role lipid and fatty acid metabolism were identified at lower levels in hearts of CVB3 infected mice by gel free proteomics. Grey bars: control; dark bars: CVB3 infected mice. THIM: 3-ketoacyl CoA thiolase, HCD2: 3-hydroxy acyl-CoA dehydrogenase, HCDH: hydroxyl acyl-CoA dehydrogenase, ACADL: long-chain specific acyl-CoA dehydrogenase, ACADV: very long-chain specific acyl-CoA dehydrogenase, ASCL1: long-chain fatty acid CoA ligase, ASC2L: acetyl- CoA synthetase 2- like, mitochondrial. **- $p < 0.05$, *- $p < 0.1$.

Using complementary techniques of 2D-DIGE and gel free LC-MS/MS analysis, protein coverage could be increased and a better understanding of the molecular changes occurring in mouse hearts infected with CVB3 could be attained.

3.2.2.5. Validation of fibrosis by Western blotting and immunohistochemical staining

Western blotting confirmed the increase in the levels of proteins CO6A1 and lumican (LUM) in dilated hearts of mice infected with CVB3 compared to controls (Fig.22). An intense signal approximately two fold stronger was observed in hearts of infected mice suffering from dilated cardiomyopathy compared to non-infected controls at the molecular weight region of 100-110kDa corresponding to the MW of CO6A1 (108kDa). A faint unspecific band was also observed slightly below 110kDa but was not consistent in all the animals. For lumican an extensive variation in abundance of the protein was observed across the individual animals. However, Western blot signals were stronger in dilated hearts after CVB3 infection compared to controls. A second band at a higher molecular weight than that of the protein was observed at 90kDa. Since lumican is a proteoglycan undergoing glycosylation, the additional band was assumed to be the glycosylated form of the protein. The results of Western blot analysis were also confirmed by immunohistochemical staining. Excessive depositions of CO6A1, CO1A1 and LUM were also observed in tissue sections confirming fibrosis at 84 d in mouse hearts infected with CVB3 (Fig.23).

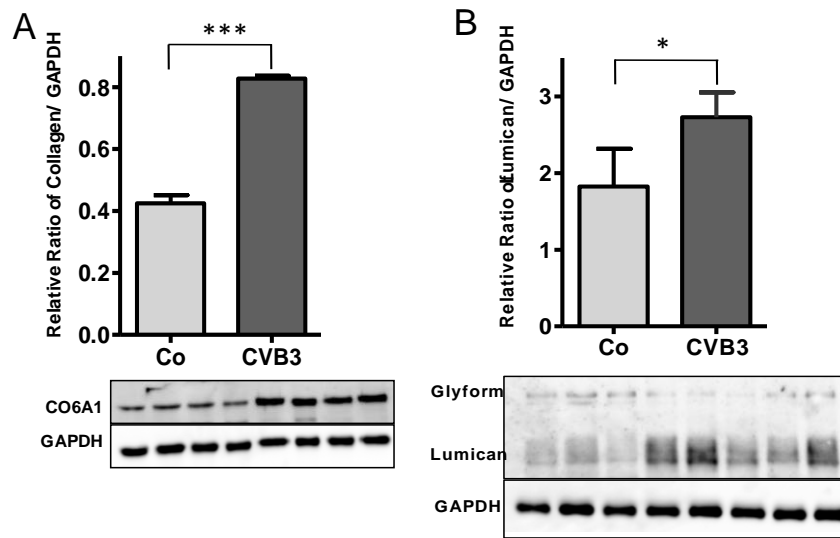


Fig. 22. Validation of fibrosis by western blotting. Western blotting confirmed the increase in extracellular matrix proteins. A-Increase in band intensity was observed for collagen 6 alpha 1 (CO6A1) by densitometry in mouse hearts infected for 84 d. B-Lumican also showed increased intensity in 84 d infected hearts compared to age-matched non-infected controls. Grey bars: control; dark bars: CVB3 infected mice ***- $p < 0.01$, *- $p < 0.1$.

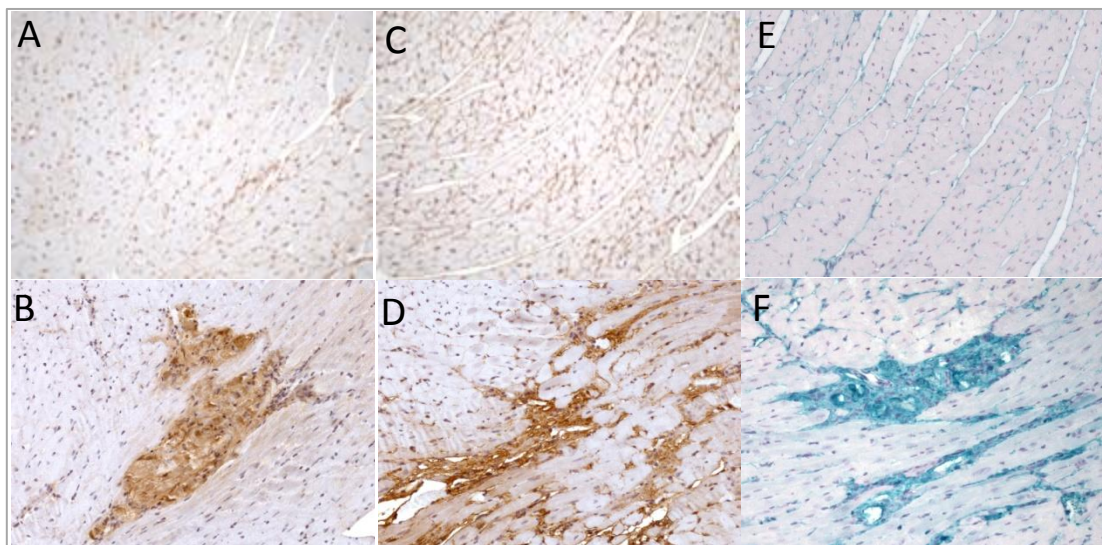


Fig. 23. Validation of fibrosis in hearts of CVB3 infected mice at day 84 p.i. by immunohistochemical staining. Representative tissue sections of hearts from non-infected mice (A, C, E) and from hearts obtained at day 84 p.i. (B, D, F), showing extensive increase of collagen type I (A,B), collagen type VI (C,D), and E,F-lumican in the dilated hearts.

3.2.3. Decreased activities of mitochondrial respiratory chain complexes in A.BY/SnJ mice hearts infected with dilated cardiomyopathy

2D-DIGE and gel-free LC-MS/MS analysis disclosed altered levels of components of complexes I, III and V in dilated hearts from mice at 84 d p.i. Though the majority of proteins decreased in diseased mice pointing to an impaired function of the electron transport chain, the results were not conclusive about the actual potential for ATP generation. Hence to obtain a better understanding of alterations, enzyme activity assays for complexes I-IV of the electron transport chain were performed. The activity assays were performed at the Dept. of Cardiology, Charité, Berlin under the supervision of Dr. Andrea Dörner.

Six animals were considered from each group and the experiments were conducted according to a protocol standardised in the lab (Walther et al., 2007). The activities of the complexes I-IV were observed to have decreased (ratio of means: CI- 0.81, CII-0.77, CIII-0.87, CIV-0.75) in mice infected with CVB3 compared to healthy controls (Fig.24). These experiments confirmed impaired function of electron transport chain.

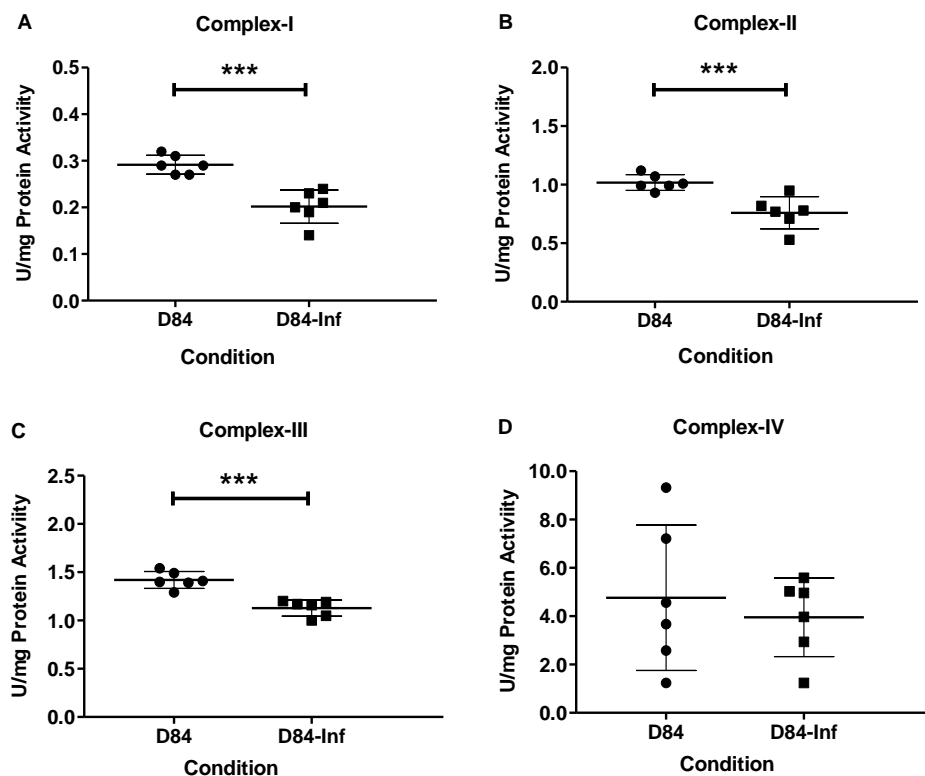


Fig. 24. DCM related changes in the activities of respiratory ETC. A.BY/SnJ mice infected with CVB3 showed decrease in the activities of Complexes I-IV (A-D) of respiratory electron transport chain indicating decreased energy metabolism as a consequence of virus induced dilated cardiomyopathy. Complex I showed 0.69 fold decrease in the activity in infected mice compared to healthy controls. Fold changes of complex II and complex III were 0.75 and 0.80 respectively. Due to high variation in control mice, for complex IV no significant alteration in activity was detected. *** indicate $p < 0.01$.

3.2.4. Phosphorylation of proteins associated to dilated hearts of CVB3 infected A.BY/SnJ mice

Protein phosphorylation is an important post translational modification influencing the function and regulation of proteins. Serine, threonine and tyrosine residues are prone to phosphorylation. Phosphorylation of serine is more widely observed than threonine and tyrosine. With respect to cardiac proteins, phosphorylation is an important event to study. Documented reports exist of phosphorylation of contractile and extracellular matrix proteins in heart. Besides, phosphorylation is also known to influence signalling pathways such as integrin and AKT signalling. Hence in order to study the changes in protein phosphorylation due to CVB3 infection, 2DE was employed with subsequent fluorescence staining. Selected spots were subjected to mass spectrometry analyses.

100µg of pooled sample each from mouse hearts infected for 84 d and non-infected hearts (n=4) were separated using two dimensional gel electrophoresis in the pI range 4-7. The gels were then stained overnight with ProQ diamond as described in 2.3.1. which specifically stains the phosphorylated proteins. Subsequently, the gels were stained with Sypro Ruby stain to detect the total cardiac protein (Fig.25).

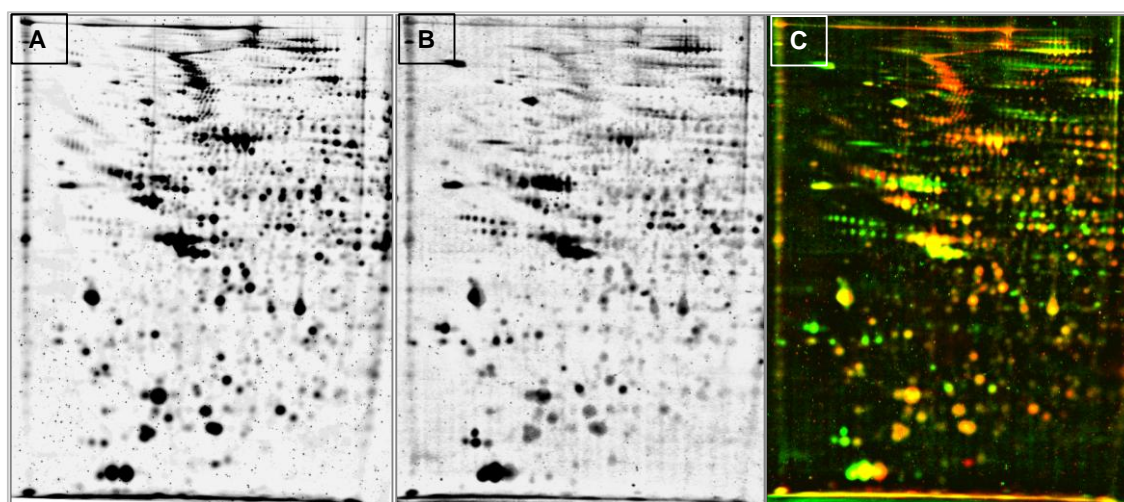


Fig. 25. Identification of phosphorylated proteins by ProQ staining. Representative image documenting the phosphorylation of proteins. A-Total heart protein pattern shown by Sypro ruby staining shows more spots. B-Staining of phosphorylated proteins by ProQ staining. C-Dual channel overlay of Sypro and ProQ stained images. Spots in red represent total protein staining Sypro image and spots in green represent probably phosphorylated proteins displaying higher signal intensity in the ProQ image than in the Sypro Ruby image.

For cutting and identification of the proteins in spots with specific staining by ProQ, three Coomassie stained preparative gels were prepared. Although a higher protein amount was loaded on the gel, only thirty four of the selected spots were visible in the Coomassie stained gel and were further processed. Twenty out of thirty four spots were identified using neutral loss method as mentioned in Materials & Methods (2.3.2.). Of these, phosphorylated peptides were observed for six proteins confirming phosphorylation of the proteins. Heat shock protein 90 beta (HS90B), heat shock protein beta-1 (HSPB1), myosin regulatory light chain 2, ventricular/cardiac muscle isoform (MLRV), myosin light chain, atrial isoform (MLRa), actin, aortic smooth muscle (ACTA), 2-oxoisovalerate dehydrogenase subunit alpha, mitochondrial (ODBA) and phosphoglucomutase-1(PGM1) were identified as phosphorylated. HSPB1 (1.15), HS90B (1.24), MLRv (1.30) and ACTA (1.23) displayed an increase in phosphorylation whereas ODBA (0.37) and PGM1 (0.71) displayed decrease in phosphorylation in diseased hearts compared to healthy controls. Two phosphorylated peptides with serine (S1) and threonine (T6) phosphorylations were identified for protein ODBA whereas two peptides with phosphorylated serine (S3) were identified for PGM1. In MLRv, two serines, S6 and S10 were identified as phosphorylated on the same peptide and tyrosine (Y3) was identified as phosphorylated in ACTA (Table 19). The remaining identified proteins for which phosphorylation could not be confirmed are listed in the appendix (A3.2.4)

The low number of identified phosphorylation sites can be explained by the concentration of phosphorylated proteins on the gel. The majority of the spots excised were faint and hence though the protein could be identified, the phosphorylated peptides couldn't be assigned. Enrichment of the phosphopeptides and identification by gel-free LC-MS/MS analysis might increase the access to the phospho sites resulting in increased number of identifications of phosphorylation sites. Unfortunately such experiments couldn't be performed in the framework of the current study.

The current study reports the changes in phosphorylation of proteins in chronic stages of Cocksackie viral infection where dilated cardiomyopathy sets in. This is in correlation with earlier reported protein phosphorylation during early stages of viral myocarditis in A.BY/SnJ mice (Hammer et al., 2010). MLRv was identified to show an increase in phosphorylation in A.BY mouse hearts 28 d p.i. and the trend appears to continue into the chronic stages of infection/dilated cardiomyopathy.

Table 19. Proteins displaying changes in phosphorylation in mouse hearts infected with CVB3 for 84 d compared to age-matched non-infected control hearts

Swissprot Entry name	Protein Annotation	Phosphorylated peptide	Phospho site	Ratio	MH+	monoisotopic m/z	ΔCn	Xcorr	pRS probability	pRS Score
HS90B_MOUSE	Heat shock protein β 1	EKEI s DDDEAEEK	S(5) Phospho	1.24	1630.6375	815.8223	0.000	4.06	100%	111
		IEDV G sDEEDDSGKDKK	S(6) Phospho		1945.7925	973.3999	0.000	2.54	100%	132
MLRV_MOUSE	Myosin regulatory light chain 2, ventricular/cardiac muscle isoform	IEGG s SNVFSmFEQTQIQEFK	S(6) Phospho	1.30	2658.1933	886.73596	0.000	5.61	93.20%	133
		IEGGSSNVF s mFEQTQIQEFK	S(10) Phospho		2502.094	834.7028	0.063	5.49	89.60%	144
ACTA_MOUSE	Actin, aortic smooth muscle	QE y DEAGPSIVHR	Y(3) Phospho	1.23	1580.6675	790.8374	0.000	2.73	100%	63
ODBA_MOUSE	2-oxoisovalerate dehydrogenase subunit alpha, mitochondrial	IGHHS t SDDSSAYR	T(6) Phospho	0.37	1612.6407	806.824	0.054	3.3	86%	80
		s VDEVNYWDK	S(1) Phospho		1334.5334	667.7703	0.000	2.98	100%	120
HSPB1_MOUSE	Heat shock protein beta-1	QL s SGVSEIR	S(3) Phospho	1.15	1155.5425	578.2749	0.000	2.67	99.80%	90
		SP s WEPFR	S(3) Phospho		1085.4457	543.2265	0.000	2.38	99.70%	42
PGM1_MOUSE	Phosphoglucosyltransferase-1	AIGGIIL T A s HNPGGPNGDFGIK	S(10) Phospho	0.71	2286.1292	762.7146	0.000	4.65	95.70%	57

Ratio- intensity of phosphorylated spots in 84d p.i./intensity of phosphorylated spots in 84d (control)

3.3. Age related changes in the protein profile of non-infected A.BY/SnJ mice hearts

Virus-induced myocarditis and subsequent dilated cardiomyopathy progress over a period of 90 days (Klingel et al., 1992) during which the mice also age. Since aging is one of the important factors contributing to heart diseases, studying the age related changes in healthy non-infected mouse hearts is also of interest. To understand the changes in the proteome profile of aging hearts, proteomic analyses was performed for hearts of 4 months old mice in comparison to those of 1 month old mice (controls) using 2D-DIGE and gel free LC-MS/MS analysis as described earlier.

3.3.1. 2D-DIGE analysis of age dependent changes in the proteome profile of mouse hearts

Quantitative analysis by Delta2D and Genespring software showed 176 spots passing one-way ANOVA with $p < 0.05$ and fold difference of > 1.5 representing age related changes out of 1683 spots. Fifty eight spots showed higher intensities in 4 months old hearts whereas one hundred and eighteen spots showed lower intensities compared to 1 month old controls.

The spots were excised from three silver stained preparative gels and were subjected to mass spectrometric analysis using an LTQ-Orbitrap XL mass spectrometer after overnight trypsin digestion as described in the material and methods section. A representative gel image displaying locations of the identified spots is shown below (Fig. 26). In total, eighty six spots were identified which accounted for forty eight distinct proteins (Table 20). Forty out of fifty eight spots showing increased intensity and forty six of one hundred eighteen spots showing decreased intensity with aging of mice were identified.

The low proportion of identifications in spots with decreased intensity in the 4 months hearts can be attributed to two factors namely- the spots being very faint on the gel and the high abundance of myosin-6 (MYH6) degradation fragments widely distributed on the gel. This was evident from the fact that 27 of the 46 spots repressed in 4 months hearts were identified to be MYH6. It can also be that the high abundance of MYH6 degradation products on the gel masked the identification of other low abundant proteins.

pI 4.0

pI 7.0

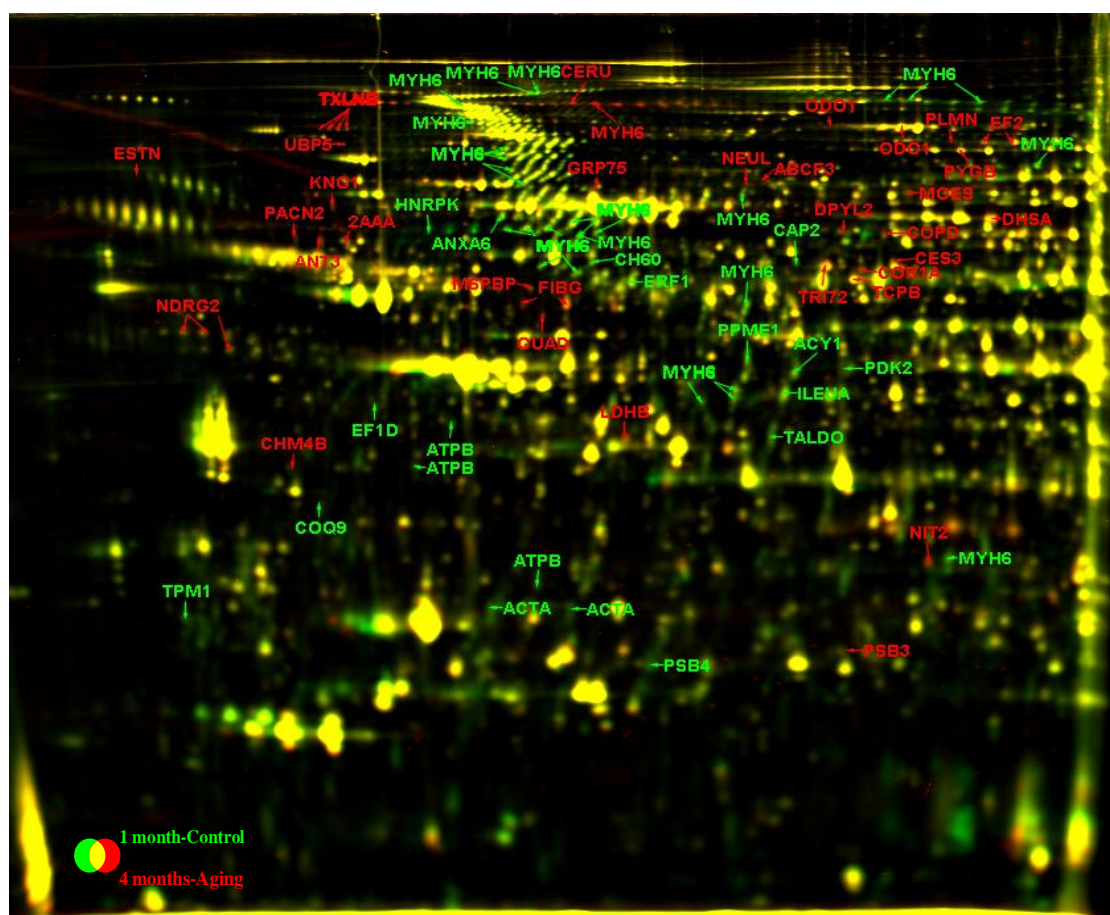


Fig. 26. Dual channel overlay displaying a comparison of protein patterns of hearts of 4 months and 1 month old mice. Protein spots in red and green colour indicate increased and decreased intensities of protein spots during aging and the spots in yellow indicate proteins that do not show significant changes within the comparison. Labels in red indicate the identified proteins for spots with increased intensity, and labels in green indicate protein identifications for the spots observed at lower intensities.

Eight proteins—elongation factor 2 (EF-2), beta-taxilin (TXLNB), fibrinogen gamma (FIBG), protein NDRG2 (NDRG2), 2-oxoglutarate dehydrogenase (ODO1), and actin, aortic smooth muscle isoform (ACTA) were identified in more than one spot on the gel. These proteins were identified in the same molecular weight range as their predicted mass and hence cannot be considered as degradation products. However, one particular protein ATP synthase β subunit, mitochondrial (ATPB) was identified as multiple spots in the lower molecular weight region. It appears that truncation of this protein occurs in hearts of younger mice which was not as prominent in older ones.

Table 20. Proteins displaying age dependent intensity changes in hearts of 4 months old mice in comparison to those of 1 month old mice identified from 2D-DIGE

Swissprot Entry	Acc no.	Protein Annotation	Spot-ID	Peptide Count	Seq. Coverage (%)	Fold Change	Direction	p-Value	Protein Score	CV 1Month	CV 4Months	CV*
Cytoplasm												
P58252	EF2	Elongation factor 2	2 spots	14	16.3	3.0-5.0	↑	6.88E-03	140.20	38.72	9.11	55.23
Q9WVE8	PACN2	Protein kinase C and casein kinase substrate in neurons protein 2	ID374568	5	10.5	3.6	↑	4.42E-02	50.16	67.93	42.40	82.88
Q9JHW2	NIT2	Nitrilase homolog 2	ID106905	6	29	2.1	↑	6.99E-03	60.23	23.58	9.37	35.38
O08553	DPYL2	Dihydropyrimidinase-related protein 2	ID106504	10	20.3	2.0	↑	3.58E-02	100.23	31.85	26.83	43.83
P80314	TCPB	T-complex protein 1 subunit beta	ID106568	9	19.6	2.0	↑	9.30E-05	90.25	6.56	5.25	32.43
Q9DBG5	PLIN3	Mannose-6-phosphate receptor-binding protein 1	ID106596	10	17.6	2.0	↑	3.58E-02	100.23	32.33	16.78	36.05
Q76MZ3	2AAA	Serine/threonine-protein phosphatase 2A 65 kDa regulatory subunit A alpha isoform	ID106526	10	16.8	1.9	↑	8.93E-03	100.28	21.94	10.01	35.93
Q9R1P1	PSB3	Proteasome subunit beta type-3	ID106979	5	22.4	1.7	↑	4.34E-02	50.23	23.86	9.34	24.47
Q9D8B3	CHM4B	Charged multivesicular body protein 4b	ID236029	5	20.1	1.6	↑	1.32E-02	50.22	20.75	20.13	32.65
O89053	COR1A	Coronin-1A	ID120818	12	21	1.6	↑	1.57E-02	120.17	10.94	15.92	27.07
Q5XJY5	COPD	Coatmer subunit delta	ID106498	7	12.9	1.6	↑	1.35E-02	70.20	11.84	16.51	26.94
P16125	LDHB	L-lactate dehydrogenase B chain	ID171779	9	27.2	1.5	↑	3.18E-03	90.20	10.96	6.15	19.54
Q9QYG0	NDRG2	Protein NDRG2	3 spots	3	0.097	1.5	↑	8.98E-03	0.00	13.42	12.77	23.12
Q99JW2	ACY1	Aminoacylase-1	ID106719	5	17.9	0.7	↓	2.62E-03	50.21	12.40	18.79	35.80
Q8BWY3	ERF1	Eukaryotic peptide chain release factor subunit 1	ID106578	8	19.9	0.6	↓	2.32E-03	80.19	12.55	8.93	31.19
P58771	TPM1	Tropomyosin alpha-1 chain	ID106970	5	13.7	0.6	↓	1.73E-03	46.20	14.61	14.76	35.85
Q9D154	ILEUA	Leukocyte elastase inhibitor A	ID106744	11	24.5	0.6	↓	3.22E-03	110.21	11.70	15.88	33.91
P99026	PSB4	Proteasome subunit beta type-4	ID283773	2	5.7	0.5	↑	1.93E-03	20.21	18.55	7.72	42.67
P14824	ANXA6	Annexin A6	ID652661	25	34.5	0.5	↓	8.95E-03	250.28	21.87	18.36	44.74
Q93092	TALDO	Transaldolase	ID106797	5	16.9	0.5	↓	8.13E-03	50.16	19.12	10.50	43.64
P62737	ACTA	Actin, aortic smooth muscle	2 spots	4	11.9	0.5	↓	2.03E-04	40.16	13.99	13.82	44.59
Q02566	MYH6	Myosin-6	28 spots	5	2.8	0.4	↓	1.24E-02	50.17	91.23	34.48	138.87
P61979	HNRPK	Heterogeneous nuclear ribonucleoprotein K	ID106517	9	15.8	0.1	↓	1.57E-02	90.23	42.51	107.78	104.33

Swissprot Entry	Acc no.	Protein Annotation	Spot-ID	Peptide Count	Seq. Coverage (%)	Fold Change	Direction	p-Value	Protein Score	CV 1Month	CV 4Months	CV*
Mitochondria												
Q8K2B3	DHSA	Succinate dehydrogenase [ubiquinone] flavoprotein subunit	ID106429	11	16.6	2.9	↑	3.03E-03	110.23	6.76	22.42	57.11
Q91YP2	NEUL	Neurolysin	ID307182	7	11.8	1.9	↑	1.98E-02	70.20	25.92	10.12	29.09
P38647	GRP75	Stress-70 protein	ID133104	16	29.2	1.5	↑	1.54E-02	160.27	20.55	9.40	25.21
Q60597	ODO1	2-oxoglutarate dehydrogenase E1 component	2 spots	10	0.12	1.5	↑	4.46E-03	0.00	12.70	8.82	21.82
Q9JK42	PDK2	Pyruvate dehydrogenase [lipoamide] kinase isozyme 2	ID176784	8	25.3	0.7	↓	1.35E-02	78.26	13.54	12.11	27.34
Q8K1Z0	COQ9	Ubiquinone biosynthesis protein COQ9	ID114165	3	8.3	0.6	↓	1.84E-02	30.18	25.31	9.89	42.75
P63038	CH60	60kDa heat shock protein	ID624781	12	22.9	0.5	↓	2.31E-02	120.26	27.40	7.87	47.92
P56480	ATPB	ATP synthase subunit beta	3 spots	10	17.6	0.4	↓	4.13E-04	100.21	17.22	13.65	51.46
Endoplasmic Reticulum												
Q8VCT4	CES3	Carboxylesterase 3	ID310987	4	7.6	2.0	↑	4.62E-02	40.17	6.22	39.62	53.15
P23953	EST1C	Liver carboxylesterase N	ID106359	6	12.8	1.9	↑	5.63E-03	60.19	17.64	17.40	36.85
Cell Membrane												
Q1XH17	TRI72	Tripartite motif-containing protein 72	ID106550	15	28.9	1.7	↑	3.33E-03	150.24	7.80	19.64	31.74
P26041	MOES	Moesin	ID653997	15	19.1	1.6	↑	2.88E-02	150.26	20.82	15.44	27.52
Q9CYT6	CAP2	Adenylyl cyclase-associated protein 2	ID122705	7	14.7	0.6	↓	4.31E-02	70.20	29.39	25.48	47.29
Secreted/Extracellular Matrix												
P32261	ANT3	Antithrombin-III	ID106524	10	27.7	4.0	↑	1.90E-02	100.21	56.33	24.29	69.34
Q8VCM7	FIBG	Fibrinogen gamma chain	2 spots	16	40.6	2.4-3.6	↑	6.78E-05	160.27	9.53	13.46	44.20
P20918	PLMN	Plasminogen	ID612408	15	19.8	2.5	↑	4.28E-03	150.27	26.54	17.08	49.38
O08677	KNG1	Kininogen-1	ID106457	7	10.7	2.2	↑	1.96E-02	70.22	31.41	21.73	44.68
Q61147	CERU	Ceruloplasmin	ID106156	18	14.1	1.9	↑	1.05E-02	180.21	16.38	21.98	38.22

Swissprot Entry	Acc no.	Protein Annotation	Spot-ID	Peptide Count	Seq. Coverage (%)	Fold Change	Direction	p-Value	Protein Score	CV 1Month	CV 4Months	CV*
Unclassified												
Q8VBT1	TXLNB	Beta-taxilin	4 spots	19	21.9	2.0-3.0	↑	1.61E-02	190.23	31.98	6.88	42.40
Q8K268	ABCF3	ATP-binding cassette sub-family F member 3	ID106401	7	11.7	1.8	↑	7.40E-03	70.22	14.14	18.35	33.78
Q9R111	GUAD	Guanine deaminase	ID137693	12	26.9	1.8	↑	4.23E-02	120.22	32.03	5.63	33.72
P56399	UBP5	Ubiquitin carboxyl-terminal hydrolase 5	ID371765	7	10	1.7	↑	7.41E-03	70.21	10.90	20.54	34.28
Q8CI94	PYGB	Glycogen phosphorylase, brain form	ID106268	8	0.077	1.6	↑	5.53E-04	0.00	7.86	9.71	25.64
P57776	EF1D	Elongation factor 1- delta	ID106771	7	22.1	0.5	↓	4.20E-03	70.20	25.78	21.98	50.66
Q8BVQ5	PPME1	Protein phosphatase methyl esterase 1	ID106704	9	17.1	0.4	↓	1.45E-02	90.20	26.92	25.83	51.19

*Acc.no-Accession number * CV- Coefficient of variation, Fold change- protein intensity ratio of 4 months old mouse hearts to 1 month old control hearts, Direction- age associated increase (↓) or decrease (↑) in protein levels

3.3.2. Gel free LC-MS/MS analysis of age dependent changes in the proteome profile of mice heart

Heart protein extracts (2µg) from individual animals of each group 4 months and 1 month old mice were digested initially with Lys C (1:100) for 3h and trypsin (1:10) was then added for overnight (16h) digestion at 37°C. A total of 357 proteins with at least two unique peptides per protein were identified by LTQ-Orbitrap XL mass spectrometer. Around 38% of the proteins identified have pI>7 which falls beyond the pI range of 2D-DIGE used and hence helped to improve the protein coverage. Also 94 of the identified proteins belong to either cell-, mitochondrial-, endoplasmic- or cytoplasmic- membrane (Fig.27A).

For quantitation of the proteins by spectral counting, the assigned spectra for the proteins were considered and a normalization factor was calculated as described earlier (section 2.2.8.4). Proteins with sum of the spectra ≥ 6 in at least one of the two conditions were considered for quantitation which resulted in 310 proteins out of 357 suitable for quantitation (Appendix A3.3.2). The proteins were then filtered for those passing student's *t*-test with $p \leq 0.1$ and ratio of means ≥ 1.2 . Fifty eight proteins showed significant changes in their levels due to aging (Table 21). 43% of the regulated proteins were either hydrophobic membrane proteins or had pI > 7 (Fig.27B).

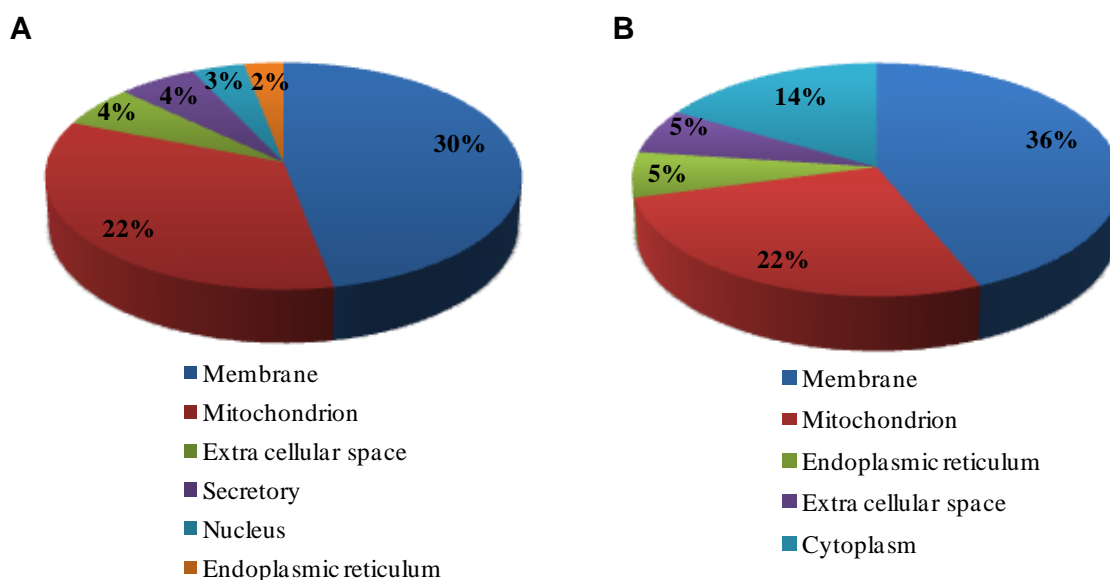


Fig. 27. Subcellular location of proteins covered by gel free LC-MS/MS analysis. The largest fraction of the proteins identified by gel free analysis are membrane proteins which includes outer- and inner mitochondrial membrane, cytoplasmic- and ER membrane. A-subcellular location of total proteins quantified (310). B-subcellular location of proteins displaying altered levels (58).

Table 21. Proteins displaying age dependent changes in hearts of 4 months old mice in comparison to those of 1 month old mice identified from gel-free analysis

Swissprot Entry	Protein Annotation	Acc. No	Mol.Wt	pI	No. of peptides	Sum of Norm. Spectra		Seq. Coverage (%)	Fold Change	Direction	p-value	Coeff. Of Var (CV)	
						4months	1Month					4Months	1Month
Mitochondria (incl. inner and outer membrane)													
BDH	D-beta-hydroxybutyrate dehydrogenase	Q80XN0	38 kDa	8.62	4	2.00	18.30	18%	12.2	↑	3.08E-03	0.00	35.58
ODBA	2-oxoisovalerate dehydrogenase subunit alpha	P50136	50 kDa	6.05	3	3.16	7.05	10%	3.0	↑	3.14E-02	73.42	35.15
IDH3G	Isocitrate dehydrogenase [NAD] subunit gamma	P70404	43 kDa	8.66	2	7.48	15.45	13%	2.8	↑	3.27E-02	74.15	30.69
NDUB9	NADH dehydrogenase [ubiquinone] 1 beta subcomplex subunit 9	Q9CQJ8	22 kDa	7.84	2	10.56	18.60	27%	2.3	↑	8.40E-02	100.92	16.76
NDUA9	NADH dehydrogenase [ubiquinone] 1 alpha subcomplex subunit 9	Q9DC69	43 kDa	9.48	3	13.76	21.15	14%	2.0	↑	9.85E-02	80.55	20.44
COX6C	Cytochrome c oxidase subunit 6C	Q9CPQ1	8 kDa	10.13	3	9.74	14.85	26%	2.0	↑	8.86E-02	77.94	16.69
CPT1B	Carnitine palmitoyl transferase 1B	Q924X2	88 kDa	8.65	6	15.52	21.75	8%	1.9	↑	4.80E-02	19.92	34.56
ACS2L	Acetyl-coenzyme A synthetase 2-like	Q99NB1	75 kDa	5.98	6	16.54	20.40	14%	1.6	↑	2.45E-03	19.35	0.00
MMSA	Methylmalonate-semialdehyde dehydrogenase	Q9EQ20	58 kDa	7.02	8	24.51	29.85	15%	1.6	↑	3.30E-02	31.32	13.57
CPT2	Carnitine palmitoyl transferase 2	P52825	74 kDa	7.95	6	18.99	22.50	14%	1.6	↑	4.95E-02	7.17	28.94
NDUBA	NADH dehydrogenase [ubiquinone] 1 beta subcomplex subunit 10	Q9DCS9	21 kDa	8.36	4	35.06	40.95	32%	1.6	↑	5.57E-02	20.34	25.21
MPCP	Phosphate carrier protein	Q8VEM8	40 kDa	9.11	6	43.41	49.50	20%	1.5	↑	1.21E-02	21.02	7.35
ETFD	Electron transfer flavoprotein-ubiquinone oxidoreductase	Q921G7	68 kDa	6.47	11	48.33	54.30	20%	1.5	↑	6.81E-03	13.81	10.66
ACOT2	Acyl-coenzyme A thioesterase 2	Q9QYR9	50 kDa	6.14	3	11.01	11.85	7%	1.4	↑	8.24E-02	33.04	6.58
NNTM	NAD(P) transhydrogenase	Q61941	114 kDa	6.45	10	58.14	62.55	13%	1.4	↑	3.41E-02	15.67	17.06
ODO1	2-oxoglutarate dehydrogenase E1 component	Q60597	116 kDa	6.05	20	119.28	124.35	26%	1.4	↑	5.47E-02	21.62	13.34
AT5F1	ATP synthase subunit b	Q9CQQ7	29 kDa	8.55	5	28.21	28.95	15%	1.4	↑	2.18E-02	15.54	9.71
CMC1	Calcium-binding mitochondrial carrier protein Aralar1	Q8BH59	75 kDa	8.43	8	36.81	36.60	19%	1.3	↑	5.18E-02	16.68	12.78
ATPA	ATP synthase subunit alpha	Q03265	60 kDa	8.28	22	872.14	541.50	50%	0.8	↓	1.33E-02	6.52	6.23
ATPD	ATP synthase subunit delta	Q9D3D9	18 kDa	4.46	2	39.39	24.30	14%	0.8	↓	7.53E-03	3.88	8.55
VDAC1	Voltage-dependent anion-selective channel protein 1	Q60932	32 kDa	8.55	8	95.84	59.10	33%	0.8	↓	3.53E-02	10.35	2.64
NDUA7	NADH dehydrogenase [ubiquinone] 1 alpha subcomplex subunit 7	Q9Z1P6	13 kDa	10.17	3	43.82	26.10	28%	0.8	↓	7.61E-03	7.96	1.99

Swissprot Entry	Protein Annotation	Acc. No	Mol.Wt	pI	No. of peptides	Sum of Norm. Spectra		Seq. Coverage (%)	Fold Change	Direction	p-value	Coeff. Of Var (CV)	
						4months	1Month					4Months	1Month
Mitochondria (continued)													
IMMT	Mitochondrial inner membrane protein	Q8CAQ8	84 kDa	6.18	13	97.73	57.60	17%	0.8	↓	6.93E-02	12.08	15.65
NDUA4	NADH dehydrogenase [ubiquinone] 1 alpha subcomplex subunit 4	Q62425	9 kDa	9.52	3	67.82	39.90	37%	0.8	↓	5.36E-02	10.65	15.35
ATPO	ATP synthase subunit O	Q9DB20	23 kDa	9.8	7	110.04	64.05	50%	0.8	↓	9.99E-02	15.99	15.54
ATP5H	ATP synthase subunit d	Q9DCX2	19 kDa	5.53	11	202.24	110.70	66%	0.7	↓	8.59E-02	20.71	8.99
CH60	60 kDa heat shock protein	P63038	61 kDa	5.35	15	159.56	85.95	33%	0.7	↓	5.81E-02	17.55	14.36
CYC	Cytochrome c, somatic	P62897	12 kDa	9.61	5	151.65	73.35	49%	0.6	↓	2.11E-02	18.07	1.97
PHB	Prohibitin	P67778	30 kDa	5.57	3	24.53	11.85	10%	0.6	↓	5.06E-02	23.23	6.58
ODPB	Pyruvate dehydrogenase E1 component subunit beta	Q9D051	39 kDa	5.39	9	126.89	58.80	34%	0.6	↓	1.48E-02	14.89	19.01
ECH1	Delta(3,5)-Delta(2,4)-dienoyl-CoA isomerase	O35459	36 kDa	6.01	4	30.91	13.80	20%	0.6	↓	6.69E-02	28.91	9.96
COQ9	Ubiquinone biosynthesis protein C	Q8K1Z0	35 kDa	4.93	4	31.72	13.95	13%	0.6	↓	8.91E-02	30.33	28.18
CX7A1	Cytochrome c oxidase polypeptide 7A1	P56392	9 kDa	8.71	2	33.80	10.35	29%	0.4	↓	1.44E-02	8.23	77.82
NDUB4	NADH dehydrogenase [ubiquinone] 1 beta subcomplex subunit 4	Q9CQC7	15 kDa	9.89	2	25.68	6.90	27%	0.4	↓	7.14E-03	9.41	78.26
Cytoplasm													
GDIB	Rab GDP dissociation inhibitor beta	Q61598	51 kDa	5.93	4	3.16	9.15	11%	3.9	↑	5.18E-03	73.42	22.54
ACTS	Actin, alpha skeletal muscle	P68134	42 kDa	5.23	12	509.27	651.60	51%	1.7	↑	1.37E-02	20.40	17.75
TERA	Transitional endoplasmic reticulum ATPase	Q01853	89 kDa	5.14	11	33.24	35.25	13%	1.4	↑	9.94E-02	28.10	17.55
PEBP1	Phosphatidylethanolamine-binding protein 1	P70296	21 kDa	5.19	7	52.04	50.70	64%	1.3	↑	8.32E-02	20.38	10.85
DESM	Desmin	P31001	53 kDa	5.21	23	234.48	146.25	51%	0.8	↓	3.16E-02	8.11	7.64
ALDR	Aldose reductase	P45376	36 kDa	6.79	4	23.48	12.75	11%	0.7	↓	3.38E-02	12.95	16.17
TAGL	Transgelin	P37804	23 kDa	8.86	2	20.22	10.95	12%	0.7	↓	6.50E-02	18.56	12.33
PGK1	Phosphoglycerate kinase 1	P09411	45 kDa	8.02	6	49.78	18.30	15%	0.5	↓	3.42E-02	28.12	24.75
Cell Membrane													
CD36	Platelet glycoprotein 4	Q08857	53 kDa	8.61	2	12.41	21.15	6%	2.3	↑	2.56E-02	56.93	20.44
EHD4	EH domain-containing protein 4	Q9EQP2	61 kDa	6.33	6	28.18	14.70	9%	0.7	↓	2.01E-02	15.18	3.53

Swissprot Entry	Protein Annotation	Acc. No	Mol.Wt	pI	No. of peptides	Sum of Norm. Spectra		Seq. Coverage (%)	Fold Change	Direction	p-value	Coeff. Of Var (CV)	
						4months	1Month					4Months	1Month
Cell Membrane													
CD36	Platelet glycoprotein 4	Q08857	53 kDa	8.61	2	12.41	21.15	6%	2.3	↑	2.56E-02	56.93	20.44
EHD4	EH domain-containing protein 4	Q9EQP2	61 kDa	6.33	6	28.18	14.70	9%	0.7	↓	2.01E-02	15.18	3.53
Endoplasmic Reticulum													
CACP	Carnitine O-acetyl transferase	P47934	71 kDa	8.63	6	30.44	33.75	15%	1.5	↑	5.66E-03	6.26	13.49
PDIA1	Protein disulfide-isomerase	P09103	57 kDa	4.75	2	12.11	2.55	6%	0.3	↓	2.44E-02	34.50	71.32
Extracellular Matrix													
LAMA2	Laminin subunit alpha-2	Q60675	343 kDa	5.77	9	22.41	32.70	3%	1.9	↑	5.37E-02	63.26	4.20
CO1A2	Collagen alpha-2(I) chain	Q01149	130 kDa	10	4	72.45	25.20	3%	0.5	↓	5.58E-02	35.05	27.28
CO1A1	Collagen alpha-1(I) chain	P11087	138 kDa	9.28	2	36.89	12.00	2%	0.4	↓	1.14E-02	20.74	37.00
Nucleus													
LMNA	Lamin-A/C	P48678	74 kDa	6.54	4	41.68	9.60	4%	0.3		1.81E-02	28.29	74.41
Uncategorised													
ARHL1	[Protein ADP-ribosylarginine] hydrolase-like protein 1	Q8BGK2	40 kDa	5.62	3	4.58	12.15	13%	3.5	↑	3.87E-02	112.66	36.35
MYG	Myoglobin	P04247	17 kDa	7.23	9	186.77	299.25	61%	2.1	↑	3.46E-03	35.02	6.70
HBA	Hemoglobin subunit alpha	P01942	15 kDa	8.08	6	384.52	395.25	43%	1.4	↑	7.99E-02	24.48	13.17
HBB1	Hemoglobin subunit beta-1	P02088	16 kDa	7.26	5	201.95	189.60	39%	1.3	↑	5.71E-02	15.31	7.84
PGAM2	Phosphoglycerate mutase 2	O70250	29 kDa	8.65	6	63.21	39.45	21%	0.8	↓	5.53E-02	7.83	12.20
TNNT2	Troponin T, cardiac muscle	P50752	36 kDa	4.98	6	110.80	61.35	20%	0.7	↓	8.99E-02	17.70	18.97
ANXA5	Annexin A5	P48036	36 kDa	4.83	5	27.45	11.85	17%	0.6	↓	7.64E-02	32.06	6.58

*Norm. spectra-Normalized spectra, Fold change- mean spectral count ratio of 4 months old mouse heart proteins to 1 month old control hearts, Direction- age associated increase (↑) or decrease (↓) in protein levels

A majority of mitochondrial proteins were found with altered levels in the hearts of four months old mice compared to younger animals. Proteins involved in lipid metabolism and transport such as carnitine O-palmitoyltransferase 1, muscle isoform (CPT1B), carnitine O-palmitoyltransferase 2, mitochondrial (CPT2), carnitine O-acetyltransferase (CACP), acetyl-coenzyme A synthetase 2-like, mitochondrial (ACS2L), and D-beta-hydroxybutyrate dehydrogenase, mitochondrial (BDH) were identified in higher amounts in 4 months old animals compared to 1 month old ones. Particularly, BDH was observed at very high levels with a ratio of spectral means of approximately 12. Furthermore, a number of components of respiratory electron transport chain like NADH dehydrogenase [ubiquinone] 1 beta subcomplex subunit 4 (NDUB4), subunit 9 (NDUB9), subunit 10 (NDUBA), NADH dehydrogenase [ubiquinone] 1 alpha subcomplex subunit 9, mitochondrial (NDUA9) of complex I, cytochrome c, somatic (CYC), cytochrome c oxidase polypeptide 7A1, mitochondrial (CX7A1), ATP synthase subunit alpha, mitochondrial (ATPA) and ATP synthase subunit delta, mitochondrial (ATPD) were observed at higher levels in hearts of 4 months old mice. In contrast, proteins CX7A1, CYC, ATPA, and ATPD were observed at decreased amounts in these animals. The results for complex I subunits were inconclusive with NDUB4 identified at lower amounts, whereas NDUB9, NDUBA and NDUA were identified at higher amounts in hearts 4 months of age. All together, these findings indicate impaired mitochondrial function. Other proteins like Rab GDP dissociation inhibitor beta (GDIB), protein disulfide-isomerase (PDIB), lamin-A/C (LMNA), and 78 kDa glucose-regulated protein (GRP78) were among those which showed strong alterations due to aging in 4 months old animals compared to younger mice.

3.3.3. Comprehensive analysis of the data of the 2D-DIGE and gel free LC-MS/MS analysis

After removing the redundant hits, proteins from both 2D-DIGE and gel-free analyses were loaded together into the PANTHER software suite for the prediction of functional significance. Protein transport (17), lipid metabolism (19), carbohydrate metabolism (15), cell morphogenesis (13), and respiratory electron transport chain (12) were among protein classes significantly altered due to aging (Fig.28).

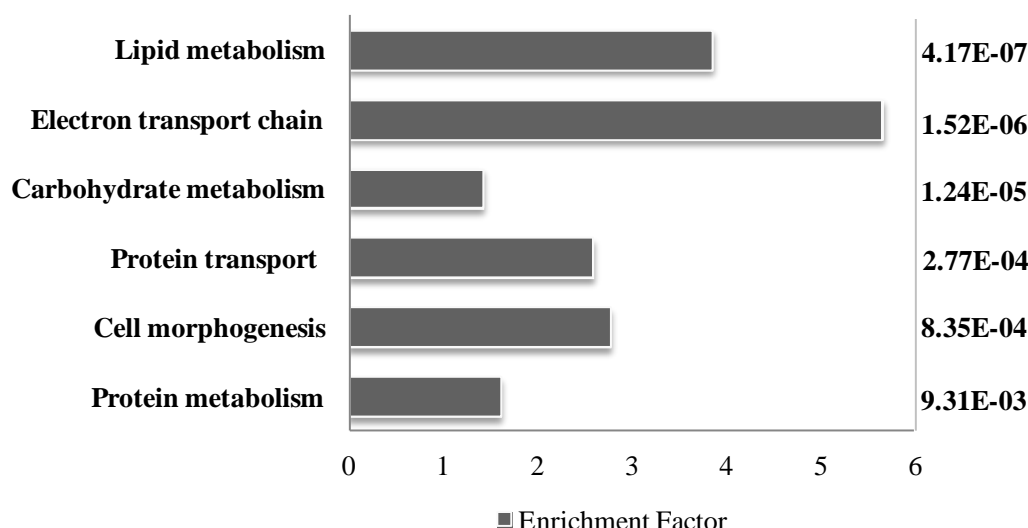


Fig. 28. Cardiac protein classes displaying age-related alterations in intensity. Functional classification of the identified proteins was done using the PANTHER software suite. The enrichment factor for the protein class is calculated by taking the ratio of the number of expected genes (PANTHER) to the number of identified proteins per class of protein. p-value as given by PANTHER (www.pantherdb.org).

Proteins with a function in intracellular transport such as beta-taxilin (TXLNB), Rab GDP dissociation inhibitor beta (GDIB), and [protein ADP-ribosylarginine] hydrolase-like protein 1 (ARHL1) were identified at very high levels in old mouse hearts. Proteins tripartite motif 72 (TRI72), coronin-1A (COR1A), and transitional endoplasmic reticulum ATPase (TERA)/valosin containing protein also involved in protein transport showed significantly higher levels in older mice.

Proteins belonging to the inner or outer mitochondrial membrane and mitochondrial matrix proteins involved in lipid metabolism and respiratory electron transport chain also showed significant changes in their levels. Carnitine-O-palmitoyltransferase 1, muscle isoform (CPT1B), carnitine-O-palmitoyltransferase 2, mitochondrial (CPT2), carnitine-O-acetyltransferase (CACP), D-beta-hydroxybutyrate dehydrogenase, mitochondrial (BDH), acetyl-coenzyme A synthetase 2-like, mitochondrial (ACS2L) involved in lipid metabolism were identified in higher amounts in older mice compared to younger ones (Fig. 29).

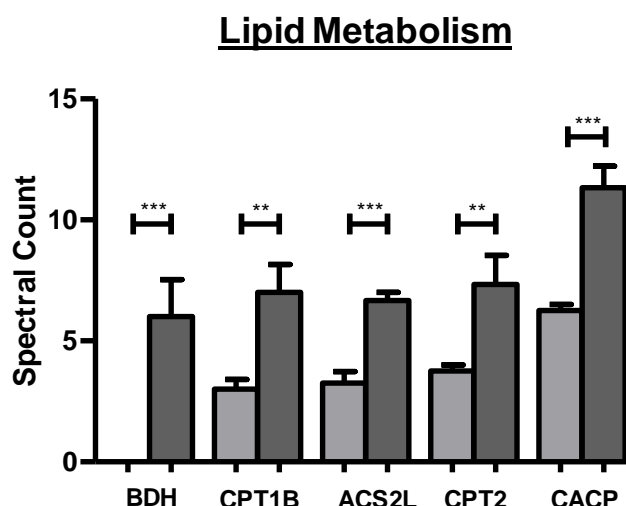


Fig. 29. Age dependent increase in abundance of proteins involved in lipid metabolism. High levels of proteins involved in lipid metabolism were observed in hearts of 4 months old mice in comparison to those of 1 month old animals suggesting increased energy production by lipid metabolism. Protein abundance in hearts of 1 month old mice: (grey bars), of 4 months old mice (dark bars). BDH-D-beta-hydroxybutyrate dehydrogenase, mitochondrial, CPT1B-carnitine O-palmitoyltransferase 1, muscle isoform, ACS2L-acetyl-coenzyme A synthetase 2-like, mitochondrial, CPT2-carnitine O-palmitoyltransferase 2, mitochondrial, CACP-carnitine O-acetyltransferase. ** indicates $p \leq 0.05$ and *** indicates $p \leq 0.01$.

Besides lipid metabolism, proteins involved in respiratory electron transport chain were also identified in altered levels in 4 months old hearts compared to hearts of younger mice. As mentioned above, subunits of complex I, II and IV were observed at higher levels in hearts of older mice (Fig. 30). However, different subunits of complex V- ATP synthase subunit alpha, mitochondrial (ATPA), ATP synthase subunit delta, mitochondrial (ATPD), ATP synthase subunit O, mitochondrial (ATPO), and ATP synthase subunit d, mitochondrial (ATP5H) were observed in lower amounts in 4 months old mice compared to 1 month animals except for ATP synthase subunit b, mitochondrial (AT5F1) which was identified in higher amounts (Fig. 30A).

Such contrasting results were also observed for cytochrome c oxidase of Complex IV and for Complex I by LC-MS analysis. Cytochrome c oxidase polypeptide 7A1, mitochondrial (CX7A1) of complex IV was identified at lower amounts in aging mice whereas cytochrome c oxidase subunit 6c was identified at higher amounts (Fig. 30B) whereas 3 subunits of NADH dehydrogenase (ubiquinone)1 –alpha and beta subcomplex subunit 9 NDUA9 and NDUB9, and beta subcomplex of subunit 10 (NDUBA) were identified in higher amounts whereas, alpha subcomplex subunit 7, mitochondrial (NDUA7), as well as alpha and beta subcomplexes of subunit 4, (NDUA4 and NDUB4) were identified in lower amounts in 4

months old mice (Fig.30C). On the other hand, succinate dehydrogenase was identified at higher amounts in 4 months old mice in DIGE analysis (Fig. 30D).

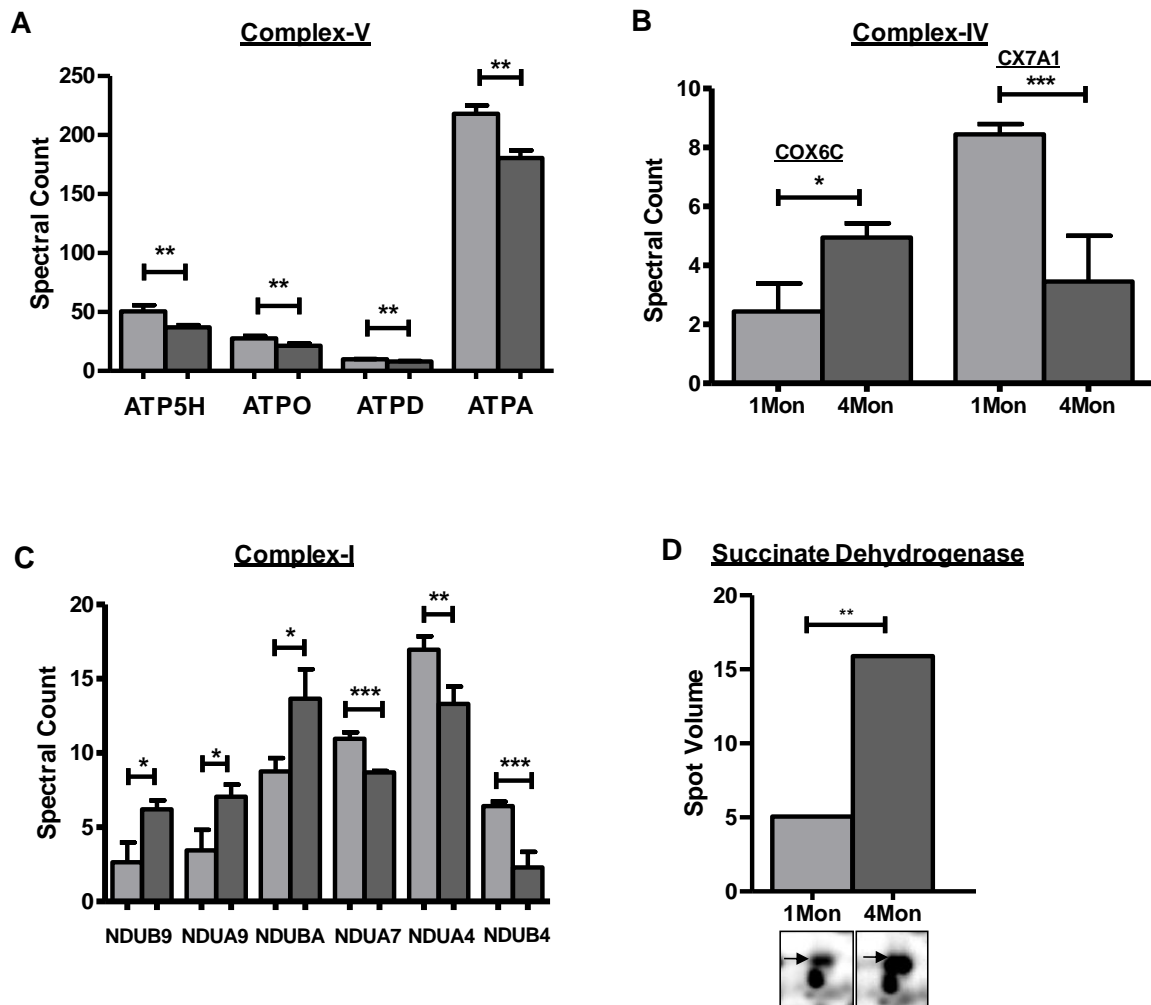


Fig. 30. Age dependent changes in abundance of proteins of the electron transport chain in hearts of mice. Different subunits of respiratory electron transport chain were affected due to aging in mice hearts. Grey bars: level in hearts of 1 month old animals, dark bars: level in hearts of 4 months old mice. A- subunits of ATP synthase (complex V) identified by gel-free analysis - ATP5H- ATP synthase subunit d, mitochondrial, ATPO- ATP synthase subunit O, mitochondrial, ATPD- ATP synthase subunit delta, mitochondrial, ATPA- ATP synthase subunit alpha, mitochondrial. B- cytochrome c oxidase subunit 6C (COX6C) and polypeptide 7A1, mitochondrial (CX7A1). C-subunits of complex I: NADH dehydrogenase [ubiquinone] 1 beta subcomplex subunit 9 (NDUB9), NADH dehydrogenase [ubiquinone] 1 alpha subcomplex subunit 9, mitochondrial (NDUA9), NADH dehydrogenase [ubiquinone] 1 beta subcomplex subunit 10 (NDUBA), NADH dehydrogenase [ubiquinone] 1 alpha subcomplex subunit 7 (NDUA7), NADH dehydrogenase [ubiquinone] 1 alpha subcomplex subunit 4 (NDUA4), NADH dehydrogenase [ubiquinone] 1 beta subcomplex subunit 4 (NDUBA). D- succinate dehydrogenase (2D DIGE results) of electron transport chain. **p-value \leq 0.05, *** indicates p \leq 0.01 and * indicates p \leq 0.1.

Besides the functional classes mentioned above, a small number of proteins (4) involved in muscle contraction- troponin T, cardiac muscle (TNNT2), transgelin (TAGL), tropomyosin 1 alpha chain (TPM1) and myosin-6 (multiple spots in 2D-DIGE of MYH6) were observed in lower amounts in hearts of 4 months old animals suggesting a slightly altered muscle contraction compared to younger mice.

Using complementary techniques of 2D-DIGE and LC-MS/MS analysis proved advantageous in gaining a comprehensive understanding of the age dependent changes occurring in mouse hearts at the cellular and molecular level. Around 30 proteins showing age dependent changes in the DIGE analysis were also identified with at least two peptides in LC-MS/MS but were not found to be regulated. This might be due to the different quantitation approaches employed which focus in LC-MS/MS on the analysis of the total protein amount whereas in the 2D-DIGE different species of one protein are analysed separately. LC-MS/MS analysis provided a more complex view of the alterations of metabolic proteins.

3.3.4. Validation of proteins displaying age dependent changes in A.BY/SnJ mice hearts by immunohistochemistry

Heterogeneous nuclear ribonucleoprotein K (HNRPK) involved in RNA processing displayed decreased levels whereas Rab GDP dissociation inhibitor beta (GDIB) and stress protein 70 (GRP75) involved in intracellular protein transport were identified at higher levels in hearts of older mice compared to hearts of younger animals. The altered expression of these three proteins in tissue was confirmed by immunohistochemical staining (Fig.31)

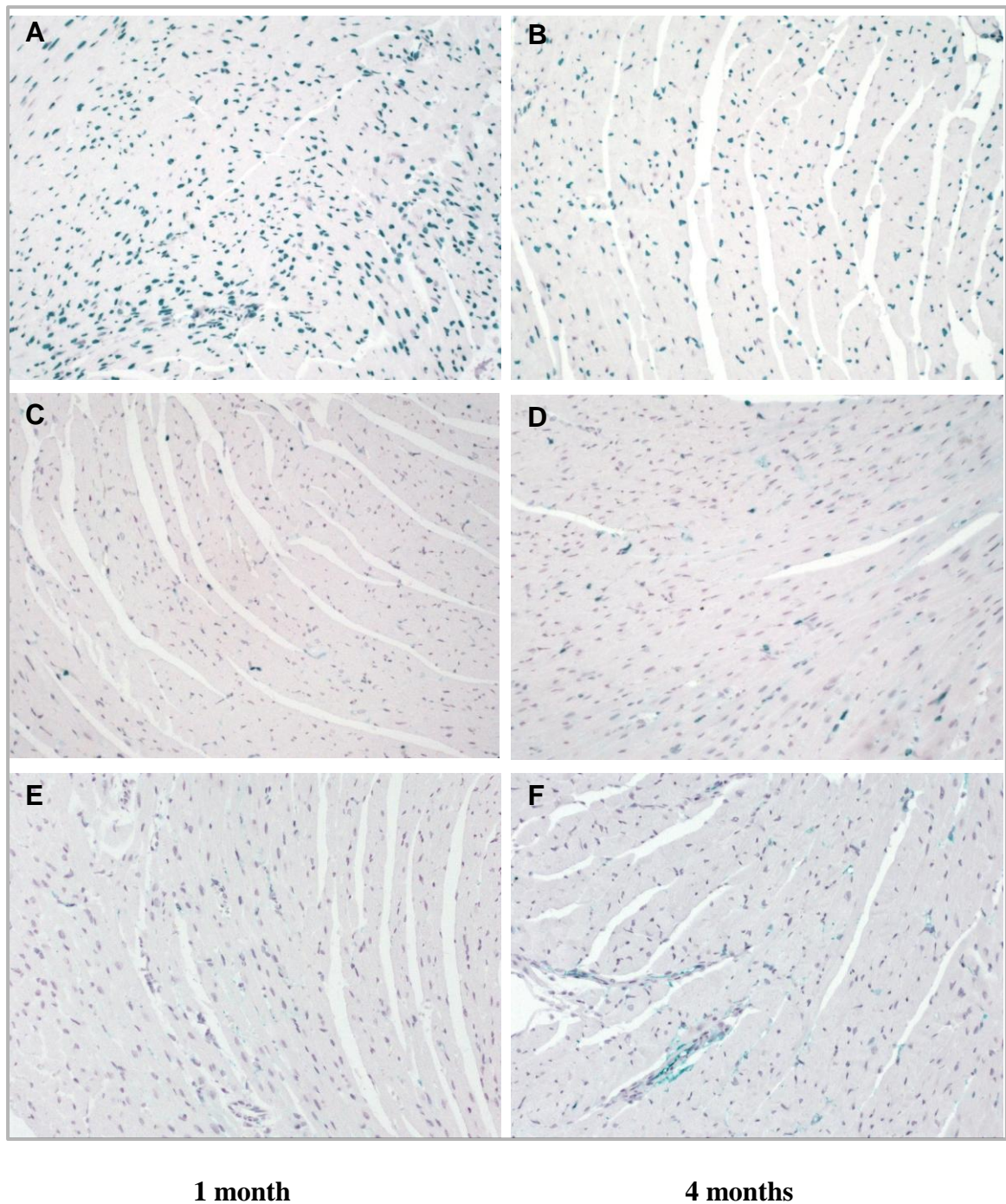


Fig. 31. Validation of age dependent changes in the level of proteins by immunohistochemical staining. A,B-represent immunohistochemical staining of heterogeneous nuclear ribonucleoprotein K (HNRPK) C,D-represent immunohistochemical staining of Rab GDP dissociation inhibitor beta (GDIB) E,F-represent immunohistochemical staining of stress protein70 (GRP75) in A.BY/SnJ mouse hearts.

3.4. Analyses of heart tissues of rats overexpressing ANT-1 in comparison to wild type animals

3.4.1. Changes in the total proteome of adenine nucleotide translocase 1/ANT1 over expressing (ANT-OE) rat hearts in comparison to wild type hearts

Mitochondria are the primary source of energy in the cell where ATP is generated. Adenine nucleotide translocase (ANT) helps in the exchange of ADP and ATP across the mitochondrial inner membrane into the cytoplasm. Of the different isoforms, over expression of the ANT 1 isoform has been reported to play a cardioprotective role and influence various cellular processes (McLeod et al., 2004). Hence, in order to characterize the changes in the total proteome of the heart due to over expression of ANT1, comparative proteomic analysis of non-infected 3 months old ANT-OE Wister rats and wild type animals (WT) was performed.

After protein digestion and MS analysis, the raw files were loaded into the Rosetta Elucidator software for quantitative analysis based on the peptide intensities. Quality control check across all isotope groups extracted after retention time shift alignment of chromatograms displayed that the animals within each group were found to be homogeneous. The coefficients of variation among the animals within each group were around 20-25% indicating that there were no outliers within the groups (Fig.32).

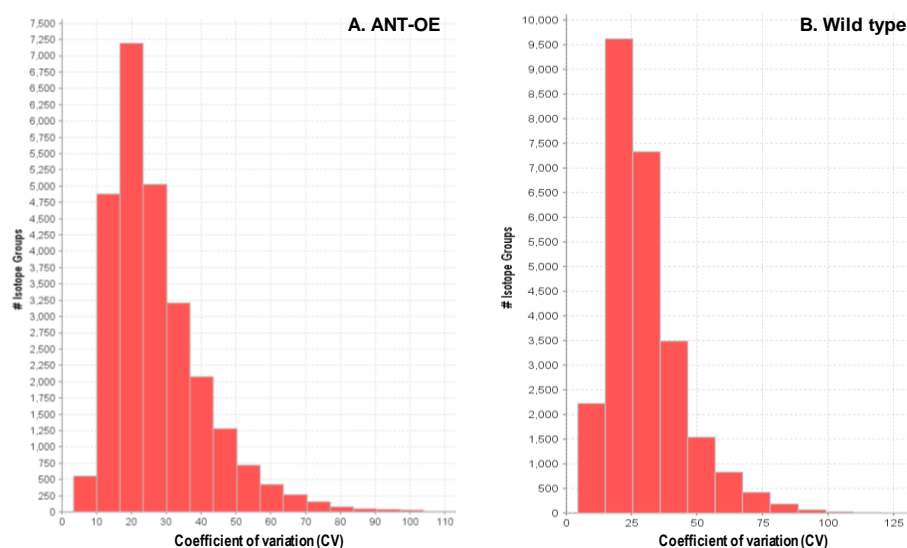


Fig. 32. Coefficients of variation among animals of each group based on the identified isotope groups. Quality control analysis by Rosetta Elucidator revealed minimal difference among animals of each group with animals showing 20-25% coefficient of variation (CV). A- CV based on isotope groups identified in all the 6 ANT over-expressing animals and B- CV based on isotope groups identified in all the 6 wild type animals. The graphs depict the CVs inclusive of the two technical replicates for each animal in each of the groups.

The samples were then searched against NCBI rat forward reverse database version 2007. Four hundred and forty three proteins were identified with at least 2 unique peptides per protein (Appendix.A3.4.1a.). For quantitation of differences between the groups an adapted in-house workflow was applied as specified in Materials & Methods section 2.2.8.5. Pair wise ratios were built from the mean and standard deviation of the intensity between the groups WT and ANT-OE were calculated. Proteins satisfying student's *t*-test with $p \leq 0.05$ and intensity ratio fold change of > 1.2 were considered to show significant changes in ANT-OE compared to WT controls. Eighty seven proteins were observed to be satisfying the above statistical cuts (Appendix.3.4.1).

Sixty proteins showed higher intensities in ANT-OE rats and twenty seven proteins were observed at lower intensities in ANT-OE compared to WT rats. Amine oxidase /monoamine oxidase type A was observed to show maximum increase in intensity with 1.66 fold difference compared to wild type animals illustrating the rather minor global influence of ANT overexpression on the left ventricle protein pattern in 3 months old rats. Besides that, proteins of the heat shock protein family and muscle contractile proteins were identified predominantly in the analysis followed by proteins involved in cell signalling and interaction. Heat shock protein 1 alpha, heat shock protein 4, heat shock protein 27kDa protein 1 and protein 2 were identified to have 1.2 -1.4 times higher intensities in ANT-OE rats compared to WT controls. Myosin-11, myosin heavy chain polypeptide 9, myosin heavy chain 7, myosin light chain, polypeptide 6 and tropomyosin 1 alpha isoform i also showed 1.2-1.5 times higher intensities in ANT-OE animals. Besides these, proteins alpha actinin 4, laminin alpha-4 chain precursor and laminin beta 2 also showed increased intensities in ANT-OE rats. Interestingly, only cytochrome c oxidase, subunit II of respiratory electron transport chain showed increased levels in ANT-OE rats. Intensities of NADH dehydrogenase (ubiquinone) Fe-S protein 4, 18kDa and NADH dehydrogenase subunit 4 showed around 1.5 fold decrease in ANT-OE rats compared to WT.

Though we could identify different subunits of ATP synthase F0 and F1 complex, cytochrome c oxidase, and NADH dehydrogenase of the electron transport chain, these proteins did not satisfy the applied statistical filters. Surprisingly, no significant difference was observed also for ANT1/solute carrier family 25, member 4 which was identified with five peptides but revealed only a factor of 1.09 at a p-value of 0.14. For a comprehensive understanding of the changes occurring in the transgenic ANT-OE animals, the proteins displaying statistically significant differences were further analysed using Ingenuity systems

Pathway Analysis (IPA). Proteins involved in three biological processes namely - interleukin signalling, mitochondrial dysfunction and glycolysis were predominantly affected in ANT-OE animals compared to WT controls (Table 22).

Table 22. Protein classes significantly altered in ANT-OE rats. Proteins altered in ANT-OE animals were assigned to interleukin signalling, mitochondrial dysfunction and glycolysis by predictive pathway analysis (IPA). Fold change of protein abundance in ANT-OE rats compared to that in WT animals is given as “ratio” and the corresponding decrease (↓) or increase (↑) in protein levels is indicated as direction.

Biological process	Protein	Ratio	Direction
Integrin linked kinase signalling	Myosin 11	1.54	↑
	Myosin heavy chain, polypeptide 7	1.49	↑
	Alpha actinin 4	1.46	↑
	Filamin-A	1.43	↑
	Fibronectin 1	1.43	↑
	Myosin, heavy polypeptide 9	1.29	↑
	Alpha isoform of regulatory subunit A, protein phosphatase 2	1.28	↑
	Integrin beta 1	1.27	↑
	Integrin linked kinase	1.21	↑
Mitochondrial function	Amine oxidase [flavin-containing] A (Monoamine oxidase type A)	1.66	↑
	Cytochrome c oxidase subunit II	1.34	↑
	Ubiquinol-cytochrome c reductase binding protein	0.58	↓
	NADH dehydrogenase (ubiquinone) Fe-S protein 4, 18kDa	0.62	↓
	NADH dehydrogenase subunit 4	0.67	↓
	Succinate dehydrogenase complex, subunit A, flavoprotein	0.81	↓
Glycolysis	Aldehyde dehydrogenase 2	1.63	↑
	Aldolase A	1.30	↑
	Aldehyde dehydrogenase family 7, member A1	1.24	↑
	Phosphoglycerate mutase 1	0.79	↓
	Aldehyde dehydrogenase family 9, subfamily A1	0.81	↓

Proteins such as myosin 11, myosin heavy chain polypeptide 7, myosin heavy polypeptide 9, and tropomyosin alpha 1 isoform were assigned to cell morphology and development by IPA analysis. Besides tissue development, these proteins are also involved in a network with other proteins such as integrin beta 1, integrin linked kinase aiding in cell signalling (Fig.33).

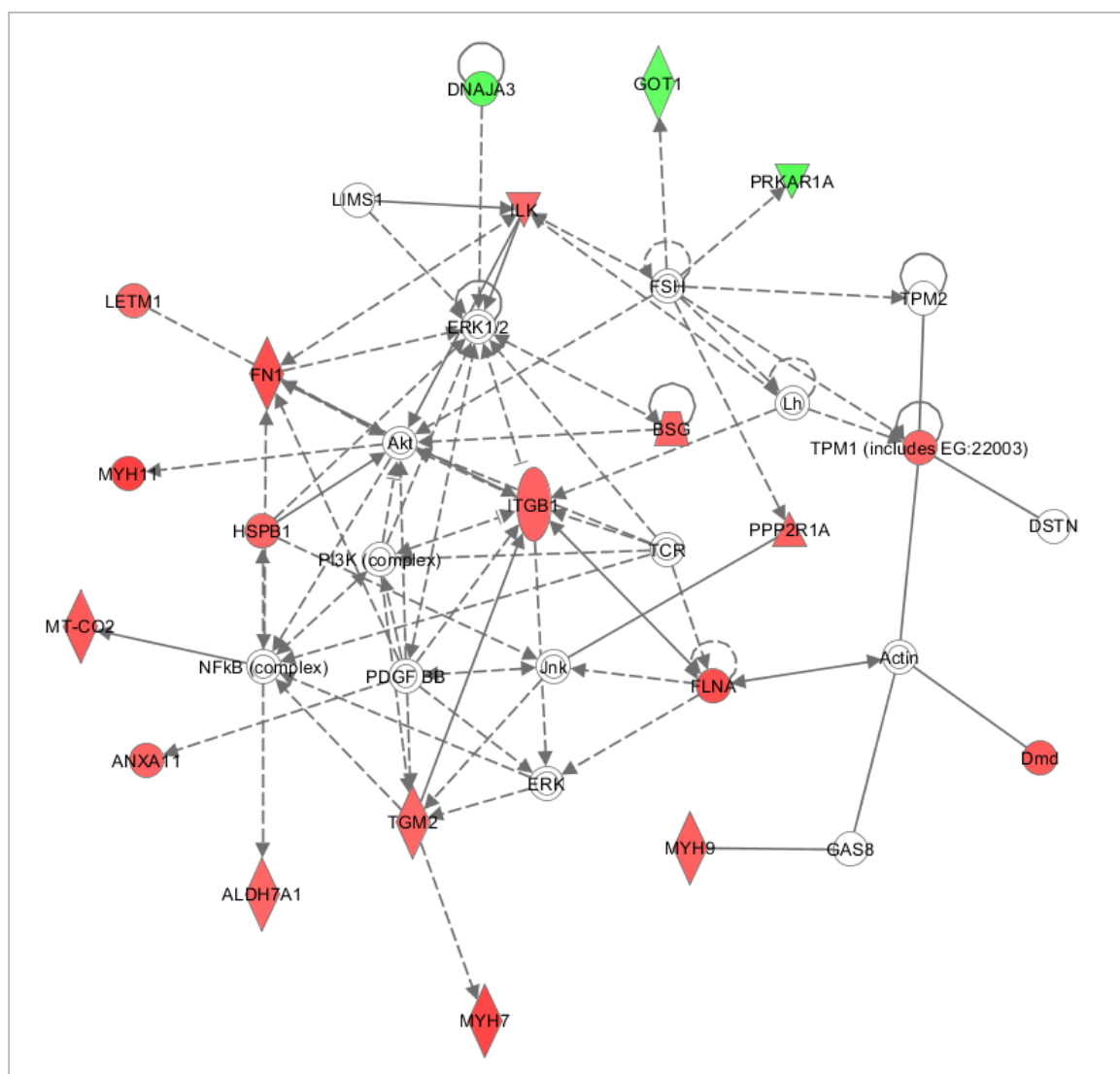


Fig. 33. Network of proteins involved in cell signalling. IPA analysis identified a set of proteins involved in tissue development which also play a role in cell signalling. Red markings show proteins with increased levels in ANT-OE animals and green markings indicate proteins whose amounts were reduced in ANT-OE rats compared to WT. FN1-Fibronectin1, ITGB1-integrin beta 1, PPP2R1A- protein phosphatase 2, regulatory subunit A, alpha, TPM1- tropomyosin alpha 1, FLNA-filamin alpha, ILK1- integrin linked kinase 1, LETM1-leucine zipper-EF-hand containing transmembrane protein 1, MYH11-myosin 11, BSG-basigin, HSPB1-heat shock 27kDa protein 1, MT-CO2- cytochrome c oxidase II, ALDH7A1-aldehyde dehydrogenase 7, member A1, ANXA11- annexin A11, MYH7- myosin heavy chain, polypeptide 7, TGM2- transglutaminase 2, MYH9-myosin, heavy polypeptide 9, Dmd- dystrophin, PPKAR1A- protein kinase, cAMP dependent, regulatory, type I, alpha, GOT- glutamic oxaloacetic transaminase 1 (aspartate transaminase), DNAJA3-DNA J (Hsp 70) analog, subfamily A, member 3.

Besides cell signalling, proteins involved in respiratory electron transport chain appeared to have been influenced in ANT-OE animals. Except for monoamine oxidase and cytochrome c oxidase subunit II, the rest of the proteins identified in the process were observed in lower amounts in transgenic rats compared to wild type rats (Fig.34). This implies a decreased or altered mitochondrial function and energy production in ANT-OE rats.

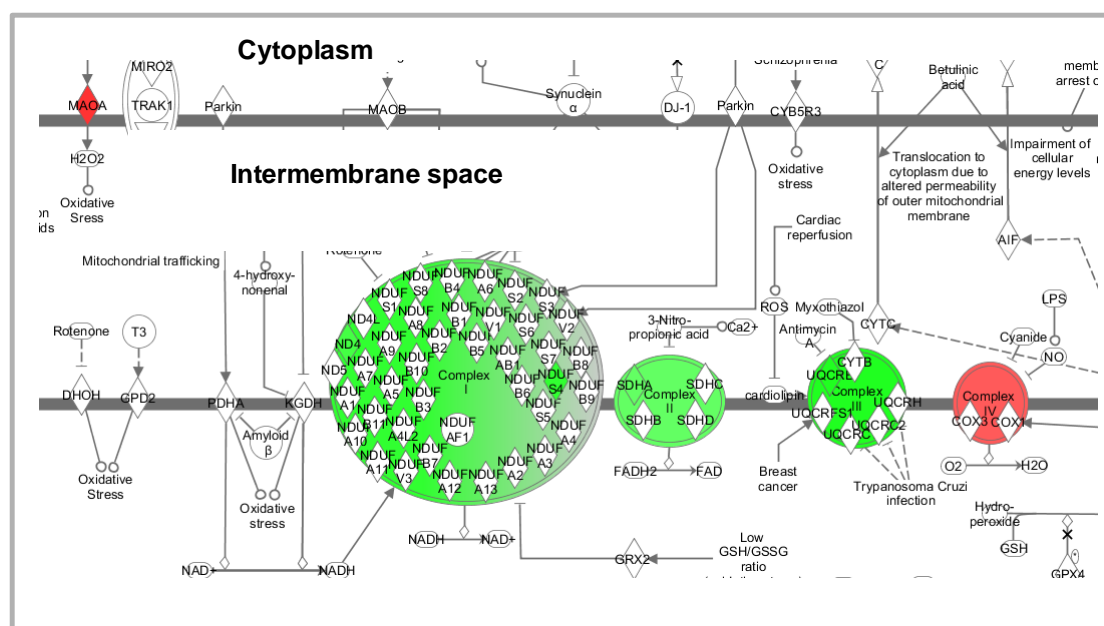


Fig. 34. Altered mitochondrial function in ANT-OE rats. Proteins NADH dehydrogenase (ubiquinone) Fe-S protein 4, 18kDa, NADH dehydrogenase subunit 4 of complex-I, succinate dehydrogenase complex, subunit A, flavoprotein of Complex –II, ubiquinol-cytochrome c reductase binding protein of complex-III were found to have decreased in ANT-OE while cytochrome c oxidase subunit II of complex-IV showed increased levels in ANT-OE rats. Also protein monoamine oxidase A (MAOA) involved in oxidative stress response showed increased levels in ANT-OE rats compared to controls.

From the above analysis, it could be concluded that the over expression of ANT1 in rat hearts resulted in increased muscle contractility and an increased integrin signalling. Also an increase in the glycolytic enzymes was observed in ANT-OE hearts compared to controls. However a decrease in the levels of proteins of respiratory electron transport chain except complex IV was detected.

3.4.1.1. Influence of ANT1 over expression on protein oxidation in ANT OE whole hearts

Over expression of ANT1 protein has been reported to rectify defective mitochondrial function and increase energetic coupling of oxidative phosphorylation (Walther et al., 2007, Wang et al., 2009). Hence, in order to determine the influence of ANT1 over-expression on oxidation of proteins, an oxyblot was performed to analyse the difference in protein oxidation between ANT-OE and WT rats.

Using an Oxyblot detection kit (Millipore, Germany), proteins carbonylated due to oxidation can be detected. The carbonyl groups of the protein side chains are converted to 2,4-dinitrophenylhydrazone on reaction with 2,4-dinitrophenylhydrazine (DNPH). This method provides the advantage of highlighting individual oxidized proteins from a complex mixture.

The oxidative state of the proteins can be analyzed by comparing the signal intensity of the bands across different groups. Six rats each from groups WT and ANT-OE were considered for detection of changes in oxidation due to over expression of ANT1. However, Oxyblot analysis revealed no significant differences in the intensity of the bands of oxidized proteins between WT and ANT-OE animals (Fig.35).

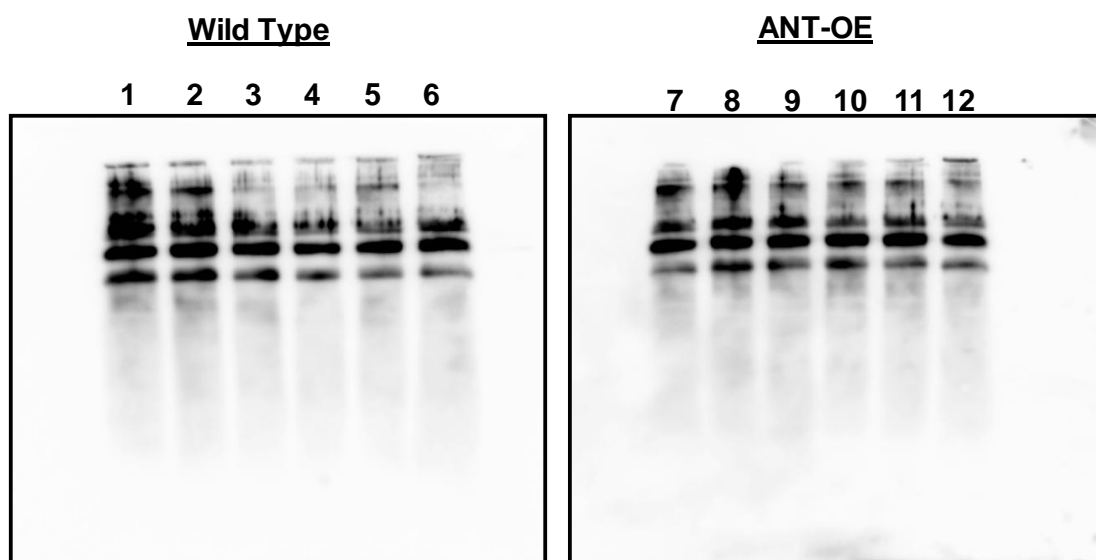


Fig. 35. Detection of protein oxidation in extracts of WT and ANT-OE rats. Oxyblot analysis did not reveal significant changes in the band intensity of oxidised proteins in ANT-OE rats compared to WT controls.

3.4.2. Influence of ANT1 over expression on the heart mitochondrial proteome of rats infected with CVB3

Protein extracts from the mitochondrial fractions of hearts from 8 months old Wister rats overexpressing adenine nucleotide translocase 1 (ANT-OE) infected with CVB3 were prepared in the laboratory of Dr. Andrea Dörner, Department of Cardiology, Charité-Universitätsmedizin, Campus Benjamin Franklin, Berlin. Mitochondria of 8 months old wild type (WT) rat hearts infected with CVB3 were considered as controls for the comparison.

2 µg of protein with two technical replicates from individual animals from each group, the WT and ANT-OE rat hearts (n=4) were considered for proteolytic digestion. After MS analysis, the raw files from LTQ-Orbitrap Velos mass spectrometer were loaded into Rosetta Elucidator software for quantitative analysis of the samples based on the identified peptide intensities. A quality check regarding variation of isotope groups of samples within a group (ANT OE and control) displayed different coefficients of variation (Fig. 36). The control

group showed higher variation in average (30-40%) than those of the ANT-OE group (20-30%).

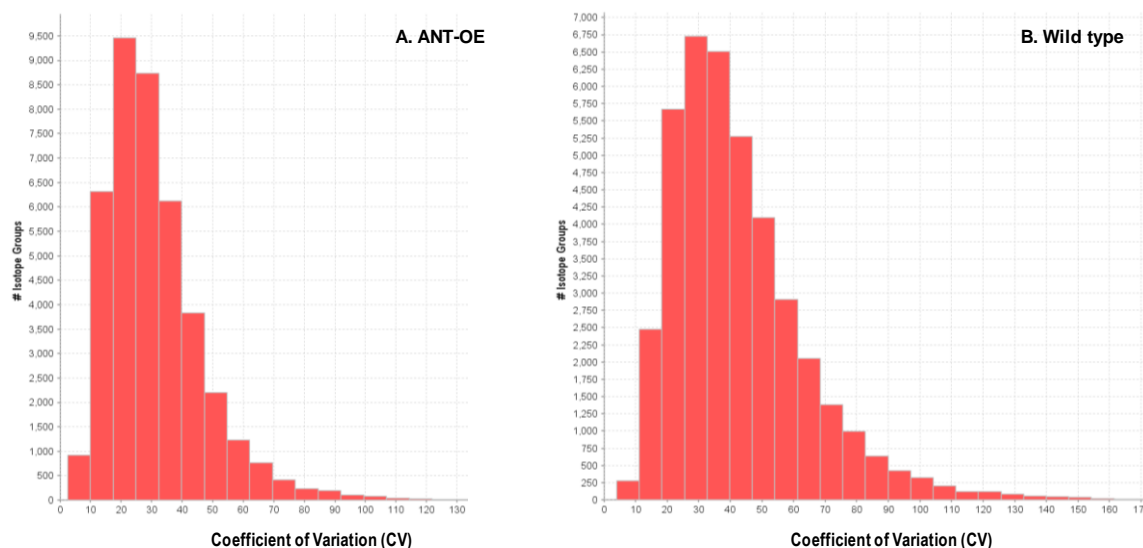


Fig. 36. Coefficients of variation (CV) within ANT-OE and WT animals based on the identified isotope groups. A- CV based on isotope groups identified in mitochondrial fractions of four ANT-OE rats infected with CVB3; B- CV based on isotope groups identified in wild type animals. The graphs depict the CVs inclusive of the two technical replicates for each animal in each of the groups.

These variations became also obvious looking at a principal component analysis (PCA) based on the identified isotope groups. PCA showed inter individual differences of the mitochondrial extracts within the groups, which seem to be stronger in the group of WT infected with CVB3 than in the group of ANT overexpressing animals (Fig.37).

Elucidator analysis resulted in 370 proteins identified with a minimum of two peptides when searched against NCBI rat forward reverse database, version 2007 (Appendix A3.4.2a). Eighty three proteins showing ratio fold difference of ≥ 1.2 and passing statistical significance of $p \leq 0.05$ were considered as showing disease dependent changes in infected ANT-OE mitochondrial fractions compared to infected WT controls (Appendix A3.4.2). Of eighty three proteins, a high number of proteins (55) were observed to have decreased in infected ANT-OE mitochondrial fractions compared to controls. Proteins of the electron transport chain complexes I, II, IV and V such as NADH dehydrogenase (ubiquinone) Fe-S protein 1, 4 and 5b, NADH dehydrogenase (ubiquinone) flavoprotein 1 and 2, as well as NADH dehydrogenase (ubiquinone) 1 alpha subcomplex 2 and 7, succinate dehydrogenase Ip subunit, cytochrome c oxidase polypeptide VIIa, and the gamma and delta subunit of ATP

synthase, H⁺ transporting, mitochondrial F1 complex, were identified lower amounts in infected ANT-OE rats than in the WT.

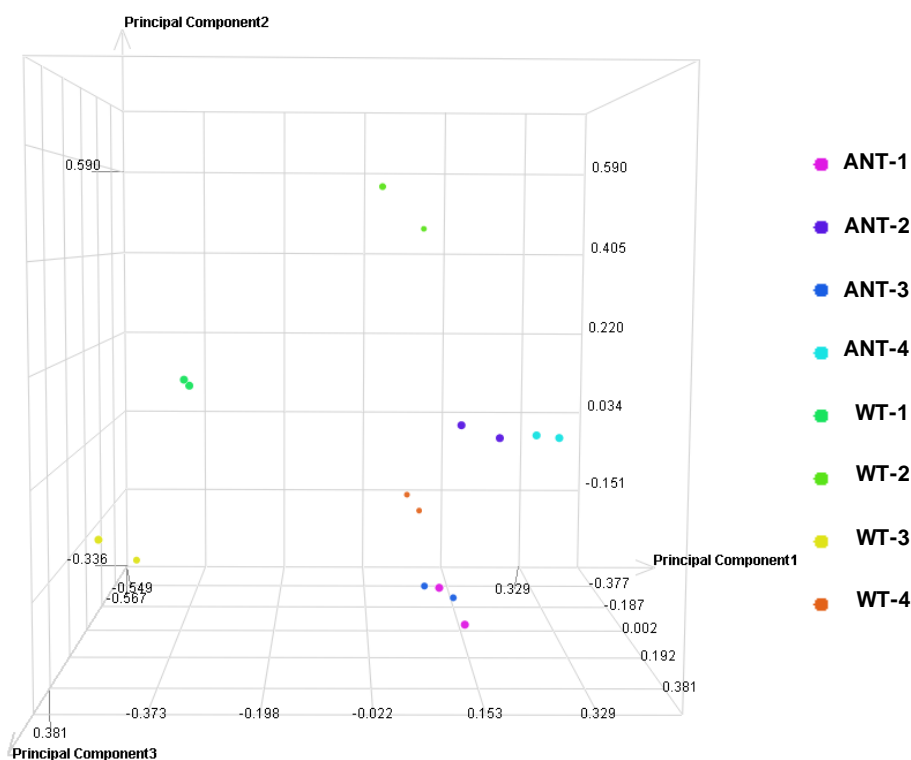


Fig. 37. Principal component analysis based on identified isotope groups from mitochondrial extracts of 8 months old ANT-OE and WT rats infected with CVB3. PCA analysis shows the variation among the animals especially in the WT group. Each group consists of mitochondrial extracts of four animals and two technical replicates per animal were measured. The colour codes on the right side of the figure describe the animals belonging to each group.

Besides electron transport chain, proteins of the cardiac contractile apparatus- troponin 1, type 3, troponin T2, cardiac, tropomyosin 1, alpha isoform I, myosin-binding protein C, cardiac-type, myosin, light polypeptide 3 and myosin heavy chain, polypeptide 6 were also identified to have decreased in infected ANT-OE group. Furthermore, extracellular matrix proteins laminin gamma-1 chain and collagen alpha-1(VI) chain were identified at lower levels in the infected transgenic animals. In contrast levels of maleylacetoacetate isomerase (MAAI) /glutathione S-transferase zeta 1 protein was more than 2 fold higher in the mitochondrial fractions of transgenic animals compared to wild type controls.

Though ANT1/ solute carrier family 25, member 4 was over expressed in the rats, the protein was not identified as significantly altered in the analysis. ANT1 identified with six peptides was observed to show ratio fold difference of 1.18 with a p value of 0.15. Analysis of the mitochondrial fractions of the hearts revealed many proteins related to cytoplasm, secretory and extracellular matrix which is intriguing. Out of the 83 proteins showing ANT-OE dependent changes due to infection compared to WT infected animals, 29 proteins belonged to either mitochondria-, mitochondrial matrix or inner or outer membrane of the mitochondria. Other than the mitochondria, the proteins are either cytoplasmic, membrane, endoplasmic reticulum with a few secreted proteins. 35 of 83 proteins couldn't be mapped for their sub-cellular location (Fig.38).

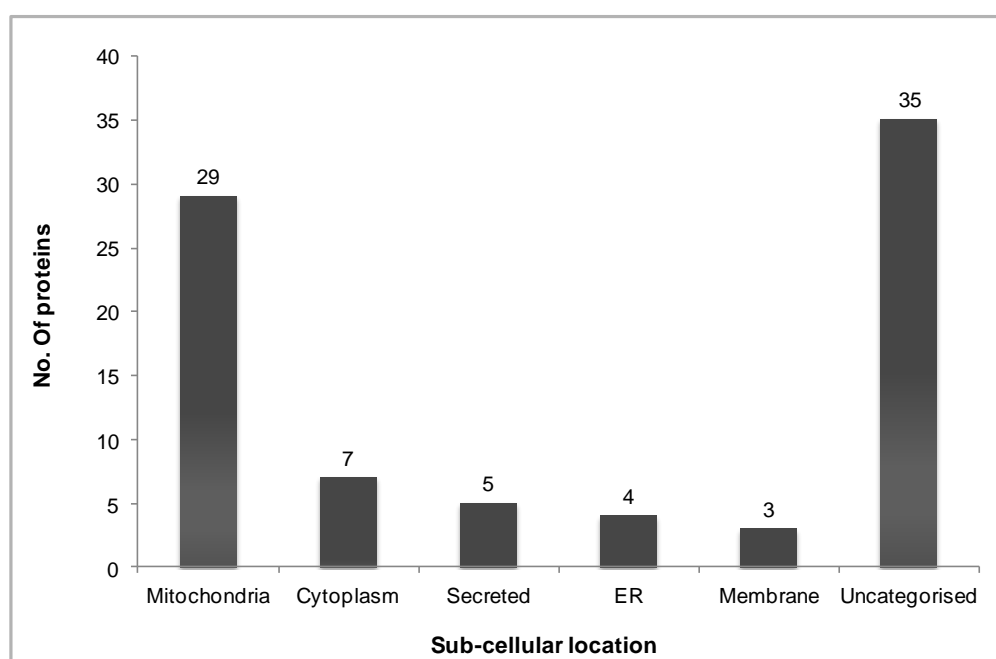


Fig. 38. Sub-cellular location of proteins displaying ANT-OE dependent changes compared to WT upon CVB3 infection.

In order to understand the physiological significance of the results, the regulated proteins were loaded into Ingenuity Pathway Analysis (IPA). Proteins related to mitochondrial dysfunction, fatty acid metabolism and cellular assembly and organization and molecular transport were shown to have been significantly affected in mitochondrial fractions of CVB3 infected ANT-OE rats compared to infected WT animals. Whereas proteins involved in molecular transport such as solute carrier family 27 (fatty acid transporter), member 1, and nicotinamide nucleotide transhydrogenase displayed significantly higher levels in CVB3 infected transgenic rats, proteins of fatty acid metabolism such as hydroxyacyl coA dehydrogenase/ mitochondrial trifunctional protein, alpha subunit, mitochondrial trifunctional protein, beta subunit/ 3-ketoacyl CoA thiolase and acetyl-CoA acyltransferase 2 were observed at lower levels in infected transgenic rat hearts besides decreased levels of mitochondrial respiratory electron transport chain (Fig. 39). Proteins related to cellular assembly organization and muscular dysfunction such as troponin T2, collagen 6, alpha 3, laminin gamma 1, tropomyosin 1 alpha, isoform a and myosin heavy chain 6 showed decreased levels in infected WT rat hearts (Table 23).

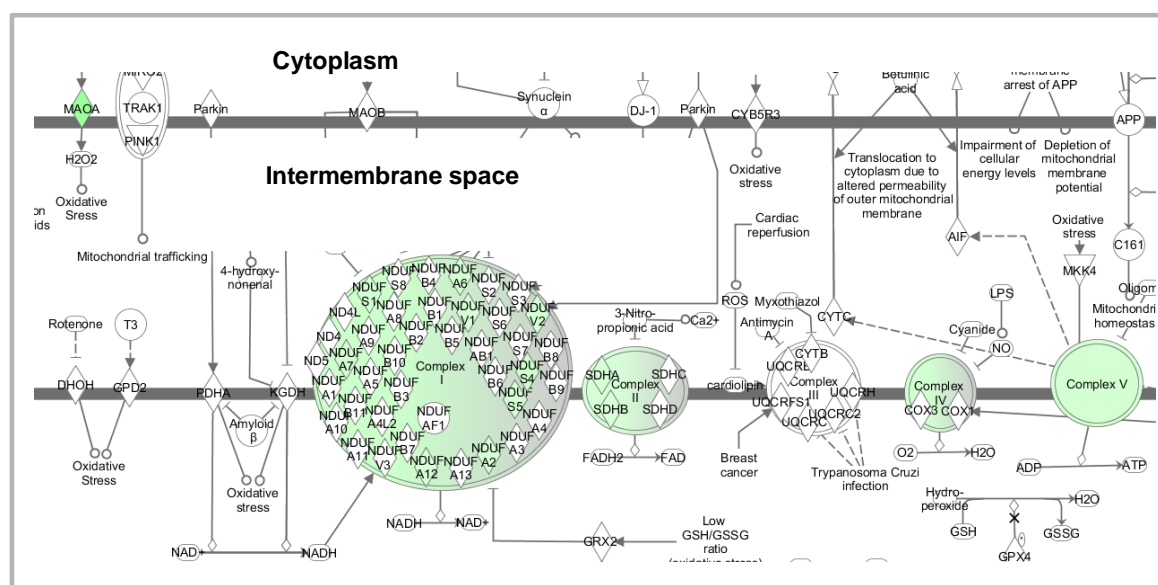


Fig. 39. Mitochondrial dysfunction in mitochondrial fractions of ANT-OE rat hearts infected with CVB3. Proteins belonging to complexes I, II, IV and V of respiratory chain were identified at decreased levels in infected mitochondrial fractions of ANT-OE rat hearts pointing towards decreased mitochondrial function.

Table 23. Significantly altered protein classes in mitochondrial fractions of 8 months old, CVB3 infected rat hearts. Ingenuity pathway analysis revealed three major functional protein classes, predicted as significantly different in CVB3 infected ANT-OE rats compared to CVB3 infected WT rats. Fold change of protein abundance in ANT-OE rats compared to that in WT animals is given as “ratio” and the corresponding decrease (↓) or increase (↑) in protein levels is indicated as direction.

Biological Function	Protein	Ratio	Direction
Mitochondrial dysfunction	Monoamine oxidase	0.33	↓
	Catalase	0.63	↓
	NADH dehydrogenase (ubiquinone) Fe-S protein 4, 18kDa	0.65	↓
	NADH dehydrogenase (ubiquinone) 1 alpha subcomplex, 7	0.71	↓
	Cytochrome c oxidase subunit Vb	0.73	↓
	NADH dehydrogenase (ubiquinone) 1 alpha subcomplex, 6	0.73	↓
	ATP synthase, H ⁺ transporting, mitochondrial F1 complex, gamma subunit	0.73	↓
	NADH dehydrogenase (ubiquinone) Fe-S protein 1, 75kDa	0.74	↓
	NADH dehydrogenase (ubiquinone) flavoprotein 2	0.74	↓
	NADH dehydrogenase (ubiquinone) Fe-S protein 5b	0.76	↓
	NADH dehydrogenase (ubiquinone) flavoprotein 1, 51kDa	0.77	↓
	NADH dehydrogenase (ubiquinone) 1 alpha subcomplex, 2	0.79	↓
	Cytochrome c oxidase subunit VIIa-H	0.79	↓
	Succinate dehydrogenase complex, subunit A, flavoprotein (Fp)	0.82	↓
	Succinate dehydrogenase Ip subunit	0.83	↓
Fatty acid metabolism	Carnitine palmitoyltransferase 2	1.23	↑
	Mitochondrial trifunctional protein, alpha subunit	0.80	↓
	Mitochondrial trifunctional protein, beta subunit	0.81	↓
	Acetyl-Coenzyme A acyltransferase 2	0.68	↓
Cell assembly organisation	Troponin 1, type 3	0.42	↓
	Troponin T2, cardiac	0.50	↓
	Tropomyosin 1, alpha isoform a	0.53	↓
	Vimentin	0.56	↓
	Vinculin	0.58	↓
	Myosin-binding protein C, cardiac-type	0.63	↓
	Laminin gamma-1 chain precursor	0.64	↓
	Myosin, light polypeptide 3	0.68	↓
	Myosin heavy chain, polypeptide 6	0.70	↓
	Alpha 3 type VI collagen isoform 1 precursor	0.73	↓
Molecular transport	Solute carrier family 27 (fatty acid transporter), member 1	2.16	↑
	Nicotinamide nucleotide transhydrogenase	1.74	↑
	Basigin	1.60	↑

In summary, the comparative proteomic analysis of the mitochondrial fractions of CVB3 infected ANT-OE and WT rats pointed towards decreased mitochondrial function and energy production coupled with decreased myocardial contractility.

3.5. Proteomic analysis of dilated cardiomyopathy in rats immunized with peptides of Fcγ receptor

The samples for the proteomic analysis were acquired from Dr. Lars Herda, Department of Cardiology, University Medicine Greifswald.

Cell lysis during infection induces autoimmune reaction against cardiac proteins. Due to the existence of a broad variety of cardiac autoantibodies against intracellular antigens, a common mediator of the autoimmune reaction was assumed. Staudt et al. hypothesized that Fc gamma receptor on the surface of cardiomyocytes might act as a crosslinker of autoantibodies triggering an intracellular signal leading to damage of the heart muscle cells (Staudt et al., 2007). Peptides of intracellular proteins such as troponin I and myosin heavy chain 6 have been shown to initiate autoimmune reactions leading to dilated cardiomyopathy. Since Fc gamma receptors are expressed on the cardiomyocytes, a model was established to investigate if such a reaction can also be triggered by peptides of Fc gamma receptor. Animals were immunized with antigenic peptides against Fc fragments eliciting an immune response and further upon dilated cardiomyopathy were induced (personal communication Lars Herda).

In order to understand the changes in the protein profile of animals immunized with peptides 1 and 2 for FcγIIa (CD-32) receptor (as mentioned in materials & methods section), mass spectrometric analysis of protein extracts from whole hearts was performed. The animals immunized with peptide 1 of FcγIIa receptor were designated as FcR group and those immunized with peptide 2 of FcγIIa receptor were designated as FcR2 group. Animals injected with adjuvants (KLH) bound to GST were considered as controls. A total of 303 proteins were identified with two or more unique peptides per protein (Appendix A3.5a). Proteins passing students *t*-test with $p \leq 0.05$ and ratio fold difference in intensities > 1.2 were considered as significantly changed in either FcR (peptide 1) or FcR2 (peptide2) rats compared to KLH controls. Forty three proteins were identified to have passed the above statistical thresholds in FcR rats compared to controls and forty nine proteins showed statistically significant changes in FcR2 rats compared to controls (Appendix A3.5). Seventy percent of the proteins were observed to have been identified in

both comparisons indicating that the FcR and FcR2 groups do not differ much among each other (Fig.40).

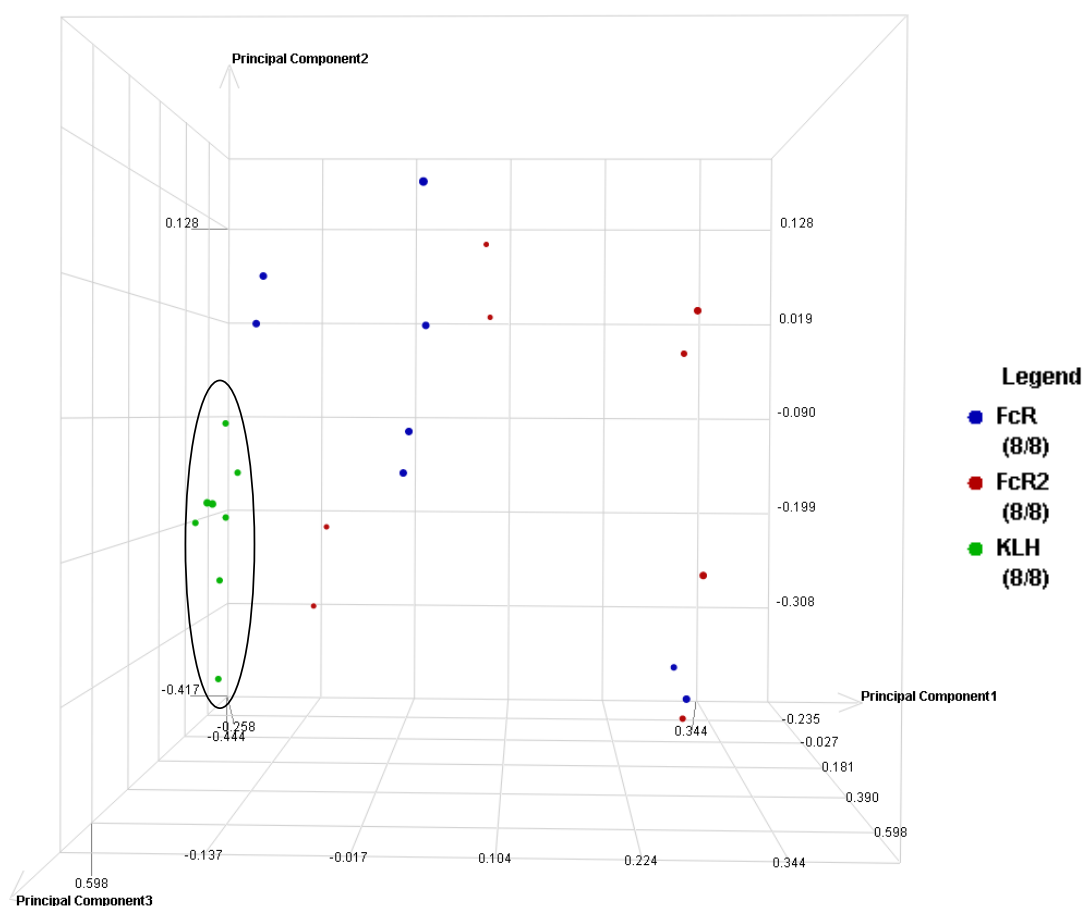


Fig. 40. Principal component analysis (PCA) based on the proteins altered in rats immunized with peptides 1 and 2 of Fc gamma receptor. PCA analysis of four animals with two technical replicates each per group shows differentiation between the control rats (circled-KLH) and rats immunized with peptide 1 (FcR) and peptide 2 (FcR2) of Fc gamma receptor indicating large differences between the control and immunized animals.

The data were analysed using Ingenuity Pathways Analysis (IPA) to perform a functional categorization of the identified proteins. Three major pathways namely, acute phase response signalling, and ILK signalling were highlighted as affected in the heart due to the immunization and the initiated processes. Of these, acute phase response signalling was observed to have significantly altered with 6 out of 9 proteins showing a fold difference of greater of 1.5 in their intensities (Table 24).

Table 24. Proteins displaying changes due to immunization in both FcR and FcR2 animals compared to KLH controls. Alterations in the protein levels as a result of immunization in FcR and FcR2 rats compared to KLH control animals is given as “ratio” and the corresponding decrease (↓) or increase (↑) in protein levels is indicated as direction.

Biological process	Protein Annotation	Ratio		Direction
		FcR	FcR2	
Acute phase response signalling	Apolipoprotein A-I	5.3	7.0	↑
	Fibrinogen, alpha polypeptide	2.8	3.2	↑
	Fibrinogen, beta polypeptide	2.6	2.9	↑
	Fibrinogen, gamma polypeptide	2.5	2.5	↑
	Inter-alpha-inhibitor H4 heavy chain	2.2	2.0	↑
	Complement component 3	1.2	-	↑
	Transferrin	0.6	0.4	↓
	Albumin	0.7	0.4	↓
	Hemopexin	0.7	0.5	↓
Urea cycle	Catalase	1.5	1.4	↑
	Creatine kinase, brain	0.8	0.7	↓
	Creatine kinase, mitochondrial 1, ubiquitous	0.8	0.8	↓
ILK signalling	PREDICTED: similar to Actin, cytoplasmic 2	1.4	1.4	↑
	PREDICTED: similar to Filamin-A (Filamin-1)	1.7	1.7	↑
	PREDICTED: similar to myosin, light polypeptide 6	1.3	-	↑
	Vimentin	1.4	1.5	↑
Nitrogen metabolism	Carbonic anhydrase 2	2.0	2.0	↑
	Transglutaminase 2, C polypeptide	1.3	1.3	↑
Cell/ Tissue morphology	Myelin protein zero	5.9	13.7	↑
	Phospholamban	1.8	2.0	↑
	Annexin A2	1.2	1.3	↑
Mitochondrial dysfunction	PREDICTED: similar to Amine oxidase (Monoamine oxidase type A)	0.8	0.8	↓
Glycolysis	Phosphoglycerate mutase 2	0.8	0.7	↓
	Enolase 3, beta	0.7	0.7	↓
Amino acid metabolism	Prolyl 4-hydroxylase, beta polypeptide	1.3	1.4	↑
	Branched chain aminotransferase 2, mitochondrial	0.8	0.8	↓
Molecular Transport	PREDICTED: similar to Hemoglobin beta-2 subunit	1.4	1.3	↑
	Myoglobin	0.7	0.8	↓
Unclassified		2.4	2.9	↑
	Pregnancy-zone protein			
	Murinoglobulin 1 homolog	2.5	2.8	↑
	Kininogen 1	2.8	2.6	↑
	Alpha-1-inhibitor III	1.7	2.0	↑
	Adenine phosphoribosyl transferase (predicted)	0.8	0.8	↓
	PREDICTED: similar to myosin light chain 2, precursor lymphocyte-specific	0.7	0.7	↓

The rats immunized with peptides 1 and 2 of Fc gamma receptor were not significantly different from each other. The FcR and FcR2 groups were observed to align together in PCA plot compared to KLH controls (Fig.3.5a). Eight proteins were found to be uniquely identified in FcR rats whereas fourteen proteins were found to be unique to FcR2 (Table 25).

Table 25. Proteins identified unique to FcR and FcR2 rats compared to KLH controls

gi Number	Protein Annotation	Fold change	Direction
Proteins unique to FcR rats			
17985949	Hemoglobin beta chain complex	1.51	↑
40445397	Beta-globulin	1.45	↑
6981010	Hemoglobin alpha 1 chain	1.42	↑
109481431	Myosin light polypeptide 6	1.27	↑
11693172	Calreticulin	1.23	↑
8393024	Complement component 3	1.22	↑
62078857	Hypothetical protein LOC313163	1.22	↑
61556832	Adenine phosphoribosyl transferase	0.77	↓
Proteins unique to FcR2 rats			
6981022	Hexokinase 1	1.94	↑
13928744	Transgelin	1.84	↑
6978491	Aldehyde reductase 1	1.52	↑
8392983	Biglycan	1.50	↑
27688933	Collagen alpha-1(I) chain precursor	1.48	↑
13591983	Lumican	1.45	↑
13929178	Fibrillin 1	1.35	↑
109473201	PREDICTED: similar to Filamin-C (Filamin-2) isoform 2	1.21	↑
62646841	PREDICTED: similar to Calcium-binding mitochondrial carrier protein Aralar2 (Solute carrier family 25 member 13)	0.83	↓
13786200	Voltage-dependent anion channel 1	0.83	↓
61557218	Chaperone, ABC1 activity of bc1 complex like	0.83	↓
27661165	NADH dehydrogenase [ubiquinone] iron-sulfur protein 8, mitochondrial	0.82	↓

The proteins that displayed alterations in level in rats immunized with peptides 1 and 2 of Fc gamma receptor were largely the same indicating that the response to immunization with different peptides is not significantly different. Plasma proteins like hemoglobins and complement component were more prominent in rats immunized with peptide 1 whereas metabolic enzymes and extracellular matrix proteins pointing to fibrosis were more prominent in the animals immunized with peptide 2 of Fc gamma receptor. Myelin proteins zero, apolipoprotein A1, fibrinogen alpha polypeptide were identified at higher

levels in Fc gamma receptor immunized animals compared to controls. Myelin protein zero and apolipoprotein A1 were observed at greater than fivefold change in their intensities in FcR rats. Different isoforms of fibrinogens, namely, fibrogen alpha polypeptide, beta and gamma polypeptide were identified to have greater than two fold difference in their intensities compared to controls. Murinoglobulin, haemoglobin subunit beta-2, haemoglobin beta chain complex, haemoglobin alpha chain and myoglobin displayed elevated levels in FcR rats. In contrast, metabolic enzymes such as phosphoglycerate mutase 2, branched chain aminotransferase 2, enolase 3 showed lower intensities in FcR rats. Besides these, creatine kinase mitochondrial 1, ubiquitous and creatine kinase, brain also showed lower intensities compared to KLH controls.

A comprehensive picture of the protein changes in DCM rats immunized with peptides 1 and 2 of Fc gamma receptor showed an increased acute phase response signalling and interleukin signalling and reduced metabolic proteins compared to KLH controls. However, a few other structural proteins such as procollagen, type I, alpha 1, lumican, fibrillin besides fibrinogens and vimentin were also observed in higher amounts in Fc receptor immunized rats than in KLH controls. More over IPA analysis revealed acute phase response signalling proteins such as alpha, beta, gamma, inter alpha trypsin inhibitor H4. Proteins involved in metabolism such as creatine kinase B, branched chain aminotransferase are observed to have either directly or indirectly involved in interleukin-6 based protein network (Fig.41).

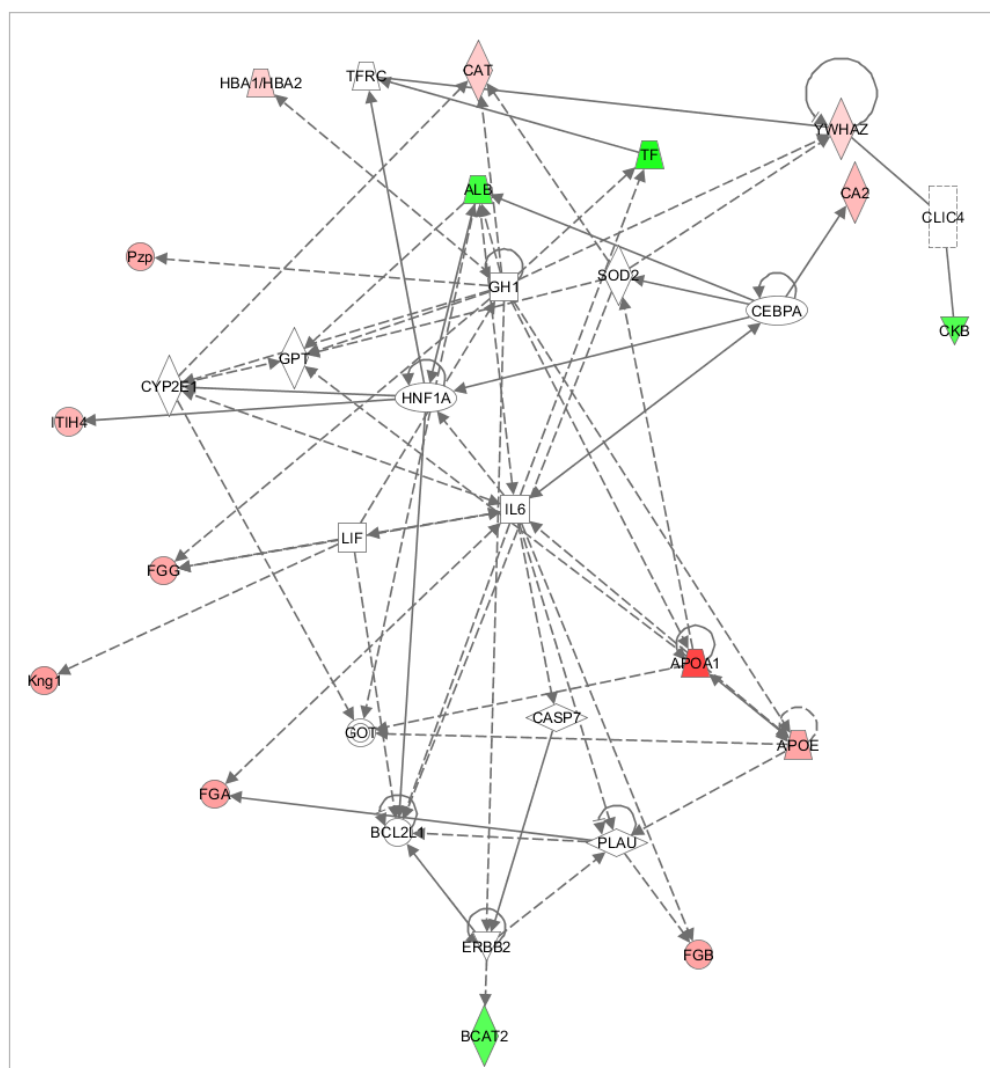


Fig. 41. Network of proteins involved in acute phase response and metabolism. Fibrinogens and other structural proteins were identified as strongly increased whereas proteins of metabolism and transport such as BCAT2, CKB, ALB and TF displayed lower levels in rats after immunization with peptides against Fc gamma receptor than in control animals. Pzp-pregnancy zone protein, FGG-fibrinogen gamma polypeptide, Kng1-kininogen 1, HBA1-hemoglobin alpha 1, CAT-catalase, CA2, carbonic anhydrase-2, FGB-fibrinogen beta polypeptide, FGA- fibrinogen alpha polypeptide, APOE-apolipoprotein E, APOA1- apolipoprotein A1, HK1, hexokinase 1, CKB-creatine kinase, brain, BCAT2, branched chain aminotransferase 2, ITIH4-inter alpha trypsin inhibitor, TF-transferrin, YWAZ-tyrosine-3-monooxygenase.

In summary, the current analysis shows acute phase response and fibrosis as dominant effects in rat hearts as a result of immunization with anti-CD32 peptides. This analysis provides an overview of the changes occurring in rats developing cardiomyopathy upon active immunization with antigenic peptides against cardiomyocyte Fc γ receptor and provides the basis for integrative analysis of the hemodynamic parameters recorded for the animal model with the molecular signature at the experimental end point.

4. Discussion

Dilated cardiomyopathy (DCM) is characterized by left ventricular dilation associated with systolic dysfunction ultimately leading to heart failure and death. It is one of the major causes of heart transplantation. Of the several causes of disease, virus induced dilated cardiomyopathy and in particular infection by coxsackievirus is most often associated with the disease. Viral myocarditis was best studied in mice since murine models of myocarditis mimic human myocarditis. The susceptibility of mice to the disease varies as certain strains of mice are resistant while others are susceptible to disease due to the genetic variability among the strains (Leipner et al., 2004, Esfanderei & McManus, 2008). A.BY is one strain which is susceptible to viral myocarditis by coxsackievirus infection and over a period of 90 days mice develop dilated cardiomyopathy leading to heart failure (Klingel et al., 1993, Esfanderei & McManus, 2008).

Much of the work in cardiovascular proteomics to characterize the disease status in human and animal models so far has been performed by two dimensional gel electrophoresis (2-DE). Comparative 2-DE analysis was used to screen right atrial samples from explanted hearts of 13 patients suffering from end-stage DCM with 15 control patients and 52 spots were reported to show DCM associated changes (Pleissner et al., 1997). In another experiment, proteomic analysis of patients with end stage heart failure either due to DCM or ischemic heart disease revealed significant changes in 93 proteins from 1600 spots (Corbett et al., 1998). Around 100 proteins have been identified to undergo disease dependent changes in expression by 2-DE in human, canine and bovine models of dilated cardiomyopathy (DCM). Using human heart tissue for proteomic studies introduces certain complications such as tissue heterogeneity, genetic variability, disease state, medical history and therapeutic intervention as well as the limited availability of the material. An alternative to overcome such problems is to employ animal models of human heart disease (McGregor & Dunn, 2003). Experimental animal models of heart disease in dog, rabbit, goat or swine are supposedly not very conclusive due to problems with their respective databases (Bukowska et al., 2004). Hence, rat and mice models of disease offer a better alternative. Moreover it has been established that murine models of viral myocarditis mimic human disease (Klingel et al., 1992). However, very few comparative proteomic studies exist to understand the differences between diseased and healthy mice. A systematic proteomic and transcriptomic analyses of DCM was performed in a murine

phospholamban mutant (R9C) to understand the changes in the protein profile in comparison to wild type mice. Changes in protein expression in the left ventricular proteome at three distinct stages (early, mid and late) of disease development were characterized in the phospholamban mutants (Gramolini et al., 2007, Gramolini et al., 2008). Earlier studies in A.BY mice have documented the time course of disease associated changes in the protein expression from acute to chronic phases of CVB3 induced dilated cardiomyopathy using 2D-DIGE (Hammer et al., 2010). The current study is the first to characterize the global changes in the protein profile at end-stage heart failure i.e. dilated cardiomyopathy in A.BY/SnJ mice at 84 days post infection with CVB3 using complementary techniques of 2D-DIGE and gel-free LC-MS/MS analysis.

4.1. Dilated cardiomyopathy associated changes in A.BY/SnJ mice hearts at 84 days post CVB3 infection

Early stages of CVB3 induced myocarditis in A.BY/SnJ mice were characterized with strong viral replication leading to large zones with necrotic myocytes, presence of mononuclear inflammatory cells, focal lesions and increased IL-6 expression at 8 d p.i. in the acute phase of the disease. During chronic myocarditis at 28 d p.i., the extent of inflammation decreased and the focal lesions were replaced by fibrosis, however the viral RNA still persisted despite a decrease in viral replication (Hammer et al., 2010). In the current study, tissue sections of A.BY/SnJ mouse hearts at 84 d p.i. showed dilation of the ventricle and severe fibrosis characterizing end-stage heart failure or dilated cardiomyopathy. Viral RNA, though at low levels, was observed by in situ hybridization indicating that the presence of viral RNA is important in the progression of the disease. Viral RNA was also observed in the myocardium of patients with myocarditis and dilated cardiomyopathy (Kandolf & Hofschneider, 1989). Though similar findings were reported in A.CA/SnJ mice, it was restricted only to 30d p.i. /chronic myocarditis (Klingel et al., 1992). The current study is the first to report the presence of trace amounts of viral RNA even after long term disease progression at end stage heart failure in A.BY/SnJ mice.

A total of 101 distinct proteins displaying DCM associated changes have been identified in infected mouse hearts compared to controls using complementary techniques of 2D-DIGE and gel-free LC-MS/MS analysis. 2D-DIGE was one of the earliest methods to separate closely related proteins (Klose et al., 1975, O' Farrell et al., 1975, Gorg et al., 2004) and enables the observation of changes on protein species level. Protein species comprise

proteins derived from one gene occurring in multiple forms due to RNA splicing, post-translational modification (PTM) or degradation (Jungblut et al., 2008). Therefore, 2D-DIGE is useful to assess to what extent PTM and degradation of proteins occur in the dilated murine hearts. Proteins collagen 6 alpha 1 (CO6A1), haptoglobin (HPT), serine protease inhibitor A3K (SPA3K), myosin regulatory light chain, ventricular isoform (MLRv), actin aortic, smooth muscle isoform (ACTA), 2-oxoisovalerate dehydrogenase (ODHA) were identified as chain or groups of spots indicating the existence of these proteins as several protein species. Furthermore, myosin and tropomyosin were detected at spot positions aside from their predicted molecular weight giving hints for degradation of these proteins. However, gel based proteomics is limited in resolving membrane proteins and proteins with extreme pI (Gorg et al., 2004, Gygi et al., 2000). To overcome these limitations and to increase protein coverage, complementary gel-free LC-MS/MS analysis was performed. 40% of the total proteins identified by gel-free LC-MS/MS analysis and around 30% of the proteins displaying DCM associated changes have pI >7. This finding clearly indicates the need for extending the pI-range of proteins covered by the analyses above pI 4-7. Moreover, 26% of the total proteins and 22% of the regulated proteins identified by gel-free analysis are membrane bound belonging to either outer or inner mitochondrial membrane, cytoplasmic- or endoplasmic reticulum membrane. A comprehensive analysis of 2D-DIGE and gel-free LC-MS/MS experiments pointed towards extensive fibrosis and left ventricular remodeling in DCM hearts accompanied with compromised myocardial contractility and a decreased energy metabolism. Proteins of energy metabolism such as those involved in respiratory electron transport chain and fatty acid metabolism and proteins of extracellular matrix were extensively identified by gel-free LC-MS/MS analysis whereas muscle contractile proteins, proteins of immunity and defense, carbohydrate metabolism and protein metabolism were identified by 2D-DIGE analysis.

4.1.1. Dilated cardiomyopathy is associated with an increase in fibrosis as a consequence of cardiac remodeling

Extracellular matrix proteins collagen 6 alpha 1 (CO6A1) and collagen 6 alpha 2 (CO6A2), besides collagen 1 alpha 1 (CO1A1) were observed to have increased in diseased hearts compared to controls. Extracellular matrix (ECM) produced by cardiac fibroblasts in the heart is dynamic and is continuously regulated by fibroblasts under normal and pathological conditions. Dependent on physiological status and the external

stimuli, fibroblasts change in their proliferation, migration, collagen deposition and matrix metalloproteinase (MMP) production. Cardiac fibroblasts differentiate into myofibroblasts with an enhanced capacity to secrete ECM. Elevated levels of type VI collagen play a key role in pathological remodeling via induction of myofibroblast differentiation which could lead to fibrosis (Naugle et al., 2006, Engvall et al., 1986). The myofibroblasts work in concert with fibroblasts in wound healing followed by apoptosis of myofibroblasts. When apoptosis is compromised, prolonged activity of these two types of cells causes excessive ECM accumulation. This in turn leads to stiffness and fibrosis affecting myocardial viscoelasticity initiating ventricular systolic and diastolic dysfunction (Shamhart et al., 2010, Sylvia et al., 2003). In homeostasis, coordinated degradation and synthesis of ECM components controls ECM turnover. MMPs and TIMPs – tissue inhibitors of MMPs-are the regulators of ECM homeostasis. An imbalance between these proteinases results in changes in ECM turnover thereby initiating pathologic remodeling. This leads to excess accumulation of collagen and fibroblasts.

Left ventricular dilation and cardiac fibrosis are hallmarks of inflammatory dilated cardiomyopathy. Collagen 6 acts as an adhesive structure in the basement membrane and interacts with other ECM components. Increase in levels of CO6A1 can be interpreted as an extension of fibrosis from chronic myocarditis into end stage dilated cardiomyopathy as it was also observed at higher levels in chronic stages of myocarditis in A.BY/SnJ mice (Hammer et al., 2010). Interstitial fibrosis and cardiac dysfunction in hypertrophic cardiomyopathy have also been correlated to elevated levels of type VI Collagen (Kitamura et al., 2001). Besides, enhanced fibrosis is also characterized by excessive accumulation of collagen I causing impaired diastolic function (Kania et al., 2009) as also observed in the current study. Accumulation of collagen I is responsible for fibrotic stiffening of the myocardium and was shown to be 3 times elevated in explanted hearts of patients with idiopathic dilated cardiomyopathy (Weber KT, 1989, Polyakova et al., 2011).

Interaction partners of collagen such as decorin (PGS2) and lumican (LUM) were also observed as elevated in hearts of DCM mice compared to healthy controls. Decorin, an ubiquitous chondroitin / dermatan sulfate proteoglycan is associated with tissues rich in type I and type III collagen and is known to co-localize with large helical collagen fibers (Bianco et al., 1990, Thieszen et al., 1995). In myocardial infarction, it is reported that fibrosis of the left ventricle occurs rapidly during recovery phase and the collagen concentration doubles. Decorin expression supposedly occurs subsequent to the

accumulation of collagen. Increase in the collagen and decorin concentration in the recovery phase post-MI indicates that decorin expression and collagen cross-linking might be related (Zimmerman et al., 2001). Lumican is another known interaction partner of collagens. Lumican co-localizes with fibrillar collagens in the corneal stroma and its mRNA was found to be expressed in human skeletal muscle, heart, liver pancreas, brain, placenta, lung and intervertebral discs (Blochberger et al., 1992, Grover et al., 1995). In ischemic and re-perfused heart tissues, lumican was observed to be highly expressed in the fibrotic lesions (Baba et al., 2001). Lumican protein has been correlated with collagen fibrillogenesis of intimal thickening in atherosclerosis. When expressed at high levels, it is thought to contribute to assembly of collagen fibers (Onda et al., 2002). Thus, increase in the levels of extracellular matrix proteins like collagens and their interaction partners suggests extensive fibrosis as a consequence of cardiac remodeling associated to cardiac dysfunction in A.BY/SnJ at 84 d p.i.

4.1.2. Compromised myocardial contractility as a result of virus induced dilated cardiomyopathy

Dilated cardiomyopathy is associated with decreased or compromised myocardial contractility. The results of the present study support the assumption that both thick and thin filaments of the myocardium are affected in DCM. Thick filament proteins myosin heavy chain 6 (MYH6), myosin regulatory light chain 2 (MRLC2) and myosin regulatory light chain 2, ventricular form (MLRv/MLC2) were observed at decreased levels in dilated hearts compared to healthy controls. Also a profound decrease in RNA expression of MYH6/ myosin heavy chain, cardiac muscle, alpha isoform (α -MHC) was observed in myocardial failure compared to non-failing ventricular myocardium in humans (Lowes et al., 1997). Down regulation of α -MHC and up-regulation of myosin heavy chain, cardiac muscle, beta isoform (β -MHC) / myosin heavy chain 7 (MYH7) gene expression can lead to the development of myocardial dysfunction and cardiomyopathy (Jones et al., 1996). However MYH7 could not be identified in the current analysis, but only represents about 1 % of the total myosin content in the heart (Carniel et al., 2005) and therefore, probably has been below the detection level. MYH6 was observed in multiple spots in the DIGE analysis and was distributed over the whole gel at molecular weights lower than expected (223kDa). The identified MYH6 fragments did not contain the N-terminal part and hence were not functional since the N-terminal region of MYH6 is responsible for its actin binding and ATPase activity (Krenz et al., 2007). Degradation products of MYH6 were

also reported in chronic stages of myocarditis in A.BY/SnJ mice (Hammer et al., 2010) and in other mammals (Cicek et al., 2002). The reason for the degradation of MYH6 is not clear yet.

Myosin regulatory light chain (MRLC2), an interaction partner for myosin heavy chain, was observed to have decreased in A.BY/SnJ mice hearts with DCM. In patients with dilated cardiomyopathy, a lower MRLC2 gene expression level was observed, too (Trahair et al., 1993). MRLC2 interacts with a C-terminal α -helix forming the myosin heavy chain lever arm and influences the stiffness and flexibility of the myosin head. Based on the position of regulatory light chain at the fulcrum of the lever arm, the protein plays a significant role in modulating cardiac contractility (Hopkins et al., 1998, Rayment et al., 1993). Phosphorylation of MRLC2 triggers conformational changes in the protein which regulates contraction of the myofibrils by modulating myosin ATPase activity (Margossian et al., 1985). However, MRLC2 was not identified as phosphorylated in the current study. On the other hand, myosin regulatory light, ventricular form (MLRv/MLC2) showed increased phosphorylation in DCM hearts compared to controls. In isolated thin filaments, phosphorylation of MLRv/MLC2 caused displacement of the crossbridges away from the thick filaments due to electrostatic repulsion between the phosphate group and the fixed charge on the surface of the filament whereas in intact myofilaments, MLC-2 phosphorylation displaces crossbridges closer to actin (thin filament) increasing the possibility of binding but slows relaxation (Fig.42). Myosin light chain kinase (MLCK) is involved in the phosphorylation and thereby regulation of MLC2. Calcium and protein calmodulin activate cardiac MLCK (Levine et al., 1996, Patel et al., 1998).

Mice with decreased gene expression of cardiac MLCK have been reported to develop cardiac hypertrophy and fibrosis (Ding et al., 2010). However, MLCK could not be identified in the current analysis and though calmodulin was observed in higher amounts in DCM hearts by gel-free LC-MS/MS, the difference was not statistically significant. It has been postulated that dysregulation of calcium/calmodulin, phosphorylation/dephosphorylation or down regulation of MLC2 gene expression could play a role in a common pathway leading to apoptosis and progressive dysfunction (Pauly 2011). Phosphorylations of MyBPC and MLRv (MLC2) were reported to correlate with virus infection related changes in the chronic stages of myocarditis in A.BY/SnJ mice (Hammer et al., 2010). Phosphorylation of MLRv in the late stages of the disease (84 d p.i) suggests the continuous existence of a higher proportion of this modified protein in acute

and chronic myocarditis as well as DCM which might be a protective mechanism against apoptosis and dysfunction. In skeletal and cardiac muscle where thin filaments play an active role in the contraction, regulatory light chain phosphorylation is thought to play a modulatory role than activate contraction (Moss et al., 2006, Ding et al., 2010).

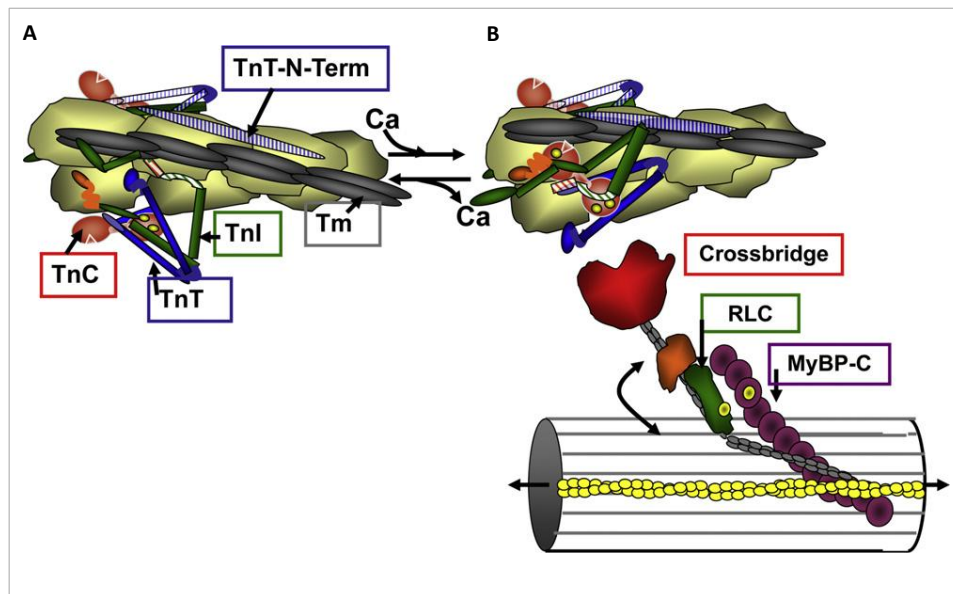


Fig. 42. Illustration of the transition between diastole and systole within a region of overlap between thick and thin filaments of the cardiac sarcomere. A-diastole: The relaxed state is shown with thin filament troponins (TnC, TnT, TnI) and tropomyosin(Tm) blocking the reaction of crossbridges with actin. B-systole: The binding of Ca^{2+} to TnC releases Tm and TnI from the blocking position, and crossbridges (fastened to associating light chains (RLC) and MyBP-C), react with actin and mechanically work to pull the thin filaments towards the center of the sarcomere. The net negative charges (illustrated by yellow circles) induced by phosphorylation of both the N-terminus of RLC and the cardiac-specific domain of MyBP-C, create an opposition between RLC and MyBP-C, which might contribute to the positioning of myosin heads relative to actin (Adopted and modified from Scruggs & Solaro, 2011).

As observed above, cardiac muscle contraction and relaxation is regulated by the intracellular Ca^{2+} concentration. Alterations in the thin filaments of the myocardium such as those found in the present study for troponin T2 and tropomyosin- α also influence the contractility. Troponin T plays a role in changing from calcium insensitive troponin C–troponin I complex to a calcium sensitive form in Mg^{2+} -ATPase system (Robinson et al., 2002). During systole, the rise in free calcium promotes Ca^{2+} binding to cardiac troponin C. This leads to the translocation of cardiac troponin I and tropomyosin away from the outer domain of the actin filaments, allowing for interaction of crossbridges and the generation of tension. During diastole Ca^{2+} levels decline and Ca^{2+} dissociates from cardiac troponin C, and the inhibitory actions of cardiac troponin I and tropomyosin are

restored (Gordon et al., 2000, Li et al., 2004). Decrease in the levels of troponin T2 and tropomyosin 1 alpha in A.BY mice hearts at the end stages of viral dilated cardiomyopathy along with decreased levels of thick filament proteins might be responsible for cardiac dysfunction and reduced left ventricular ejection fraction observed in dilated cardiomyopathy.

4.1.3. Dilated cardiomyopathy is associated with decreased levels of proteins involved in energy metabolism

Heart and in particular myocytes involved in contractility depend on mitochondria for their energy supply. β -oxidation of fatty acids and respiratory electron transport chain in mitochondria are the major sources of ATP for the adult heart (Casademont et al., 2002, van der Vusse et al., 1992, Lopaschuk et al., 2010, Ingwall, 2009). Fatty acid metabolism can have a profound effect on heart failure and mitochondria play an important role in various cardiac pathologies like cardiomyopathy and congestive heart failure (CHF) (Marin-Garcia et al., 1995, Stanley et al., 2005, Gustafsson et al., 2008).

Enough evidence exists on decreased expression and activity of proteins involved in cardiac fatty acid uptake and fatty acid oxidation in heart failure suggesting impaired mitochondrial function. Proteins involved in β -oxidation of fatty acid were identified in lower levels indicating a decrease in the fatty acid oxidation in idiopathic cardiomyopathy (iDCM) (Davila-Roman et al., 2002). Proteins 3-methylcrotonyl CoA carboxylase (MCCA), long chain fatty acid CoA ligase 1 (ACSL1) and ornithine aminotransferase levels decreased in the current analysis in dilated A.BY/SnJ mice hearts as compared to controls. Similar results on the fatty acid oxidation enzymes were reported at the gene level in the Incyte cDNA array mouse model with elevated mtDNA mutations which develop four chambered dilated cardiomyopathy (Zhang et al., 2005). mRNA levels of long chain acyl CoA dehydrogenase and mRNA and protein expression of medium chain acyl CoA dehydrogenase enzymes involved in fatty acid β -oxidation were observed to have decreased in explanted hearts of patients with end stage heart failure compared to controls (Sack et al., 1996). Very long chain acyl CoA dehydrogenase (VCAD) observed at lower levels in A.BY/SnJ hearts showed a similar decrease in gene expression in patients with hypertrophy (Barger et al., 1999). The decreased levels of proteins related to fatty acid β -oxidation suggest a decreased energy supply to the heart. The decrease in the expression of fatty acid β -oxidation enzymes, though not clearly understood so far, is

speculated to be due to reduced activation of gene expression by the PPAR α pathway (Berger et al., 2000). An increase in the glycolytic enzymes which might compensate the lower activity of beta-oxidation was not observed in the current analysis.

Besides fatty acid metabolism, another important pathway which influences energy supply to the heart is the electron transport chain. Components of the electron transport chain were found in lower amounts especially for complexes I, II, III, IV and V. However, the decrease in the levels was not consistent for all subunits of the complexes. Earlier reports on electron transport chain (ETC) complexes in failing hearts have also shown differences in the expression of subunits using 2-DE (Agnetti et al., 2010). A more valuable conclusion on the importance of the obvious imbalance between ETC complex subunits could be drawn by activity measurements. The significant decrease in the activity observed in dilated A.BY/SnJ mice hearts points towards a lowered energy production. Similar findings were reported for a canine model of iDCM. Activities of complex I and V were identified to have reduced by 60% and 50% in Doberman pinscher dogs suffering from iDCM (McCutcheon et al., 1992). Similar phenomena in the content and activity of complex III and IV of ETC were observed in isolated mitochondrial particles from DCM patients who received heart transplants. Complex III activity was also reported to decrease in patients with iDCM (Buchwald et al., 1990, Jarreta et al., 2000, Quigley et al., 2000).

4.1.4. Changes in the phosphorylation of proteins associated with virus induced dilated cardiomyopathy in mice hearts 84 d p.i.

Earlier studies during acute and chronic stages of myocarditis in A.BY/SnJ mice have shown increased phosphorylation of muscle contractile proteins such as myosin regulatory light chain and myosin binding protein C besides desmin and Rab GDP dissociation inhibitor beta (Hammer et al., 2010). Monitoring the changes in the phosphorylation of the proteins during later stages of the disease i.e. end stage dilated cardiomyopathy, would improve understanding of the changes in the behaviour of the proteins in response to disease.

Analysis of the ProQ stained gels revealed altered phosphorylation for about 30 spots. However, for only six of them the phosphorylation site could be identified. The majority of the phosphoprotein spots were very faint indicating the small fraction of total protein indeed modified by PTM. The low protein amount in the spot together with the weak signal intensity of phosphopeptides analysed in positive mode of MS might have

hampered the identification of many of the phosphosites. An increase of the phosphorylated species was observed for heat shock protein beta 1/Hsp 25 (HSPB1), heat shock protein 90 beta (HS90B), myosin regulatory light chain ventricular isoform (MLRv) and actin aortic, smooth muscle (ACTA) while a decrease in the phosphorylation was observed for proteins 2-oxoisovalerate dehydrogenase subunit alpha, mitochondrial (ODBA) and phosphoglucomutase 1 (PGM1). Influence of phosphorylation of contractile proteins was discussed in the earlier section (4.1.2).

Furthermore, increase in the phosphorylation of heat shock proteins has been interpreted to be a protective mechanism under diseased conditions. Increase in the phosphorylation of Hsp 27, the human homologue of mouse Hsp25 was observed in hearts of patients with ischemia/ reperfusion damage or dilated cardiomyopathy (Lutsch et al., 1997). A similar increase in Hsp 27 phosphorylation was also observed in canines with congestive heart failure (Dohke et al., 2006). Viruses belonging to families herpesviridae, papillomaviridae, paramyxoviridae, flaviviridae, togaviridae, retroviridae and hepadnaviridae were reported to induce Hsp 25/27 expression or phosphorylation (Li et al., 2010). Murine Hsp25 was reported to inhibit apoptosis both upstream and downstream of cytochrome c release from mitochondria (Arya et al., 2007).

The physiological effect of decrease or increase in phosphorylation of 2-oxoisovalerate dehydrogenase phosphorylation is not known, however, an increase in the phosphorylation of PGM1 might play a protective role in inhibiting apoptosis and glucose metabolism as a cell survival technique (Danial et al, 2003). It is documented to be phosphorylated by p21 activated kinase 1 (PAK1) which helps in increased conversion of glucose-1-phosphate to glucose-6-phosphate towards utilisation in pentose phosphate pathway (Gururaj et al., 2004). However, in the current analysis, a decrease in the phosphoglucomutase 1 phosphorylation was observed which in turn fits to the missing induction of glycolysis in the DCM hearts.

From the above analysis, it can be inferred that an increase in the phosphorylation of contractile proteins and heat shock proteins acts as a cell survival compensatory mechanism during virus induced dilated cardiomyopathy.

In summary, an impaired mitochondrial function characterized by decreased energy production was observed in the dilated hearts of A.BY/SnJ mice affected with dilated cardiomyopathy upon CVB3 infection. A similar decrease in the expression of genes

related to fatty acid metabolism and mitochondrial respiratory chain was also observed in another mouse model susceptible to viral infection (BALB/c mice model) leading to dilated cardiomyopathy (Xu et al., 2010). Impaired mitochondrial function is multifaceted with consequences of decreased availability of ATP, contractile defects and myocardial structural changes (Casademont et al., 2002), as it was also observed in the current analysis. Implementing complementary techniques of 2D-DIGE and gel free LC-MS/MS analysis helped in attaining a comprehensive picture of the changes in the protein profile of mice hearts affected with coxsackievirus induced dilated cardiomyopathy.

4.2. Age dependent changes in the proteome profile of A.BY/SnJ mouse hearts

As seen above in the case of viral dilated cardiomyopathy, the disease progresses over a period of 3-4 months during which the animals also age. It is well documented that aging is one of the many factors that makes the heart susceptible to diseases such as congestive heart failure (CHF), coronary heart disease, atherosclerosis, myocardial infarction, hypertension etc.. Aging can cause an increase in cardiac arrhythmias as well as diastolic and systolic dysfunction which can ultimately lead to cardiac failure and death. Thus, the chances of developing arteriosclerosis increase significantly with aging and there exists a difference in cardiac remodeling due to aging as well (Oxenham et al., 2003, Olivetti et al., 1990, Shih et al., 2010, Lakatta et al 2002). In order to understand and interpret if the changes observed in diseased condition are purely due to infection/ disease and to avoid the influence of age in the outcome of the disease, it becomes imperative to use age matched controls. However, studying the changes in the heart due to aging is also equally important given the role of age in susceptibility of the disease. Proteomics offers the tools for studying global changes in the proteome profile of hearts due to aging. Several proteomic studies exist characterizing the changes in the protein profile due to aging in young and old hearts in rat, monkey, bovine and murine models. Most of the studies were performed comparing hearts from 3-5 months old animals with 12-26 months old ones (Dai et al., 2008, Kwong et al., 2000). Also most of these studies were done using conventional 2DE (Kim et al., 2007, Kanski et al., 2005, Yan et al., 2004, Kiri et al., 2005) while a few studies also applied the more advanced iTRAQ technology (Grant et al., 2009, Walther et al., 2010). Analysis of aging in murine models was performed primarily in C57BL/6J mice (Chakravarti et al., 2008, Walther et al, 2010). The current proteomic analysis is unique from other studies in characterizing the global changes in protein profile of A.BY/SnJ mice at a much earlier time span of mouse life by comparing hearts of 1

month and 4 months old mice. The fact that 96 distinct proteins altered in this time span clearly shows that alterations occur during aging and have to be considered in designing the experiments.

4.2.1. Altered mitochondrial function in 4 months old A.BY/SnJ mice hearts

Mitochondria play a significant role in aging. Altered mitochondrial function might lead to increased oxidative stress which causes oxidative damage to proteins associated with aging (Lenaz et al., 2002, Chakravarti et al., 2007). Fifteen proteins involved in respiratory electron transport chain were identified in by gel-free LC-MS/MS in the current analysis. Though the total protein content for each of the complexes of respiratory chain did not show significant differences, individual subunits of complex I, IV and V showed changes in the levels due to aging. Of these, most prominent changes were observed for complex V/ATP synthase with protein species of ATP5H, ATPO, ATPD and ATPA subunits identified in lower amounts in 4 months old hearts. Decrease in the levels of ATP synthase complex proteins point towards decreased ATP production in the cell. Similar results were reported in aging rat and mice hearts where different subunits of ATP synthase showed ambiguity. This is postulated to be due to either post-translational modification or proteolysis of the molecule (Chakravarti et al, 2008). ATPB however was identified as degradation products on the gel in our DIGE analysis.

Complex I subunits have also been reported to show inconsistent differences in left ventricles of aged rats (Chakravarti et al, 2008, Grant et al, 2009). Similar changes have also been reported at the RNA level earlier with respect to aging mice. mRNA of complexes I-IV like NADH subunit 1, cytochrome c oxidase subunit 3 and cytochrome b were observed in reduced levels in old hearts compared to young hearts in C57BL/6 mice where 20 months old animals were compared to 4 months old animals (Bodyak et al., 2002). This indicates altered mitochondrial function during aging but does not produce a clear picture on the total outcome though it leans towards reduced ATP synthesis. Also activity assays could not provide a clear picture of the respiratory chain regulation due to aging. Although imbalance in protein levels of the subunits of electron transport chain complexes was associated with lower activities, such measurements were not possible within the timeframe of this study. However, Kwong et al. reported a minor increase of about 10% in C-II and C-IV activities in a comparison of 30 months old C57BL/6J mice with 12 months and 3.5 months old animals (Kwong et al., 2000).

Another pathway which was significantly influenced in 4 months old mice hearts is fatty acid metabolism. Proteins BDH, CPT1B, CPT2, ACS2L, CACP located either in mitochondria, endoplasmic reticulum, or peroxisomes were identified in higher amounts in 4 months old hearts. BDH/3-hydroxybutyrate dehydrogenase showed maximum difference in the protein amount in old hearts. It catalyzes the formation of acetoacetate into β -hydroxybutyrate and its expression was reported to have increased in ischemia as a protective mechanism (Kim et al., 2006). Proteins carnitine palmitoyl transferase 1 (CPT1) and carnitine palmitoyl transferase 2 (CPT2) are involved in the cellular fatty acid utilization. Especially CPT1 is involved in the long chain fatty acid uptake which is a rate limiting step in fatty acid oxidation, whereas CPT2 majorly catalyses the hydrolyses of the transported molecules in fatty acid acyl CoA and carnitine in the mitochondrium (Fig.43). In mammals, continuous circulation of lipids is under the influence of CPT1 gene transcription which is known to be activated by long chain fatty acids via PPAR α . In PPAR α k.o. mice, a decreased expression of muscle CPT1 was observed to effect the chief energy production (Brandt et al., 1998).

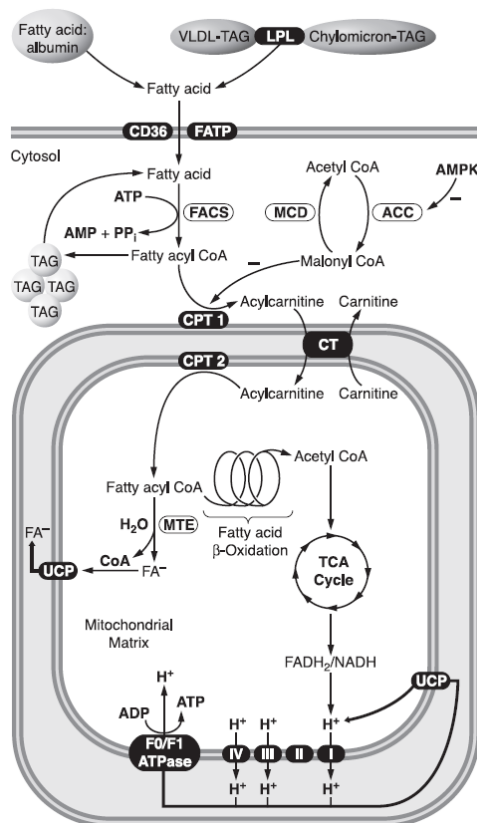


Fig. 43. Fatty acid metabolism in the heart. Fatty acids are taken up by the heart CD36/FATP transporters. Inside the cytosolic compartment of the cardiac myocyte, fatty acids are esterified to fatty acyl CoA by fatty acyl coA synthase (FACS). The acyl group of fatty acyl CoA is transferred to carnitine via carnitine palmitoyltransferase (CPT 1). Acylcarnitine is then shuttled into the mitochondria, where it is converted back to fatty acyl CoA by carnitine palmitoyl transferase (CPT 2). Most of fatty acyl CoA enters the fatty acid - oxidation cycle, whose products enter mitochondrial respiratory chain via TCA cycle for ATP synthesis (Adapted from Lopaschuk et al., 2010).

Besides CPT1 and CPT2 in the hearts, an increase in the levels of carnitine acetyl transferase was observed with longer life time of mice. Although the carnitine level was not measured within this study, this finding might be interpreted as a compensatory effect, because decreased levels of this molecule, cardiolipin and impaired pyruvate metabolism were reported in aged rats (Paradies et al., 1990). In turn, administration of acetyl-L-carnitine to old rats (28 months) restored the metabolic functions such as pyruvate oxidation and transport compared to young rats (5 months) (Paradies et al., 1999). Other mitochondrial enzymes such as long chain acyl CoA dehydrogenase, very long chain acyl CoA dehydrogenase, short chain acyl CoA dehydrogenase involved in fatty acid metabolism were also identified in the current analysis, however, were not observed as significantly regulated in the 4 months old mice hearts. Therefore, taking all data together, an increased fatty acid turn over can be supposed which might reflect the higher energy demands of mice hearts at this age.

4.2.2. Increased intracellular protein transport in 4 months old A.BY/SnJ mice hearts compared to young 1 month old hearts

An increase in the levels of proteins involved in protein transport/vesicular transport was observed in 4 months old mice hearts compared to 1 month old mice hearts. Among them β -taxilin (TXLNB) was identified in multiple spots indicating the existence of different species of this protein displaying approximately three fold increase in intensity. The protein is abundantly expressed in skeletal muscle and heart and is involved in the transport of vesicles to the plasma membrane. β -taxilin is considered to be the human homologue of chicken MDP77 as it shares 57% amino acid sequence homology. Increased transcript levels were observed in chicken during development (Yoshida et al., 2005, Nogami et al., 2004, Fujimori et al., 2002). However, the physiological role of this protein in heart is not yet clearly understood.

Another protein involved in vesicular transport and membrane trafficking with higher level in older mice was tripartite motif-containing protein 72 (TRI72) or Mitsugmin 53 (MG53), a skeletal and cardiac muscle specific protein. It was observed that over expression of MG53 in mice enhanced vesicular trafficking to sarcolemmal membrane and knock-out of MG53 impeded myoblast differentiation in mice (Masumiya et al., 2009, Cai et al., 2009,). Furthermore, trafficking of intracellular vesicles to the injury site in the muscle is mediated by TRI72. Rab GDP dissociation inhibitor beta (GDIB), also involved in vesicular transport showed strong changes in 4 months old mice hearts compared to young 1 month old hearts. Rab proteins, due to their association with secretory and endocytic pathways, play an important role in regulation of vesicular transport and help in docking of transport vesicles with their corresponding acceptor membranes (Yang et al., 1994). Increased levels of transitional endoplasmic reticulum ATPase (TERA)/ Valosin-containing protein might point to alterations of protein-protein interactions in membrane transport by its association with clathrin-a structural protein involved in receptor-mediated endocytosis (Pleasure et al., 1993). However, much less is known about the role of these transport proteins in mouse hearts. Increase in the levels of the proteins involved in protein/vesicular transport can be inferred as a secondary effect leading to endoplasmic reticulum associated protein degradation (ERAD) by either proteasome or macroautophagy pathway. Stress protein-70 (GRP75) involved in the protein recognition step of ERAD (Vembar, 2008) was also observed at increased levels in 4 months old hearts compared to young 1 month hearts in A.BY/ SnJ mice.

Using complementary methods of DIGE and LC-MS/MS, the current study is the first to identify proteins taxilin-beta (TXLNB), carnitine-O-palmitoyltransferase-1, muscle isoform (CPT1B), carnitine-O-palmitoyltransferase 2, mitochondrial (CPT2), in relation to aging and in A.BY/SnJ mice hearts. However, the current analysis also identified proteins similar to earlier reports of aging in mice and rat hearts. In C57BL/6 mice, transcripts of HSP70 (GRP75), cytochrome c and tropomyosin alpha 1 showed lower levels in aging when 4 months mice hearts were compared to 20 months hearts (Bodyak et al., 2002). Similar results were observed in our analysis at an earlier time point in A.BY/SnJ mice hearts at the proteome level. For most of the proteins such as lactate dehydrogenase B chain (LDHB), mortalin (GRP75), translation elongation factor 2 (EF2), myoglobin (MYG), phosphoglycerate kinase 1 (PGK1), desmin (DESM), voltage dependent anion channel 1 (VDAC1) altered in 4 months old A.BY mice, a negative correlation between level and age was also reported in CB6F1 mice (Dai et al., 2008). Also the changes due to aging in the current study share close similarities to those when hearts of young 4 months old rats were compared to 26 months old animals analysing iTRAQ labelled protein extracts (Grant et al., 2009). 11 proteins identified within this study were also identified in our analysis. Proteins such as pyruvate dehydrogenase E1 component subunit beta, mitochondrial (ODPB), phosphoglycerate kinase 1 (PGK1), hemoglobin alpha (HBA), hemoglobin 1 β (HBB), desmin (DESM), troponin T2 (TNNT2), tropomyosin alpha 1 (TPM1), cytochrome c, somatic (CYC) and voltage dependent anion channel-1 (VDAC1) were identified in lower levels in old animals similar to that of reported by Grant et al. (2009).

In conclusion, protein/vesicular transport, lipid metabolism and mitochondrial electron transport chain which play important role in the survival and energy production of the cell are altered already in young mice. Increase in carnitine transferases might be interpreted as a compensation of decreased ATP production and as a protective mechanism against apoptosis. The occurrence and therefore the response on apoptotic events might be supported by increased levels of GRP75 for which anti-apoptotic role in vascular smooth cells was reported earlier (Taurin et al., 2002). In total, due to the unexpected extensive changes within 3 months of mice life span, all experimental setups should include age matched controls in order to adjust for age related differences.

4.3. Alterations in the whole heart proteome of rats due to over expression of Adenine nucleotide translocase 1

Heart tissue is replete with mitochondria and the experiments in A.BY mice point towards compromised energy metabolism in the heart under disease conditions. Especially the components of respiratory electron transport chain were observed to be predominantly influenced in dilated cardiomyopathy as shown above (section 4.1.3). Decrease in the activities of the complexes I-IV in mice suffering from dilated cardiomyopathy indicate decreased energy/ATP production and henceforth decreased energy supply to the heart. The transport or exchange of ADP/ATP across mitochondrial membrane is carried out by a carrier protein adenine nucleotide translocase (ANT). ANT1 overexpression has been reported to play a protective role by preventing cardiac dysfunction in hypertrophic and diabetic cardiomyopathy (Walther et al., 2007, Wang et al., 2009). To understand the influence of ANT in the heart, the changes in the proteome profile of transgenic rat hearts over expressing ANT protein against wild type rat hearts were studied.

Three months old ANT-OE rats have collected somewhat more weight and hearts have non-significant higher ejection fraction, larger inner diameter of the ventricle and slightly hypertrophic phenotype (personal communication, Andrea Dörner). On the molecular level predictive pathway analysis revealed integrin-linked kinase signalling predominantly altered in ANT-OE rat hearts. Proteins myosin 11, myosin heavy polypeptide 9, myosin heavy chain polypeptide 7, filamin, fibronectin, integrin $\beta 1$, and integrin linked kinase (ILK) were observed at higher levels in ANT-OE rat hearts compared to WT hearts. ILK is associated with regulation of cell proliferation, differentiation, migration and also in the regulation of several signalling pathways. It is also known to interact with the cytoplasmic domains of $\beta 1$ and $\beta 3$ integrins and can phosphorylate myosin light chain and its regulators (Persad et al., 2003, Legate et al., 2006) which would fit to the slightly improved hemodynamics in these animals. Besides the indication of increased cellular growth and proliferation, it also points towards protein phosphorylation in ANT-OE rat hearts. ILK also has a role in cell-matrix adhesion and actin cytoskeleton reorganization and regulates cell matrix and cadherin mediated cell-cell contact (Nikolopoulos et al., 2002, Chen et al., 2006). Although in the current study the molecules cadherin 2, cadherin 13 and catenin (cadherin associated protein) involved in cell-cell contact were identified, no significant alterations were found in ANT-OE rat hearts.

Besides being involved in ILK signalling, myosins along with other proteins such as dystrophin and tropomyosin 1, alpha isoform, are also responsible for cell structure/assembly and muscle contraction and were identified in higher amounts in ANT-OE rat hearts than in hearts of the wild type. Similar increase in the levels of myofibrillar proteins belonging to both thick and thin filaments was also reported in isolated cardiomyocytes from transgenic ANT-OE rat hearts (Vogelpohl et al., 2011). While a significant elevation in total left ventricular myosin heavy chain protein was observed in the isolated cardiomyocytes of rat, different isoforms of myosin heavy chain protein were identified as increased in whole heart tissue of ANT-OE rats compared to wild type controls suggesting increased contractile function. Increased cardiac contraction and relaxation is thought to be influenced by Ca^{+2} re-uptake by a set of proteins such as SERCA2a, plasma membrane Ca^{2+} ATPase (PMCA) and $\text{Na}^{2+}/\text{Ca}^{2+}$ exchanger (NCX). While protein amounts of SERCA2a and PMCA were elevated in isolated cardiomyocytes of transgenic hearts, such a phenomenon could not be observed in the current analysis.

Increase in amounts of proteins of the contractile apparatus in transgenic ANT over expressed hearts has been linked to increase in the cell size of the cardiomyocytes which contributes to elevated contractile function and preservation of cell structure. Intact cell structure with an organized contractile apparatus has been hypothesized to improve the function of heart and enhance the survival (Vogelpohl et al., 2011, Walther et al., 2007).

Furthermore, correlation of ANT-OE with heat shock protein levels was observed. Four proteins belonging to the heat shock family namely- heat shock protein 1 alpha, heat shock protein 4, heat shock protein 27kDa protein 1 and protein 2 showed higher levels in transgenic ANT-OE hearts than in wild type control rats. In mice, the activity and expression of ANT has been reported to be influenced by heat shock transcription factor 1 (HSF1). HSF1 is responsible for the transcriptional activation of mammalian HSPs and in mice, it is reported to regulate the expression of heat shock proteins such as Hsp 25 and Hsp 70. Deficiency of HSF1 in *hsf1* $-/-$ mice reportedly decreases the functional activity of ANT1 resulting in a decrease in ADP/ATP exchange besides a selective repression of Hsps in the heart (Yan et al., 2002). Though HSF1 was not identified in the mass spectrometric analysis of ANT-OE hearts, the increase in the amounts of Hsps observed in the transgenic hearts might be a secondary effect of overexpression of ANT.

On the other hand, proteins of the mitochondria were identified to have decreased in ANT-OE rats except for monoamine oxidase A and cytochrome c oxidase subunit II which were identified at increased amounts by mass spectrometry. Though different subunits of NADH complex, cytochrome c oxidase and ATP synthase were identified, they were not found to be significantly altered in ANT-OE hearts. Also protein adenine nucleotide translocase 1/ solute carrier family 25, member 4 did not show significant change in transgenic hearts although it was shown that ANT1 is expressed in the rat model over a time span up to 8 months. Also in isolated rat left ventricular mitochondria, ANT protein amounts in transgenic animals did not show significant increase than in wild type (Walther et al., 2007). The amount of ANT is hypothesized to adapt to the ATP production and the amount of mitochondria in the cell (Dorner et al., 1999). However, such a conclusion cannot be derived from the current analysis and hence a more in-depth analysis of the total ANT protein content and its activity might provide a better idea.

In summary, the current proteomic analysis provides an overview of the influence of ANT1 over expression in rat hearts. This knowledge was seen as a starting point to analyse the influence of ANT-OE under pathologic conditions.

4.3.1. Comparative proteomic analysis of mitochondrial fractions of rat hearts over expressing adenine nucleotide translocase 1 and wild type hearts upon infection with Coxsackievirus B3

Analysis of the mitochondrial fractions revealed significant changes in mitochondrial proteins and structural proteins within the groups. This might be due to differences in the preparation of the mitochondrial fractions from the infected hearts. One-third of the total identified proteins as well as of the regulated proteins were observed to be of mitochondrial origin. However, the identification a number of structural proteins poses question on the purity of the mitochondrial fractions obtained.

Decrease in the proteins of the respiratory electron transport chain belonging to complexes I, II, IV and V hints towards compromised mitochondrial function associated with CVB3 infection in ANT-OE hearts compared to controls. CVB3 associated decrease in the activities of complexes I-IV was also observed in A.BY/SnJ mice 84 d p.i. as discussed earlier. However, the activities of respiratory chain complexes were observed to have increased in double transgenic overexpressing ANT1 and renin (ANT/REN-OE) rat models of hypertension induced heart disease suggesting protective role of ANT-OE

(Walther et al., 2007). The results from the current analysis do not hint towards such a conclusion. The proteins of respiratory transport chain in ANT-OE infected rats did not show any difference in the behaviour when compared to a similar disease model of A.BY/SnJ mice without overexpression of ANT1. However, the infection and therefore the predicted death and lysis of myocytes in the hearts might impair the former positive effect of higher ANT-1 levels. Furthermore, proteins of fatty acid metabolism displayed decreased levels in infected ANT-OE rats. These enzymes (hydroxyacyl CoA dehydrogenase/ mitochondrial trifunctional protein, alpha subunit, mitochondrial trifunctional protein, beta subunit/ 3-ketoacyl CoA thiolase and acetyl-CoA acyltransferase 2) also displayed reduced levels in CVB3 infected A.BY/SnJ mice 84 d p.i. Decreased levels of these proteins suggests a decreased fatty acid oxidation as also observed in case of hypertrophied left ventricles in spontaneously hypertensive rats (Zamorano-Leon et al., 2009).

Among those altered, transport proteins were observed to have increased in infected ANT-OE hearts whereas contractile proteins and cell signalling proteins were found to be decreased compared to infected WT hearts. Proteins such as solute carrier family 27 (fatty acid transporter), member 1/fatty acid transporter protein 1 and nicotinamide nucleotide transhydrogenase showed strong increase in their levels. Solute carrier family 27 member 1 protein is hypothesized to act synergistically in the uptake of long chain fatty acids (LCFAs). LCFAs might be transported into the cell by either binding directly to FATP complexes or can alternatively bind to CD36 on the membrane which in turn transfers the LCFAs to FATP complex for transport into the cell (Glatz et al., 1997, Stahl, 2004). This hints towards an increased fatty acid uptake probably associated to ANT1 over expression which might be a compensatory mechanism to decreased fatty acid oxidation. Higher levels were also observed for nicotinamide transhydrogenase, another transporter protein located within the inner mitochondrial membrane which forms NADPH from NAD^+ via transport of protons across inner membrane from cytosol to the mitochondrial matrix (Earle et al, 1978). In contrast, gene expression, activity and protein amount were observed in decreased levels in explanted heart biopsies from patients with end stage heart failure (Sheeran et al., 2010). Thus, the higher levels of nicotinamide transhydrogenase protein in mitochondrial fractions of infected ANT-OE rat hearts can be attributed to ANT over-expression. On the other hand, the higher number of the transmembrane ANT1 molecule probably might influence the membrane structure thereby impairing other proteins and

protein complexes leading to a compensating higher expression of them. Furthermore, higher amount of basigin/CD147/EMMPRIN involved intracellular transport was also observed. CD147 is thought to interact with solute carrier 16 A1 (SLC16A1) and solute carrier 1 A3 (SLC1A3) (Kirk et al., 2000). SLC16A1 was also identified to have increased the current analysis however the difference was not statistically significant. In humans with left ventricular heart failure, CD147/EMMPRIN (extracellular matrix metalloproteinase inducer) has been reported to increase MMP expression (Spinale et al., 2000). Its role in MMP activation in the current study could not be predicted. However, the increase in the levels of basigin might be interpreted as a secondary effect of the increase in SLC16A1.

Furthermore, lower levels of structural proteins such as vimentin, vinculin, alpha 3 type VI collagen and laminin gamma 1 were observed in samples of ANT-OE mice which would point towards a compromised structural integrity of the heart. Interestingly it also emphasizes the lower extent of fibrosis at this stage of the disease. Decreased cardiac fibrosis due to ANT1 over expression has been reported in rat models of hypertension induced heart disease (Walther et al., 2007). Besides fibrotic proteins, decrease in contractile proteins such as myosin heavy chain 6, tropomyosin alpha 1, isoform a, troponin 1, type 3, troponin T2 and myosin-binding protein C, cardiac type were observed. This is in contradiction to the increase of the proteins of the contractile apparatus reported for isolated rat cardiomyocytes (Vogelpohl et al., 2011). Decrease in contractile proteins levels in infected ANT-OE rats is more prominent than in CVB3 infected ABY/Sn.J mice 84 d p.i. as discussed earlier. Though protein tropomyosin alpha 1 was identified at lower amounts in DIGE analysis, it was identified as a degradation product and moreover no difference in total protein levels were identified for proteins troponin C, troponin I and troponin T by spectral counting in CVB3 infected A.BY/SnJ mice hearts whereas a strong decrease in troponin 1, type 3 and troponin T2 were observed in infected ANT-OE rats compared to infected WT animals. These findings point towards decreased myocardial contractility in infected ANT-OE rat hearts.

In conclusion, CVB3 infection of ANT1 overexpressing rats resulted in more severe decreased mitochondrial function, reduced myocardial contractility and an increase of transporter proteins in the hearts than in those of the WT. Furthermore, a slightly reduced fibrosis was observed in ANT-OE rat hearts. Altogether, no protective effect of ANT-1 on

heart protein profile could be observed in comparison with that in hearts of the infected WT.

4.4. Proteomic analysis of experimental rat model developing dilated cardiomyopathy and severe heart failure after immunization with peptides of Fc receptor gamma IIa(CD32)

Besides as a consequence of viral infection, as discussed earlier, autoimmune causes are also responsible for the development of dilated cardiomyopathy. Several studies exist on experimental autoimmune myocarditis (EAM) leading to dilated cardiomyopathy. EAM has been established in mice and rat models by immunization with cardiac myosin (Neu et al., 1987, Kodama et al., 1990). DBA/2 mice reportedly develop myocarditis upon injection of cardiac myosin specific antibodies (Liao et al., 1995, Kuan et al., 2000). Chronic autoimmune myocarditis was observed in lewis rats 6 months post infusion of activated T-cells specific for a 17 amino acid peptide from rat cardiac myosin (Ratcliffe et al., 2000). Also BALB/c mice deficient for the immune regulatory program death receptor (PD-1) are reported to generate autoantibodies against cardiac troponin I which results in cardiac dysfunction similar to human DCM (Nishimura et al., 2001, Okazaki et al., 2003). Besides autoantibodies against cardiac myosin and troponin I, Fc receptors and in particular FcγIIa (CD-32) receptors are considered as risk factors for autoimmune disease (Hogarth, 2002). Fc receptors play an important role in immune regulation and mediate immune responses and have been implicated to be involved in autoimmune diseases (Gessner et al., 1998). Therefore, an experimental model for autoimmune induced dilated cardiomyopathy leading to left ventricular dilatation and reduced cardiac function based on the active immunization of lewis rat hearts with peptides of the FcγIIa was established in the Clinic for Internal Medicine at the University Medicine Greifswald. The application of the anti-CD32 antibody was shown to have an acute negative inotropic effect on isolated cardiomyocytes in comparison to control (Staudt et al., 2007). The loss of the negative inotropic effects in the presence of corresponding inhibitors gave preliminary evidence of Fcγ receptor IIa coupled src kinase to be involved in the pathologic process (Herda et al., unpublished).

Proteomic analyses of 5 months old rat hearts immunized with FcγIIa peptides in comparison to controls performed within this thesis revealed a significant increase in the levels of acute phase response proteins and proteins involved in integrin linked kinase

signalling. Fibrinogens-alpha, beta and gamma were identified at higher levels in rats with autoimmune cardiomyopathy compared to controls. Fibrinogen is expressed exclusively in hepatocytes and interleukin-6 (IL-6) plays an important role in the induction of fibrinogen as a part of acute phase response. IL-6 induced fibrinogen expression, besides serum amyloid protein A, C-reactive protein and haptoglobin, is also reported in chronic inflammatory processes as periodontal disease and hypertrophied adipocytes affected by hyperglycemia (McCarty et al., 1999, Gabay et al., 1999). The levels of fibrinogen are supposedly influenced by inflammation and immune disease and reports earlier have suggested that fibrinogen is a marker of cardiovascular disease and should be included in cardiovascular profiles (Reinhart, 2003, Ernst, 1993). Besides fibrinogen regulation, IL-6 also plays a crucial role in the development of autoimmune disease by bridging innate and adaptive immunity via regulation of complement C3, which was also observed at higher levels in the current study. BALB/c IL-6 $-/-$ mice immunized with peptide derived from α -MHC displayed reduction in innate and adaptive immune responses linked to myocarditis (Eriksson et al., 2003). Hence, increase in complement C3 in the current study in rats can be interpreted as a consequence of autoimmune disease and as associated with dilated cardiomyopathy.

Inter- alpha inhibitor heavy chain H4/ inter-alpha trypsin inhibitor heavy chain H4 (ITIH4) also belongs to the group of acute phase response glycoproteins identified at higher levels after immunization in the current study. It is mainly synthesized in the liver and has been proposed to be a precursor of plasma kallikrein-generated bioactive peptides (Song et al., 1996, Pu et al., 1994, Nishimura, 1995). Inter alpha inhibitor proteins are a family of serine protease inhibitors and are usually present in very high concentrations in plasma. These proteins were reported to play a role in inflammation, wound healing and cancer metastasis (Josic et al., 2006). The anti-inflammatory role of inter alpha inhibitor proteins was discovered by the enhanced plasmin inhibitory activity of inter alpha inhibitor proteins. Plasmin is a serine protease involved in the activation of matrix metalloproteinases associated with inflammation (Wisniewski et al., 1996, Kobayashi et al., 1996). Overall an increase in the levels of these acute phase response proteins hints towards acute inflammation as a consequence of autoimmunization associated with or leading to development of dilated cardiomyopathy.

Increased levels were also observed for proteins involved in integrin linked kinase signalling. Thus a higher amount of filamins- A and C were detected in rats with

autoimmune dilated cardiomyopathy. Filamins are actin binding proteins involved in stabilizing actin filament networks linking them to cell membrane facilitating cell signalling important for cell motility. Positioned at both the leading edge and the rear of polarized motile cells, they influence the nature of cytoplasmic protrusions and retractions by directly regulating actin cytoskeleton remodeling (Stossel et al., 2001). Filamin A is thought to promote integrin-ligand interactions by binding to cytoplasmic domain of $\beta 1$ -integrin and facilitates inside-out signalling (D'Addario et al., 2001). Integrins and filamins regulate activities of each other and the mechanical stress delivered through $\beta 1$ integrin recruits both filamin A and F-actin to focal adhesions with $\beta 1$ integrin (Glogauer et al., 1998). Mutations in filamin A have been suspected as causes of most common genetic heart valvular disorders and cardiac vascular dystrophy (Kyndt et al., 2007). Loss of filamin expression in mice is reported to cause severe defects in the formation of vasculature and in bone development (Hart et al., 2006, Feng et al., 2006, Zhou et al., 2007). Moreover filamins and their binding partners- vimentin, integrin $\beta 1$, F-actin are involved in cell adhesion, spreading and migration (Nakamura et al., 2011). In the current study, besides filamin A and C, increased levels of vimentin and actin were also observed. The mRNA and protein levels of vimentin are also reported to have increased in explanted human failing hearts with DCM (Heling et al., 2000). Vimentin, an intermediate filament of fibroblasts and endothelial cells is an indicator of cellularity of the interstitium (Traub, 1985). These results indicate filamins along with their interaction partners are involved in increased cell signalling in autoimmune dilated cardiomyopathy.

Besides being involved in integrin linked kinase signalling, vimentin also plays a role in fibrosis. Other fibrosis proteins such as lumican, procollagen alpha 1, type 1 have also been identified at higher levels in the current study. Fibrosis leads to increased stiffness and loss of ventricular compliance. Additionally, an increase in the amounts of cytoskeleton associated proteins such as vimentin, desmin, vinculin and tubulin are correlated to reduced function in heart failure (Schaper et al., 1991). Though the proteins desmin, tubulin and vinculin were identified in the current analysis, these proteins did not show significant difference in their levels in disease hearts compared to controls.

Muscle contractile proteins troponin T2, troponin I, myosin heavy chain, polypeptide 6, myosin light chain 2, ventricular isoform though were covered in the current study, did not differ between immunised animals and controls. Thus, the decrease of fractional shortening observed (Herda, unpublished data) does not obviously occur due to lower

abundance of contractile proteins in the heart. However, it might be a consequence of a change in the levels of other proteins such as fatty acid binding protein. The current study showed an increase in the levels of fatty acid binding protein 4 (FABP4) in immunized animals. Fatty acid binding proteins are members of highly conserved cytosolic proteins having a high affinity for long chain fatty acids. FABP4 was reported to be involved in intracellular trafficking of fatty acids (Hertzel & Bernlohr, 2000). FABP4 induced decrease in fractional shortening was reported in adult rat cardiomyocytes. Moreover FABP4 was also reported to reduce/inhibit cardiac contraction (Lamounier-Zepter et al., 2000). Besides, two isoforms of creatine kinase namely, creatine kinase, brain isoform and creatine kinase, mitochondrial were identified at lower levels in infected hearts compared to controls. Creatine kinase converts creatine phosphate and ADP to ATP and creatine in correlation to energy demand (Wallimann, 1994, Saks et al., 1980). Reduced levels of creatine kinase and decrease in creatine kinase activity have been associated to decreased energy metabolism in experimental and clinical models of heart failure (Ingwall et al., 1985, Nascimben et al., 1996). Impaired contractile function was observed in creatine kinase-null mice due to impaired mechanical response to adrenergic stimulation (Crozatier et al., 2002). Recently, improved contractile function as a result of improved creatine kinase related energy metabolism was reported in heart failure mice conditionally over expressing myofibrillar creatine kinase (Gupta et al., 2012). Another protein phospholamban, associated with calcium binding and contractility was also observed to have increased in the current study. Abnormal calcium handling by proteins sarcoplasmic/endoplasmic reticulum Ca^{+2} ATPase 2 (SERCA2a) and phospholamban has been reported in cardiac pathological conditions (Haghighi et al., 2004, Rodriguez & Kranias et al., 2005). SERCA2a is regulated by phospholamban by direct protein-protein interaction (MacLennan & Kranias, 2003). Dephosphorylated phospholamban inhibits SERCA2a activity whereas phosphorylation of phospholamban at ser-16 or Thr-17 reverses the inhibition and activates SERCA2a (Kimura et al., 1997, Asahi et al., 1999, Mattiazzi et al., 2005). But in the current analysis, though SERCA2a was observed to have decreased in immunized animals, the difference was not observed to be statistically significant. Since SERCA2a is involved in myocardial contractility through regulating the cytoplasmic Ca^{+2} during relaxation (MacLennan et al., 1997), its decreased levels paired with increased phospholamban levels hints towards impaired myocardial function. Though a decrease in myocardial contractile proteins was not obvious, decreased levels of creatine

kinase, SERCA2a and increased levels of FABP4 and phospholamban might be an indicator of depressed contractility in immunized animals.

Besides the above described proteins, myelin protein zero, a protein of the peripheral nervous system was identified to have expressed in very high amounts in the current analysis. However, the reason behind such a high expression of the protein in heart is not clearly understood.

In summary, the current analysis proves an acute inflammatory response corresponding to active immunization with peptides of FcγIIa. Though a clear cut indication of decrease in myocardial contractility by decrease of sarcomeric proteins was not observed, alterations in the levels of proteins related to or influencing myocardial contractility and Ca^{2+} homeostasis support the compromised contractile function recorded by hemodynamic measures.

Using proteomics approaches, the current thesis focuses on the analysis of global changes in the protein profile of hearts of animal models of virus induced and autoimmunity induced dilated cardiomyopathy. Decreased energy metabolism and compromised myocardial contractility were prominently observed in viral models of cardiomyopathy whereas severe acute phase response signalling was observed in autoimmune model of dilated cardiomyopathy. This study provides insights into the changes occurring at the molecular level in diseased hearts which serve as indicators for cardiac dysfunction. These observations can act as the starting point for a further analysis into the behaviour of dilated cardiomyopathy and in finding ways to counteract the disease.

5. References

- Agnetti, G., N. Kaludercic, et al. Modulation of mitochondrial proteome and improved mitochondrial function by biventricular pacing of dyssynchronous failing hearts. *Circ Cardiovasc Genet* 3(1): 78-87.
- Ahmad, F., J. G. Seidman, et al. (2005). The genetic basis for cardiac remodeling. *Annu Rev Genomics Hum Genet* 6: 185-216.
- Alban, A., S. O. David, et al. (2003). A novel experimental design for comparative two-dimensional gel analysis: two-dimensional difference gel electrophoresis incorporating a pooled internal standard. *Proteomics* 3(1): 36-44.
- Arber, S., J. J. Hunter, et al. (1997). MLP-deficient mice exhibit a disruption of cardiac cytoarchitectural organization, dilated cardiomyopathy, and heart failure. *Cell* 88(3): 393-403.
- Arya, R., M. Mallik, et al. (2007). Heat shock genes - integrating cell survival and death. *J Biosci* 32(3): 595-610.
- Asahi, M., Y. Kimura, et al. (1999). Transmembrane helix M6 in sarco(endo)plasmic reticulum Ca(2+)-ATPase forms a functional interaction site with phospholamban. Evidence for physical interactions at other sites. *J Biol Chem* 274(46): 32855-32862.
- Baba, H., T. Ishiwata, et al. (2001). Expression and localization of lumican in the ischemic and reperfused rat heart. *Jpn Circ J* 65(5): 445-450.
- Badorff, C., G. H. Lee, et al. (1999). Enteroviral protease 2A cleaves dystrophin: evidence of cytoskeletal disruption in an acquired cardiomyopathy. *Nature Medicine* 5(3): 320-326.
- Barger, P. M. and D. P. Kelly (1999). Fatty acid utilization in the hypertrophied and failing heart: molecular regulatory mechanisms. *Am J Med Sci* 318(1): 36-42.
- Baumer, A. T., M. Flesch, et al. (2000). Antioxidative enzymes in human hearts with idiopathic dilated cardiomyopathy. *Journal of Molecular and Cellular Cardiology* 32(1): 121-130.
- Belzacq, A. S., H. L. Vieira, et al. (2003). Bcl-2 and Bax modulate adenine nucleotide translocase activity. *Cancer Res* 63(2): 541-546.
- Bendig, J. W., O. M. Franklin, et al. (2003). Coxsackievirus B3 sequences in the blood of a neonate with congenital myocarditis, plus serological evidence of maternal infection. *J Med Virol* 70(4): 606-609.
- Bergelson, J. M., J. A. Cunningham, et al. (1997). Isolation of a common receptor for Coxsackie B viruses and adenoviruses 2 and 5. *Science* 275(5304): 1320-1323.
- Berger, J. and D. E. Moller (2002). The mechanisms of action of PPARs. *Annu Rev Med* 53: 409-435.

- Beynon, R. J., M. K. Doherty, et al. (2005). Multiplexed absolute quantification in proteomics using artificial QCAT proteins of concatenated signature peptides. *Nat Methods* 2(8): 587-589.
- Bianco, P., L. W. Fisher, et al. (1990). Expression and localization of the two small proteoglycans biglycan and decorin in developing human skeletal and non-skeletal tissues. *J Histochem Cytochem* 38(11): 1549-1563.
- Blochberger, T. C., J. P. Vergnes, et al. (1992). cDNA to chick lumican (corneal keratan sulfate proteoglycan) reveals homology to the small interstitial proteoglycan gene family and expression in muscle and intestine. *Journal of Biological Chemistry* 267(1): 347-352.
- Bodyak, N., P. M. Kang, et al. (2002). Gene expression profiling of the aging mouse cardiac myocytes. *Nucleic Acids Res* 30(17): 3788-3794.
- Boros, P., J. M. Chen, et al. (1990). Autoimmune mice make anti-Fc gamma receptor antibodies. *J Exp Med* 171(5): 1581-1595.
- Bottero, V., F. Rossi, et al. (2001). Ikappa b-alpha, the NF-kappa B inhibitory subunit, interacts with ANT, the mitochondrial ATP/ADP translocator. *J Biol Chem* 276(24): 21317-21324.
- Bousette, N., T. Kislinger, et al. (2009). Large-scale characterization and analysis of the murine cardiac proteome. *J Proteome Res* 8(4): 1887-1901.
- Bowles, N. E., M. L. Rose, et al. (1989). End-stage dilated cardiomyopathy. Persistence of enterovirus RNA in myocardium at cardiac transplantation and lack of immune response. *Circulation* 80(5): 1128-1136.
- Boyle, A. J., H. Shih, et al. (2011). Cardiomyopathy of aging in the mammalian heart is characterized by myocardial hypertrophy, fibrosis and a predisposition towards cardiomyocyte apoptosis and autophagy. *Exp Gerontol* 46(7): 549-559.
- Brandt, J. M., F. Djouadi, et al. (1998). Fatty acids activate transcription of the muscle carnitine palmitoyltransferase I gene in cardiac myocytes via the peroxisome proliferator-activated receptor alpha. *J Biol Chem* 273(37): 23786-23792.
- Breuker, K., M. Jin, et al. (2008). Top-down identification and characterization of biomolecules by mass spectrometry. *J Am Soc Mass Spectrom* 19(8): 1045-1053.
- Brink, T. C., C. Regenbrecht, et al. (2009). Activation of the immune response is a key feature of aging in mice. *Biogerontology* 10(6): 721-734.
- Brink, T. C., L. Demetrius, et al. (2009). Age-related transcriptional changes in gene expression in different organs of mice support the metabolic stability theory of aging. *Biogerontology* 10(5): 549-564.
- Buchwald, A., H. Till, et al. (1990). Alterations of the mitochondrial respiratory chain in human dilated cardiomyopathy. *Eur Heart J* 11(6): 509-516.

- Bukowska, A., U. Lendeckel, et al. (2004). Proteomics in myocardial diseases. *Pathology, Research and Practice* 200(2): 135-145.
- Buse, C., F. Altmann, et al. (2008). Discovering novel targets for autoantibodies in dilated cardiomyopathy. *Electrophoresis* 29(6): 1325-1332.
- Caforio, A. L., M. Grazzini, et al. (1992). Identification of alpha- and beta-cardiac myosin heavy chain isoforms as major autoantigens in dilated cardiomyopathy. *Circulation* 85(5): 1734-1742.
- Cai, C., H. Masumiya, et al. (2009). MG53 nucleates assembly of cell membrane repair machinery. *Nat Cell Biol* 11(1): 56-64.
- Carniel, E., M. R. Taylor, et al. (2005). Alpha-myosin heavy chain: a sarcomeric gene associated with dilated and hypertrophic phenotypes of cardiomyopathy. *Circulation* 112(1): 54-59.
- Carolyn Y. Ho and Christine E. Seidman (2003). *Principles of Molecular Medicine*, Chapter 53. Elsevier publishers.
- Casademont, J. and O. Miro (2002). Electron transport chain defects in heart failure. *Heart Fail Rev* 7(2): 131-139.
- Chakravarti, B., M. Oseguera, et al. (2008). Proteomic profiling of aging in the mouse heart: Altered expression of mitochondrial proteins. *Archives of Biochemistry and Biophysics* 474(1): 22-31.
- Chau, D. H., J. Yuan, et al. (2007). Coxsackievirus B3 proteases 2A and 3C induce apoptotic cell death through mitochondrial injury and cleavage of eIF4GI but not DAP5/p97/NAT1. *Apoptosis* 12(3): 513-524.
- Chen, X. and B. M. Gumbiner (2006). Crosstalk between different adhesion molecules. *Curr Opin Cell Biol* 18(5): 572-578.
- Cho, C. T., K. K. Feng, et al. (1982). Role of antiviral antibodies in resistance against coxsackievirus B3 infection: interaction between preexisting antibodies and an interferon inducer. *Infect Immun* 37(2): 720-727.
- Chow, L. H., C. J. Gauntt, et al. (1991). Differential effects of myocarditic variants of Coxsackievirus B3 in inbred mice. A pathologic characterization of heart tissue damage. *Lab Invest* 64(1): 55-64.
- Cicek, G., E. Schiltz, et al. (2002). Analysis of mitochondrial antigens reveals inner membrane succinate dehydrogenase flavoprotein subunit as autoantigen to antibodies in anti-M7 sera. *Clinical and Experimental Immunology* 128(1): 83-87.
- Clark, M. E., P. M. Lieberman, et al. (1993). Direct cleavage of human TATA-binding protein by poliovirus protease 3C in vivo and in vitro. *Mol Cell Biol* 13(2): 1232-1237.
- Claycomb, W. C., N. A. Lanson, Jr., et al. (1998). HL-1 cells: a cardiac muscle cell line that contracts and retains phenotypic characteristics of the adult cardiomyocyte. *Proc Natl Acad Sci U S A* 95(6): 2979-2984.

- Corbett, J. M., H. J. Why, et al. (1998). Cardiac protein abnormalities in dilated cardiomyopathy detected by two-dimensional polyacrylamide gel electrophoresis. *Electrophoresis* 19(11): 2031-2042.
- Coyne, C. B. and J. M. Bergelson (2006). Virus-induced Abl and Fyn kinase signals permit coxsackievirus entry through epithelial tight junctions. *Cell* 124(1): 119-131.
- Crozatier, B., T. Badoual, et al. (2002). Role of creatine kinase in cardiac excitation-contraction coupling: studies in creatine kinase-deficient mice. *Faseb J* 16(7): 653-660.
- D'Addario, M., P. D. Arora, et al. (2001). Cytoprotection against mechanical forces delivered through beta 1 integrins requires induction of filamin A. *J Biol Chem* 276(34): 31969-31977.
- Daeron, M. (1997). Fc receptor biology. *Annu Rev Immunol* 15: 203-234.
- Dai, D. F. and P. S. Rabinovitch (2009). Cardiac aging in mice and humans: the role of mitochondrial oxidative stress. *Trends Cardiovasc Med* 19(7): 213-220.
- Dai, Q., G. P. Escobar, et al. (2008). The left ventricle proteome differentiates middle-aged and old left ventricles in mice. *J Proteome Res* 7(2): 756-765.
- Dai, Q., G. P. Escobar, et al. (2008). The left ventricle proteome differentiates middle-aged and old left ventricles in mice. *J Proteome Res* 7(2): 756-765.
- Danial, N. N., C. F. Gramm, et al. (2003). BAD and glucokinase reside in a mitochondrial complex that integrates glycolysis and apoptosis. *Nature* 424(6951): 952-956.
- Davila-Roman, V. G., G. Vedala, et al. (2002). Altered myocardial fatty acid and glucose metabolism in idiopathic dilated cardiomyopathy. *J Am Coll Cardiol* 40(2): 271-277.
- Diedrich, M., J. Tadic, et al. (2007). Heart protein expression related to age and sex in mice and humans. *Int J Mol Med* 20(6): 865-874.
- Ding, P., J. Huang, et al. (2010). Cardiac myosin light chain kinase is necessary for myosin regulatory light chain phosphorylation and cardiac performance in vivo. *J Biol Chem* 285(52): 40819-40829.
- Doedens, J. R. and K. Kirkegaard (1995). Inhibition of cellular protein secretion by poliovirus proteins 2B and 3A. *Embo J* 14(5): 894-907.
- Dohke, T., A. Wada, et al. (2006). Proteomic analysis reveals significant alternations of cardiac small heat shock protein expression in congestive heart failure. *J Card Fail* 12(1): 77-84.
- Dorner, A., M. Olesch, et al. (1999). Transcription of the adenine nucleotide translocase isoforms in various types of tissues in the rat. *Biochimica et Biophysica Acta (BBA) - Biomembranes* 1417(1): 16-24.

- Dorner, A., S. Giessen, et al. (2006). An isoform shift in the cardiac adenine nucleotide translocase expression alters the kinetic properties of the carrier in dilated cardiomyopathy. *Eur J Heart Fail* 8(1): 81-89.
- Dunn, M. J. (1987). Two-dimensional gel electrophoresis of proteins. *J Chromatogr* 418: 145-185.
- Earle, S. R., W. M. Anderson, et al. (1978). Evidence that reconstituted bovine heart mitochondrial transhydrogenase functions as a proton pump. *FEBS Lett* 91(1): 21-24.
- Ehrenfeld, E. (1982). Poliovirus-induced inhibition of host-cell protein synthesis. *Cell* 28(3): 435-436.
- Engvall, E., H. Hessel, et al. (1986). Molecular assembly, secretion, and matrix deposition of type VI collagen. *J Cell Biol* 102(3): 703-710.
- Eriksson, U., R. Ricci, et al. (2003). Dendritic cell-induced autoimmune heart failure requires cooperation between adaptive and innate immunity. *Nature Medicine* 9(12): 1484-1490.
- Ernst, E. (1993). Fibrinogen as a cardiovascular risk factor--interrelationship with infections and inflammation. *Eur Heart J* 14 Suppl K: 82-87.
- Esfandiarei, M. and B. M. McManus (2008). Molecular biology and pathogenesis of viral myocarditis. *Annual Review of Pathology* 3: 127-155.
- Fatkin, D. and R. M. Graham (2002). Molecular mechanisms of inherited cardiomyopathies. *Physiological Reviews* 82(4): 945-980.
- Feng, Y., M. H. Chen, et al. (2006). Filamin A (FLNA) is required for cell-cell contact in vascular development and cardiac morphogenesis. *Proc Natl Acad Sci U S A* 103(52): 19836-19841.
- Flanagan, J. B., R. F. Petterson, et al. (1977). Covalent linkage of a protein to a defined nucleotide sequence at the 5'-terminus of virion and replicative intermediate RNAs of poliovirus. *Proc Natl Acad Sci U S A* 74(3): 961-965.
- Fujimori, K. E., A. Uyeda, et al. (2002). Regulatory expression of MDP77 protein in the skeletal and cardiac muscles. *FEBS Lett* 529(2-3): 303-308.
- Fuse, K., G. Chan, et al. (2005). Myeloid differentiation factor-88 plays a crucial role in the pathogenesis of Coxsackievirus B3-induced myocarditis and influences type I interferon production. *Circulation* 112(15): 2276-2285.
- Gabay, C. and I. Kushner (1999). Acute-phase proteins and other systemic responses to inflammation. *N Engl J Med* 340(6): 448-454.
- Gauntt, C. J., S. M. Tracy, et al. (1995). Coxsackievirus-induced chronic myocarditis in murine models. *Eur Heart J* 16 Suppl O: 56-58.

- Gay, R. T., S. Belisle, et al. (2006). An aged host promotes the evolution of avirulent coxsackievirus into a virulent strain. *Proc Natl Acad Sci U S A* 103(37): 13825-13830.
- Ge, Y., I. N. Rybakova, et al. (2009). Top-down high-resolution mass spectrometry of cardiac myosin binding protein C revealed that truncation alters protein phosphorylation state. *Proc Natl Acad Sci U S A* 106(31): 12658-12663.
- Gerber, S. A., J. Rush, et al. (2003). Absolute quantification of proteins and phosphoproteins from cell lysates by tandem MS. *Proc Natl Acad Sci U S A* 100(12): 6940-6945.
- Gessner, J. E., H. Heiken, et al. (1998). The IgG Fc receptor family. *Ann Hematol* 76(6): 231-248.
- Glatz, J. F., F. A. van Nieuwenhoven, et al. (1997). Role of membrane-associated and cytoplasmic fatty acid-binding proteins in cellular fatty acid metabolism. *Prostaglandins Leukot Essent Fatty Acids* 57(4-5): 373-378.
- Glogauer, M., P. Arora, et al. (1998). The role of actin-binding protein 280 in integrin-dependent mechanoprotection. *J Biol Chem* 273(3): 1689-1698.
- Godeny, E. K. and C. J. Gauntt (1987). Murine natural killer cells limit coxsackievirus B3 replication. *J Immunol* 139(3): 913-918.
- Goldmacher, V. S., L. M. Bartle, et al. (1999). A cytomegalovirus-encoded mitochondria-localized inhibitor of apoptosis structurally unrelated to Bcl-2. *Proc Natl Acad Sci U S A* 96(22): 12536-12541.
- Gordon, A. M., E. Homsher, et al. (2000). Regulation of contraction in striated muscle. *Physiol Rev* 80(2): 853-924.
- Gorg, A., W. Weiss, et al. (2004). Current two-dimensional electrophoresis technology for proteomics. *Proteomics* 4(12): 3665-3685.
- Graham, B. H., K. G. Waymire, et al. (1997). A mouse model for mitochondrial myopathy and cardiomyopathy resulting from a deficiency in the heart/muscle isoform of the adenine nucleotide translocator. *Nat Genet* 16(3): 226-234.
- Gramolini, A. O., T. Kislinger, et al. (2007). Analyzing the cardiac muscle proteome by liquid chromatography-mass spectrometry-based expression proteomics. *Methods Mol Biol* 357: 15-31.
- Gramolini, A. O., T. Kislinger, et al. (2008). Comparative proteomics profiling of a phospholamban mutant mouse model of dilated cardiomyopathy reveals progressive intracellular stress responses. *Molecular and Cellular Proteomics* 7(3): 519-533.
- Grant, J. E., A. D. Bradshaw, et al. (2009). Quantification of protein expression changes in the aging left ventricle of *Rattus norvegicus*. *J Proteome Res* 8(9): 4252-4263.

- Grover, J., X. N. Chen, et al. (1995). The human lumican gene. Organization, chromosomal location, and expression in articular cartilage. *J Biol Chem* 270(37): 21942-21949.
- Gupta, A., A. Akki, et al. (2012). Creatine kinase-mediated improvement of function in failing mouse hearts provides causal evidence the failing heart is energy starved. *J Clin Invest* 122(1): 291-302.
- Gururaj, A., C. J. Barnes, et al. (2004). Regulation of phosphoglucomutase 1 phosphorylation and activity by a signaling kinase. *Oncogene* 23(49): 8118-8127.
- Gustafsson, A. B. and R. A. Gottlieb (2008). Heart mitochondria: gates of life and death. *Cardiovasc Res* 77(2): 334-343.
- Gustafsson, A. B. and R. A. Gottlieb (2008). Heart mitochondria: gates of life and death. *Cardiovasc Res* 77(2): 334-343.
- Gygi, S. P., G. L. Corthals, et al. (2000). Evaluation of two-dimensional gel electrophoresis-based proteome analysis technology. *Proc Natl Acad Sci U S A* 97(17): 9390-9395.
- Haghighi, K., K. N. Gregory, et al. (2004). Sarcoplasmic reticulum Ca-ATPase-phospholamban interactions and dilated cardiomyopathy. *Biochemical and Biophysical Research Communications* 322(4): 1214-1222.
- Hammer, E., M. Goritzka, et al. (2011). Characterization of the human myocardial proteome in inflammatory dilated cardiomyopathy by label-free quantitative shotgun proteomics of heart biopsies. *J Proteome Res* 10(5): 2161-2171.
- Hammer, E., T. Q. Phong, et al. (2010). Viral myocarditis induced by Coxsackievirus B3 in A.BY/SnJ mice: analysis of changes in the myocardial proteome. *Proteomics* 10(9): 1802-1818.
- Hart, A. W., J. E. Morgan, et al. (2006). Cardiac malformations and midline skeletal defects in mice lacking filamin A. *Hum Mol Genet* 15(16): 2457-2467.
- Heeneman, S., J. P. Cleutjens, et al. (2003). The dynamic extracellular matrix: intervention strategies during heart failure and atherosclerosis. *J Pathol* 200(4): 516-525.
- Heling, A., R. Zimmermann, et al. (2000). Increased expression of cytoskeletal, linkage, and extracellular proteins in failing human myocardium. *Circ Res* 86(8): 846-853.
- Herbert, B. (1999). Advances in protein solubilisation for two-dimensional electrophoresis. *Electrophoresis* 20(4-5): 660-663.
- Hertzel, A. V. and D. A. Bernlohr (2000). The mammalian fatty acid-binding protein multigene family: molecular and genetic insights into function. *Trends Endocrinol Metab* 11(5): 175-180.
- Hogarth, P. M. (2002). Fc receptors are major mediators of antibody based inflammation in autoimmunity. *Curr Opin Immunol* 14(6): 798-802.

- Honda, T., H. Saitoh, et al. (2000). The coxsackievirus-adenovirus receptor protein as a cell adhesion molecule in the developing mouse brain. *Brain Res Mol Brain Res* 77(1): 19-28.
- Hopkins, S. C., C. Sabido-David, et al. (1998). Fluorescence polarization transients from rhodamine isomers on the myosin regulatory light chain in skeletal muscle fibers. *Biophys J* 74(6): 3093-3110.
- Hulett, M. D. and P. M. Hogarth (1994). Molecular basis of Fc receptor function. *Adv Immunol* 57: 1-127.
- Ierino, F. L., M. S. Powell, et al. (1993). Recombinant soluble human Fc gamma RII: production, characterization, and inhibition of the Arthus reaction. *J Exp Med* 178(5): 1617-1628.
- Ingwall, J. S. (2009). Energy metabolism in heart failure and remodelling. *Cardiovasc Res* 81(3): 412-419.
- Ingwall, J. S., M. F. Kramer, et al. (1985). The creatine kinase system in normal and diseased human myocardium. *N Engl J Med* 313(17): 1050-1054.
- Jacotot, E., K. F. Ferri, et al. (2001). Control of mitochondrial membrane permeabilization by adenine nucleotide translocator interacting with HIV-1 viral protein rR and Bcl-2. *J Exp Med* 193(4): 509-519.
- Jarreta, D., J. Orús, et al. (2000). Mitochondrial function in heart muscle from patients with idiopathic dilated cardiomyopathy. *Cardiovascular Research*.
- Jones, W. K., I. L. Grupp, et al. (1996). Ablation of the murine alpha myosin heavy chain gene leads to dosage effects and functional deficits in the heart. *J Clin Invest* 98(8): 1906-1917.
- Josic, D., M. K. Brown, et al. (2006). Proteomic characterization of inter-alpha inhibitor proteins from human plasma. *Proteomics* 6(9): 2874-2885.
- Jungblut, P. R., H. G. Holzthutter, et al. (2008). The speciation of the proteome. *Chemistry Central Journal* 2: 16.
- Kandolf, R. and P. H. Hofschneider (1989). Viral heart disease. *Springer Semin Immunopathol* 11(1): 1-13.
- Kania, G., P. Blyszczuk, et al. (2009). Mechanisms of cardiac fibrosis in inflammatory heart disease. *Trends Cardiovasc Med* 19(8): 247-252.
- Kanski, J., A. Behring, et al. (2005). Proteomic identification of 3-nitrotyrosine-containing rat cardiac proteins: effects of biological aging. *Am J Physiol Heart Circ Physiol* 288(1): H371-381.
- Kashimura, T., M. Kodama, et al. (2004). Spatiotemporal changes of coxsackievirus and adenovirus receptor in rat hearts during postnatal development and in cultured cardiomyocytes of neonatal rat. *Virchows Arch* 444(3): 283-292.

- Kearney, M. T., J. M. Cotton, et al. (2001). Viral myocarditis and dilated cardiomyopathy: mechanisms, manifestations, and management. *Postgraduate Medical Journal* 77(903): 4-10.
- Kim, H., S. Eliuk, et al. (2007). 2D gel proteomics: an approach to study age-related differences in protein abundance or isoform complexity in biological samples. *Methods Mol Biol* 371: 349-391.
- Kim, N., Y. Lee, et al. (2006). Potential biomarkers for ischemic heart damage identified in mitochondrial proteins by comparative proteomics. *Proteomics* 6(4): 1237-1249.
- Kimura, Y., K. Kurzydowski, et al. (1997). Phospholamban inhibitory function is activated by depolymerization. *J Biol Chem* 272(24): 15061-15064.
- Kiri, A. N., H. C. Tran, et al. (2005). Proteomic changes in bovine heart mitochondria with age: using a novel technique for organelle separation and enrichment. *J Biomol Tech* 16(4): 371-379.
- Kirk, P., M. C. Wilson, et al. (2000). CD147 is tightly associated with lactate transporters MCT1 and MCT4 and facilitates their cell surface expression. *Embo J* 19(15): 3896-3904.
- Kishimoto, C., K. Kuribayashi, et al. (1985). Immunologic behavior of lymphocytes in experimental viral myocarditis: significance of T lymphocytes in the severity of myocarditis and silent myocarditis in BALB/c-nu/nu mice. *Circulation* 71(6): 1247-1254.
- Kitamura, M., M. Shimizu, et al. (2001). Collagen remodeling and cardiac dysfunction in patients with hypertrophic cardiomyopathy: the significance of type III and VI collagens. *Clin Cardiol* 24(4): 325-329.
- Klingel, K. and R. Kandolf (1993). The role of enterovirus replication in the development of acute and chronic heart muscle disease in different immunocompetent mouse strains. *Scand J Infect Dis Suppl* 88: 79-85.
- Klingel, K., C. Hohenadl, et al. (1992). Ongoing enterovirus-induced myocarditis is associated with persistent heart muscle infection: quantitative analysis of virus replication, tissue damage, and inflammation. *Proc Natl Acad Sci U S A* 89(1): 314-318.
- Klingel, K., M. Sauter, et al. (2004). Molecular pathology of inflammatory cardiomyopathy. *Med Microbiol Immunol* 193(2-3): 101-107.
- Klose, J. (1975). Protein mapping by combined isoelectric focusing and electrophoresis of mouse tissues. A novel approach to testing for induced point mutations in mammals. *Humangenetik* 26(3): 231-243.
- Kobayashi, H., J. Gotoh, et al. (1996). Inter-alpha-trypsin inhibitor bound to tumor cells is cleaved into the heavy chains and the light chain on the cell surface. *J Biol Chem* 271(19): 11362-11367.

- Kodama, M., Y. Matsumoto, et al. (1990). A novel experimental model of giant cell myocarditis induced in rats by immunization with cardiac myosin fraction. *Clin Immunol Immunopathol* 57(2): 250-262.
- Koike, H., T. Kanda, et al. (2001). Reduction of viral myocarditis in mice lacking perforin. *Res Commun Mol Pathol Pharmacol* 110(3-4): 229-237.
- Koolwijk, P., G. T. Spierenburg, et al. (1989). Interaction between hybrid mouse monoclonal antibodies and the human high-affinity IgG FcR, huFc gamma RI, on U937. Involvement of only one of the mIgG heavy chains in receptor binding. *J Immunol* 143(5): 1656-1662.
- Krenz, M., S. Sadayappan, et al. (2007). Distribution and structure-function relationship of myosin heavy chain isoforms in the adult mouse heart. *The Journal of Biological Chemistry* 282(33): 24057-24064.
- Kuan, A. P., L. Zuckier, et al. (2000). Immunoglobulin isotype determines pathogenicity in antibody-mediated myocarditis in naive mice. *Circ Res* 86(3): 281-285.
- Kühl, U. and H. P. Schultheiss (2009). Viral myocarditis: diagnosis, aetiology and management. *Drugs* 69(10): 1287-1302.
- Kuhl, U., M. Pauschinger, et al. (2005). Viral persistence in the myocardium is associated with progressive cardiac dysfunction. *Circulation* 112(13): 1965-1970.
- Kurlander, R. J. (1983). Blockade of Fc receptor-mediated binding to U-937 cells by murine monoclonal antibodies directed against a variety of surface antigens. *J Immunol* 131(1): 140-147.
- Kwong, L. K. and R. S. Sohal (2000). Age-related changes in activities of mitochondrial electron transport complexes in various tissues of the mouse. *Arch Biochem Biophys* 373(1): 16-22.
- Kyndt, F., J. P. Gueffet, et al. (2007). Mutations in the gene encoding filamin A as a cause for familial cardiac valvular dystrophy. *Circulation* 115(1): 40-49.
- Kyu, B., A. Matsumori, et al. (1992). Cardiac persistence of cardioviral RNA detected by polymerase chain reaction in a murine model of dilated cardiomyopathy. *Circulation* 86(2): 522-530.
- Laemmli, U. K. (1970). Cleavage of structural proteins during the assembly of the head of bacteriophage T4. *Nature* 227(5259): 680-685.
- Lakatta, E. G. (2003). Arterial and cardiac aging: major shareholders in cardiovascular disease enterprises: Part III: cellular and molecular clues to heart and arterial aging. *Circulation* 107(3): 490-497.
- Lakatta, E. G. and D. Levy (2003). Arterial and cardiac aging: major shareholders in cardiovascular disease enterprises: Part II: the aging heart in health: links to heart disease. *Circulation* 107(2): 346-354.

- Lamounier-Zepter, V., C. Look, et al. (2009). Adipocyte fatty acid-binding protein suppresses cardiomyocyte contraction: a new link between obesity and heart disease. *Circ Res* 105(4): 326-334.
- Lamphear, B. J., R. Yan, et al. (1993). Mapping the cleavage site in protein synthesis initiation factor eIF-4 gamma of the 2A proteases from human Cocksackievirus and rhinovirus. *J Biol Chem* 268(26): 19200-19203.
- Lane, J. R., D. A. Neumann, et al. (1993). Role of IL-1 and tumor necrosis factor in coxsackie virus-induced autoimmune myocarditis. *J Immunol* 151(3): 1682-1690.
- Latif, N., C. S. Baker, et al. (1993). Frequency and specificity of antiheart antibodies in patients with dilated cardiomyopathy detected using SDS-PAGE and western blotting. *Journal of the American College of Cardiology* 22(5): 1378-1384.
- Lauber, W. M., J. A. Carroll, et al. (2001). Mass spectrometry compatibility of two-dimensional gel protein stains. *Electrophoresis* 22(5): 906-918.
- Legate, K. R., E. Montanez, et al. (2006). ILK, PINCH and parvin: the tIPP of integrin signalling. *Nat Rev Mol Cell Biol* 7(1): 20-31.
- Leipner, C., K. Grun, et al. (2004). Cocksackievirus B3-induced myocarditis: differences in the immune response of C57BL/6 and Balb/c mice. *Medical Microbiology and Immunology* 193(2-3): 141-147.
- Lenaz, G., C. Bovina, et al. (2002). Role of mitochondria in oxidative stress and aging. *Ann N Y Acad Sci* 959: 199-213.
- Lenaz, G., C. Bovina, et al. (2002). Role of mitochondria in oxidative stress and aging. *Ann N Y Acad Sci* 959: 199-213.
- Levine, R. J., R. W. Kensler, et al. (1996). Myosin light chain phosphorylation affects the structure of rabbit skeletal muscle thick filaments. *Biophys J* 71(2): 898-907.
- Levy, S. E., Y. S. Chen, et al. (2000). Expression and sequence analysis of the mouse adenine nucleotide translocase 1 and 2 genes. *Gene* 254(1-2): 57-66.
- Li, L., J. R. Sevinsky, et al. (2010). Proteomic analysis reveals virus-specific Hsp25 modulation in cardiac myocytes. *J Proteome Res* 9(5): 2460-2471.
- Li, M. X., X. Wang, et al. (2004). Structural based insights into the role of troponin in cardiac muscle pathophysiology. *J Muscle Res Cell Motil* 25(7): 559-579.
- Li, Y., T. Bourlet, et al. (2000). Enteroviral capsid protein VP1 is present in myocardial tissues from some patients with myocarditis or dilated cardiomyopathy. *Circulation* 101(3): 231-234.
- Liao, L., R. Sindhvani, et al. (1995). Antibody-mediated autoimmune myocarditis depends on genetically determined target organ sensitivity. *J Exp Med* 181(3): 1123-1131.
- Lilley, K. S. and D. B. Friedman (2004). All about DIGE: quantification technology for differential-display 2D-gel proteomics. *Expert Rev Proteomics* 1(4): 401-409.

- Limas, C. J., I. F. Goldenberg, et al. (1995). Soluble interleukin-2 receptor levels in patients with dilated cardiomyopathy. Correlation with disease severity and cardiac autoantibodies. *Circulation* 91(3): 631-634.
- Lindsey, M. L., D. K. Goshorn, et al. (2005). Age-dependent changes in myocardial matrix metalloproteinase/tissue inhibitor of metalloproteinase profiles and fibroblast function. *Cardiovasc Res* 66(2): 410-419.
- Liu, H., R. G. Sadygov, et al. (2004). A model for random sampling and estimation of relative protein abundance in shotgun proteomics. *Anal Chem* 76(14): 4193-4201.
- Liu, P., K. Aitken, et al. (2000). The tyrosine kinase p56lck is essential in coxsackievirus B3-mediated heart disease. *Nature Medicine* 6(4): 429-434.
- Lodge, P. A., M. Herzum, et al. (1987). Coxsackievirus B-3 myocarditis. Acute and chronic forms of the disease caused by different immunopathogenic mechanisms. *Am J Pathol* 128(3): 455-463.
- Lopaschuk, G. D., J. R. Ussher, et al. (2010). Myocardial fatty acid metabolism in health and disease. *Physiol Rev* 90(1): 207-258.
- Lowes, B. D., W. Minobe, et al. (1997). Changes in gene expression in the intact human heart. Downregulation of alpha-myosin heavy chain in hypertrophied, failing ventricular myocardium. *Journal of Clinical Investigation* 100(9): 2315-2324.
- Lu, P., C. Vogel, et al. (2007). Absolute protein expression profiling estimates the relative contributions of transcriptional and translational regulation. *Nature Biotechnology* 25(1): 117-124.
- Lutsch, G., R. Vetter, et al. (1997). Abundance and location of the small heat shock proteins HSP25 and alphaB-crystallin in rat and human heart. *Circulation* 96(10): 3466-3476.
- MacLennan, D. H., M. Asahi, et al. (2003). The regulation of SERCA-type pumps by phospholamban and sarcolipin. *Ann N Y Acad Sci* 986: 472-480.
- MacLennan, D. H., T. Toyofuku, et al. (1997). Sites of regulatory interaction between calcium ATPases and phospholamban. *Basic Res Cardiol* 92 Suppl 1: 11-15.
- Malmstrom, J., M. Beck, et al. (2009). Proteome-wide cellular protein concentrations of the human pathogen *Leptospira interrogans*. *Nature* 460(7256): 762-765.
- Margossian, S. S. (1985). Reversible dissociation of dog cardiac myosin regulatory light chain 2 and its influence on ATP hydrolysis. *J Biol Chem* 260(25): 13747-13754.
- Marin-Garcia, J., M. J. Goldenthal, et al. (1995). Impaired mitochondrial function in idiopathic dilated cardiomyopathy: biochemical and molecular analysis. *J Card Fail* 1(4): 285-291.
- Maron, B. J., J. A. Towbin, et al. (2006). Contemporary definitions and classification of the cardiomyopathies: an American Heart Association Scientific Statement from the Council on Clinical Cardiology, Heart Failure and Transplantation Committee;

- Quality of Care and Outcomes Research and Functional Genomics and Translational Biology Interdisciplinary Working Groups; and Council on Epidemiology and Prevention. *Circulation* 113(14): 1807-1816.
- Martino, T. A., P. Liu, et al. (1994). Viral infection and the pathogenesis of dilated cardiomyopathy. *Circulation Research Journal Of The American Heart Association* 74(2): 182-188.
- Masumiya, H., Y. Asaumi, et al. (2009). Mitsugumin 53-mediated maintenance of K⁺ currents in cardiac myocytes. *Channels (Austin)* 3(1): 6-11.
- Mattiazzi, A., C. Mundina-Weilenmann, et al. (2005). Role of phospholamban phosphorylation on Thr17 in cardiac physiological and pathological conditions. *Cardiovascular Research* 68(3): 366-375.
- McCarty, M. F. (1999). Interleukin-6 as a central mediator of cardiovascular risk associated with chronic inflammation, smoking, diabetes, and visceral obesity: down-regulation with essential fatty acids, ethanol and pentoxifylline. *Med Hypotheses* 52(5): 465-477.
- McCutcheon, L. J., C. R. Cory, et al. (1992). Respiratory chain defect of myocardial mitochondria in idiopathic dilated cardiomyopathy of Doberman pinscher dogs. *Can J Physiol Pharmacol* 70(11): 1529-1533.
- McDonald, W. H. and J. R. Yates, 3rd (2003). Shotgun proteomics: integrating technologies to answer biological questions. *Curr Opin Mol Ther* 5(3): 302-309.
- McGregor, E. and M. J. Dunn (2006). Proteomics of the heart: unraveling disease. *Circulation Res* 98(3): 309-321.
- McLeod, C. J., A. P. Jeyabalan, et al. (2004). Delayed ischemic preconditioning activates nuclear-encoded electron-transfer-chain gene expression in parallel with enhanced postanoxic mitochondrial respiratory recovery. *Circulation* 110(5): 534-539.
- McManus, B. M., L. H. Chow, et al. (1993). Direct myocardial injury by enterovirus: a central role in the evolution of murine myocarditis. *Clin Immunol Immunopathol* 68(2): 159-169.
- McMullen, J. R. and G. L. Jennings (2007). Differences between pathological and physiological cardiac hypertrophy: novel therapeutic strategies to treat heart failure. *Clin Exp Pharmacol Physiol* 34(4): 255-262.
- Miller, I., J. Crawford, et al. (2006). Protein stains for proteomic applications: which, when, why? *Proteomics* 6(20): 5385-5408.
- Milner, D. J., G. Weitzer, et al. (1996). Disruption of muscle architecture and myocardial degeneration in mice lacking desmin. *J Cell Biol* 134(5): 1255-1270.
- Mohan, S. B., M. Parker, et al. (2002). Idiopathic dilated cardiomyopathy: a common but mystifying cause of heart failure. *Cleveland Clinic Journal of Medicine* 69(6): 481-487.

- Moss, R. L. and D. P. Fitzsimons (2006). Myosin light chain 2 into the mainstream of cardiac development and contractility. *Circulation Research Journal Of The American Heart Association* 99(3): 225-227.
- Nakamura, F., T. P. Stossel, et al. (2011). The filamins: organizers of cell structure and function. *Cell Adh Migr* 5(2): 160-169.
- Nascimben, L., J. S. Ingwall, et al. (1996). Creatine kinase system in failing and nonfailing human myocardium. *Circulation* 94(8): 1894-1901.
- Naugle, J. E., E. R. Olson, et al. (2006). Type VI collagen induces cardiac myofibroblast differentiation: implications for postinfarction remodeling. *Am J Physiol Heart Circ Physiol* 290(1): H323-330.
- Neilson, K. A., N. A. Ali, et al. Less label, more free: Approaches in label-free quantitative mass spectrometry. *Proteomics* 11(4): 535-553.
- Neu, N., K. W. Beisel, et al. (1987). Autoantibodies specific for the cardiac myosin isoform are found in mice susceptible to Coxsackievirus B3-induced myocarditis. *Journal of Immunology* 138(8): 2488-2492.
- Neu, N., N. R. Rose, et al. (1987). Cardiac myosin induces myocarditis in genetically predisposed mice. *J Immunol* 139(11): 3630-3636.
- Nicholson-Weller, A. and C. E. Wang (1994). Structure and function of decay accelerating factor CD55. *J Lab Clin Med* 123(4): 485-491.
- Nigro, V., Y. Okazaki, et al. (1997). Identification of the Syrian hamster cardiomyopathy gene. *Hum Mol Genet* 6(4): 601-607.
- Nikolopoulos, S. N. and C. E. Turner (2002). Molecular dissection of actopaxin-integrin-linked kinase-Paxillin interactions and their role in subcellular localization. *J Biol Chem* 277(2): 1568-1575.
- Nishimura, H., I. Kakizaki, et al. (1995). cDNA and deduced amino acid sequence of human PK-120, a plasma kallikrein-sensitive glycoprotein. *FEBS Lett* 357(2): 207-211.
- Nishimura, H., T. Okazaki, et al. (2001). Autoimmune dilated cardiomyopathy in PD-1 receptor-deficient mice. *Science* 291(5502): 319-322.
- Nogami, S., S. Satoh, et al. (2004). Identification and characterization of taxilin isoforms. *Biochem Biophys Res Commun* 319(3): 936-943.
- Noutsias, M., H. Fechner, et al. (2001). Human coxsackie-adenovirus receptor is colocalized with integrins alpha(v)beta(3) and alpha(v)beta(5) on the cardiomyocyte sarcolemma and upregulated in dilated cardiomyopathy: implications for cardiotropic viral infections. *Circulation* 104(3): 275-280.
- O'Farrell, P. H. (1975). High resolution two-dimensional electrophoresis of proteins. *J Biol Chem* 250(10): 4007-4021.

- Okazaki, T., Y. Tanaka, et al. (2003). Autoantibodies against cardiac troponin I are responsible for dilated cardiomyopathy in PD-1-deficient mice. *Nature Medicine* 9(12): 1477-1483.
- Olson, T. M., V. V. Michels, et al. (1998). Actin mutations in dilated cardiomyopathy, a heritable form of heart failure. *Science* 280(5364): 750-752.
- Onda, M., T. Ishiwata, et al. (2002). Expression of lumican in thickened intima and smooth muscle cells in human coronary atherosclerosis. *Exp Mol Pathol* 72(2): 142-149.
- Opiteck, G. J. and J. W. Jorgenson (1997). Two-dimensional SEC/RPLC coupled to mass spectrometry for the analysis of peptides. *Anal Chem* 69(13): 2283-2291.
- Pallansch, M. A. (1997). Coxsackievirus B epidemiology and public health concerns. *Curr Top Microbiol Immunol* 223: 13-30.
- Paradies, G. and F. M. Ruggiero (1990). Age-related changes in the activity of the pyruvate carrier and in the lipid composition in rat-heart mitochondria. *Biochim Biophys Acta* 1016(2): 207-212.
- Paradies, G., G. Petrosillo, et al. (1999). The effect of aging and acetyl-L-carnitine on the pyruvate transport and oxidation in rat heart mitochondria. *FEBS Lett* 454(3): 207-209.
- Patel, J. R., G. M. Diffie, et al. (1998). Phosphorylation of myosin regulatory light chain eliminates force-dependent changes in relaxation rates in skeletal muscle. *Biophys J* 74(1): 360-368.
- Pauly, D. F. (2011). The slow cardiac myosin regulatory light chain in heart failure. *Clin Cardiol* 34(1): 10-11.
- Pauschinger, M., K. Chandrasekharan, et al. (2004). Viral heart disease: molecular diagnosis, clinical prognosis, and treatment strategies. *Medical Microbiology and Immunology (Berl)* 193(2-3): 65-69.
- Pavelka, N., M. L. Fournier, et al. (2008). Statistical similarities between transcriptomics and quantitative shotgun proteomics data. *Mol Cell Proteomics* 7(4): 631-644.
- Persad, S. and S. Dedhar (2003). The role of integrin-linked kinase (ILK) in cancer progression. *Cancer Metastasis Rev* 22(4): 375-384.
- Pleasure, I. T., M. M. Black, et al. (1993). Valosin-containing protein, VCP, is a ubiquitous clathrin-binding protein. *Nature* 365(6445): 459-462.
- Pleissner, K. P., P. Soding, et al. (1997). Dilated cardiomyopathy-associated proteins and their presentation in a WWW-accessible two-dimensional gel protein database. *Electrophoresis* 18(5): 802-808.
- Polyakova, V., I. Loeffler, et al. (2011). Fibrosis in endstage human heart failure: Severe changes in collagen metabolism and MMP/TIMP profiles. *Int J Cardiol* 151(1): 18-33.

- Portman, M. A. (2002). The adenine nucleotide translocator: regulation and function during myocardial development and hypertrophy. *Clin Exp Pharmacol Physiol* 29(4): 334-338.
- Prasad, T. S., K. Kandasamy, et al. (2009). Human Protein Reference Database and Human Proteinpedia as discovery tools for systems biology. *Methods Mol Biol* 577: 67-79.
- Pu, X. P., A. Iwamoto, et al. (1994). Purification and characterization of a novel substrate for plasma kallikrein (PK-120) in human plasma. *Biochim Biophys Acta* 1208(2): 338-343.
- Quigley, A. F., R. M. Kapsa, et al. (2000). Mitochondrial respiratory chain activity in idiopathic dilated cardiomyopathy. *J Card Fail* 6(1): 47-55.
- Ratcliffe, N. R., J. Hutchins, et al. (2000). Chronic myocarditis induced by T cells reactive to a single cardiac myosin peptide: persistent inflammation, cardiac dilatation, myocardial scarring and continuous myocyte apoptosis. *J Autoimmun* 15(3): 359-367.
- Ravetch, J. V. and S. Bolland (2001). IgG Fc receptors. *Annu Rev Immunol* 19: 275-290.
- Rayment, I., H. M. Holden, et al. (1993). Structure of the actin-myosin complex and its implications for muscle contraction. *Science* 261(5117): 58-65.
- Reinhart, W. H. (2003). Fibrinogen--marker or mediator of vascular disease? *Vasc Med* 8(3): 211-216.
- Robinson, P., M. Mirza, et al. (2002). Alterations in thin filament regulation induced by a human cardiac troponin T mutant that causes dilated cardiomyopathy are distinct from those induced by troponin T mutants that cause hypertrophic cardiomyopathy. *The Journal of Biological Chemistry* 277(43): 40710-40716.
- Rodriguez, P. and E. G. Kranias (2005). Phospholamban: a key determinant of cardiac function and dysfunction. *Arch Mal Coeur Vaiss* 98(12): 1239-1243.
- Rose, N. R. and S. L. Hill (1996). Autoimmune myocarditis. *International Journal of Cardiology* 54(2): 171-175.
- Rutschow, S., S. Leschka, et al. (2010). Left ventricular enlargement in coxsackievirus-B3 induced chronic myocarditis--ongoing inflammation and an imbalance of the matrix degrading system. *Eur J Pharmacol* 630(1-3): 145-151.
- Sack, M. N., T. A. Rader, et al. (1996). Fatty acid oxidation enzyme gene expression is downregulated in the failing heart. *Circulation* 94(11): 2837-2842.
- Saks VA. Creatine kinase isozymes and the control of cardiac contraction. In: Jacobus WE, Ingwall JS, eds. *Heart Creatine Kinase*. Baltimore, Maryland, USA: Williams & Wilkins; (1980):109-124.
- Schaper, J., R. Froede, et al. (1991). Impairment of the myocardial ultrastructure and changes of the cytoskeleton in dilated cardiomyopathy. *Circulation* 83(2): 504-514.

- Schmidt, R. E. and J. E. Gessner (2005). Fc receptors and their interaction with complement in autoimmunity. *Immunol Lett* 100(1): 56-67.
- Schonberger, J. and C. E. Seidman (2001). Many roads lead to a broken heart: the genetics of dilated cardiomyopathy. *Am J Hum Genet* 69(2): 249-260.
- Schultheiss, H. P. (1992). Dysfunction of the ADP/ATP carrier as a causative factor for the disturbance of the myocardial energy metabolism in dilated cardiomyopathy. *Basic Res Cardiol* 87 Suppl 1: 311-320.
- Schultheiss, H. P. and H. D. Bolte (1985). Immunological analysis of auto-antibodies against the adenine nucleotide translocator in dilated cardiomyopathy. *J Mol Cell Cardiol* 17(6): 603-617.
- Schultheiss, H. P. and M. Klingenberg (1984). Immunochemical characterization of the adenine nucleotide translocator. Organ specificity and conformation specificity. *Eur J Biochem* 143(3): 599-605.
- Schultheiss, H. P., U. Kuhl, et al. (2011). The management of myocarditis. *Eur Heart J* 32(21): 2616-2625.
- Schulze, K., B. F. Becker, et al. (1989). Antibodies to the ADP/ATP carrier, an autoantigen in myocarditis and dilated cardiomyopathy, penetrate into myocardial cells and disturb energy metabolism in vivo. *Circulation Research Journal Of The American Heart Association* 64(2): 179-192.
- Schulze, K., B. F. Becker, et al. (1990). Antibodies to ADP-ATP carrier--an autoantigen in myocarditis and dilated cardiomyopathy--impair cardiac function. *Circulation* 81(3): 959-969.
- Schwimmbeck, P. L., N. K. Schwimmbeck, et al. (1993). Mapping of antigenic determinants of the adenine-nucleotide translocator and coxsackie B3 virus with synthetic peptides: use for the diagnosis of viral heart disease. *Clin Immunol Immunopathol* 68(2): 135-140.
- Scruggs, S. B. and R. J. Solaro (2011). The significance of regulatory light chain phosphorylation in cardiac physiology. *Arch Biochem Biophys* 510(2): 129-134.
- Seko, Y., H. Tsuchimochi, et al. (1990). Expression of major histocompatibility complex class I antigen in murine ventricular myocytes infected with Cocksackievirus B3. *Circ Res* 67(2): 360-367.
- Seko, Y., N. Takahashi, et al. (1997). Expression of cytokine mRNAs in murine hearts with acute myocarditis caused by coxsackievirus b3. *J Pathol* 183(1): 105-108.
- Shamhart, P. E. and J. G. Meszaros (2010). Non-fibrillar collagens: key mediators of post-infarction cardiac remodeling? *J Mol Cell Cardiol* 48(3): 530-537.
- Sheeran, F. L., J. Rydstrom, et al. (2010). Diminished NADPH transhydrogenase activity and mitochondrial redox regulation in human failing myocardium. *Biochim Biophys Acta* 1797(6-7): 1138-1148.

- Shen, Y. and R. D. Smith (2002). Proteomics based on high-efficiency capillary separations. *Electrophoresis* 23(18): 3106-3124.
- Shenoy-Scaria, A. M., J. Kwong, et al. (1992). Signal transduction through decay-accelerating factor. Interaction of glycosyl-phosphatidylinositol anchor and protein tyrosine kinases p56lck and p59fyn 1. *J Immunol* 149(11): 3535-3541.
- Shi, Y., C. Chen, et al. (2009). Cardiac deletion of the Coxsackievirus-adenovirus receptor abolishes Coxsackievirus B3 infection and prevents myocarditis in vivo. *J Am Coll Cardiol* 53(14): 1219-1226.
- Shih, H., B. Lee, et al. (2011). The aging heart and post-infarction left ventricular remodeling. *J Am Coll Cardiol* 57(1): 9-17.
- Silva, J. C., M. V. Gorenstein, et al. (2006). Absolute quantification of proteins by LCMS^E: a virtue of parallel MS acquisition. *Mol Cell Proteomics* 5(1): 144-156.
- Simkhovich, B. Z., P. Marjoram, et al. (2003). Age-related changes of cardiac gene expression following myocardial ischemia/reperfusion. *Arch Biochem Biophys* 420(2): 268-278.
- Song, J., M. Patel, et al. (2006). Quantification of fragments of human serum inter-alpha-trypsin inhibitor heavy chain 4 by a surface-enhanced laser desorption/ionization-based immunoassay. *Clin Chem* 52(6): 1045-1053.
- Spinale, F. G., M. L. Coker, et al. (2000). A matrix metalloproteinase induction/activation system exists in the human left ventricular myocardium and is upregulated in heart failure. *Circulation* 102(16): 1944-1949.
- Stahl, A. (2004). A current review of fatty acid transport proteins (SLC27). *Pflugers Arch* 447(5): 722-727.
- Stanley, W. C., F. A. Recchia, et al. (2005). Myocardial substrate metabolism in the normal and failing heart. *Physiol Rev* 85(3): 1093-1129.
- Staudt, A. and S. B. Felix (2007). Immunoabsorption in dilated cardiomyopathy. *Transfusion and Apheresis Science* 37(2): 187-190.
- Stepien, G., A. Torroni, et al. (1992). Differential expression of adenine nucleotide translocator isoforms in mammalian tissues and during muscle cell differentiation. *J Biol Chem* 267(21): 14592-14597.
- Stossel, T. P., J. Condeelis, et al. (2001). Filamins as integrators of cell mechanics and signalling. *Nat Rev Mol Cell Biol* 2(2): 138-145.
- Sullivan, T., D. Escalante-Alcalde, et al. (1999). Loss of A-type lamin expression compromises nuclear envelope integrity leading to muscular dystrophy. *J Cell Biol* 147(5): 913-920.
- Sylvén, C., L. Lin, et al. (1993). Ventricular adenine nucleotide translocator mRNA is upregulated in dilated cardiomyopathy. *Cardiovasc Res* 27(7): 1295-1299.

- Tamir, I., J. C. Stolpa, et al. (2000). The RasGAP-binding protein p62dok is a mediator of inhibitory FcγRIIB signals in B cells. *Immunity* 12(3): 347-358.
- Taurin, S., V. Seyrantepe, et al. (2002). Proteome analysis and functional expression identify mortalin as an antiapoptotic gene induced by elevation of [Na⁺]_i/[K⁺]_i ratio in cultured vascular smooth muscle cells. *Circ Res* 91(10): 915-922.
- Thiesen, S. L. and T. H. Rosenquist (1995). Expression of collagens and decorin during aortic arch artery development: implications for matrix pattern formation. *Matrix Biol* 14(7): 573-582.
- Towbin, J. A. and N. E. Bowles (2002). The failing heart. *Nature* 415(6868): 227-233.
- Trahair, T., T. Yeoh, et al. (1993). Myosin light chain gene expression associated with disease states of the human heart. *Journal of Molecular and Cellular Cardiology* 25(5): 577-585.
- Traub, P. (1985). Are intermediate filament proteins involved in gene expression? *Ann N Y Acad Sci* 455: 68-78.
- Treuting, P. M., N. J. Linford, et al. (2008). Reduction of age-associated pathology in old mice by overexpression of catalase in mitochondria. *J Gerontol A Biol Sci Med Sci* 63(8): 813-822.
- van der Vusse, G. J., J. F. Glatz, et al. (1992). Fatty acid homeostasis in the normoxic and ischemic heart. *Physiol Rev* 72(4): 881-940.
- Van Dyke, T. A. and J. B. Flanagan (1980). Identification of poliovirus polypeptide P63 as a soluble RNA-dependent RNA polymerase. *J Virol* 35(3): 732-740.
- van Kuppeveld, F. J., J. G. Hoenderop, et al. (1997). Coxsackievirus protein 2B modifies endoplasmic reticulum membrane and plasma membrane permeability and facilitates virus release. *Embo J* 16(12): 3519-3532.
- Vembar, S. S. (2008). One step at a time: endoplasmic reticulum- associated degradation. *Nat Rev Mol Cell Biol* 9(12): 944-957.
- Ventoso, I., S. E. MacMillan, et al. (1998). Poliovirus 2A proteinase cleaves directly the eIF-4G subunit of eIF-4F complex. *FEBS Lett* 435(1): 79-83.
- Vogelpohl, I., R. Vetter, et al. (2011). Transgenic overexpression of heart-specific adenine nucleotide translocase 1 positively affects contractile function in cardiomyocytes. *Cell Physiol Biochem* 27(2): 121-128.
- Wallimann, T. and W. Hemmer (1994). Creatine kinase in non-muscle tissues and cells. *Mol Cell Biochem* 133-134: 193-220.
- Walther, D. M. and M. Mann (2011). Accurate quantification of more than 4000 mouse tissue proteins reveals minimal proteome changes during aging. *Mol Cell Proteomics* 10(2): M110 004523.

- Walther, T., C. Tschope, et al. (2007). Accelerated Mitochondrial Adenosine Diphosphate/Adenosine Triphosphate Transport Improves Hypertension-Induced Heart Disease. *Circulation* 115(3): 333-344.
- Wang, Y., L. Ebermann, et al. (2009). Myocardial overexpression of adenine nucleotide translocase 1 ameliorates diabetic cardiomyopathy in mice. *Exp Physiol* 94(2): 220-227.
- Weber, K. T. (1989). Cardiac interstitium in health and disease: the fibrillar collagen network. *J Am Coll Cardiol* 13(7): 1637-1652.
- Wei, L., C. Cai, et al. (2009). Dual-drug delivery system based on hydrogel/micelle composites. *Biomaterials* 30(13): 2606-2613.
- Wisniewski, H. G., J. C. Hua, et al. (1996). TNF/IL-1-inducible protein TSG-6 potentiates plasmin inhibition by inter-alpha-inhibitor and exerts a strong anti-inflammatory effect in vivo. *J Immunol* 156(4): 1609-1615.
- Wolters, D. A., M. P. Washburn, et al. (2001). An automated multidimensional protein identification technology for shotgun proteomics. *Anal Chem* 73(23): 5683-5690.
- Wong, J. W., M. J. Sullivan, et al. (2008). Computational methods for the comparative quantification of proteins in label-free LCn-MS experiments. *Brief Bioinform* 9(2): 156-165.
- Woodruff, J. F. and J. J. Woodruff (1974). Involvement of T lymphocytes in the pathogenesis of coxsackie virus B3 heart disease. *J Immunol* 113(6): 1726-1734.
- Xu, J., H. G. Nie, et al. (2011). Down-regulated energy metabolism genes associated with mitochondria oxidative phosphorylation and fatty acid metabolism in viral cardiomyopathy mouse heart. *Mol Biol Rep* 38(6): 4007-4013.
- Yajima, T. and K. U. Knowlton (2009). Viral myocarditis: from the perspective of the virus. *Circulation* 119(19): 2615-2624.
- Yan, L. J., E. S. Christians, et al. (2002). Mouse heat shock transcription factor 1 deficiency alters cardiac redox homeostasis and increases mitochondrial oxidative damage. *Embo J* 21(19): 5164-5172.
- Yan, L., H. Ge, et al. (2004). Gender-specific proteomic alterations in glycolytic and mitochondrial pathways in aging monkey hearts. *J Mol Cell Cardiol* 37(5): 921-929.
- Yang, C., V. I. Slepnev, et al. (1994). Rab proteins form in vivo complexes with two isoforms of the GDP-dissociation inhibitor protein (GDI). *J Biol Chem* 269(50): 31891-31899.
- Yates, J. R., 3rd (2004). Mass spectral analysis in proteomics. *Annu Rev Biophys Biomol Struct* 33: 297-316.
- Yoneda, S., K. Senda, et al. (1979). Experimental study of virus myocarditis in culture. *Jpn Circ J* 43(11): 1048-1054.

- Yoshida, K., S. Nogami, et al. (2005). Interaction of the taxilin family with the nascent polypeptide-associated complex that is involved in the transcriptional and translational processes. *Genes Cells* 10(5): 465-476.
- Young, L. H., S. V. Joag, et al. (1990). Perforin-mediated myocardial damage in acute myocarditis. *Lancet* 336(8722): 1019-1021.
- Yuan, C., Y. Guo, et al. (2006). Myosin binding protein C is differentially phosphorylated upon myocardial stunning in canine and rat hearts-- evidence for novel phosphorylation sites. *Proteomics* 6(14): 4176-4186.
- Zamorano-Leon, J. J., J. Modrego, et al. (2010). A proteomic approach to determine changes in proteins involved in the myocardial metabolism in left ventricles of spontaneously hypertensive rats. *Cell Physiol Biochem* 25(2-3): 347-358.
- Zhang, D., U. R. Ezekiel, et al. (2005). Gene expression profile in dilated cardiomyopathy caused by elevated frequencies of mitochondrial DNA mutations in the mouse heart. *Cardiovasc Pathol* 14(2): 61-69.
- Zhou, X., J. Boren, et al. (2007). Filamins in cardiovascular development. *Trends Cardiovasc Med* 17(7): 222-229.
- Zimmerman, S. D., D. P. Thomas, et al. (2001). Time course of collagen and decorin changes in rat cardiac and skeletal muscle post-MI. *Am J Physiol Heart Circ Physiol* 281(4): H1816-1822.

Acknowledgements

First and foremost, I'd like to express my thanks and gratitude to Prof. Dr. Uwe Völker, Director, Interfaculty Institute for Genetics and Functional Genomics for providing me the opportunity of pursuing my doctoral studies in the Dept. of Functional Genomics. I'd also like to thank him for the guidance and support provided within and beyond the lab which made my stay productive.

I am especially thankful to Dr. Elke Hammer for supervising and guiding me through my Ph.d. Her constant support and encouragement helped in the fruitful completion of the thesis and publications for which I express my deep gratitude. Working under her guidance provided me a learning experience and her immense knowledge in proteomics and mass spectrometry is intriguing and something which I will always look upto.

I'd also like thank Dr. Leif Steil for his continuous help and guidance in planning, execution and in trouble shooting without which some of the major experiments of the thesis could not be performed and interpreted.

Furthermore I'd like to thank Dr. Karin Klingel, Dept. of Molecular Pathology, University Medicine, Tübingen for providing the A.BY heart tissue samples and helping out with the validation experiments. I'd also like to thank Dr. Stephan Felix and Dr. Lars Herda of Dept. of Cardiology, University Medicine, Greifswald, for providing the samples for the study. I'd like to express my gratitude to Dr. Andrea Dörner, Charité, Berlin for graciously providing the samples for the study and for the help, support and generosity shown during the my week long stay in her lab. I'd also like to thank Ms. Inga Vogelpohl for taking out her precious time to perform the acitivity measurements during this week.

I'd like to thank Dr.Sabine Ameling for taking out her time and helping me out with my thesis.I'm also thankful to my other lab members and colleagues who provided a friendly, happy and congenial environment. Katrin Darm and Katrin Schocknecht have been extremely helpful through out my doctoral studies for which I express my gratitude. Finally I'd like to thank my friends Praveen, Rasmita, Priyanka, Ravi Kumar, Marc Schaffer and Martin for their timely advice and encouragement.

Erklärung

Hiermit erkläre ich, dass diese Arbeit bisher von mir weder an der Mathematisch-Naturwissenschaftlichen Fakultät der Ernst-Moritz-Arndt-Universität Greifswald noch einer anderen wissenschaftlichen Einrichtung zum Zwecke der Promotion eingereicht wurde.

Ferner erkläre ich, daß ich diese Arbeit selbständig verfasst und keine anderen als die darin angegebenen Hilfsmittel benutzt und keine Textabschnitte eines Dritten ohne Kennzeichnung übernommen habe.

Krishnatej Nishtala, 2. April, 2012

Krishnatej Nishtala

Curriculum Vitae

Personal Details

Name	Krishnatej Nishtala
Date of Birth	16.08.1981
Place of Birth	Kakinada
Nationality	Indian

Educational Qualifications

- 1. Primary School (1984-1990):** Aditya Public School, Kakinada, India
- 2. Secondary School (1990-1998):** Nava Bharat Public High School, Kakinada, India
- 3. Bachelor in Pharmacy (1999-2003):** Vishwa Bharathi College of Pharmaceutical Sciences, Guntur affiliated to JNTU, Hyderabad, India
- 4. Masters in Biotechnology (2004-2006):** Acharya Nagarjuna University, Guntur, India

Work Experience

- 1. 2006-2007:** Research Assistant at Centre for Biotechnology, Acharya Nagarjuna University, Guntur, India
- 2. 2007 - 2008:** Research Assistant in Proteomics Research Facility at Centre for Cellular and Molecular Biology (CCMB), Hyderabad, India

Doctoral Study (since 09/2008): Doctoral student at Interfakultary Institute for Genetics and Functional Genomics, Dept. of Functional Genomics, Ernst-Moritz-Arndt-University, Greifswald, Germany

Publications

Krishnatej Nishtala, Truong Q. Phong, Leif Steil, Martina Sauter, Manuela G. Salazar, Reinhard Kandolf, Heyo K. Kroemer, Stephan B. Felix, Uwe Völker, Karin Klingel and Elke Hammer (2011). Virus-induced dilated cardiomyopathy is characterized by increased levels of fibrotic extracellular matrix proteins and reduced amounts of energy-producing enzymes. *Proteomics* 2011, 11, 4310–4320.

Krishnatej Nishtala, Truong Q. Phong, Leif Steil, Manuela G. Salazar, Reinhard Kandolf, Heyo K. Kroemer, Stephan B. Felix, Uwe Völker, Karin Klingel and Elke Hammer (2011). Characterisation of age related changes in the proteome of four months old A.BY/SnJ mice heart using 2D-DIGE and LC- MS analysis (manuscript for submission).

Abstracts/Poster presentations:

1. Poster presentation titled “Comprehensive analysis of changes in the proteome occurring in ABY/SnJ mice infected with Cocksackievirus B3 (CVB3) using 2D-DIGE and LC-MS/MS” at Proteomic forum 2011, Freie Universität, Berlin, Germany.
2. Poster presentation titled “Characterisation of virus induced dilated cardiomyopathy in ABY/SnJ mice hearts using a proteomics approach” at 4th EU- Summer School in Proteomic Basics 2010, Brixen, South Tyrol, Italy.
3. Poster presentation titled “Exploring the molecular events occurring during dilated cardiomyopathy (DCM) in murine animal models” at Proteomic forum 2009, Freie Universität, Berlin, Germany.
4. Abstract titled “Comparison of experimental methods for the identification of membrane proteins from MPI reference specimen” accepted for The joint 2nd Pacific Rim International conference on Protein science and the 4th Asian-Oceania Human proteome Organization, AOHUPO Conference 2008, Abstract No.110.
5. Abstract titled “Study of proteins during grain development in rice and their relevance to grain weight” accepted for the International Proteomics Conference, Human Proteomics Organisation (HUPO) 2007, is published in the Journal Molecular and Cellular Proteomics(MCP) Abstract No.HA-0921.

Appendix

A3.2.4. identifications from probable phosphorylated spots in mice hearts infected with CVB3 compared to 84d non-infected mice hearts.

Acc.No	Protein Annotation	No. of Peptides	Protein score	Seq. Coverage (%)	Mol.Wt (kDa)	pI	Fold Change
P51667	Myosin regulatory light chain 2, ventricular/cardiac muscle isoform	7	182.65	61.5	18.9	4.9	0.6
P62259	14-3-3 protein epsilon	24	558.57	83.1	29.2	4.7	0.3
Q91WD5	NADH dehydrogenase [ubiquinone] iron-sulfur protein 2	12	107.79	41.7	52.6	7.0	1.6
Q91WD5	NADH dehydrogenase [ubiquinone] iron-sulfur protein 2	20	502.99	58.1	52.6	7.0	0.6
P80314	T-complex protein 1 subunit beta	16	113.17	51.6	57.4	6.4	0.5
P14152	Malate dehydrogenase	23	773.91	67.1	36.5	6.6	0.1
P14152	Malate dehydrogenase	12	130.95	40.7	36.5	6.6	0.5
O08553	Dihydropyrimidinase-related protein 2	20	331.25	61.0	62.2	6.4	0.7
Q9D0F9	Phosphoglucomutase-1	24	275.50	63.4	61.5	6.8	0.9
Q60597	2-oxoglutarate dehydrogenase	36	581.31	51.2	116.4	6.8	1.2
Q9EQP2	EH domain-containing protein 4	21	168.29	46.8	61.4	6.8	1.3
P56480	ATP synthase subunit beta	45	3470.90	83.7	56.3	5.3	0.9
P56480	ATP synthase subunit beta	45	2257.35	85.4	56.3	5.3	0.8

Fold change- Intensity ratio of phospho spots at 84 d p.i. to 84 d control phospho spots.

A3.4.1. List proteins displaying ANT-OE dependent changes in 8 months old transgenic rat hearts compared to WT animals.

gi Number	Protein Annotation	Symbol (IPA)	Peptide count	Seq.Coverage (%)	Subcellular location	Mol.wt (Da)	pI	Fold change	p-value	Coefficient of Variation (CV)		CV
										ANT-OE	WT	
Proteins displaying ratios ≥ 1.2 in ANT-OE hearts												
34933197	PREDICTED: similar to Amine oxidase A (Monoamine oxidase type A)	MAOA	5	40.2	Cytoplasm	27182.7	9.40	1.7	1.30E-02	51.02	41.97	35.23
109509021	PREDICTED: similar to C50H11.1		3	23.2	Cytoplasm	93611.4	6.36	1.7	8.71E-06	26.90	13.34	34.84
14192933	Aldehyde dehydrogenase 2	ALDH2	10	25.6	Extracellular Space	56488.4	6.63	1.6	6.82E-26	30.17	18.32	33.80
16924006	Complement component 9	C9	3	8.3	Cytoplasm	63762.5	5.83	1.5	9.53E-05	45.66	28.84	30.46
109487680	Myosin-11 (Myosin heavy chain, smooth muscle isoform)	MYH11	4	3.2	Cytoplasm	63980.5	6.22	1.5	1.00E-02	43.91	52.81	30.03
8393807	Myosin heavy chain, polypeptide 7	MYH7	12	10.5	Cytoplasm	223083.0	5.64	1.5	4.00E-03	40.78	35.16	27.66
77539778	Alpha actinin 4	ACTN4	2	8.7	Cytoplasm	104915.0	5.27	1.5	2.63E-05	29.09	33.31	26.33
109462323	Filamin-A	FLNA	3	23.0	Extracellular Space	321328.5	6.12	1.4	8.00E-03	44.77	30.13	25.08
9506703	Fibronectin 1	FN1	4	2.6	Cytoplasm	272511.2	5.50	1.4	1.11E-08	35.94	26.45	25.00
57114342	Lactate dehydrogenase D	LDHD	2	6.0	Cytoplasm	54292.2	5.78	1.4	5.19E-05	37.72	37.74	24.89
28467005	Heat shock protein 1, alpha	HSP90AA1	2	5.7	Nucleus	84814.9	4.93	1.4	1.36E-08	36.15	24.36	23.56
16924004	Cysteine-rich protein 3	CSRP3	2	18.0	Cytoplasm	20802.7	8.81	1.4	1.00E-03	46.29	19.04	23.38
15805031	Eukaryotic translation elongation factor 1 alpha 2	EEF1A2	2	2.5	Cytoplasm	48574.8	5.59	1.4	3.15E-05	35.30	17.69	22.15
109481431	PREDICTED: similar to myosin, light polypeptide 6, alkali, smooth muscle and non-muscle	EEF1A2	2	1.0	Cytoplasm	157166.1	8.48	1.4	2.91E-06	36.30	28.36	21.81
58615680	Cytochrome c oxidase subunit II	MT-CO2	3	15.9	Plasma Membrane	25928.3	4.61	1.3	5.74E-07	36.58	24.03	20.71
52630316	Dystrophin isoform Dp71ab	Dmd	2	11.4	Cytoplasm	40132.7	5.84	1.3	2.00E-03	38.01	29.93	20.45

gi Number	Protein Annotation	Symbol (IPA)	Peptide count	Seq.Coverage (%)	Subcellular location	Mol.wt (Da)	pI	Fold change	p-value	Coefficient of Variation (CV)		CV
										ANT-OE	WT	
62651145	PREDICTED: similar to Protein C14orf159, mitochondrial precursor	C14orf159	2	12.6	Plasma Membrane	51044.1	8.61	1.3	3.00E-03	36.75	38.37	20.40
47058982	Erythroid spectrin beta	SPTB	5	4.2	Extracellular Space	246328.6	5.18	1.3	9.65E-04	22.34	17.91	20.00
109510183	PREDICTED: similar to Laminin alpha-4 chain precursor	LAMA4	2	23.2	Cytoplasm	93611.4	6.36	1.3	7.73E-06	29.61	24.25	19.85
83977457	3-hydroxyisobutyrate dehydrogenase	HIBADH	4	23.3	Cytoplasm	35302.7	8.73	1.3	4.58E-05	38.39	24.74	19.60
6978487	Aldolase A	ALDOA	4	25.8	Extracellular Space	39351.9	8.30	1.3	4.16E-04	43.62	17.34	18.60
109503793	PREDICTED: similar to Inter-alpha-trypsin inhibitor heavy chain H1 precursor	ITIH1	2	20.1	Cytoplasm	79854.7	6.65	1.3	1.00E-03	32.72	25.11	18.58
24025637	Heat shock protein 4	HSPA4	4	7.5	Cytoplasm	94056.5	5.13	1.3	4.45E-04	38.53	33.89	18.33
6981236	Myosin, heavy polypeptide 9	MYH9	4	4.0	unknown	226338.1	5.49	1.3	3.96E-05	26.93	18.59	17.85
109459168	PREDICTED: similar to Hemoglobin beta-2 subunit (Hemoglobin beta-2 chain)	LOC100134871	3	3.5	Cytoplasm	93168.5	6.02	1.3	1.00E-03	29.61	23.13	17.73
9506467	Carbonyl reductase	CBR1	3	24.5	Cytoplasm	30578.1	8.21	1.3	5.00E-02	40.60	31.52	17.70
55926139	Alpha isoform of regulatory subunit A, protein phosphatase 2	PPP2R1A	3	15.1	Extracellular Space	65322.6	5.00	1.3	2.99E-04	31.79	26.80	17.48
109505096	PREDICTED: similar to Nidogen-1 precursor (Entactin)	NID1	2	7.1	Nucleus	137039.1	5.24	1.3	1.23E-05	30.79	19.10	16.93
34869683	PREDICTED: similar to purine-nucleoside phosphorylase	PNP	3	40.2	Cytoplasm	27182.7	9.40	1.3	3.62E-04	31.90	26.23	16.90
109479984	PREDICTED: similar to Adenylosuccinate synthetase isozyme 1 isoform 2	Adss1l	2	14.2	Plasma Membrane	50250.4	8.60	1.3	7.00E-03	33.28	19.98	16.78

gi Number	Protein Annotation	Symbol (IPA)	Peptide count	Seq.Coverage (%)	Subcellular location	Mol.wt (Da)	pI	Fold change	p-value	Coefficient of Variation (CV)		CV
										ANT-OE	WT	
8393636	Integrin beta 1	ITGB1	3	6.1	Nucleus	88494.6	5.77	1.3	4.28E-04	35.80	28.33	16.56
58865414	Annexin A11	ANXA11	3	7.6	Cytoplasm	54160.5	7.53	1.3	2.00E-03	36.79	25.57	16.38
109463865	PREDICTED: similar to sorbin and SH3 domain containing 1 isoform 3	SORBS3	6	6.9	Plasma Membrane	43609.3	6.34	1.3	9.92E-04	38.93	23.87	16.39
21326447	EH-domain containing 4	EHD4	2	6.3	Plasma Membrane	61467.6	6.33	1.3	1.00E-03	35.64	28.68	16.08
9845234	Annexin A2	ANXA2	3	12.7	Cytoplasm	38678.2	7.55	1.3	2.62E-04	33.40	27.90	16.07
51948400	NAD(P)H dehydrogenase, quinone 2	NQO2	3	18.2	Plasma Membrane	26275.2	6.90	1.3	2.00E-03	37.69	29.75	15.80
16758606	Arg/Abl-interacting protein ArgBP2	Sorbs2	4	6.8	Plasma Membrane	134053.4	8.70	1.3	8.00E-03	45.65	22.24	15.69
7709992	Basigin	BSG	2	10.3	Cytoplasm	29585.5	5.12	1.2	4.00E-03	42.30	25.29	15.50
62078483	OCIA domain containing 1	OCIAD1	2	21.5	Cytoplasm	27659.1	6.97	1.2	1.30E-02	42.47	29.44	15.44
13591983	Lumican	LUM	2	7.4	Extracellular Space	38279.0	6.00	1.2	4.80E-02	41.47	25.42	15.39
42476287	Transglutaminase 2, C polypeptide	TGM2	9	21.4	Extracellular Space	76935.7	4.95	1.2	2.57E-06	35.19	17.13	15.37
12831225	Murinoglobulin 1 homolog	Mug1	2	18.8	Cytoplasm	165326.2	6.00	1.2	2.90E-02	29.32	21.27	15.28
14010865	Heat shock 27kDa protein 1	HSPB1	2	16.1	Cytoplasm	22821.6	6.12	1.2	8.34E-08	32.68	22.04	15.27
13592093	Suppression of tumorigenicity 13	ST13	2	6.0	Cytoplasm	41279.5	5.28	1.2	8.37E-04	32.63	20.10	15.19
48675845	5-aminoimidazole-4-carboxamide ribonucleotide formyltransferase/IMP cyclohydrolase		3	8.3	Cytoplasm	64208.4	6.69	1.2	8.38E-06	32.38	25.20	15.09
62664437	PREDICTED: similar to aldehyde dehydrogenase family 7, member A1	ALDH7A1	3	2.1	Cytoplasm	109837.9	6.04	1.2	5.00E-03	41.61	27.51	15.11

gi Number	Protein Annotation	Symbol (IPA)	Peptide count	Seq.Coverage (%)	Subcellular location	Mol.wt (Da)	pI	Fold change	p-value	Coefficient of Variation (CV)		CV
										ANT-OE	WT	
34858394	PREDICTED: similar to Bcl-2-like 13 protein	BCL2L13	3	40.2	Cytoplasm	27182.7	9.40	1.2	4.00E-03	37.46	28.61	14.91
109465995	PREDICTED: similar to mitochondrial ribosomal protein S36	MRPS36	2	1.0	Cytoplasm	140882.1	8.71	1.2	5.00E-03	43.82	20.56	14.92
78000203	Tropomyosin 1, alpha isoform i	TPM1	3	11.7	Cytoplasm	28528.7	4.71	1.2	2.02E-07	31.80	26.94	14.35
6981142	Laminin, beta 2	LAMB2	2	2.3	Cytoplasm	196473.8	6.35	1.2	1.00E-02	41.11	20.96	14.22
6981324	Prolyl 4-hydroxylase, beta polypeptide	P4HB	3	7.1	Extracellular Space	56864.2	4.82	1.2	4.12E-04	35.80	19.97	14.25
18266692	Selenium binding protein 2	SELENBP1	3	12.7	Cytoplasm	52532.1	6.10	1.2	6.76E-05	31.57	18.84	14.27
18426864	Heat shock 27kD protein 2	HSPB2	2	18.1	Nucleus	20346.7	5.27	1.2	5.67E-04	38.41	23.67	13.99
109482276	PREDICTED: similar to C33H5.19		2	9.4	Cytoplasm	24912.0	7.74	1.2	2.00E-03	35.06	19.85	13.83
16923998	Heterogeneous nuclear ribonucleoprotein K	HNRNPK	2	9.1	Plasma Membrane	50976.2	5.39	1.2	4.00E-03	34.60	26.49	13.72
19173772	Integrin linked kinase	ILK	2	4.6	Plasma Membrane	51373.2	8.30	1.2	4.55E-05	32.87	21.96	13.72
31542380	Carboxylesterase 3		2	7.4	Extracellular Space	62147.2	6.10	1.2	3.90E-02	30.31	28.78	13.71
13929056	Basal cell adhesion molecule	BCAM	2	6.1	Cytoplasm	67511.7	5.52	1.2	6.00E-03	34.41	21.14	13.61
109487472	PREDICTED: similar to alpha 3 type VI collagen isoform 1 precursor	COL6A3	2	15.4	Cytoplasm	343536.5	5.97	1.2	1.00E-02	32.01	20.50	13.38
55742827	Rho GDP dissociation inhibitor (GDI) alpha	ARHGDI A	2	15.2	Cytoplasm	23407.4	5.12	1.2	1.00E-03	36.96	18.94	13.07
54400736	Leucine zipper-EF-hand containing transmembrane protein 1	LETM1	2	3.7	Cytoplasm	83059.8	6.23	1.2	7.00E-03	36.44	25.43	12.91

gi Number	Protein Annotation	Symbol (IPA)	Peptide count	Seq.Coverage (%)	Subcellular location	Mol.wt (Da)	pI	Fold change	p-value	Coefficient of Variation (CV)		CV
										ANT-OE	WT	
Proteins displaying ratios ≤ 1.2 in ANT-OErats												
77993368	Hypothetical protein LOC619561		7	22.3	Cytoplasm	67886.5	8.39	0.8	2.00E-03	21.59	16.04	13.25
6980970	Glutamate oxaloacetate transaminase 1	GOT1	8	34.1	Cytoplasm	46328.6	6.28	0.8	2.00E-03	28.05	25.96	13.32
18426858	Succinate dehydrogenase complex, subunit A, flavoprotein (Fp)	SDHA	12	31.1	Cytoplasm	71615.2	6.75	0.8	4.00E-03	31.22	24.17	14.35
75905479	Aldehyde dehydrogenase family 9, subfamily A1	ALDH9A1	3	7.4	Cytoplasm	54050.1	6.31	0.8	5.00E-03	27.03	10.27	14.41
109477971	PREDICTED: ribosomal protein S7	RPS7	3	5.7	Cytoplasm	164010.0	5.50	0.8	8.36E-04	31.03	20.49	14.82
74024923	Sulfite oxidase	SUOX	2	9.0	Cytoplasm	60805.8	6.32	0.8	1.20E-02	27.85	24.07	15.13
34856307	PREDICTED: similar to Deoxyguanosine kinase, mitochondrial precursor (dGK)	DGUOK	2	40.2	Cytoplasm	27182.7	9.40	0.8	2.00E-02	40.55	17.29	15.31
27685797	PREDICTED: similar to thioesterase superfamily member 2	ACOT13	3	6.5	Cytoplasm	49670.8	4.78	0.8	5.45E-04	30.34	25.18	16.25
16757984	Phosphoglycerate mutase 1	PGAM1	4	31.5	Cytoplasm	28645.7	6.20	0.8	6.00E-03	26.36	24.71	16.55
19705465	ATP synthase, H+ transporting, mitochondrial F0 complex, subunit b, isoform 1	ATP5F1	6	28.9	Cytoplasm	28868.8	9.39	0.8	8.00E-03	21.65	23.01	16.84

gi Number	Protein Annotation	Symbol (IPA)	Peptide count	Seq.Coverage (%)	Subcellular location	Mol.wt (Da)	pI	Fold change	p-value	Coefficient of Variation (CV)		CV
										ANT-OE	WT	
84370368	DnaJ (Hsp40) homolog, subfamily A, member 3 isoform 2	DNAJA3	2	23.3	Cytoplasm	35302.7	8.73	0.8	2.30E-02	30.39	16.74	17.40
18426866	Acetyl-Coenzyme A acyltransferase 2	ACAA2	13	58.9	unknown	41870.9	8.09	0.8	9.00E-03	24.46	27.17	17.68
6981396	Protein kinase, cAMP dependent regulatory, type I, alpha	PRKAR1A	3	15.5	Cytoplasm	43095.0	5.27	0.8	4.29E-05	24.57	19.07	18.32
56912206	Hypothetical protein LOC310201		2	16.7	Cytoplasm	27902.9	6.24	0.8	7.00E-03	21.47	20.35	19.05
109473821	PREDICTED: similar to T- complex protein 1 subunit eta (TCP-1-eta)	CCT7	2	0.5	Nucleus	542698.9	6.00	0.8	4.10E-02	25.15	19.65	19.26
6978705	Carnitine palmitoyltransferase 2	CPT2	8	21.3	Cytoplasm	74110.3	6.89	0.8	8.00E-03	30.59	23.29	20.25
52345435	Adenosine kinase	ADK	2	11.4	Cytoplasm	40132.7	5.84	0.7	6.00E-03	21.79	23.46	21.24
19705527	Basic leucine zipper and W2 domains 2	BZW2	3	14.1	Cytoplasm	48049.2	6.26	0.7	5.00E-03	23.51	22.07	21.73
12018270	Pyridoxine 5-phosphate oxidase	PNPO	3	24.1	Cytoplasm	30184.4	8.66	0.7	2.70E-02	40.60	30.85	24.27
72255509	Proteasome (prosome, macropain) 26S subunit, non- ATPase, 2	PSMD2	2	4.5	Cytoplasm	100187.6	5.08	0.7	6.00E-03	34.80	16.69	25.17

gi Number	Protein Annotation	Symbol (IPA)	Peptide count	Seq.Coverage (%)	Subcellular location	Mol.wt (Da)	pI	Fold change	p-value	Coefficient of Variation (CV)		CV
										ANT-OE	WT	
58615686	NADH dehydrogenase subunit 4	MT-ND4	3	14.6	Cytoplasm	51782.8	9.45	0.7	3.20E-02	27.25	32.35	27.16
67078526	UDP-glucose pyrophosphorylase 2	UGP2	2	7.9	Cytoplasm	57023.4	7.18	0.7	3.35E-05	22.81	19.75	27.59
13162363	Heart fatty acid binding protein	FABP3	3	24.8	Cytoplasm	14774.7	5.90	0.7	2.37E-04	22.85	11.52	29.45
48675862	Mitochondrial acyl-CoA thioesterase 1	ACOT2	4	35.5	Cytoplasm	49629.1	8.16	0.6	1.60E-02	29.06	23.44	30.40
68341995	NADH dehydrogenase (ubiquinone) Fe-S protein 4, 18kDa (NADH-coenzyme Q reductase)	NDUFS4	4	34.3		19740.6	10.14	0.6	8.58E-04	26.11	26.29	33.43
109458613	PREDICTED: similar to ubiquinol-cytochrome c reductase binding protein	UQCRB	2	3.5		93168.5	6.02	0.6	3.27E-05	15.16	16.03	38.92

Fold change- Ratio of protein intensities of ANT over expressing (ANT-OE) rat hearts to that of Wild type hearts (WT)

A3.4.2. Proteins displaying infection dependent changes in mitochondrial fractions of CVB3 infected ANT-OE rats compared to infected WT rats

gi number	Protein annotation	Symbol	No.of peptides	Seq.Coverage (%)	Sub-cellular location	Mol. Wt (Da)	pI	Fold change	p-value	Coefficient of variation (CV)		CV
											ANT	WT
Proteins displaying ratios ≥ 1.2 in infected ANT-OE hearts												
109479712	PREDICTED: similar to Maleylacetoacetate isomerase	Gstz1	2		Cytoplasm			2.7	1.30E-02	55.77	65.04	64.50
50054324	Solute carrier family 27 (fatty acid transporter), member 1	SLC27A1	3	7.0		71347.11	8.77	2.2	4.81E-06	31.99	53.46	52.15
61557127	Nicotinamide nucleotide transhydrogenase	NNT	29	38.6	Mitochondria	113869.42	8.02	1.7	2.10E-02	39.40	79.55	38.20
109509021	PREDICTED: similar to C50H11.1	MUT	2					1.7	2.58E-06	15.63	53.97	37.13
109485854	PREDICTED: similar to Methylmalonyl-CoA mutase, mitochondrial precursor		3		Mitochondria			1.7	3.00E-03	12.84	86.98	36.84
48675862	Mitochondrial acyl-CoA thioesterase 1	ACOT2	4	31.8		49629.10	8.16	1.6	3.40E-02	30.52	54.76	32.77
7709992	Basigin	BSG	3	14.3	Membrane	29585.48	5.12	1.6	3.80E-02	43.78	78.14	32.42
109460735	PREDICTED: similar to glycoprotein, synaptic 2	RGD1560015	2					1.6	3.20E-02	30.88	78.83	31.12
11693174	Branched chain aminotransferase 2	BCAT2	6	20.1	Mitochondria	44275.52	8.46	1.5	6.09E-06	12.69	38.14	28.56
109461122	PREDICTED: similar to isochorismatase domain containing 2 isoform 1	ISOC2	2		Mitochondria			1.5	6.30E-05	17.66	48.00	27.96
62078677	Hypothetical protein LOC303606	CCDC47	2	8.7		55732.67	4.74	1.5	7.00E-03	26.76	58.03	26.62
76563946	Calsequestrin 2	CASQ2	10	33.3	Sarcoplasmic reticulum lumen	49402.65	4.14	1.4	7.46E-06	12.92	55.76	25.22

gi number	Protein annotation	Symbol	No.of peptides	Seq.Coverage (%)	Sub-cellular location	Mol. Wt (Da)	pI	Fold change	p-value	Coefficient of variation (CV)		CV
										ANT	WT	
61889092	Adenylate kinase 1	AK1	2	13.4	Cytoplasm	21583.76	7.66	1.4	9.00E-03	15.01	38.58	24.58
21489987	Chloride ion pump-associated 55 kDa protein	PCYOX1	2	7.7	Lysosome.	56287.64	6.62	1.4	1.00E-02	23.63	62.27	23.80
40254785	Lysosomal membrane glycoprotein 2	LAMP2	2	4.6		45143.76	8.02	1.4	8.36E-09	13.14	60.46	22.59
9506497	Clathrin, heavy polypeptide (Hc)	CLTC	3	3.4	Cytoplasm	191598.66	5.50	1.4	3.00E-02	15.25	66.37	22.51
77404380	Hypoxia up-regulated 1	Kat3	2		Endoplasmic reticulum lumen			1.4	2.00E-03	15.95	66.23	22.31
62543563	Kynurenine aminotransferase III	RTN4IP1	2	8.8		51044.10	8.61	1.4	3.20E-02	23.05	61.70	22.31
109510252	PREDICTED: similar to Reticulon-4-interacting protein 1	HYOU1	3		Mitochondria			1.4	2.00E-03	12.64	43.94	21.70
109467479	PREDICTED: similar to Lipoamide acyltransferase component of branched-chain alpha-keto acid dehydrogenase complex	DBT	3		Mitochondria			1.4	3.10E-02	20.01	58.67	21.28
6978515	Apolipoprotein A-I	APOA1	2	15.1	Secreted	30062.13	5.52	1.3	5.78E-06	11.25	43.96	20.92
8393913	Propionyl Coenzyme A carboxylase, beta polypeptide	PCCB	9	24.0		58626.24	7.19	1.3	2.00E-02	17.87	56.32	20.82
47058982	Erythroid spectrin beta	SPTB	8	6.8		246328.58	5.18	1.3	2.10E-02	23.27	45.23	17.09
54633307	RN protein	OPA1	12	21.6		111247.96	7.01	1.3	2.00E-03	15.58	49.50	16.23
19705527	Basic leucine zipper and W2 domains 2	BZW2	2	7.2		48049.21	6.26	1.3	1.90E-02	22.24	51.33	15.99

gi number	Protein annotation	Symbol	No.of peptides	Seq.Coverage (%)	Sub-cellular location	Mol. Wt (Da)	pI	Fold change	p-value	Coefficient of variation (CV)		CV
										ANT	WT	
6981168	Lipoprotein lipase	LPL	3	10.5	Membrane	53082.36	8.36	1.3	6.00E-03	27.58	43.86	15.89
6978705	Carnitine palmitoyltransferase 2	CPT2	16	31.3	Mitochondria	74110.34	6.89	1.2	5.17E-04	15.15	45.27	14.61
109508535	PREDICTED: similar to vacuolar protein sorting 35	VPS35	2		Cytoplasm			1.2	1.30E-02	19.99	52.56	13.58
Proteins displaying ratios ≤1.2 in infected ANT-OE hearts												
109477603	PREDICTED: similar to succinate dehydrogenase Ip subunit	SDHB	9		Mitochondria			0.8	4.10E-02	8.44	30.73	13.14
18426858	Succinate dehydrogenase complex, subunit A, flavoprotein (Fp)	SDHA	25	46.6	Mitochondria	71615.20	6.75	0.8	4.70E-02	7.49	26.49	13.52
109459862	PREDICTED: similar to AHNAK nucleoprotein isoform 1	AHNAK	4					0.8	2.03E-06	13.18	41.24	13.94
21955146	Translocase of inner mitochondrial membrane 13 homolog	TIMM13	3	36.8	Mitochondria	10457.94	8.42	0.8	1.40E-02	9.79	28.02	14.38
19424338	Mitochondrial trifunctional protein, beta subunit	HADHB	18	47.4	Mitochondria	51414.47	9.50	0.8	4.00E-03	6.75	31.25	14.61
27689507	PREDICTED: similar to Polymerase I and transcript release factor	PTRF	5					0.8	3.81E-04	13.71	35.34	14.55
18677763	Mitochondrial trifunctional protein, alpha subunit	HADHA	20	46.0	Mitochondria	82512.92	9.11	0.8	4.90E-02	8.24	29.95	15.09
20301954	Apolipoprotein E	APOE	3	16.1	Secreted	36037.82	5.53	0.8	2.00E-03	15.59	32.36	15.17
109462848	PREDICTED: similar to Tu translation elongation factor	TUFM	10		Mitochondria			0.8	3.70E-02	18.04	26.81	15.53

gi number	Protein annotation	Symbol	No.of peptides	Seq.Coverage (%)	Sub-cellular location	Mol. Wt (Da)	pI	Fold change	p-value	Coefficient of variation (CV)		CV
										ANT	WT	
21326447	EH-domain containing 4	EHD4	5	14.8		61467.60	6.33	0.8	2.00E-03	15.92	48.49	15.74
109461624	PREDICTED: similar to Cytochrome c oxidase polypeptide VIIa-heart, mitochondrial precursor	COX7A1	2					0.8	2.40E-02	23.62	46.11	16.11
109481873	PREDICTED: similar to 13kDa differentiation-associated protein	NDUFA12	8					0.8	2.70E-02	12.10	33.37	16.20
47058998	TOM22 protein	TOMM22	2	16.2	Mitochondria	15490.65	4.27	0.8	1.31E-05	12.92	31.44	16.38
61557085	Spectrin beta 2	SPTBN1	4	2.7		273586.47	5.50	0.8	4.00E-03	14.64	32.28	16.69
109473321	PREDICTED: similar to coiled-coil-helix-coiled-coil-helix domain containing 3	CHCHD3	6		Membrane			0.8	3.00E-03	17.80	25.24	17.16
27682913	PREDICTED: similar to NADH dehydrogenase (ubiquinone) 1 alpha subcomplex, 2	NDUFA2	4					0.8	3.00E-02	9.61	23.44	18.14
55741424	NADH dehydrogenase (ubiquinone) flavoprotein 1, 51kDa	NDUFV1	17	47.8	Mitochondria	50730.98	8.37	0.8	1.30E-02	11.03	25.65	18.55
66730360	Microtubule-associated protein 4	MAP4	4	7.8		110300.76	4.63	0.8	6.00E-03	9.31	47.80	19.05
6981010	Hemoglobin alpha 1 chain	HBA1/HBA2	6					0.8	1.80E-02	12.29	24.42	19.07
72086149	NADH dehydrogenase (ubiquinone) Fe-S protein 5b	NDUFS5	3	29.2	Mitochondria	12699.77	9.10	0.8	2.00E-03	12.59	27.13	19.14
40445397	Beta-glo	HBB	3	35.4		16037.47	6.75	0.8	4.50E-02	23.60	27.71	19.18
77917570	Endonuclease G	ENDOG	3	13.6		32267.73	9.54	0.8	5.31E-04	15.29	28.62	19.52

gi number	Protein annotation	Symbol	No.of peptides	Seq.Coverage (%)	Sub-cellular location	Mol. Wt (Da)	pI	Fold change	p-value	Coefficient of variation (CV)		CV
										ANT	WT	
51092268	NADH dehydrogenase (ubiquinone) flavoprotein 2	NDUFV2	6	36.3	Mitochondria	27378.34	6.23	0.7	8.00E-03	9.51	29.66	20.32
52138635	Electron-transferring-flavoprotein dehydrogenase	ETFDH	15	29.5		68164.07	7.33	0.7	3.90E-02	6.67	14.75	20.85
53850628	NADH dehydrogenase (ubiquinone) Fe-S protein 1, 75kDa	NDUFS1	27	47.9	Mitochondria	79412.33	5.65	0.7	1.40E-02	8.94	24.89	20.93
39930503	ATP synthase, H+ transporting, mitochondrial F1 complex, gamma subunit	ATP5C1	9	29.5		32996.03	9.06	0.7	4.40E-02	8.91	10.94	21.41
17985949	Hemoglobin beta chain complex	HBB	4	27.9		15979.39	7.87	0.7	1.50E-02	16.50	25.91	21.38
109509939	PREDICTED: similar to Collagen alpha-1(VI) chain precursor	COL6A1	2		Extracellular matrix			0.7	2.00E-02	16.63	26.99	21.49
27663138	PREDICTED: similar to NADH dehydrogenase (ubiquinone) 1 alpha subcomplex, 6 (B14)		4					0.7	1.20E-02	12.20	24.27	21.63
27664028	PREDICTED: similar to tetratricopeptide repeat domain 11	NDUFA6	3					0.7	2.00E-03	20.93	34.16	21.88
16758362	Cytochrome c oxidase subunit Vb	COX5B	4	36.4	Mitochondria	13914.92	7.68	0.7	2.90E-02	17.86	23.70	21.94
34328536	Single-stranded DNA binding protein 1	SSBP1	2	19.9	Mitochondria	17454.93	9.84	0.7	5.00E-03	18.18	29.07	22.41
17105350	2,4-dienoyl CoA reductase 1	DECR1	5	22.7	Mitochondria	36203.82	9.18	0.7	5.00E-03	14.02	31.00	22.57
78214350	Hypothetical protein LOC498909	COQ9	6	30.1		35145.61	5.50	0.7	3.30E-02	23.02	26.25	23.50
27717677	PREDICTED: similar to NADH dehydrogenase (ubiquinone) 1 alpha subcomplex, 7 (B14.5a)	NDUFA7	3					0.7	1.00E-02	17.35	26.05	23.57

gi number	Protein annotation	Symbol	No.of peptides	Seq.Coverage (%)	Sub-cellular location	Mol. Wt (Da)	pI	Fold change	p-value	Coefficient of variation (CV)		CV
										ANT	WT	
8393804	Myosin heavy chain, polypeptide 6		10	25.4		223508.36	5.59	0.7	3.00E-05	17.55	33.49	24.55
109506033	PREDICTED: similar to actinin alpha 2	ACTN2	6					0.7	7.00E-03	30.22	31.53	26.10
18426866	acetyl-Coenzyme A acyltransferase 2	ACAA2	17	54.9		41870.92	8.09	0.7	6.24E-04	21.48	46.85	26.20
6981240	Myosin, light polypeptide 3	MYL3	5	48.5		22156.20	5.03	0.7	1.00E-03	17.45	29.29	26.52
11968118	Desmin	DES	8	31.3	Cytoplasm	53456.71	5.21	0.7	3.00E-03	16.97	22.86	27.42
68341995	NADH dehydrogenase (ubiquinone) Fe-S protein 4, 18kDa	NDUFS4	8	52.0	Mitochondria	19740.63	10.14	0.7	1.00E-02	16.93	23.43	29.98
62659497	PREDICTED: similar to Laminin gamma-1 chain precursor	LAMC1	3		Extracellular matrix			0.6	8.88E-05	20.97	26.71	31.29
109470313	PREDICTED: similar to Myosin- binding protein C, cardiac-type	MYBPC3	9					0.6	1.00E-03	20.37	28.11	32.15
6978607	Catalase	FGA	7	17.8	Peroxisome	59757.20	7.07	0.6	1.00E-03	14.89	40.98	32.16
56797757	Fibrinogen, alpha polypeptide	CAT	3	4.9		86656.85	5.52	0.6	5.25E-05	9.72	29.21	32.20
16758586	Succinate-CoA ligase, GDP-forming, alpha subunit	SUCLG1	4	22.2	Mitochondria	35031.63	9.54	0.6	1.50E-02	16.21	7.61	35.53
20806153	ATP synthase, H+ transporting, mitochondrial F1 complex, delta subunit precursor	VCL	2	13.7	Mitochondria	17595.07	5.16	0.6	2.50E-02	14.83	13.85	35.91
109502103	PREDICTED: similar to Vinculin (Metavinculin)	ATP5D	4					0.6	2.00E-03	16.83	19.95	37.22
14389299	Vimentin	VIM	6	21.0	Nucleus matrix	53732.73	5.06	0.6	2.10E-05	17.12	25.34	38.96

gi number	Protein annotation	Symbol	No.of peptides	Seq.Coverage (%)	Sub-cellular location	Mol. Wt (Da)	pI	Fold change	p-value	Coefficient of variation (CV)		CV
										ANT	WT	
78000203	Tropomyosin 1, alpha isoform i	TPM1	2	11.7		28528.73	4.71	0.5	2.00E-03	11.92	28.27	43.51
6981666	Troponin T2, cardiac		5	24.7		35730.28	4.95	0.5	1.00E-03	12.24	19.17	47.19
62650782	PREDICTED: similar to Y45G12B.3	TNNT2	3					0.5	2.76E-09	20.07	49.66	51.20
8394469	Troponin 1, type 3	TNNI3	4	20.9		24159.67	9.57	0.4	6.88E-04	13.32	21.80	57.50
34933197	PREDICTED: similar to Amine oxidase A (Monoamine oxidase type A)	MAOA	11		Mitochondria			0.3	1.03E-04	35.08	68.88	70.91
19705431	Albumin	ALB	2	3.6	Secreted	68718.74	6.09	0.1	1.64E-04	30.94	73.40	105.70

Fold change- Ratio of protein intensities in mitochondrial fractions of ANT over expressing (ANT-OE) rat hearts infected with CVB3 to that of infected Wild type hearts (WT)

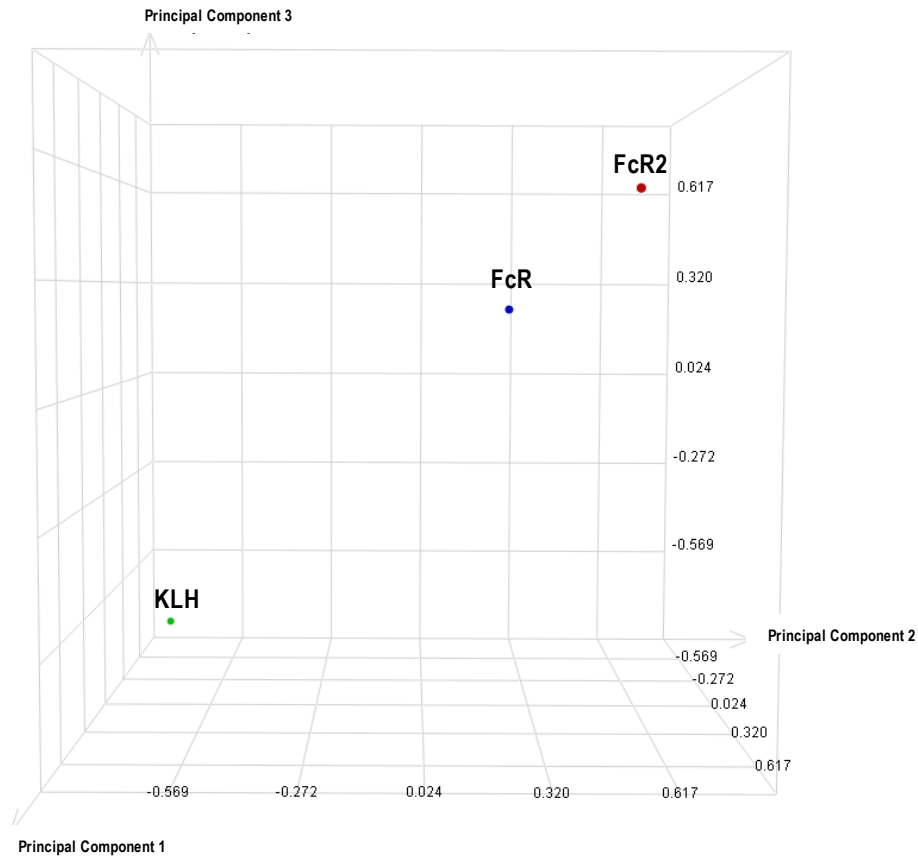


Fig. 3.5a. Principal component analysis (PCA) based on the identified isotope groups in rats immunized with peptides 1 and 2 of Fc gamma receptor. PCA analysis shows clear differentiation between the control rats (KLH) and rats immunized with peptide 1 (FcR) and peptide 2 (FcR2) of Fc gamma receptor. FcR2 rats differ the most from KLH whereas FcR and FcR2 rats grouped close to each other.

A 3.5 Proteins displaying autoimmune disease associated changes in 5 months old rats immunized with peptides 1 and 2 of Fcγ receptor compared to controls

gi Number	Protein Annotation	Symbol (IPA)	No. of peptides	Seq.Coverage (%)	Subcellular location	Mol.Wt (Da)	pI	Fold Change	p-value	Coefficient of variation (CV)		CV
										KLH	FcR*	
Proteins displaying ratios ≥ 1.2 in FcR immunized rats												
8393778	Myelin protein zero	MPZ	2	8.9	Plasma Membrane	27669.8	9.48	13.7	1.00E-02	53.43	77.82	122.16
6978515	Apolipoprotein A-I	APOA1	8	39.0	Extracellular Space	30062.1	5.52	7.0	3.00E-03	51.78	82.80	105.99
56797757	Fibrinogen, alpha polypeptide	FGA	11	22.8	Extracellular Space	86656.9	5.52	3.2	2.94E-06	52.88	45.52	74.66
21955142	Pregnancy-zone protein	Pzp	16	19.3	Extracellular Space	167159.2	6.46	2.9	8.00E-03	50.93	75.68	69.26
29789106	Fibrinogen, beta polypeptide	FGB	14	41.3	Extracellular Space	54303.3	7.89	2.9	1.05E-05	52.08	47.36	68.50
12831225	Murinoglobulin 1 homolog	Mug1	5	21.4	Extracellular Space	165326.2	5.68	2.8	1.00E-03	51.05	47.15	66.67
80861401	Kininogen 1	Knq1	2	11.2	Extracellular Space	47764.2	6.29	2.6	6.31E-15	58.88	48.50	63.09
61098186	Fibrinogen, gamma polypeptide	FGG	6	10.5	Extracellular Space	49651.7	5.85	2.5	4.16E-05	52.50	46.47	60.58
20301954	Apolipoprotein E	APOE	4	13.5	Extracellular Space	36037.8	5.53	2.3	3.25E-04	42.33	54.10	56.54
9506445	Carbonic anhydrase 2	CA2	2	12.7	Cytoplasm	29113.8	6.89	2.0	2.29E-04	38.56	27.66	47.02
83816939	Alpha-1-inhibitor III		5	9.7	Extracellular Space	163773.3	5.70	2.0	4.54E-04	51.11	36.71	46.95
9506819	Inter-alpha-inhibitor H4 heavy chain	ITI4	3	7.0	Extracellular Space	103607.3	6.08	2.0	1.58E-13	45.95	33.73	46.27
12083675	Phospholamban	PLN	2	32.7	Cytoplasm	6094.5	9.15	2.0	1.22E-05	43.06	27.85	46.18
6981022	Hexokinase 1	HK1	2	3.9	Cytoplasm	102408.0	6.29	1.9	6.00E-03	43.81	31.69	45.20
13928744	Transgelin	TAGLN	4	16.9	Cytoplasm	22602.9	8.87	1.8	4.38E-04	60.18	41.60	41.72
109462323	PREDICTED: similar to Filamin-A (Alpha-filamin)	FLNA	4	4.0	Cytoplasm	281215.4	5.69	1.7	7.82E-04	51.45	46.88	37.19

gi Number	Protein Annotation	Symbol (IPA)	No. of peptides	Seq.Coverage (%)	Subcellular location	Mol.Wt (Da)	pI	Fold Change	p-value	Coefficient of variation (CV)		CV
										KLH	FcR*	
16758094	Fatty acid binding protein 4	FABP4	4	32.7	Cytoplasm	16494.3	9.10	1.6	3.14E-04	52.15	33.47	33.86
14389299	Vimentin	VIM	12	32.8	Cytoplasm	53732.7	5.06	1.5	2.90E-07	57.53	30.59	29.41
6978491	Aldehyde reductase 1	AKR1B1	2	25.3	Cytoplasm	35797.3	6.26	1.5	1.00E-03	50.34	28.08	29.30
17985949	Hemoglobin beta chain complex	HBB	4	27.9	Cytoplasm	15979.4	7.87	1.5	6.00E-03	58.31	45.09	28.84
8392983	Biglycan	BGN	2	5.7	Extracellular Space	41706.3	7.16	1.5	1.10E-02	59.97	29.51	28.40
27688933	PREDICTED: similar to procollagen, type I, alpha 1	COL1A1	4	3.6	Extracellular Space	137953.5	5.71	1.5	1.20E-02	50.46	41.45	27.18
13591983	Lumican	LUM	2	9.5	Extracellular Space	38279.0	6.00	1.5	5.00E-03	61.80	28.90	25.99
109489498	PREDICTED: similar to Actin, cytoplasmic 2	ACTG1	3	6.3	Cytoplasm	75346.4	8.54	1.4	1.21E-05	46.01	31.00	25.92
40445397	Beta-globulin	HBB	5	51.0	Cytoplasm	16037.5	6.75	1.5	3.00E-03	59.21	52.46	25.96
6978607	Catalase	CAT	3	9.9	Cytoplasm	59757.2	7.07	1.4	6.19E-04	53.75	34.47	25.07
6981010	Hemoglobin alpha 1 chain	HBA1/HBA2	4	41.6	Cytoplasm	15328.5	7.81	1.4	7.00E-03	57.32	48.67	24.7
6981324	Prolyl 4-hydroxylase, beta polypeptide	P4HB	2	4.7	Cytoplasm	56864.2	4.82	1.4	1.20E-02	47.23	32.67	24.14
13929178	Fibrillin 1	FBN1	3	3.1	Extracellular Space	312072.0	4.81	1.4	2.30E-02	64.92	33.72	21.04
9845234	Annexin A2	ANXA2	3	10.0	Plasma Membrane	38678.2	7.55	1.3	7.00E-03	48.16	34.12	19.48
109459168	PREDICTED: similar to Hemoglobin beta-2 subunit	HBB	2	53.7	Cytoplasm	15982.4	8.91	1.3	7.00E-03	55.62	26.91	18.98
42476287	Transglutaminase 2, C polypeptide	TGM2	6	20.0	Cytoplasm	76935.7	4.95	1.3	7.00E-03	53.56	37.47	18.10
109481431	PREDICTED: similar to myosin, light polypeptide 6	MYL6	2	24.5	Cytoplasm	16961.1	4.46	1.3	2.00E-03	53.69	61.3	17.02
11693172	Calreticulin	CALR	2	8.2	Cytoplasm	47995.5	4.33	1.2	2.70E-02	52.44	56.01	14.49

gi Number	Protein Annotation	Symbol (IPA)	No. of peptides	Seq.Coverage (%)	Subcellular location	Mol.Wt (Da)	pI	Fold Change	p-value	Coefficient of variation (CV)		CV
										KLH	FcR*	
62990183	Tyrosine 3-monooxygenase/tryptophan 5-monooxygenase activation protein, zeta polypeptide	YWHAZ	5	22.0	Cytoplasm	27771.1	4.73	1.2	2.00E-03	50.98	26.78	14.66
8393024	Complement component 3	C3	13	11.1	Extracellular Space	186460.4	6.12	1.2	4.50E-02	51.17	42.62	13.9
62078857	Hypothetical protein LOC313163	1700009N14Rik	2	9.7	Nucleus	24450.1	8.40	1.2	3.10E-02	50.48	70.79	13.74
109473201	PREDICTED: similar to Filamin-C, isoform 2	FLNC	6	4.4	Cytoplasm	290986.1	5.59	1.2	3.50E-02	51.75	35.22	13.22
Proteins displaying ratios ≤ 1.2 in FcR immunized rats												
62646841	PREDICTED: similar to Calcium-binding mitochondrial carrier protein Aralar2 (Solute carrier family 25 member 13)	SLC25A13	4	5.9	Cytoplasm	74398.9	8.86	0.8	1.46E-04	53.64	31.13	13.33
13786200	Voltage-dependent anion channel 1	VDAC1	4	43.1	Cytoplasm	30755.5	8.62	0.8	1.60E-05	52.98	34.13	13.39
61557218	Chaperone, ABC1 activity of bc1 complex like	ADCK3	2	6.2	Cytoplasm	72225.6	6.03	0.8	1.10E-02	55.07	29.30	13.56
27661165	PREDICTED: similar to NADH dehydrogenase (ubiquinone) Fe-S protein 8	NDUFS8	5	21.2	Cytoplasm	23970.3	5.87	0.8	3.28E-06	52.21	40.43	13.62
11693174	Branched chain aminotransferase 2, mitochondrial	BCAT2	3	12.0	Cytoplasm	44275.5	8.46	0.8	3.00E-03	53.32	35.78	13.73
60678254	Creatine kinase, mitochondrial 1, ubiquitous	CKMT1A/CKMT1B	3	8.9	Cytoplasm	46961.7	8.58	0.8	4.00E-03	50.13	35.74	14.95

gi Number	Protein Annotation	Symbol (IPA)	No. of peptides	Seq.Coverage (%)	Subcellular location	Mol.Wt (Da)	pI	Fold Change	p-value	Coefficient of variation (CV)		CV
										KLH	FcR*	
61556832	Adenine phosphoribosyl transferase (predicted)	APRT	2	12.8	Cytoplasm	19545.8	6.17	0.8	4.00E-03	49.09	46.52	17.98
11024650	Myoglobin	MB	6	38.3	Cytoplasm	17156.8	7.83	0.8	5.00E-03	54.28	32.34	18.22
34933197	PREDICTED: similar to Amine oxidase A (Monoamine oxidase type A)	MAOA	6	6.3	Cytoplasm	98074.5	6.95	0.8	7.00E-03	54.96	42.93	19.77
8393948	Phosphoglycerate mutase 2	PGAM2	4	26.1	Cytoplasm	28755.0	8.85	0.7	6.67E-06	55.02	36.87	20.64
31542401	Creatine kinase, brain	CKB	3	13.9	Cytoplasm	42712.2	5.33	0.7	2.70E-04	55.58	38.56	22.74
109495555	PREDICTED: similar to myosin light chain 2, precursor lymphocyte-specific		2	18.4		26187.9	6.72	0.7	4.40E-02	45.11	32.00	27.03
6981684	Transthyretin		5	30.6		15747.8	5.77	0.6	2.50E-02	47.48	66.44	32.19
6978477	Alpha-2-HS-glycoprotein	AHSG	4	19.9	Extracellular Space	38003.4	6.30	0.6	5.00E-03	44.45	67.79	40.72
16758014	Hemopexin	HPX	7	18.5	Extracellular Space	51290.9	7.58	0.5	3.11E-04	55.98	88.43	50.16
61556986	Transferrin	TF	19	35.5	Extracellular Space	76395.2	7.14	0.4	2.03E-07	52.42	73.47	54.85
19705431	Albumin	ALB	2	54.9	Extracellular Space	68718.7	6.09	0.4	2.48E-05	52.43	88.72	56.71
62078619	Hypothetical protein LOC299354		3	8.4		51698.6	7.12	0.4	4.47E-08	51.04	85.57	65.20

FcR*- includes proteins altered in both FcR and FcR2 models of autoimmune cardiomyopathy, Fold change- Ratio of protein intensities of FcR* rat hearts to that of KLH control hearts

Enclosures (CD)

A3.2.2.3 List of proteins identified with 2peptide confidence by gel-free LC-MS/MS analysis in A.BY/SnJ mice hearts 84d p.i.

A3.3.2 List of protein identified with 2peptide confidence by gel free LC-MS/MS analysis in 4months old A.BY/SnJ mice hearts.

A3.4.1a List of proteins identified with 2peptide confidence by gel-free LC-MS/MS analysis in 8 months old whole hearts of ANT overexpressed (ANT-OE) rats

A3.4.2a List of proteins identified with 2peptides in mitochondrial fractions of CVB3 infected ANT-OE rats compared to infected WT rats

A3.5a List of proteins identified with 2peptides in rats immunized with peptides 1 and 2 of Fc gamma receptorIIa (FcR)